# Stochastic Geometry Based Analysis of Candidate Technologies for 5G Cellular Systems

by
Sachitha Kusaladharma

A thesis submitted in partial fulfillment of the requirements for the degree of

Doctor of Philosophy
in
Communications

Department of Electrical and Computer Engineering

University of Alberta

# Abstract

Future fifth generation (5G) cellular standards incorporate new emerging technologies such as cognitive radio, device to device (D2D), interweave, energy harvesting, massive MIMO, and millimeter wave networks. However, the achievable gains of these technologies are limited by the spatial randomness of nodes and network interference.

Spatial locations of nodes are increasingly random. Characterizing the impacts of this randomness on system parameters is a main motivation of this thesis. Moreover, when two networks coexist in the same geographical area, interference occurs between the networks in addition to interference within each network. The interplay between different technologies is also of high interest as they will be deployed in tandem. Therefore, the main communication problem addressed in this thesis is the characterization of interference among spatially random nodes for co-existing networks under emerging technologies.

The main contributions of this thesis are categorized as follows: 1) Development of power control and receiver association schemes for an annular underlay CR network and investigation of their performance, 2) Development of co-operative beacon detection schemes for interweave CR networks and investigation of their performance, 3) Investigation of the feasibility of wireless energy harvesting for an underlay CR network using stochastic geometry and markov chain based models, 4) Quantifying the effect of performance degradation for an underlaid receiver when base stations use massive MIMO, and 5) Development of an analytical framework to analize performance degradation to an underlaid D2D network employing millimeter wave frequencies.

It is shown that stochastic geometry models provide vital insights into key network design considerations while incorporating most system and channel parameters. The research outcomes

will potentially improve spectral efficiency, throughput, and coverage in fifth generational (5G) cellular networks.

# Preface

Elements of Chapter 2 have been published as S. Kusaladharma, Cognitive Radio Networks, which has been accepted for publication in *Wiley Encyclopedia of Electrical and Electronic Engineering*.

Chapter 3 of this thesis has been published as S. Kusaladharma, P. Herath, and C. Tellambura, Underlay Interference Analysis of Power Control and Receiver Association Schemes, *IEEE Transactions on Vehicular Technology*, vol. 65, no. 11, pp. 89788991, November 2016 and S. Kusaladharma, P. Herath, and C. Tellambura, Impact of Transmit Power Control on Aggregate Interference in Underlay Cognitive Radio Networks, *IEEE International Conference on Communications (IEEE ICC)*, Sydney, Australia, June 2014.

Chapter 4 has been published as S. Kusaladharma and C. Tellambura, "Interweave Cognitive Networks with Cooperative Sensing," *IEEE Global Communications Conference (IEEE GLOBECOM)*, San Diego, CA, USA, December 6-10, 2015 and S. Kusaladharma and C. Tellambura, Co-operative Beacon Sensing Strategies for Spatially Random Interweave Cognitive Networks, which has been submitted to *IEEE Transactions on Cognitive Communications and Networking*.

Chapter 5 has been published as S. Kusaladharma, and C. Tellambura, Massive MIMO based underlay networks with power control, *IEEE International Conference on Communications (IEEE ICC)*, Kuala Lumpur, Malaysia, May 2016 and S. Kusaladharma and C. Tellambura, Secondary User Interference Characterization for Underlay Massive MIMO Networks with Power Control, which has been accepted for publication in *IEEE Transactions on Vehicular Technology*.

Chapter 6 has been published as S. Kusaladharma, and C. Tellambura, Performance Characterization of Spatially Random Energy Harvesting Underlay D2D Networks with Primary User Power Control, *IEEE International Conference on Communications (IEEE ICC)*, Paris, France, May 2017 and as S. Kusaladharma and C. Tellambura, Performance Characterization of Spatially Random Energy Harvesting Underlay D2D Networks with Transmit Power Control, which has

been submitted to *IEEE Transactions on Communications*.

Chapter 7 has been published as S. Kusaladharma, and C. Tellambura, Modeling Interference in Random Millimeter-wave Networks, *IEEE International Conference on Communications (IEEE ICC)*, Paris, France, May 2017.

# Acknowledgements

I would like to thank Prof. Chintha Tellambura for being an excellent supervisor and guiding me on my path of research from the beginning of my Masters in 2011 till the end of my PhD in 2017. Prof. Tellambura provided valuable insights and feedback which enabled the best research outcomes. Moreover, his suggestions on writing and presentations have been especially valuable. I also appreciate Prof. Yindi Jing, Prof. Majid Khabbazian, Prof. Ehab Elmallah, Prof. Raviraj Adve, and Prof. Duncan Elliott for being my committee members, and for providing important feedback.

I also wish to thank all my family and friends and other teachers who have helped me to come to this stage. A special thanks also goes to all present and former members of the Wireless Communications lab W5-070 who helped me immensely along the way.

$\sim$

# Contents

# List of Figures

# List of Tables

# List of symbols and notations

| Notation | Definition |
|---|---|
| $k!$ | factorial of $k$ |
| $\binom{n}{k}$ | binomial coefficient, $n$ choose $k$ |
| $\min(a_1, \ldots, a_n)$ | minimum of all scalars $a_i$ for relevant $i$ |
| $O(\cdot)$ | the remainder in series |
| $\Gamma(x, a)$ | $\int_a^\infty t^{x-1}e^{-t}dt$ |
| $\Gamma(x)$ | $\Gamma(x, 0)$ |
| ${}_2\mathcal{F}_1(,;;)$ | Gauss' Hypergeometric function [5, (eq. 9.10)] |
| ${}_2\mathcal{F}_2(,;;)$ | generalized Hypergeometric function [5, (eq. 9.14)] |
| $\mathcal{K}_\nu(\cdot)$ | modified Bessel function of the second kind [5, (eq. 8.407)] |
| $\lfloor x \rfloor$ | the largest integer less than $x$ |
| $E_n(x)$ | $\int_1^\infty \frac{e^{-xt}}{t^n}dt$ |
| $f_X(\cdot)$ | probability density function (PDF) |
| $F_X(\cdot)$ | cumulative distribution function (CDF) |
| $M_X(\cdot)$ | moment generating function (MGF) |
| $E_X[\cdot]$ | expectation with respect to $X$ |
| $\Pr[A]$ | probability of event $A$ |
| $f_X(\cdot)$ | PDF |
| $F_X(\cdot)$ | CDF |
| $Q(\cdot)$ | $Q$ function |
| Bernoulli$(p)$ | Bernoulli random variable $X$ with $\Pr[X = 1] = p$ and $\Pr[X = 0] = 1 - p$ |
| $\|\|x\|\|$ | Euclidean norm |
| $Lin(\alpha)$ | $f(t) = \frac{2t}{\alpha^2}, 0 < t < \alpha$ |

| | |
|---|---|
| $Ral(\alpha)$ | $f(t) = 2\alpha t e^{-\alpha t^2}, 0 < t < \infty$ |
| $TRal(\alpha, \beta)$ | $f(t) = \frac{2\alpha t e^{-\alpha t^2}}{1-e^{-\alpha \beta^2}}, 0 < t < \beta$ |

# Acronyms

| Acronym | Meaning |
|---|---|
| BPP | Binomial Point Process |
| CAGR | Cumulative Annual Growth Rate |
| CBS | Cooperative Beacon Sensing |
| CCDF | Complementary Cumulative Distribution Function |
| CDF | Cumulative Distribution Function |
| CLT | Central Limit Theorem |
| CR | Cognitive Radio |
| CSI | Channel State Information |
| CSMA/CA | Carrier Sense Multiple Access/ Collision Avoidance |
| CVRMSE | Coefficient of Variation of Root Mean Square Error |
| D2D | Device to Device |
| DSA | Dynamic Spectrum Access |
| DySPAN | Dynamic Spectrum Access Networks |
| FM | Frequency Modulation |
| FSL | Free Space Loss |
| GPS | Global Positioning System |
| IEEE | Institute of Electrical and Electronic Engineers |
| IoT | Internet of Things |
| ISI | Inter Symbol Interference |
| ISM | Industrial, Scientific, and Medical |
| ITU | International Telecommunication Union |
| LOS | Line-of-sight |
| LTE | Long Term Evolution |

| | |
|---|---|
| MGF | Moment Generating Function |
| MIMO | Multiple Input Multiple Output |
| NEM | Normalized Error of the Mean |
| NLOS | Non-line-of-sight |
| QoS | Quality of Service |
| PDF | Probability Density Function |
| PDP | Power Delay Profile |
| PGFL | Probability Generating Functional |
| PL | Path Loss |
| PLI | Path Loss Inversion |
| PPP | Poisson Point Process |
| PR | Primary Receiver |
| PT | Primary Transmitter |
| PU | Primary User |
| QoS | Quality of Service |
| RF | Radio Frequency |
| RFID | Radio Frequency Identification |
| RMSE | Root Mean Square Error |
| SINR | Signal to Interference and Noise Ratio |
| SNR | Signal to Noise Ratio |
| SU | Secondary User |
| TDD | Time Division Duplexing |
| UHF | Ultra High Frequency |
| WCDMA | Wideband Code Division Multiple Access |
| WiMAX | Worldwide interoperability for Microwave Access |
| WRAN | Wireless Regional Area Network |

# Chapter 1

# Introduction

The wireless communications industry has globally experienced an exponential growth over the last few decades. Currently, it supports a vast array of applications and standards. These include but are not limited to:

1. Mobile telephony,
2. Satellite communications,
3. Internet of Things (IoT),
4. Wireless sensor networks,
5. Ad-hoc networks,
6. Radar and Navigation,
7. Body area networks.

Due to these and other applications, the number of mobile devices exceeded the global population in 2014 [1]. According to Cisco, this trend is set to continue with the monthly mobile data traffic exceeding $24.3$ exabytes by 2019 [1]. By then, there will be 1.5 mobile devices per capita, and the average speed of a connection will increase to $4$Mbps. Furthermore, over $59\%$ of mobile connections arise from smartphones, and mobile to mobile connections will become the dominant category (Fig. 1.1).

To meet these increased demands for coverage, capacity, and service, the wireless industry must continuously upgrade itself, which motivates the development of the fifth generation (5G)

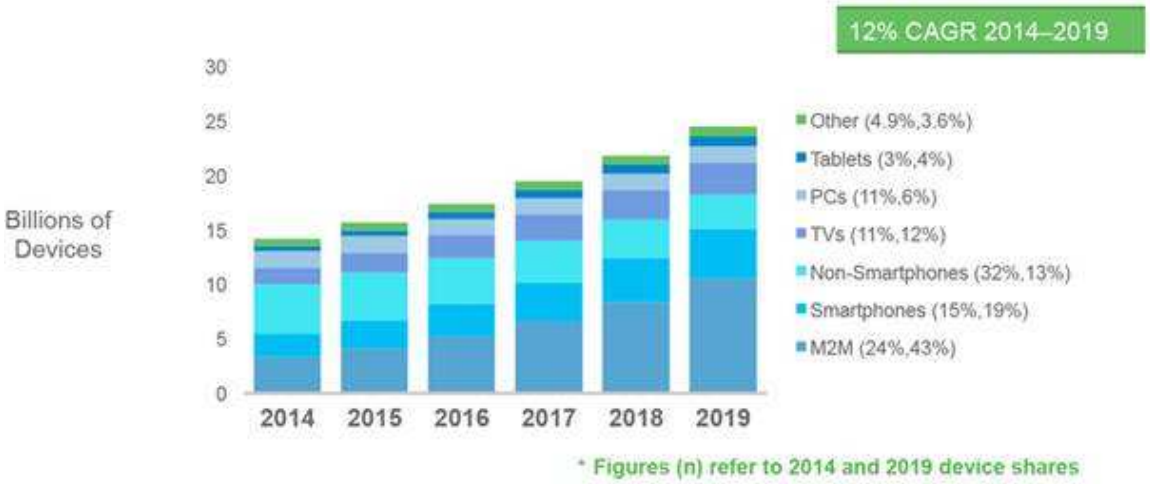


Figure 1.1: Cisco Global Devices Forecast 2014-2019 [1]

standards [6]. Candidate technologies for 5G systems include cognitive radio (CR), massive MIMO (multiple input multiple output) systems, millimeter-wave networks, and device to device (D2D) communications, and energy harvesting networks [6]–[9].

Modern wireless networks are evolving so that the locations of base stations and users do not usually conform to a pre determined layout. In particular, while the locations of base stations are conventionally modelled as a hexagonal grid, increasing irregularity is common with the introduction of heterogeneous networks comprising small cells and pico cells [2]. The location of users are almost always random. As such, conventional fixed models such as the hexagonal grid model are unrealistic and stochastic geometry models have thus gained ground within the research community [10]–[15]. Apart from modelling a realistic network scenario, they are also tractable [12] and can even approximate planned network deployments [12]. There are multiple stochastic geometry based models. For example, when the number of nodes within the total geographical area is known the Binomial point process is more accurate for node distributions (especially base stations) [16]. In contrast, the Poisson point process (PPP) is more popular due to its superior analytical tractability.

In this thesis, we will analyze the performance of proposed 5G technologies when the locations of user nodes and base stations are modelled as PPPs. First, we will provide a brief introduction of these various promising technologies next.

| Service | Frequency |
|---|---|
| E-GSM-900 (Mobile) | 880-915, 925-960 MHz |
| DCS (Mobile) | 1710-1785, 1805-1880 MHz |
| FM radio (Broadcasting) | 88-108 MHz |
| Standard C Band (Satellite Communication) | 5.850-6.425, 3.625-4.200 GHz |
| Non-directional radio beacon (Navigation) | 190-1535 kHz |

Table 1.1: Existing frequency assignment for different services.

## 1.1 Cognitive radio networks

Wireless growth is hampered due to the absence of unallocated spectrum and its inefficient uses [2]. For example, although theoretically ranging from $3$ Hz to $3000$ GHz, the prime spectrum for current wireless standards may be roughly $1-5$ GHz. This is because the spectrum below $1$ GHz has already been reserved for applications such as radar, military communications, and terrestrial radio/television while the spectrum above $5$ GHz suffers from increased attenuation and atmospheric absorption. While this efficiency of spectral usage (measured in bits per second per hertz) has steadily increased due to technical improvements such as the use of higher order modulation and adaptive techniques [17]–[21], the rate of growth has decreased recently [22]. Due to this saturation, improving spectral efficiency by other means is essential for the growth of wireless networks.

Currently, spectrum is assigned in a fixed manner by national regulatory bodies, and their main principle is to avoid radio interference, which is achieved by dividing spectrum into bands (e.g., frequency division) which are allocated to one or more services. These radio services include mobile, satellite, amateur radio, navigation and others (Table 1.1). A license gives an exclusive right to operate (transmit and receive wireless signals) in a specific frequency band, in a specific location or geographic area. But much of the licensed spectrum remains unused in practice at different times and/or locations. Those temporary spectrum slots (aka spectrum holes or white spaces) [23], [24] can be as high as $15-85\%$ of the licensed spectrum [25]. Clearly, to improve the overall spectral efficiency, unlicensed users can be allowed to access such spectrum holes. Thus, this fact suggests the need for opportunistic spectrum access without causing undue interference to licensed users [8], [26]. Such capability is the defining characteristic of cognitive radio (CR) nodes, which require algorithms and protocols for rapid spectrum sensing, coordination and cooperation. In other words, CR nodes can recognize unused parts of spectrum and adapt their communications to utilize them while minimizing the interference on licensed users.

Consequently, CR improves the overall spectrum usage, by moving away from static assignments into more dynamic forms of spectrum access. Formally, the main functionalities of CR networks include: spectrum sensing, spectrum management and decision, spectrum sharing, and spectrum mobility [2].

Thus, to enable access to idle or underutilized spectrum, CR networks have already been standardized in IEEE 802.22 WRAN (Wireless Regional Area Network) and its amendments, IEEE 802.11af for wireless LANs, IEEE 1900.x series, and has also been a motivating factor for licensed shared access (LSA) for LTE mobile operators [27]. Furthermore, test beds have been built to verify the feasibility of CR within LTE systems [28].

In the context of CR, licensed spectrum users are called primary users (PUs) and unlicensed users are called secondary users (SUs) or CR nodes (both terms are used interchangeably henceforth.) Thus, SUs must opportunistically access spectrum holes, while keeping the interference on the PU receivers at either zero or below a prescribed level. Thus, multiple secondary CR networks and a primary network can co-exist (Fig. 1.2). CR networks can be divided into two main paradigms [29]–[34]. These are interweave networks and underlay networks.

- Interweave Networks

  These hold true to the original premise of accessing whitespaces [29], and operate on an interference free basis. Thus, SUs transmit only when their sensing algorithms detect spectrum holes in real time and indicate that primary transmissions are absent. These sensing algorithms include matched filter detection, cylostationary detection, energy detection, eigenvalues based detection, waveform sensing and beacon detection [35], [36], and via a centralized system by using a geo-location database [9], [36].

- Underlay Networks

  Underlay networks operate on an interference tolerant basis, and allows simultaneous spectrum access for both primary and secondary devices [31]. However, concurrent spectrum access may significantly decrease user performance due to harmful interference. As such, transmit power control techniques and interference cancellation schemes are essential for primary and secondary networks to coexist with each other [8]. Furthermore, exclusion regions (guard regions) around primary devices where no secondary transmissions take place can also be enforced to keep the interference in check [37]. These can be enforced

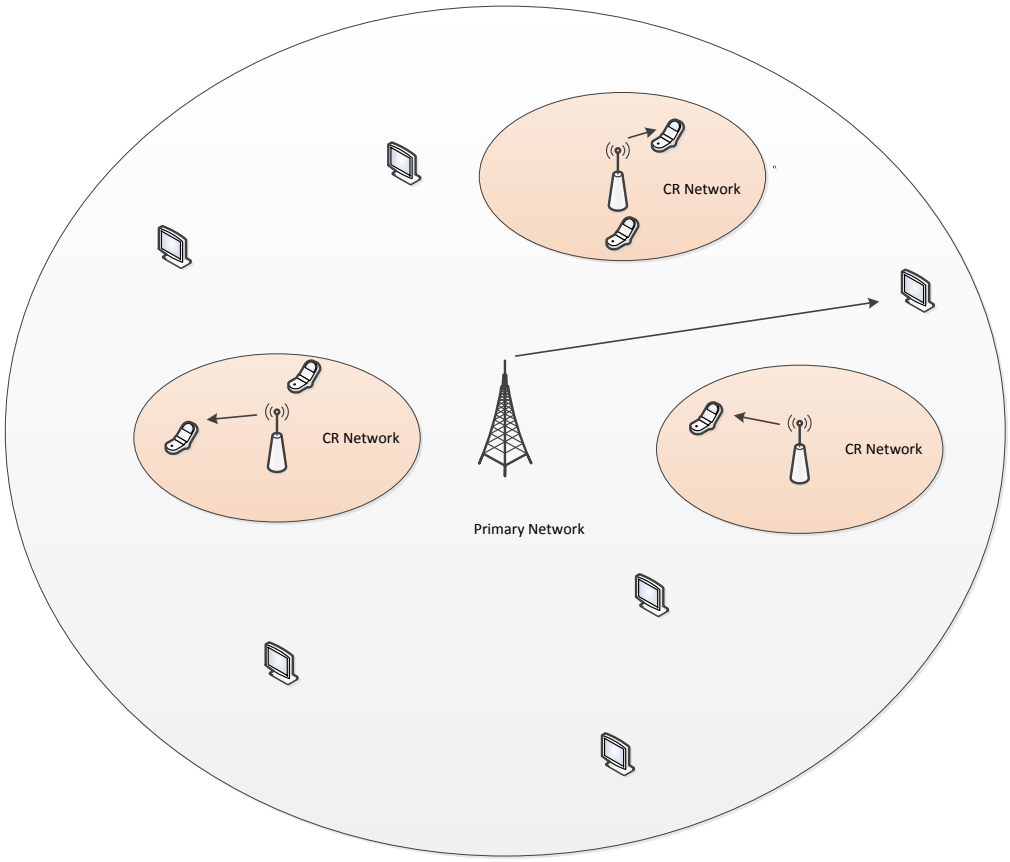


Figure 1.2: CR networks existing within a primary network [2]

either through prior location information which could be obtained through a centralized control center aided by a geo location database, GPS data, or dynamically via sensing pilot signals/acknowledgements originating from the primary nodes [38]–[40]. However, even with interference constraints, each underlay node can still achieve half of the total degrees of freedom which would have been attainable without interference constraints [41].

## 1.2 Device to device communications

Device to device communications allow two neighbouring user terminals to comunicate with each other without the base stations being involved [42], [43], and is a promising concept for future 5G systems, especially in millimeter-wave networks [43], [44]. While the base station is serving multiple users, two users may directly communicate while bypassing the base station. The network can implement minimal control procedures on the D2D communication. For example, the network may only allow communication within certain geographical areas, and maximum

transmit power limits may be enforced.

Current technologies such as Bluetooth and Wi-Fi direct utilize D2D, which has also been proposed for cellular [43]. D2D provides benefits such as lower power consumption, higher data rates, and reduced communication delay [43]. Furthermore, from the perspective of the provider, the load on the cellular network is lower, and spectral efficiency is increased. Moreover, in case of emergencies, D2D systems can potentially act as a vital tool to enable communications when the network side infrastructure is either damaged or overburdened [42], [45]. D2D is also a special case of the underlay CR paradigm.

Like the other potential 5G technologies, D2D faces numerous challenges before successful deployment. For example, security may be compromised because user information passes through other user devices [42]. Interference management is also a key concern particularly when D2D in 5G will operate within licensed cellular bands. Thus, the interference must be kept below a certain level for normal cellular communications between users and base stations. However, D2D millimeter-wave systems have certain advantages for interference management due to the high attenuation and directivity experienced [44]. Moreover, device discovery and initial session set-up is problematic. In addition, resource allocation and guaranteeing quality of service (QoS) is difficult for D2D users.

## 1.3 Massive MIMO

Massive MIMO systems enable a large number of antennas (typically tens or hundreds) to exploit the spatial dimension, and hold promise as a constituent technology for 5G systems [46]–[48]. It enables either large data rates, greater reliability, or the ability to simultaneously serve a large number of users. In a cellular set-up, the number of antennas at the user devices is limited, but a massive MIMO base station can serve a large number of users. With massive MIMO, interference management is possible by employing suitable beamforming schemes.

With massive MIMO, performance improvements over conventional MIMO in terms of reliability, spectral efficiency, and efficiency are possible [8]. Moreover, massive MIMO enables efficient multi-user MIMO communications where separate signals are sent to individual receivers using the same time-frequency slot while avoiding complex scheduling algorithms [8].

However, massive MIMO needs channel state information (CSI) of both uplink and downlink [9]. This requires the use of orthogonal pilot sequences [49]–[52]. Time division duplexing

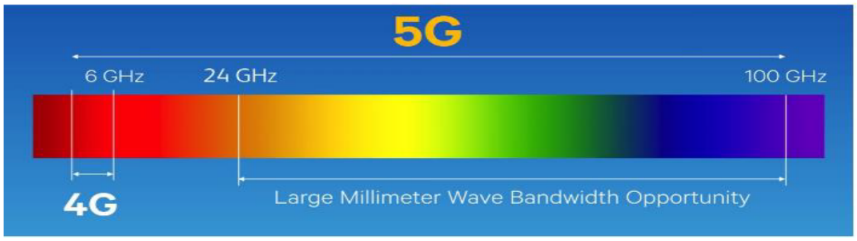


Figure 1.3: Advantages of millimeter-wave systems.

(TDD) which enables uplink pilots to be used for CSI estimation in the downlink has thus been popular [9], [53]. However, using pilot signals has two main downsides: 1) using spectral resources which may otherwise be used for data transfer, and 2) resulting interference when the same pilots are used for different terminals (named pilot contamination) [46]. The pilot lengths depend on the number of user terminals, and because the length of the pilots are constrained by the channel coherence time, the same pilot sequences have to be used in adjacent cells or within the same cell itself. The resulting inter-cell and intra-cell interference is one of the main inhibiting factors of massive MIMO [51].

## 1.4 Millimeter-wave systems

Due to congestion of the traditional spectrum, the millimeter-wave frequencies ($30 - 300$GHz) show promise for future 5G wireless systems [7], [44], [47]. Even after excluding certain subbands which may be unusable, $40\%$ of the remaining spectrum which tallies close to $100$GHz may be available over time [54]. Fig. 1.3 gives a basic idea of the vastness in millimeter-wave bands. However, it should be noted that not all of these frequencies are necessarily vacant or assigned.

Recent research has suggested that these frequencies may be able to support cellular communication provided the cell radius remains small; typically within $100 - 200$m [7]. Thus, millimeter-wave networks are ideal for cells having small radii; especially for indoor cells. Furthermore, millimeter-wave systems have potential applications within cellular backhaul, personal area networks, internet of things (IoT), and campus/enterprise networks.

While providing much needed spectrum, transitioning into the millimeter-wave frequencies provide much larger bandwidths for services compared with present usage [55]. Furthermore, given the small wavelengths at high frequencies, millimeter-wave based networks have the po-

tential to make ever smaller antennas and thus include a large number within an extremely small area [55]. This spatial condensation of antennas is expecially beneficial to incorporate techniques such as massive MIMO [55].

Before successful implementation of a 5G system on millimeter-wave frequencies, several obstacles must be overcome. First, due to the high frequencies, the path loss increases by $20$ dB for every $10$ fold increase in frequency if the electrical sizes of the antennas are kept constant [6], [9]. Moreover, the propagation laws vary for line of sight and non-line of sight paths [55]. Second, due to the sparsity of scatterers, the number of multi-path components received is significantly low. Third, millimeter-wave signals experience significant effect from blockages due to low diffraction [9], [44], and have trouble penetrating obtacles such as walls [55]. For example, at $40$GHz, there is a $178$ dB attenuation when penetrating brick walls and a $20$ dB loss when penetrating a painted board [44]. As such, the existence of a line-of-sight component varies immensely [6], and because non-line of sight paths are weak in millimeter-wave frequencies, outages can readily occur due to blockages [44]. Fourth, the absorption by air and rain is high, and within the $60$GHz band, an absorption of $15$ dB per km occurs due to oxygen [6]. Fifth, the millimeter-wave signal beams are extremely narrow and directed, and difficulties occur for users in finding base stations to associate with.

## 1.5 Energy harvesting systems

Apart from spectrum constraints, energy constraints have been recognized as a bottleneck for wireless nodes [56]. Nodes such as base stations are connected to the mains power grid while nodes such as user devices or sensor nodes are battery powered. In the case of battery powered devices, they are recharged periodically. For sensor nodes, practical considerations inhibit periodic recharging, and thus the lifetime of these devices would end whenever the battery power runs out. Moreover, there has been a global demand to reduce energy usage to aid greener technology irrespective of the availability of power sources. Specifically, the drive has been towards using less resources including energy, and reusing those resources.

Therefore, wireless underlay nodes may be powered by energy harvesting [57], which is especially attractive for small battery powered devices [58]. This harvesting from the ambient environment enables greener devices, and extends the lifetime of sensor nodes indefinitely due to the self-sustaining nature of the harvesting process. In practice, energy can be harnessed from

various environmental sources including solar energy, ambient radio frequency (RF) energy, wind energy, mechanical energy due to vibration and motion, and thermal energy among others. For the purposes of this thesis, we will be concentrating on energy harvesting from RF sources.

RF energy harvesting can itself be divided into two constituent technologies [57]. The first involves dedicated RF transmitters placed strategically. These transmitters guarantee a fixed energy source for the devices. Furthermore, the ambient power available for harvesting can be readily predicted. Moreover, whenever the energy requirement is low or non-existent, the network has the control of switching such transmitters off. However, having such dedicated infrastructure based transmitters are costly. Furthermore, if the harvesting devices are not congregated into certain geographic areas, dedicated RF transmitters become an impractical solution. This is also the case when sensor devices are placed in hostile environments. The second RF energy harvesting scheme uses ambient RF signals present in the environment. With this scheme, the use of existing RF signals increases the energy efficiency via reuse. Furthermore, because fixed infrastructure components are not needed, the cost for the network operator is significantly less. However, the actual amount of harvested energy can be extremely small. Therefore, this method is only suitable for basic devices requiring very low energy. Moreover, the harvested energy is inherently variable and unreliable.

The applications of RF energy harvesting are multi-fold. These include wireless sensor networks, RFID (radio frequency identification), internet of things (IoT), D2D networks, and body area networks. There has been ongoing research on developing specific hardware components for the energy conversion circuits. Practical RF devices have been shown to successfully harvest far field non-directive energy in both the UHF and ISM bands at power densities of $1\ \mu W/cm^2$ or lower [59]. It is expected that the capabilities of energy conversion circuits would increase over the next few years making RF energy harvesting applicable to an increased range of devices.

## 1.6 Motivation, objectives, and significance

**Motivation:** The emergence of different 5G technologies presents some critical questions. How will they perform under different system and wireless conditions? Moreover, how will the combination of different technologies perform? For example, D2D millimeter-wave links perform drastically differently compared to D2D links operating within more traditional frequency assignments. D2D with energy harvesting will have reliability and power budget related issues.

Moreover, cognitive radio base stations equipped with massive MIMO will differ in performance to conventional base stations. Such issues need to be fully addressed and well understood before 5G standardisation is complete.

The irregularity of modern wireless networks must be considered when attempting to answer these questions. To this end, we must employ stochastic geometry models which however are inherently complex. Moreover, the analytical tractability is limited. This presents a crucial challenge that must be overcome using mathematical manipulations. The wireless channel also provides many complications. For example, path loss and fading significantly hinder communications. Moreover, the effect of these on different technologies are complex. For example, millimeter-wave and massive MIMO networks behave differently from other conventional networks. As such, in analyzing the performance, these irregularities need to be properly taken into account. In addition, power control and transmitter-receiver association procedures play an integral role in limiting interference, increasing energy efficiency, and providing better coverage.

**Objectives:** Characterizing how different power control and transmitter-receiver association procedures impact the performance of future wireless technologies with stochastic geometry models is the main focus of this thesis, with spatial modelling of key 5G technologies, assessing their performance, and proposing methods for performance improvement being the key objectives. Specifically, my main goals are: 1) Developing power control and receiver association schemes for an annular underlay CR network and investigation of their performance, 2) Developing co-operative beacon detection schemes for interweave CR networks and investigation of their performance, 3) Investigating the feasibility of wireless energy harvesting for an underlay CR network using stochastic geometry and markov chain based models, 4) Quantifying the effect of performance degradation for an underlaid receiver when base stations use massive MIMO, and 5) Developing an analytical framework to analyze performance degradation to an underlaid D2D network employing millimeter-wave frequencies.

**Significance:** This work will provide essential insight into the limitations of different technologies, their strengths and weaknesses in different environments and system set-ups, and methods to overcome limitations. More specifically, how spatial randomness (e.g. random locations of users and base stations) affects the performance of D2D, CR, massive MIMO, and millimeter-wave networks has not been investigated before. This thesis fills this gap and also analyzes power controlling and receiver association techniques. Ultimately, this work may aid in the de-

velopment of 5G wireless standards that incorporate cognitive and D2D techniques to alleviate spectrum scarcity.

## 1.7 Outline of the thesis

The contributions of this thesis is presented below with respect to the different chapters.

- **Chapter 2**

  In Chapter 2, basic background concepts and models will be presented. First, small-scale fading, shadowing, path loss, spatial distribution, and others are discussed. Next, spatial modelling using stochastic geometry is introduced, and the Poisson point process is discussed in depth. Furthermore, cognitive radio, millimeter-wave networks, and energy harvesting will be introduced. Finally, the performance analysis of stochastic wireless networks is illustrated.

- **Chapter 3**

  In this Chapter 3, we present a precise, comprehensive analysis of the aggregate interference ($I$) generated from an underlay network of CR nodes employing several transmit power control and receiver association schemes. Importantly, we consider the randomness of the locations of CR transmitter nodes and receiver nodes by using two independent Poisson Point Processes. We investigate receiver association based on the distance or the instantaneous received power and transmit power control based on the maximum possible transmitter-receiver distance, fixed or location dependent cut-off power levels, feedback from the primary system, or the maximum number of available receivers. For each of these schemes, the exact moment generating function (MGF) and mean of aggregate $I$ power are derived for links with Rayleigh fading and exponential path loss. The resulting primary outage and the probability of secondary transmitter cut-off are also derived. Numerical results show that the secondary power thresholds and node densities significantly affect the aggregate $I$, primary receiver outage, and secondary transmitter cut-off arising from the different schemes.

- **Chapter 4**

  In Chapter 4, we analyze several cooperative beacon sensing (CBS) strategies given spatial randomness of SU and PU nodes, which are modeled via independent homogeneous

Poisson point processes. We consider two cases of beacon emitter placement: (1) by PU-transmitters and (2) by PU-receivers. We analyze three separate local beacon detection schemes and propose five CBS schemes. They require the sharing of SU results via a control channel subject to Rayleigh fading and path loss, and making a final decision via the OR rule. By considering the randomness of node locations, we derive both the missed detection probability, the false alarm probability, and the primary outage and show that impressive gains are achievable. For example, with PU-receiver beacons, CBS reduces missed detection by a factor of $10^4$. In contrast, with PU-transmitter beacons, the reduction diminishes with the increased cell radii, but there exists an optimum cooperation radius.

- **Chapter 5**

  In Chapter 5, we characterize the interference of an underlay device when considering the use of massive MIMO systems with pilot contamination, path-loss-inversion power control, receiver association policies, spatially random nodes and propagation characteristics with power-law path loss and Rayleigh fading. To this end, we derive the average and the MGF of the aggregate interference and its average due to both primary and underlay transmissions from nodes modeled as Poisson point processes and analyze how the interference impacts the outage performance of an underlay receiver in Chapter 5. Our analysis considers all of the above factors and both single antenna type and massive MIMO base stations. We show that massive MIMO improves the outage performance, and a higher path loss exponent reduces the outage probability. This is in contrast to single antenna systems where a higher path loss exponent increases the outage. Furthermore, it is shown that the different node densities and power thresholds significantly affect the outage performance.

- **Chapter 6**

  In Chapter 6, we assess how the energy harvest of ambient RF signals and D2D link performance are affected by spatial randomness, temporal correlations, transmit power control, and channel uncertainties. To this end, we analyze the energy harvesting process of a random (typical) D2D transmitter node, say $\mathcal{D}_t$, which can communicate with its receiver if the harvest is sufficient to meet the receiver sensitivity and channel inversion. The system model consists of (a) three independent homogeneous Poisson point processes, (b) log-distance path loss and Rayleigh fading, and (c) path loss inversion (PLI) transmit power

control. In Chapter 6, we derive the ambient radio frequency (RF) energy at $\mathcal{D}_t$, and model the harvest as a Gamma random variable. We propose four schemes: namely– single slot harvesting, multi slot harvesting, $\mathcal{N}$ slot harvesting, and hybrid harvesting. We develop a Markov chain model for success probability of these schemes, and derive the coverage of the D2D receiver. We find that a D2D receiver sensitivity between $-120$ dBm and $-100$ dBm is optimum for both single and multi-slot harvests, and that high density of primary transmitters is unfavorable to multi slot harvesting for increasing D2D link distance. Moreover, hybrid harvesting always outperforms single and $\mathcal{N}$ slot harvesting, and outperforms multi-slot harvesting except for very high path-loss conditions.

- **Chapter 7**

  D2D networks underlaying millimeter-wave cellular systems hold massive potential. However, the performance of such networks incorporating spatial randomness and power control has not yet been characterized. To fill this gap, we develop a comprehensive analysis of the performance of a D2D receiver. We model the locations of cellular transmitters and receivers as homogeneous Poisson point processes and the D2D network as a Matern cluster process, and incorporate blockages due to random objects, sectored antenna patterns, log-distance path loss, and Nakagami-$m$ fading. Furthermore, we consider path loss and antenna gain inversion based power control, and peak power constraints for D2D devices along with distinct path loss exponents and fading severities for line-of-sight and non-line-of-sight scenarios. With the aid of stochastic geometry tools, we derive closed-form expressions of the MGF of the aggregate interference experienced by a D2D receiver and its outage probability. We finally show that the feasibility of millimeter-wave D2D communication relies heavily on the D2D cluster radii, peak power thresholds, and node densities.

- **Chapter 8**

  This chapter provides an overall conclusion for the thesis, and future research directions are discussed.

# Chapter 2

# Background

This chapter provides the mathematical background for different concepts used in the rest of the thesis.

## 2.1 The wireless channel

In this section, channel impairments such as multipath propagation, the Doppler effect, small scale fading, shadowing, and path loss will be discussed briefly. The combined effect of these channel impairments on the received signal is displayed in Fig. 2.1.4.

### 2.1.1 Multipath fading and the Doppler effect

Due to multiple obstructions and scatterers in the wireless channel, the received signal is the superposition of many signals with different time delays and phases [3]. These multiple copies will cause inter symbol interference (ISI), and will severely degrade the performance of the receiver.

The power delay profile (PDP) represents the average power associated with a given multipath delay ($\tau$) [3]. The average delay and the root mean square (r.m.s.) delay are important statistics of a wireless channel. They are defined as

$$\mu_\tau = \frac{\int_0^\infty \tau P_\tau d\tau}{\int_0^\infty P_\tau d\tau}, \text{ and } \sigma_\tau = \sqrt{\frac{\int_0^\infty (\tau - \mu_\tau)^2 P_\tau d\tau}{\int_0^\infty P_\tau d\tau}}, \tag{2.1}$$

respectively, where $P_\tau$ is the power associated with a delay of $\tau$. If the symbol period is defined to be $T_s$, frequency flat fading occurs if $T_s >> \sigma_\tau$. Otherwise, the signal would experience

frequency selective fading. The term coherence bandwidth is usually defined as

$$B_{coh} \approx \frac{1}{\sigma_\tau}, \tag{2.2}$$

which is roughly the frequency range in which a signal experiences frequency flat fading.

The time variation of the channel is described by the Doppler effect, which is caused by the relative frequency shift between the received signal and the transmitted signal. If the transmitter and receiver are stationary, the Doppler shift is zero. However, when the transmitter and/or receiver move/moves, the maximum Doppler shift is given by

$$f_d = \frac{f_c v}{c}, \tag{2.3}$$

where $f_c$ is the signal frequency, $v$ is the relative velocity between the transceivers, and $c$ is the speed of light. The Doppler spectrum of the channel represents the power associated with a particular Doppler shift (between $0$ and $f_d$). In a similar manner to the PDP, the average and the r.m.s. Doppler spread can be calculated. Furthermore, the coherence time $T_{coh}$ is defined to be approximately $\frac{1}{B_d}$, where $B_d$ is the Doppler spread. If the signal period $T_s << T_{coh}$, the signal is said to undergo slow fading. Otherwise, the signal undergoes fast fading.

### 2.1.2 Small scale fading models

Small scale fading is the random fluctuation of signal amplitude over short distances, and occurs due to the effects of multipath propagation [**?**]. It can be characterized by various statistical models.

#### Rayleigh fading

Rayleigh fading is the most common model to represent wireless channels including broadcast and mobile systems. Popular due to its mathematical tractability, this model is valid when there is no line-of-sight path between the transmitter and receiver [3]. The probability density function (PDF) of the received signal power under this model is given by

$$f_\gamma(x) = e^{-x}, \quad 0 \leq x < \infty, \tag{2.4}$$

It should be noted that while the Rayleigh distribution denotes the envelope amplitude, the power is specified by an exponential distribution.

**Rician fading**

Rician fading occurs when there is a dominant line-of-sight component. This model is especially useful for channels such as satellite links. The PDF of the received signal is [60]

$$f_\gamma(x) = \frac{(K+1)}{\bar{\gamma}} e^{-\left(K+\frac{x(K+1)}{\bar{\gamma}}\right)} I_0\left(2\sqrt{\frac{xK(K+1)}{\bar{\gamma}}}\right), \quad 0 \leq x < \infty, \tag{2.5}$$

where $\bar{\gamma}$ is the average received signal power, $K$ is the ratio between the line-of-sight component power and the power of the other scatterer components, and $I_0(\cdot)$ is the modified Bessel function of the first kind.

**Nakagami-$m$ fading**

Nakagami-$m$ fading is a model proposed by [61] which fits the empirical measurements of wireless channels. Its PDF is given by

$$f_\gamma(x) = \frac{x^{m-1}}{\Gamma(m)} \left(\frac{m}{\bar{\gamma}}\right)^m e^{-\frac{mx}{\bar{\gamma}}}, \quad 0 \leq x < \infty, m > 0.5, \tag{2.6}$$

where $m$ is a parameter describing the severity of fading. The model is versatile; for example, $m = 1$ yields Rayleigh fading, and $m \to \infty$ yields the no-fading case.

### 2.1.3 Shadowing

Shadowing is the random variation of signal amplitude due to blockages from large obstacles such as mountains and buildings in the transmission path. The distances in which shadowing occurs depend on the dimensions of the obstacle causing the shadowing effect [3].

**Log-normal shadowing**

The most common model for shadowing is the log-normal shadowing model. The PDF of the ratio between transmit and receive power ($\psi$) is given by [3]

$$f_{\Psi}(\psi) = \frac{\xi}{\sqrt{2\pi}\sigma_{\psi_{dB}}\psi} e^{-\frac{(10\log_{10}(\psi)-\mu_{\psi_{dB}})^2}{\sigma^2_{\psi_{dB}}}}, \quad 0 \leq \psi < \infty, \tag{2.7}$$

where $\xi = \frac{10}{ln10}$, $\mu_{\psi_{dB}}$ is the mean of $\psi_{dB}$, and $\sigma_{\psi_{dB}}$ is the standard deviation of $\psi_{dB}$.

Because (2.7) is not mathematically tractable readily, several approximations have been proposed. One such approximation is the Gamma model [62], [63], where the two distributions show a close match except in the lower tail region. Another approximation is the mixture Gamma model developed in [64].

### 2.1.4 Path loss

Path loss is the reduction in signal amplitude over distance between the transmitter and receiver. Path loss variations only occur over large distances [3].

**Free space path loss model**

The free space path loss (FSL) model is the most simple path loss model. It can be written as

$$FSL = \left(\frac{4\pi d}{\lambda}\right)^2, \tag{2.8}$$

where $d$ is the distance between the transmitter and receiver, and $\lambda$ is the wavelength of the transmitted signal.

**Empirical path loss models**

Because free space conditions do not hold for the wireless environment which encompasses many variable factors such as buildings, trees, hills, and houses, the path loss modeling is difficult. Thus, several empirical models have been developed using real world experimental data. These include the Okumura model, Hata model, COST 231 Hata model, and COST 231 Wolfisch-Ikegami model [3].

| Environment | Path loss exponent |
|---|---|
| Free space | 2 |
| Urban cellular radio | 2.7 to 3.5 |
| Shadowed urban cellular radio | 3 to 3.5 |
| In-building line-of-sight | 1.6 to 1.8 |
| Obstructed within a building | 4 to 6 |
| Obstructed within a factory | 2 to 3 |

Table 2.1: Common path loss exponent values.

The COST 231 Hata model for path loss (PL) in dB can be written as [3]

$$\begin{aligned} PL_{dB}(d) &= 46.3 + 33.9\log_{10}(f_c) - 13.82\log_{10}(h_t) - a(h_r) \\ &+ (44.9 - 6.55\log_{10}(h_t))\log_{10}(d) + C_M, \end{aligned} \tag{2.9}$$

where $h_t$ is the transmit antenna height, $h_r$ is the receiver antenna height, $f_c$ is the transmit signal frequency, and $d$ is the distance between the transmitter and receiver. For suburbs and small cities, $a(h_r)$ is defined as

$$a(h_r) = (1.1\log_{10}(f_c) - 0.7)h_r - (1.56\log_{10}(f_c) - 0.8). \tag{2.10}$$

$C_M$ is 0 for small cities and suburbs, while it is 3 for large cities.

**Simplified path loss model**

The most common path loss model used in analysis is the simplified path loss model, and will be used in the subsequent chapters. According to this model, the power at a certain distance $r$ from the transmitter is given by

$$P(r) = P_0 \left(\frac{r_0}{r}\right)^{\alpha}, \tag{2.11}$$

where $P_0$ is the observed power at a distance $r_0$ from the transmitter, and $\alpha$ is the path loss exponent. This model includes the free space path loss model (2.8) as a special case when $\alpha = 2$. Some common path loss exponents for different environments are tabulated in Table 2.1.

Combining the effects of small scale fading, shadowing, and path loss, the received power $P_r$ can be expressed as

$$P_r = PX|h|^2 r^{-\alpha}, \tag{2.12}$$

where $P$ is the transmit power, $X$ is the shadowing gain, and $|h|^2$ is the power gain due to small

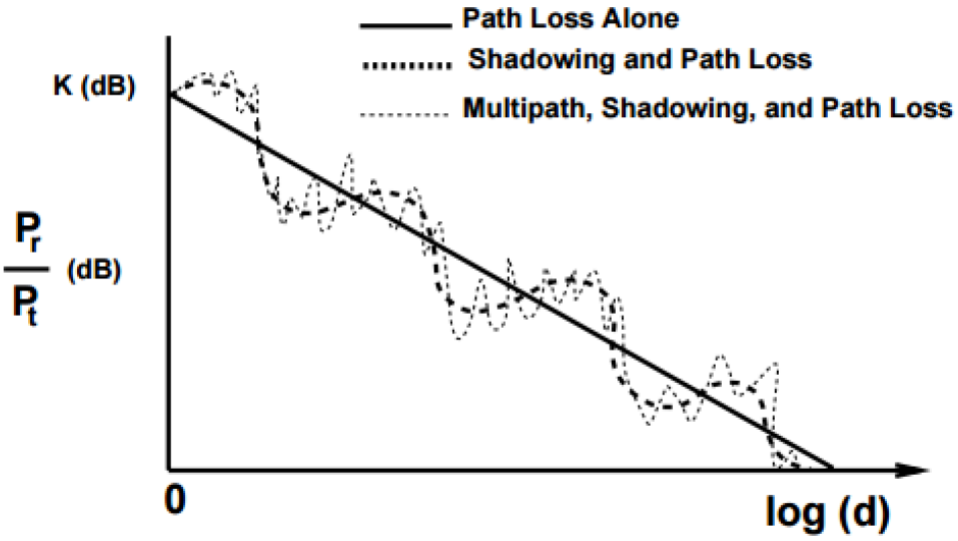


Figure 2.1: Combined effect of path loss, shadowing, and fading [3]

scale fading.

## 2.2 Spatial modelling

The locations of base stations and different user terminals do not usually conform to a pre determined setup. While the placement of base stations is not purely random, it is increasingly becoming irregular with the introduction of small cells and pico cells. The user terminals on the other hand are almost always random, and change location regularly. As such, conventional fixed models such as the hexagonal grid model do not present an accurate picture of the network. Stochastic geometry based modelling has thus gained ground within the research community [10]–[14]. In addition to providing a realistic network scenario, some stochastic models are mathematically tractable [12]. Stochastic geometry is crucial to calculate the statistical properties of such collections of points and to calculate averages over all possible realizations.

Stochastic geometry is the mathematical area dedicated to analyze random spatial patterns, or more specifically point patterns. A random point pattern or point process is a set of points (locations) which is generated randomly through some mechanism. Formally, a point process is a countable random set $\Phi = \{x_1, x_2, \dots\} \in \mathbb{R}^2$. Many different mathematical models for point processes exist. These include, but are not limited to: the binomial point process (BPP), the

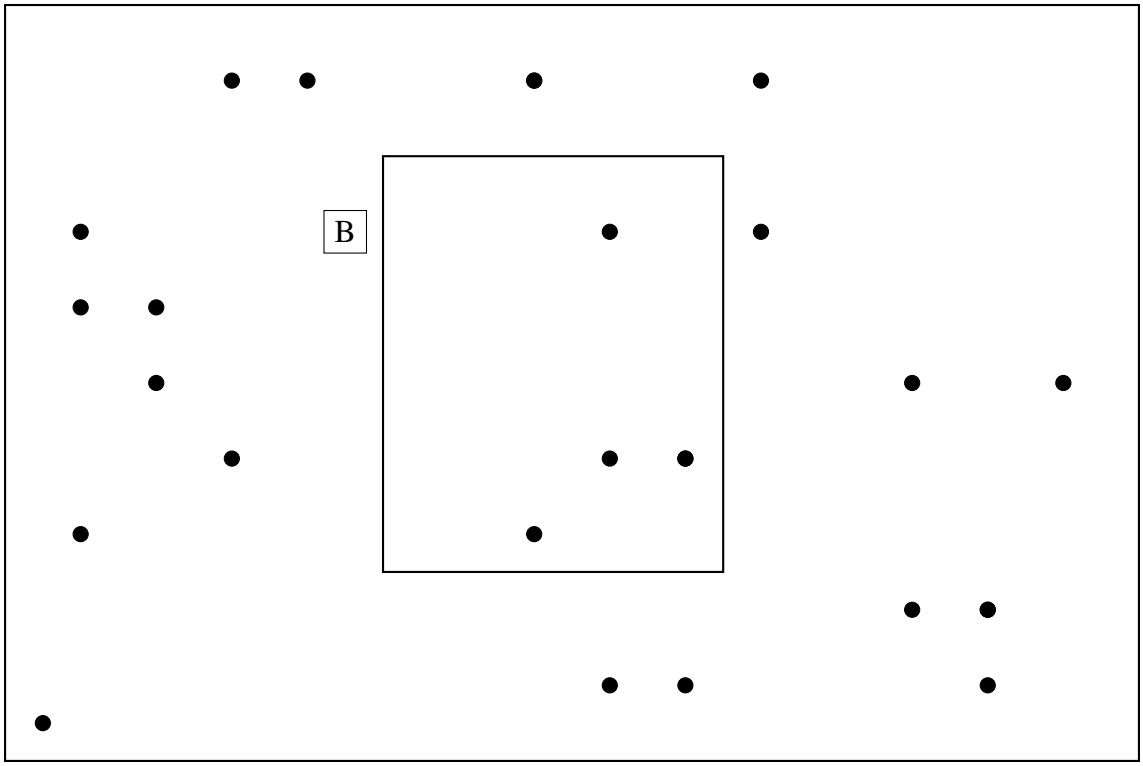

Figure 2.2: Network of nodes where the BPP is applicable.

Poisson point process (PPP), the Beta-Ginibre point process, the Matern Hardcore point process, and the cluster process.

### 2.2.1 Binomial point process

The Binomial point process (BPP) is useful to model interferers when the total number of nodes is fixed and uniformly distributed within an area [16]. For a bounded set $Z$, the total number of nodes in $B$ ($B \in Z$) is given by [65],

$$P(N(B) = n) = \begin{pmatrix} N \\ n \end{pmatrix} p^n (1-p)^{N-n}, \quad n = 0, \ldots, N \tag{2.13}$$

where $N$ is the total number of nodes in $Z$, and $p = \frac{v(B)}{v(Z)}$. Here $v(\cdot)$ represents the area. A visual representation of this concept is given in Fig. 2.2. The BPP is accurate for node distributions (especially base stations) when the number of nodes within the total geographical area is known [16].

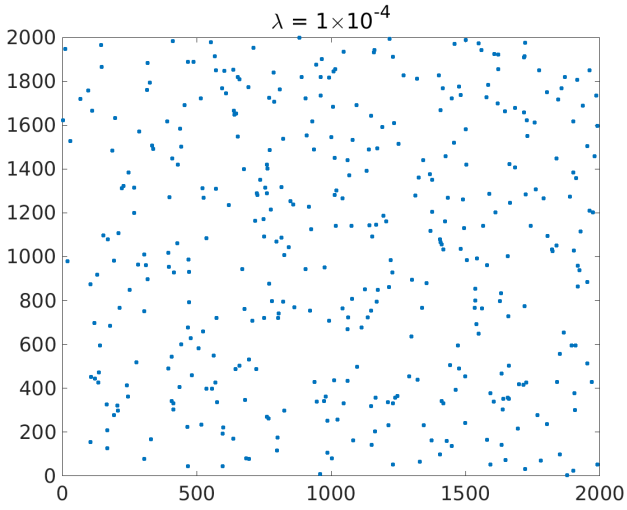


Figure 2.3: Realization of a homogenous PPP for density = $1 \times 10^{-4}$

### 2.2.2 Poisson point process

The PPP is the most popular point process model used in stochastic geometry based analysis. Within a PPP, there is no dependence between node locations and the number of nodes are random. It can be interpreted as a limiting case of the BPP. The formal definition of a PPP is as follows [66]. $\Phi$ is a point processes in $\mathbb{R}^2$ such that:

- for every bounded closed set $A$, the number $N(A)$ is Poisson distributed with mean $\lambda(A) = \int_A \lambda(x)dx$ and
$$\Pr[N(A) = n] = \frac{(\lambda(A))^n}{n!} e^{-\lambda(A)}, n = 0, 1, 2, \ldots \tag{2.14}$$
- if $A_1, A_2 \ldots, A_m$ are disjoint sets, $N(A_1), N(A_2), \ldots, N(A_m)$ are independent random variables.

The PPP has extensively been used to characterize the locations of wireless nodes in prior research [37]–[39], [67]. When the mean $\lambda(A) = \lambda A$, and if the number of points in disjoint sets are independent, the PPP is termed a homogeneous PPP, and $\lambda$ is termed the node density (Fig. 2.3). In other words, the intensity is independent of the location $x$. Conversely, when the mean is a function of the location, the resultant process is said to be inhomogeneous.

### 2.2.3 Cluster process

A cluster involves the formation of daughter processes around a parent process. If the points within a parent process $X$ is replaced with a set of points $Z_x$, the superposition of all the clus-

ter points represents the daughter process $Y = \bigcup_x Z_x$ [66]. The most commonly used cluster processes is the Matern cluster process where the parent process is a PPP in $\mathbb{R}^2$, and each cluster within the daughter process consists of $M_x$ points independently and uniformly distributed within a disc having a radius $r$ centered at $x$ where $M_x = Poisson(\mu)$, and $x$ is the location of any parent node [66]. The Matern cluster process has been extensively used in the modeling of user terminals centered around base stations in cellular networks [68]–[70].

### 2.2.4 Hardcore point process

Hardcore point processes differ from other point processes by having dependencies between the points [71]. In a practical sense, a minimum distance is enforced between different points within a realization. Hardcore processes are especially useful to model base station locations. This is because base stations would ideally have some space between each other to limit unnecessary overlap.

A hardcore process is formed after thinning an existing point process. Because this thinning procedure depends on other points of the process, it is termed as dependent thinning. If $\Phi$ is such process, each point $x$ of $\Phi$ is marked with either $0$ or $1$ depending on whether or whether not another point is present in $b(x, r)$, where $b(x, r)$ is a ball of radius $r$ with origin $x$. The elements marked with $0$ get deleted, and the remainder form a hardcore point process. While several different hardcore processes exist, the Matern hardcore process [72] is one of the most popular.

### 2.2.5 Stochastic geometry tools

When modelling nodes as a PPP, several useful stochastic geometry tools such as mapping, thinning, and clustering can be employed [66], [73].

#### Displacement/mapping theorem

Mapping refers to transforming a point process to another point process by applying a fixed transformation [66]. In formal terms, it is stated as follows [74]. If $\Phi$ is an inhomogeneous PPP on $\mathbb{R}^d$ with intensity $\Lambda$, and let $f : \mathbb{R}^d \rightarrow \mathbb{R}^s$ be measurable and $\Lambda(f^{-1}\{y\}) = 0$ for all for $y \in \mathbb{R}^s$. Assume further that $\mu(B) = \Lambda(f^{-1}\{B\})$ satisfies $\mu(B) < \infty$ for all bounded $B$. Then, $f(\Phi)$ is a non-homogeneous PPP on $\mathbb{R}^s$ with intensity $\mu$.

### Thinning

Thinning refers to a process on a PPP where some points are deleted. The remaining points are said to form a thinned PPP [66]. Each point of the process is marked with an indicator taking the values $1$ or $0$ representing whether the point is to be retained or not. When the indicators are independent of each other, it's referred to as independent thinning, while it's referred as dependent thinning when the indicators depend on each other [66]. While the resultant processes after independent thinning are also PPPs if the original process was a PPP, the resultant process after dependent thinning generally is a hardcore process. Matern type I and II [72] are commonly used hardcore processes where the thinning procedure is dependent on the distance to neighbouring nodes [66]. Hardcore processes are especially useful in modelling medium access protocols such as CSMA/CA employed in IEEE 802.11 [38].

### Campbell theorem

The Campbell theorem is useful to obtain sums over a PPP. Formally, it can be expressed as [73]

$$\mathbb{E}\left[\sum_{x\in\Phi} f(x)\right] = \int_{\mathbb{R}^2} f(x)\lambda(x)dx. \tag{2.15}$$

### Probability generating functional

The probability generating functional (PGFL) is used to derive products over a PPP, and goes hand-in-hand with the Campbell theorem. It can be expressed as

$$\mathbb{E}\left[\prod_{x\in\Phi} f(x)\right] = e^{\left(-\int_{\mathbb{R}^2}(1-f(x))\lambda(x)dx\right)}. \tag{2.16}$$

### Slivnyak theorem

The Slivnyak-Mecke theorem, commonly known simply as the Slivnyak theorem states that for a PPP $\Phi$, any new point can be added or removed from it without affecting the distributions or properties of $\Phi$. In a practical sense, if $\Phi$ is conditioned to have a point at $x$, the properties of $\Phi$ do not change as long as $x$ is not considered. This condition is formally written as [73]

$$\mathbb{P}^{!x}(E) = \mathbb{P}(E). \tag{2.17}$$

## 2.3 Power control and receiver association

### 2.3.1 Power control

The transmitter controls its power depending on the distance from the receiver, other transmissions, and channel conditions. The benefits include saving transmitter power and reducing interference. Power control methods include fixed power, distance based schemes with channel inversion, and measurement based schemes [75]. For example, open-loop and closed-loop schemes are used in Wideband Code Division Multiple Access (WCDMA) and LTE networks [76]. More complicated power control schemes involve optimizing the transmit power to achieve a certain objective. For example, power control schemes have been developed to maximize network capacity, to use the lowest energy while guaranteeing a performance threshold, and to reduce the bit error rate data rate [3].

Power control schemes have been extensively studied for a variety of settings [38], [77]–[85]. Furthermore, it is common to have a maximum allowable transmit power for networks in order to prevent interference to other co-channel users [83]. This maximum allowable transmit power can be a constant for all devices or a location dependent one. A location dependent power level is desirable because the interference from a certain user device to others depend on the specificities of the network layout. A constant maximum allowable power level may disadvantage devices which are far from their respective receivers, and which do not necessarily interfere other devices.

One disadvantage of power control schemes is the additional processing power which is required by the transmitters. This is especially true for more complicated power control structures such as water-filling [3]. Moreover, distance based power control schemes require the distance from the receiver to the transmitter known beforehand. In order to gain this information, either periodic pilot signals or information from a network control center are required. Going one step further, if channel inversion based power control is conducted, channel state information (CSI) is needed via regular pilot signals.

### 2.3.2 Receiver association

Receiver association schemes are the policies governing how a receiver is assigned to a particular transmitter or vice versa. Association can be made with the closest receiver/transmitter, the receiver/transmitter providing the best instantaneous SNR, or a random receiver/transmitter within

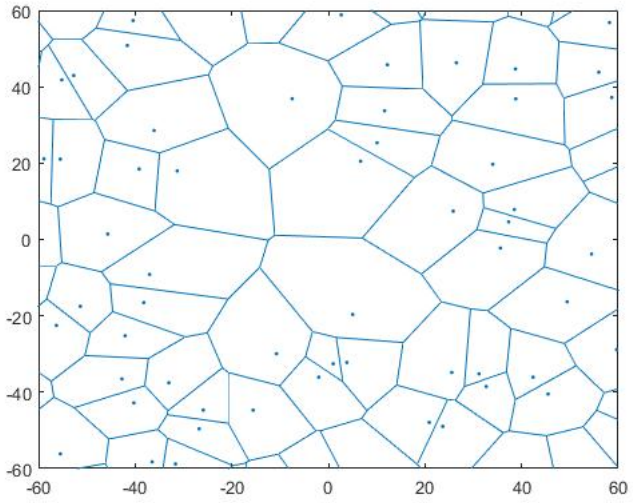


Figure 2.4: Cellular base stations and their respective Voronoi cells.

a given radius [83]. Receiver association schemes directly affect the transmit power, quality of service (QoS), handovers, and the coverage. In heterogeneous networks, networks can introduce a bias for a certain class of base stations. For example, in a hypothetical scenario of macro cells and micro cells, the network may implement a policy where a $10\,\text{dB}$ bias exists for the micro cells. In such a case, the user will connect to a micro cell even if the received signal strength of a micro cell is $10\,\text{dB}$ lower than the macro cell.

Associating with the closest base station is the most popular association scheme for cellular networks studied in research. Fig. 2.3.2 depicts a random set of base stations and their corresponding cells. Any user falling within the cell of a particular base station has that as its closest base station. Such a cellular structure is termed the Voronoi tesselation, and a cell is termed a Voronoi cell.

## 2.4 Interfernce characterization for a finite network

The total interference experienced by a user device is the combination of interference from all active co-channel devices [86], [87]. Thus, the aggregate interference $I$ may be written as

$$I = \sum_{i=1}^{N} I_i, \tag{2.18}$$

where $I_i$ is the interference caused by the $i$-th interferer, and $N$ is the number of interferers. $N$ can be a finite value or $\infty$.

The individual interference $I_i$ is written as

$$I_i = \beta_i P_i X_i |h_i|^2 r_i^{-\alpha}, \tag{2.19}$$

where $\beta_i$ is a Bernoulli random variable depending on the activity level (and spectrum identification errors if interweave CR is considered) of the $i$-th interfering device and $P_i$ is the transmit power of that $i$-th device. $X_i$, $|h_i|^2$, and $r_i$ are the shadowing gain, small scale fading gain and the distance between the $i$-th interfering device and the device in question. The path loss exponent is $\alpha$.

Since the PDF of the aggregate interference is generally intractable, an MGF (moment generating function) based approach is generally used for analysis [88]–[94]. The MGF can be obtained relatively easily because, for a sum of independent interferers, the total MGF is the product of individual MGFs [88], [93].

The MGF $M_I^i(s)$ of the interference from a single node can be written as

$$M_I^i(s) = E[e^{-sI_i}], \tag{2.20}$$

where $E[\cdot]$ denotes the expectation, and $s$ is the Laplace variable. If the individual interferers are independent and identically distributed, the MGF of the aggregate interference becomes

$$M_I(s) = (M_I^i(s))^N \tag{2.21}$$

Other valuable parameters of the aggregate interference include the mean and higher moments, and cumulants. The $n$-th moment ($\mu_n = E[I^n]$) can be obtained from the MGF $M_I(s)$ as

$$\mu_n = (-1)^n \left[ \frac{d^n}{ds^n} M_I(s) \right]_{s=0} \tag{2.22}$$

Modelling aggregate interference to fit well known distributions has been extremely popular due to the intractability of exact analysis. Typical such distributions are Gaussian, log-normal, tailed $\alpha$-stable, gamma, and as sums of normal and log-normal [88], [95]–[99]. This is generally achieved by matching moments of the aggregate interference with the corresponding moments of the well known distribution.

## 2.5 Technology specific attributes

### 2.5.1 Spectrum sensing

Spectrum sensing is one of the key aspects of CR networks. As in Chapter 1, unlicensed secondary devices can opportunistically access spectrum holes. Holes may exist in vacant, under-utilized, or occupied spectrum. Vacant spectrum is where PU activity is absent within a particular geographical area [33]. For example, this may occur when the licensee does not use the spectrum in a specific location or geographic area. Under-utilized spectrum occurs when primary user activity is only present within certain times, but absent during others. For example, cellular frequency slots may be idle at times depending on traffic levels. Even primary user occupied spectrum can be accessed by CR devices under certain conditions. For example, transmit beamforming allows the signals to focus towards the intended receiver without interfering on other devices. The primary user spectrum can thus be used at the same geographical location by CR devices without mutual interference [33].

Spectrum identification techniques include geolocation databases, in-band sensing, out-of-band sensing, interference temperature based detection and co-operative sensing [29], [33], [100], [101].

#### In-band sensing

With in-band sensing, CR devices sense the spectrum they are trying to access directly. The major in-band sensing methods involve energy detection, cyclostationary feature detection, and eigenvalue based detection [2]. These schemes are relatively easy to implement without the need for network control, dedicated devices or channels, or co-ordination between the primary and CR networks. Thus, they are popular as a means of opportunistic spectrum access where decisions can be made on the spot. However, in-band sensing is highly susceptible to corruptions from noise. The sensing CR device will not be alerted to the presence of nearby non-transmitting primary receivers. Another major disadvantage of in-band sensing is the inability to gain system level information other than about spectrum occupancy. For example, if the primary system is occupying the spectrum, there will be no information as to how long the access will take place. Similarly, when the spectrum is vacant, there is no information as to when re-occupation by the primary network will occur. As such, the CR devices have to constantly engage in sensing.

### Out-of-band beacon sensing

With this method of sensing, CR networks do not directly sense the frequency band for which spectrum access is required (In Chapter 4, we will consider this scheme). Instead, beacon signals on a dedicated out-of-band control channel (beacon) tell whether the frequency band is occupied or not by PU devices. The beacon signals are simply narrowband electromagnetic waves modulated by on-off switching [102], do not necessarily have to be continuous, and can be transmitted periodically, which will reduce additional power requirement for the PUs. Beacon signalling and beacon detection circuits can be relatively simple [103]–[105]. In addition, the beacon signals can be used to separate different primary devices using different time slots or orthogonal codes. Individually identifying different primary devices is not readily possible in many in-band spectrum identification strategies including energy detection. Furthermore, beacons provide added control mechanism to the primary devices, which can actively allow or prevent CR spectrum access dynamically. This is however not possible with in-band schemes. Such beacons have been proposed for IEEE 802.22.1 [106] and are the most suitable for CR implementation in a cellular system [101]. The SU devices detect beacon signals by comparing the received signal power in the control channel with a threshold level.

### Guard regions

Guard regions or exclusion regions are areas around primary users where CR transmissions are not allowed [37]. Typically, a guard region can be mathematically expressed as $\sum_i b(x_i, R)$, where $b(x_i, R)$ is the 2-D annular area (ball) of radius $R$ at point $x_i$. These regions are critical in underlay CR networks in order to ensure the interference temperature at a primary user receiver is maintained. Guard regions may be established around both PU transmitters and PU receivers. However, guard regions around PU receivers are more desirable because these are the devices which bear the detrimental effects of interference.

Finding distances to PU devices to establish guard regions can be accomplished either through periodic pilot channels, prior information about the network from a controller, or through GPS information. While guard regions are usually annular in shape, more complex shapes have also been researched to provide optimum CR throughput while maintaining the interference temperature on PU receivers.

### Co-operative sensing

Due to wireless channel impairments such as multipath fading, shadowing, and path loss, a CR node may not be able to detect a spectrum hole through either in-band or out-of-band sensing. In this context, co-operative sensing refers to several SUs sharing their local spectrum sensing results for an overall decision in the interweave mode of CR. Thus, it achieves better sensing performance by exploiting spatial and multiuser diversity in wireless networks [33], [100], [107]–[109]. Furthermore, minimizing the detection error and reducing individual sensing times are possible [110]. However, co-operation techniques amongst secondary users assume a substantial smount of information exchange, which is an overhead usually ignored in literature.

Co-operation techniques among secondary nodes can be broadly classified as data fusion and decision fusion [35]. In data fusion, a node amplifies and transmits the sensed information. A node may either share all the sampled information or a summary [111], and soft decision combining such as the likelihood ratio test can be used. For example, CR node $x_0$ with sensed information $F_0$. This device makes its final decision based on the combined sensed data $\{F_0, F_1, F_2, \ldots F_N\}$, where $F_1, F_2, \ldots F_N$ are the sensed information of co-operating CRs $x_1, x_2, \ldots x_N$. In contrast, in decision fusion, a CR makes a spectrum occupancy decision first, which is then broadcast. The final decision by $x_0$ is based on $\{s_0, s_1, s_2, \ldots s_N\}$ where $s_k (k \in \{0, \ldots, N\})$ is the decision of the CR $x_k$. Each node makes a binary decision about PU spectrum occupancy, which is shared. These hard decisions are combined using the AND, OR, or majority rules [35], [101]. With the AND rule, if all co-operating devices indicate a PU channel occupancy, then the spectrum is designated as occupied. On the contrary, with the OR rule, the same decision is reached even with a single occupancy indication by a co-operating device. Thus, the OR rule is more conservative in allowing spectrum access. With the majority rule, a majority of co-operating nodes must indicate spectrum occupation.

### 2.5.2 Markov chains

A Markov chain is a stochastic process which has the memoryless property. That is, the next state only depends on the present state, and not the states before. In the rest of this thesis, Markov chains will be used primarily for energy harvesting networks which consider temporal dynamics and time correlations.

Formally, a Markov chain is a sequence of random variables having the Markov property (i.

e. memorylessness). If the random variables are $X_1, X_2, X_3, \ldots, X_N, X_{N+1}$,

$$\Pr[X_{N+1} = a_{N+1} \backslash \{X_1 = a_1, X_2 = a_2, \ldots, X_N = a_N\}] = \Pr[X_{N+1} = a_{N+1} \backslash X_N = a_N]. \tag{2.23}$$

Markov chains can be illustrated via state transition diagram, where the edges represent the probability of transitioning from one state to another [112]. Equivalently, a state transition matrix can also be used to display the same information. If $Q$ is such a matrix, the probability of transitioning from state $i$ to state $j$ is represented on $Q(i, j)$.

A crucial parameter which is obtained through Markov chains is the steady state probability if it exists. For a Markov chain comprising of $N$ states, the steady state probabilities for each state can be represented as a vector $\Omega = [\omega_1 \ \omega_2 \ . \ . \ \omega_N]$. At steady state, we have

$$\Omega Q = \Omega. \tag{2.24}$$

Solving this equation while recalling that $\omega_1 + \omega_2 + \cdots + \omega_{N+1} = 1$ gives the individual steady state probabilities [57].

### 2.5.3 Millimeter wave channels

Millimeter wave channels differ from traditional microwave channels in several respects. Below, we will elaborate two defining features.

#### Blockages

Millimeter wave signals are considerably more sensitive to blockages from objects within their path compared with traditional microwave signals as the effect from diffraction is negligible [4]. There exist high penetration losses when signals traverse through materials such as concrete [4]. As such, depending on whether the transmitter-receiver pair is line-of-sight (LOS) or not, significant differences occur. For example, the LOS path loss exponents are significantly lower than those for non-line-of-sight (NLOS) environments. Furthermore, additional shadowing occurs for NLOS scenarios [4].

When modelling blockages mathematically, the most common assumption is to consider a process of random Boolean rectangles within $\mathbb{R}^2$. This process is considered to be stationary and motion invariant. The LOS and NLOS probabilities for such a process depend only on the

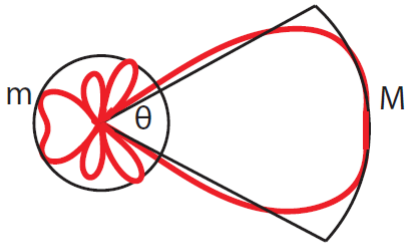


Figure 2.5: Sectored antenna pattern with a main lobe gain of $M$, a back lobe gain of $m$, and a main lobe beamwidth of $\theta$ [4].

transmitter receiver distance $r$. As such, we have

$$\Pr[Blocking] = \begin{cases} e^{-\beta r} & \text{LOS} \\ 1 - e^{-\beta r} & \text{NLOS} \end{cases}, \tag{2.25}$$

where $\beta$ is a constant depending on the size and density of the blocking objects.

**Sectored antenna patterns**

Under millimeter wave frequencies, large numbers of antenna elements can be packed within a small area which enables directional beamforming. This is because antenna element sizes decrease with the increase of frequency. The actual antenna patterns are undoubtedly complex, and dependent on the physical array dimensions. However, to keep the analysis concise, we can consider a sectored antenna model [113] where the antenna gain pattern is divided into discrete regions based on the angle off the boresight direction (Fig. 2.5.3). Thus, the antenna gain ($G$) can be expressed as follows:

$$G_* = \begin{cases} M & , |\theta| \leq \frac{\omega_*}{2} \\ m & , \text{otherwise} \end{cases}, \tag{2.26}$$

where $\omega_*$ is the antenna beamwidth, $\theta$ is the angle off the boresight direction, $M$ is the main lobe gain, and $m$ is the gain from the side and back lobes. This gain pattern can also be generalized for different side and back lobe gains. Moreover, it should be noted that the gains for different devices (for example for base stations and users) will differ depending on their physical antenna parameters.

# Chapter 3

# Underlay interference characterization with power control and receiver association

## 3.1 Introduction

As mentioned in Chapter 1, spectrum scarcity and under utilization are two of the factors inhibiting the growth of wireless networks, and a promising solution is to opportunistically access unused channels. To mitigate both these factors, the underlay mode is especially attractive because both primary and cognitive nodes simultaneously access spectrum slots which will enhance spectral usage and spectral efficiency. Nevertheless, due to the imposition of interference power ($I$) constraints to protect primary channels, underlay nodes must use transmit power control, which is the main limiting factor of their capacity [41].

Thus, transmit power control, contention control, and receiver association schemes must be used not only to manage primary interference, but also to improve the throughput, reliability and other quality-of-service parameters of the underlay network itself. While these schemes are widely used in wireless systems, their use in underlay networks has not been investigated extensively.

1. Power control methods have been widely used in non-cognitive set-ups to reduce the signal to interference ratio. Those include fixed power, distance based schemes with channel inversion, and measurement based schemes [75]. For example, open-loop and closed-loop schemes are used in Wideband Code Division Multiple Access (WCDMA) and Long Term Evolution (LTE) networks [76]. Although such schemes have been extensively studied for non-cognitive settings [77]–[80], how they perform in terms of minimizing the interference

from cognitive underlay networks remains to be quantified.

2. Contention control can also help to reduce interference. which limits the transmissions of a node based on its distance to other nodes [38]. These can be employed together with or independently from power control schemes, and have been shown to significantly reduce the mean $I$ [38].

3. Receiver association schemes specify which receiver is selected by a transmitter. They can be based on the distance, the instantaneous signal to noise ratios (SNRs), or the received powers of pilot signals of the transmitter-receiver channels [114]. For example, the transmitter can be associated with the nearest receiver, or the receiver with the highest received power.

While the aforementioned schemes do help to reduce the interference from cognitive nodes, additional reduction of $I$ is possible via two other mechanisms: namely, instituting cut-off transmit powers for SU-transmitters and enforcing exclusion regions around the primary nodes. The cut-off transmit power, which is the maximum transmit power level allowed for SU-transmitters can either be a constant or location dependent. An exclusion (guard) region around the primary nodes defines a region where cognitive nodes are barred from transmitting. These can be enforced either through prior location information which could be obtained through a centralized control center aided by GPS data, or dynamically via sensing pilot signals/acknowledgements originating from the primary nodes [38]–[40].

### 3.1.1 Prior research

Aggregate $I$ of random cognitive networks has been extensively analyzed including statistical interference models, exact analysis, and performance bounds [37], [39], [87], [88], [93], [95], [96], [98], [115]–[121]. For example, [39] provides a statistical model for $I$ considering path loss, small scale fading, shadowing, sensing techniques, and also investigates the effects of primary network transmit power control. Interference in a spectrum sensing framework [115] and heterogeneous networks (networks with multiple tiers of nodes) with macro base stations and cognitive femto access points [116] have been analyzed. On the other hand, [37] derives the moment generating function (MGF) and cumulants of $I$ for a finite annular field of interferers. Centralized and distributed power control schemes for a D2D network are proposed in [118]. A normal and

log-normal sum approximation is developed in [96], while [93] approximates the interference with the nearest neighbor's interference. The average $I$ considering intra-cognitive user interference has been derived in [119], while a coverage analysis of two tier networks is performed in [120]. The MGF of the underlay $I$ is analyzed and approximated in [88] while considering the effects of shadowing. Moreover, [95] investigates the effects of the exclusion zone radius and the number of cognitive nodes whereas [98] analyses the probability density function (PDF) of the interference under different exclusion regions. Reference [87] analyzes $I$ due to beacon misdetection for hybrid underlay-interweave networks, while [122] develops a foundation for designing wireless networks with secrecy exploiting intrinsic spatial and channel properties of the wireless environment. Bounds for interference and outage probability are derived and a method involving Poisson cluster processes to model the interference is proposed in [121] for active cognitive nodes outside primary node guard regions following a Poisson hole process, while power control strategies based on single node optimal power control and the Nash equilibrium for interference limited Poisson distributed nodes are studied in [123]. Furthermore, [71] proposes a technique to estimate access point throughput in dense random CSMA (Carrier Sense Multiple Access) networks, and extends the results when the access points form a Matern-hardcore process using an computationally efficient procedure.

### 3.1.2 Motivation

Thus, prior research has not completely analyzed the impact of power control, receiver association, and contention control schemes on $I$ (interference on primary network) and on the performance of the cognitive network itself. Publications [37], [95], [119] have assumed a constant transmit power for cognitive nodes, and in the case of [71] for the transmitting access points. Whilst enabling analytical tractability, this assumption may not hold because the actual transmit powers depend on several factors including the receiver association policy, the distance to the intended receiver, and the cut-off transmit power. Thus, all such factors must be considered in a more comprehensive analysis. While a channel inversion based power controlling scheme and a threshold scheduling scheme are proposed in [124] for an infinite network, [124] does not consider different receiver association models and guard regions. Furthermore, cut-off thresholds or maximum allowable receiver distances are not considered for the power control schemes. A comprehensive analysis is given by [38], which provides a rigorous analysis of power control,

contention control, and hybrid power-contention control schemes by deriving the primary receiver interference in an underlay network with exclusion regions. The power control technique adopted in [38] limits the mutual interference among SU-transmitters but only considers one spatial point process for cognitive nodes. No distinction is thus made between a transmitter node and receiver node. In contrast, we differentiate cognitive transmitters and receivers by modeling them as two separate spatial point processes, which allows for more detailed analysis of the system. Our approach also focuses on guaranteeing a certain level of performance for the SU-receivers. Therefore, our work complements [38] and develops several interference management schemes. These schemes thus enable various trade-offs among performance objectives, thereby offering a more flexible system analysis and design perspective. Finally, the primary objective of this chapter is to provide an exact analysis of the aggregate $I$ for the proposed association and power control policies in underlay networks.

### 3.1.3 Contributions

We propose several interference management schemes for the cognitive nodes, derive the MGF and mean aggregate $I$ and analyze the outage of the primary receiver. The proposed schemes are as follows:

- Nearest receiver association with power control schemes based on: 1) cognitive transmitter-receiver distance $r_c$ 2) $r_c$ and a constant cut-off power level 3) $r_c$ and a location dependent cut-off power level.
- Nearest-$M$ receiver association with the power control scheme based on the transmitter receiver distance $r_{c,k}$ and a constant cut-off power level.
- Best received power association (when channel state information (CSI) is available) with the following: 1) power control based on the transmitter receiver distance, the channel state information, and a constant cut-off power level 2) constant powered transmission with self deactivation based on the estimated received power at the receiver.
- Nearest-$M$ receiver association and transmission restrictions based on distance to other receivers.
- Iterative changing of the cut-off transmit power level based on the primary receiver performance with a nearest receiver association, a power control scheme based on the transmitter

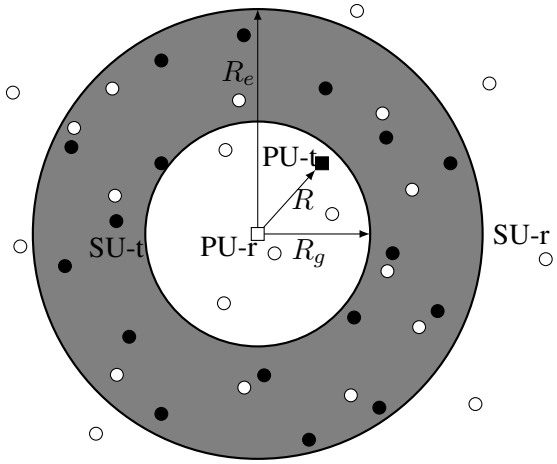


Figure 3.1: Sytem model. The PU-receiver is located at (0,0). Active SU-transmitters are in the shaded area. Respectively, $R_g$, $R_e$, and $R$ denote the guard distance, the outer distance, and the primary transmitter-receiver distance.

receiver distance and, a cut-off power level.

The MGF is an extremely important tool for deriving various statistics. For instance, while immediately providing moments, which can be used for moment matching purposes, it can also be used for evaluations bit error rates and outage [89], [125]. Furthermore, the probability of a cognitive transmitter being cut-off is derived. Moreover, for the best received power association, we will use stochastic-geometry tools including the Mapping and Marking theorems [73] to derive the distance distribution to a cognitive receiver having the best received power.

The following system-model assumptions are made: 1) the CR transmitter and receiver nodes form two independent homogeneous PPPs [73], 2) the exclusion zone around the primary receiver (Fig. 3.1) is perfectly enforced, 3) The links experience exponential path-loss and Rayleigh fading, and 4) SU-transmitters know the distances to SU-receivers (either via pilot signals, or through information stored in a database).

This chapter is organized as follows. Section II introduces the spatial and signal models. Section III derives the MGF and mean of the aggregate $I$ for the proposed transmission schemes, while Section IV derives the outage probability of the PU-receiver. Section V provides numerical results, and Section VI concludes the chapter.

## 3.2 System model

This section introduces both the spatial and signal models.

### 3.2.1 Spatial model and assumptions

- Without loss of generality, the primary user receiver (PU-receiver) is located at the center with a distance $R$ from the PU transmitter. We will consider multiple stochastic PU transmitter receiver pairs within Chapter 5.

- The active SU-transmitters are located in a finite annular area (Fig. 3.1). (While this model is simplistic, it is analytically tractable, and provides key insights. The model will be generalized in Chapter 5) The circle of radius $R_g$ around the PU-receiver is the exclusion zone, which plays an important role to limit the interference [37]. The value of $R_g$ will be decided based on the maximum admissible outage probability for a primary receiver. The SU-transmitters within the exclusion zone do not transmit or must use a different frequency block. We further assume that the SU-transmitters lie within a finite outer radius of $R_e$ in order to provide a more general analysis (the secondary network may form a single cluster where a finite $R_e$ may be the most appropriate). Note that a field of active SU-transmitters distributed in the entire $\mathbb{R}^2$ is a special case of our model when $R_g \to 0$ and $R_e \to \infty$. The SU-receivers are distributed in $\mathbb{R}^2$.

- Because the number and locations of SU-transmitters and receivers are random, they must be modeled by a spatial stochastic process [13], [14], [117]. For this purpose, independent conditional homogeneous PPPs with intensities $\lambda_t$ and $\lambda_r$ respectively are used. We will denote them as $\Phi_t$ and $\Phi_r$, and the number of nodes within an area $A$ follows (2.14).

Let $\phi_{t,i}$ denote the $i$-th cognitive transmitter located at $x_i \in \Phi_t$ when it exists. Thus, the distance to the PU-receiver from $\phi_{t,i}$ $r_i$ is $r_i = ||x_i||$, $R_g < r_i < R_e$. The distribution of $r_i$ is obtained as follows. Because $\Phi_t$ is a homogeneous PPP, the CDF of $r_i$ becomes $F_{r_i}(x) = \frac{\pi(x^2 - R_g^2)}{A_t}$, $R_g < x < R_e$, where $A_t = \pi\left(R_e^2 - R_g^2\right)$. Differentiating this CDF yields the PDF [88]

$$f_{r_i}(x) = \begin{cases} 2\frac{\pi x}{A_t} & , R_g < x < R_e \\ 0 & , \text{otherwise} \end{cases} . \tag{3.1}$$

Let $\phi_{r,k\backslash i}$ denote the $k$-th closest receiver from $\phi_{t,i}$ located at $y_{k\backslash i} \in \Phi_r$. We will require the distribution of the distance to $\phi_{r,k\backslash i}$ from $\phi_{t,i}$, which we will denote as $r_{c,k}$ where $r_{c,k} = ||y_{k\backslash i} - x_i||$. Because $\Phi_r$ and $\Phi_t$ are stationary, $r_{c,k}$ is equivalent to the distance to the $k$-th nearest

node in a PPP from any given location. The probability of having at least $k$ nodes within a circle of radius $x$ is given by;

$$\Pr[Nodes \geq k] = 1 - \sum_{i=0}^{k-1} \frac{(\lambda_r \pi x^2)^i}{i!} e^{-\lambda_r \pi x^2}, 0 < x < \infty.$$

Thus, the PDF of $r_{c,k}$ is thus obtained from (3.2) as [126], [127]

$$f_{r_{c,k}}(x) = \frac{2(\pi\lambda_r)^k}{(k-1)!} x^{2k-1} e^{-\pi\lambda_r x^2}, 0 < x < \infty. \tag{3.2}$$

When $k = 1$, we get the distance distribution to the nearest receiver node from $\phi_{t,i}$ ($r_{c,1}$). We will refer this distance as $r_c$ for brevity.

In the subsequent analysis, we assume that all $\phi_{t,i}$ in the annular region with $R_g < ||x_i|| < R_e$ are active simultaneously. However, this is a worst-case assumption designed to glean maximum primary interference level. Nevertheless, there is no loss of generality in this assumption because if some transmitters are inactive, we can model this on-off behaviour by assigning a transmission probability $\beta < 1$ to each node. By using independent thinning [73], our derived expressions can then be adapted by replacing $\lambda_t$ with $\beta\lambda_t$.

We will investigate nearest receiver association, the best received power association, and the $k$-th nearest receiver association when closer receivers are unavailable. Practical applications for such networks can include ad-hoc networks, wireless sensor networks, and cellular networks [128].

### 3.2.2 Signal model

- All radio links experience path-loss, and the power law path loss model (log-distance path loss model) [3] is assumed. Accordingly, the received power at a distance $r$ from the transmitter may be expressed as $P_r = Pr^{-\alpha}$, where $\alpha$ is the path-loss exponent, and the constant $P = P_0 r_0^{\alpha}$ is termed the power level. The path-loss exponent varies between 1.6 (same floor in office buildings) to 6.5 (built up areas) [3]. To complete this model, $P_0$ is the received power at a reference distance of $r_0$. Typically, $r_0$ varies from 1 m ( pico cells ) to 1 km (macro cells). For a given $r_0$, the received power $P_0$ depends on the frequency, antenna heights, buildings and other factors.

- Small-scale fading is modeled by the Rayleigh model, for which the PDF of the $i$-th channel power gain is Exponential and is given by (2.4).

The interference from $\phi_{t,i}$, $I_i$ can thus be written as [37]

$$I_i = P_i |h_i|^2 r_i^{-\alpha}, \tag{3.3}$$

where $r_i$ and $P_i$ are respectively the distance from the PU-receiver and the power of $\phi_{t,i}$. The aggregate interference $I$ is [37]

$$I = \sum_{i=1}^{N} I_i, \tag{3.4}$$

where $N$ is the number of SU-transmitters.

### 3.2.3 Power control and association model

The following receiver association schemes are considered for cognitive nodes:

- **Nearest association**: a transmitter thus is connected with its nearest receiver (denoted as $\phi_{r,1\backslash i}$). The benefits are: (1) instantaneous channel state information (CSI) is not required, (2) the highest received power averaged over small scale fading is achieved, and (3) the distance to the nearest receiver may be found readily.

- **Nearest-$M$ association**: a transmitter thus selects a neighbor within its $M$ closest neighbors. Of course, $M = 1$ is the above case. The transmitter successively checks the availability of a receiver, starting from the closest node to the farthest one in the set. Such an association rule comes into the fray when closer receivers are unavailable, and is thus a generalization of the enarest association scheme.

- **Best received power association**: a transmitter is associated with the receiver having the highest received power. We will denote this receiver as $\phi_{r,p\backslash i}$. The receiver thus may or may not be the nearest. Such schemes require the use of periodic pilot/beacon signals from the receivers to obtain CSI [129]. These schemes are thus more complex than the nearest association schemes.

For each of the above association techniques, we assume that a receiver may be associated with more than one transmitter at a given time[1]. Moreover, although there will be certain correlations in the transmit power of different transmitters, the impact of ignoring such correlations is minor as shown in simulations of Section V.

For each of the above schemes, we consider several power control methods at the transmitter. All the power control schemes can be summed up by the following equation for the transmit power ($P_i$):

$$P_i = \begin{cases} P_s r^{\alpha}(|h|^2)^{\mu} & , P_s r^{\alpha}(|h|^2)^{\mu} < P_c \\ 0 & , \text{otherwise} \end{cases} . \tag{3.5}$$

In this equation, $|h|^2$ and $r$ are the channel gain due to small scale fading and distance between the SU-transmitter and the associated receiver, $P_s$ is the required average received power at the SU-receiver, $P_c$ is the cut-off power level, and $\mu \in \{0, -1\}$. While it is possible to transmit at $P_c$ when the required transmit power exceeds $P_c$, we will not consider this scenario within this chapter. However, such a power control scheme is introduced in Chapter 6.

The individual power control methods are as follows:

- Path loss inversion: this negates the attenuation due to path loss and ensures a constant received power regardless of the distance. Distance information between the transmitter and the associated receiver is needed for this to be effective. ($\mu = 0$, $P_c = \infty$)

- Channel inversion: With channel inversion, the whole channel gain (path loss and small scale fading) is inverted. However, CSI of the transmitter-receiver channel is essential.

- Constant cut-off power level: $P_i < P_c$ where $P_c$ is fixed.

- Location dependent cut-off power level: $P_c$ is a function of the CR transmitter location. The premise of this is similar to a constant cut-off power level except for the fact that the cut-off power level varies by location. The interference from a cognitive node on the PU-receiver depends greatly on its distance from the PU-receiver. Thus, a constant cut-off power threshold disadvantages cognitive nodes which are far away. In this scheme, the cut-off power level may vary with its distance to the PU-receiver.

[1]The secondary network may employ multiple access techniques within the given frequency block, but a detailed discussion is out of the scope.

- Iteratively changing cut-off power: Feedback information about the interference at the primary user is used to iteratively change the cut-off power level to balance PU-receiver outage and cognitive transmitter cut-off probability.

- Constant powered transmission with self deactivation: Each transmitter employs a constant power to transmit. Before a transmission occurs, the transmitter estimates the received power level at the associated receiver, and if this falls below the required threshold, the transmission is aborted. This method also requires CSI.

Moreover, we also investigate transmission restrictions based on distances to other SU-receivers where, a SU-transmitter will refrain from transmitting if desired SU-receivers do not exist within an association region. The existence of SU-receivers within the association region can be found out using GPS information disseminated through a centralized control center.

Transmission restrictions may also be enforced based on distances to other transmitters to limit cognitive outages occurring due to mutual interference. If a SU-transmitter detects that another user is occupying the spectrum within a certain region around it (contention region), it will refrain from transmitting. Otherwise, it may transmit depending on other factors such as receiver availability, cut-off thresholds, etc. Such methods are similar to CSMA/CA employed in IEEE 802.11 [38]. The transmitting cognitive nodes follow a Matern-hardcore point process which may be analyzed based on the techniques adopted in [38], [67], [130]. However, the discussion of such schemes is out of the scope.

## 3.3 Interference analysis

This section derives the MGF and mean of $I$ under several transmission schemes for cognitive nodes, where $I$ is the aggregate interference (3.4).

The MGF of the aggregate interference is defined as $M_I(s) = E[e^{-sI}]$ [37], [117]. Let $M_{I_i}(s)$ define the MGF of $I_i$. Because of the independence, the MGF given $N$ transmitters can be written as $M_{I/N}(s) = (M_{I_i}(s))^N$. Averaging with respect to the Poisson model (2.14) yields [37], [88]

$$M_I(s) = e^{\lambda_t A_t \left(M_{I_i}(s)-1\right)}. \tag{3.6}$$

Our objective now is to find $M_{I_i}(s)$ under the following schemes.

### 3.3.1 Nearest association

Four nearest association based transmit power control schemes are developed next.

**Scheme 1 (Nearest association and path loss inversion)**

The transmitter connects to the nearest receiver ($\phi_{r,1\backslash i}$), and transmits at a power level sufficient to ensure a constant received power when averaged over small scale fading. This scheme is used extensively in the CDMA uplink to compensate the near-far problem [76], where all transmitters adjust their power such that the received power at the base station from each of them is the same.

Suppose $P_s$ is the average received power[1] ensured, and $r_c$ is the distance to the nearest receiver from $\phi_{t,i}$. Let $|g_i|^2$ be the channel gain from $\phi_{t,i}$ to its associated receiver. We need $P_s = E_{|g_i|^2}[P_i|g_i|^2 r_c^{-\alpha}]$. Therefore, the transmit power level of $\phi_{t,i}$, $P_i = P_s r_c^{\alpha}$. Substituting $P_i$ in (3.3), it is possible to write $M_{I_i}(s)$ as [88]

$$\begin{aligned} M_{I_i}(s) &= E_{|h_i|^2, r_i, r_c}[e^{-sI_i}] \\ &= E_{r_c}[E_{r_i}[E_{|h_i|^2}[e^{-sP_s r_c^{\alpha} r_i^{-\alpha} |h_i|^2}]]], \end{aligned} \tag{3.7}$$

due to the independence of $|h_i|^2$, $r_c$, and $r_i$.

To evaluate (3.7), we use a series summation based approach utilizing the fact that $(1+x)^{-1} = \sum_{k=0}^{\infty}(-x)^k$ when $|x| < 1$. $M_{I_i}(s)$ can thus be written as

$$M_{I_i}(s) = \int_0^{\infty} \int_{R_g}^{R_e} \sum_{t=0}^{\infty} (-sP_s r_c^{\alpha} r_i^{-\alpha})^t f_{r_i}(r_i) f_{r_c}(r_c) dr_i dr_c. \tag{3.8}$$

Averaging (3.8) with respect to $r_i$ and $r_c$ gives us

$$M_{I_i}(s) = \frac{2\pi}{A_t} \sum_{t=0}^{\infty} (\pi\lambda_r)^{-\frac{\alpha t}{2}} (-sP_s)^t \left( \frac{R_e^{2-\alpha t} - R_g^{2-\alpha t}}{2 - \alpha t} \right) \Gamma(\frac{\alpha t}{2} + 1), \alpha > 2. \tag{3.9}$$

From $M_{I_i}(s)$, we can find the moments of the aggregate interference readily. For example, the mean aggregate interference $E[I] = \lambda_t A_t E[I_i]$, where $E[I_i] = -\frac{d}{ds} M_{I_i}(s)|_{s=0}$. Therefore,

[1]The average received power will be the receiver sensitivity plus an appropriate fade margin.

$E[I]$ is found to be

$$E[I] = 2\pi\lambda_t P_s(\pi\lambda_r)^{-\frac{\alpha}{2}} \left(\frac{R_e^{2-\alpha} - R_g^{2-\alpha}}{2-\alpha}\right)\Gamma(\frac{\alpha}{2}+1), \alpha \neq 2. \tag{3.10}$$

This shows us that the mean interference increases linearly with the receiver sensitivity. Moreover, the interference decreases exponentially with the CR receiver density. When $\alpha \to 2$, $E[I]$ can be obtained after applying the L'Hospital's rule to (3.10) as

$$E[I]|_{\alpha\to 2} = \frac{4\pi\lambda_t P_s}{\pi\lambda_r}(\log(R_e) - \log(R_g)). \tag{3.11}$$

**Scheme 2 (Nearest association and path loss inversion with a cut-off power level)**

In Scheme 1, the cognitive transmit power can go arbitrarily high. When that happens, the resulting interference is unconstrained. This situation can be avoided by enforcing a cut-off power level [38]. Thus, Scheme 2 enforces an added constraint of a cut-off power level $P_c$, and if a cognitive node needs more power than $P_c$, it will abort transmission.

Now, the interference from the $\phi_{t,i}$ (3.3) becomes $I_i = Q_i P_i |h_i|^2 r_i^{-\alpha}$, where $Q_i = \text{Bernoulli}(q_i)$ with $q_i = \Pr[P_i < P_c] = \Pr[P_s r_c^\alpha < P_c] = 1 - e^{-\pi\lambda_r\left(\frac{P_c}{P_s}\right)^{\frac{2}{\alpha}}}$. We can now write

$$M_{I_i}(s) = 1 - q_i + \frac{2\pi^2\lambda_r}{A_t}\int_0^{\left(\frac{P_c}{P_s}\right)^{\frac{1}{\alpha}}} r_c e^{-\pi\lambda_r r_c^2}\left((\mathcal{V}(R_g)\text{–}1)R_g^2\text{–}(\mathcal{V}(R_e)\text{–}1)R_e^2\right)dr_c, \tag{3.12}$$

with $\mathcal{V}(x) = {}_2F_1\left(1, \frac{2}{\alpha}; 1+\frac{2}{\alpha}, -\frac{x^\alpha}{sP_s r_c^\alpha}\right)$. As performed in Scheme 1, we can use a series expansion, and average $M_{I_i}(s)$ to get a closed-form solution. It thus becomes

$$\begin{aligned} M_{I_i}(s) &= 1 - q_i + q_i\sum_{t=0}^{\infty}(-sP_s)^t\left(\frac{2\pi}{A_t}\int_{R_g}^{R_e} r_i^{1-\alpha t}dr_i\right)\left(\frac{2\pi\lambda_r}{q_i}\int_0^{\left(\frac{P_c}{P_s}\right)^{\frac{1}{\alpha}}} r_c^{1+\alpha t}e^{-\pi\lambda_r r_c^2}dr_c\right) \\ &= e^{-\pi\lambda_r\left(\frac{P_c}{P_s}\right)^{\frac{2}{\alpha}}} + \frac{2\pi}{A_t}\sum_{t=0}^{\infty}\left(-\frac{sP_s}{\pi^{\frac{\alpha}{2}}\lambda_r^{\frac{\alpha}{2}}}\right)^t\left(\frac{R_e^{2-\alpha t} - R_g^{2-\alpha t}}{2-\alpha t}\right) \\ &\quad\times\left(\Gamma\left(\frac{\alpha t}{2}+1\right) - \Gamma\left(\frac{\alpha t}{2}+1, \pi\lambda_r\left(\frac{P_c}{P_s}\right)^{\frac{2}{\alpha}}\right)\right), \alpha > 2. \end{aligned} \tag{3.13}$$

Similar to Scheme 1, we can obtain $E[I]$ as

$$\begin{aligned} E[I] &= 2\pi\lambda_t P_s(\pi\lambda_r)^{-\frac{\alpha}{2}}\left(\frac{R_e^{2-\alpha}-R_g^{2-\alpha}}{2-\alpha}\right) \\ &\times \left(\Gamma\left(\frac{\alpha}{2}+1\right)-\Gamma\left(\frac{\alpha}{2}+1,\pi\lambda_r\left(\frac{P_c}{P_s}\right)^{\frac{2}{\alpha}}\right)\right), \alpha\neq 2. \end{aligned} \tag{3.14}$$

**Scheme 3 (Nearest-$M$ association and path loss inversion with a cut-off power level)**

Schemes 1 and 2 assume the nearest receiver is always available for reception, which however may not be ready at a given time. Scheme 3 allows a transmitter to scan up to the $M$-th nearest receiver ($\phi_{r,M\setminus i}$) whenever necessary [114]. To analyze this scheme, we denote the probability that a receiver is available with $\beta_r$, and this probability is constant for all receivers. Moreover, the availabilities of receivers are mutually independent events.

In this scheme, each transmitter node attempts to connect to the nearest receiver. However, if this fails, a connection is attempted with the next nearest and so on till $M$ nearest receivers are scanned, or the transmission attempt is aborted. If a successful association is made, a constant averaged received power of $P_s$ to that receiver must be guaranteed. However, if this guarantee makes the transmit power exceed $P_c$, the transmission does not take place.

The interference from $\phi_{t,i}$ (3.3) is expressed as $I_i = W_i P_i |h_i|^2 r_i^{-\alpha}$. $W_i$ is a Bernoulli random variable similar to $Q_i$ of Scheme 2 with a success probability (probability of transmission) of $w_i$. This probability depends on the availability of a receiver $\beta_r$, the number of nearest receivers a transmitter is allowed an association attempt $M$, and the cut-off power level $P_c$. Thus, the success probability $w_i$ can be written as [131]

$$w_i = \beta_r \sum_{k=1}^{M}(1-\beta_r)^{k-1}p_k, \tag{3.15}$$

where $p_k$ is the probability that the transmit power of a transmitter associated with $\phi_{r,k\setminus i}$ is below the cut-off level $P_c$. This probability is thus written as $p_k = \Pr[P_s r_{c,k}^{\alpha} < P_c]$. Using the

distribution of $r_{c,k}$ (3.2), $p_k$ is found to be [131]

$$p_k = 1 - \frac{\Gamma\left(k, \pi\lambda_r \left(\frac{P_c}{P_s}\right)^{\frac{2}{\alpha}}\right)}{(k-1)!}. \tag{3.16}$$

Now, the simplified MGF of the interference from $\phi_{t,i}$ ($M_{I_i}(s)$) can be obtained in a similar way to Scheme 2 using the series summation based approach as

$$\begin{aligned} M_{I_i}(s) =& 1 - \beta_r \sum_{k=1}^{M} (1-\beta_r)^{k-1} \left(1 - \frac{\Gamma\left(k, \pi\lambda_r \left(\frac{P_c}{P_s}\right)^{\frac{2}{\alpha}}\right)}{(k-1)!}\right) \\ &+ \frac{2\pi}{A_t} \sum_{t=0}^{\infty} (-\frac{sP_s}{\pi^{\frac{\alpha}{2}} \lambda_r^{\frac{\alpha}{2}}})^t \left(\frac{R_e^{2-\alpha t} - R_g^{2-\alpha t}}{2-\alpha t}\right) \sum_{k=1}^{M} \frac{\beta_r (1-\beta_r)^{k-1}}{(k-1)!} \\ &\times \left(\Gamma\left(\frac{\alpha t}{2} + k\right) - \Gamma\left(\frac{\alpha t}{2} + k, \pi\lambda_r \left(\frac{P_c}{P_s}\right)^{\frac{2}{\alpha}}\right), \alpha > 2. \end{aligned} \tag{3.17}$$

$E[I]$ can be obtained as

$$\begin{aligned} E[I] = & 2\pi\lambda_t P_s (\pi\lambda_r)^{-\frac{\alpha}{2}} \left(\frac{R_e^{2-\alpha} - R_g^{2-\alpha}}{2-\alpha}\right) \sum_{k=1}^{M} \frac{\beta_r (1-\beta_r)^{k-1}}{(k-1)!} \\ &\times \left(\Gamma\left(\frac{\alpha}{2} + k\right) - \Gamma\left(\frac{\alpha}{2} + k, \pi\lambda_r \left(\frac{P_c}{P_s}\right)^{\frac{2}{\alpha}}\right)\right), \alpha \neq 2. \end{aligned} \tag{3.18}$$

**Scheme 4 (Nearest association and path loss inversion with a location dependent cut-off power level)**

In schemes 2 and 3, the cut-off transmit power $P_c$ is a constant. We will now consider the case where $P_c$ depends on $r_i$ and $\alpha$, and has the form $P_c = P_I r_i^{\alpha}$ for $\phi_{t,i}$, where $P_I$ is a constant threshold value. The distance to the primary receiver ($r_i$) can be obtained through periodic acknowledgement signals from it [40].

The probability of $P_i < P_c$ ($q_i$) would thus be $1 - e^{-\pi\lambda_r r_i^2 \left(\frac{P_I}{P_s}\right)^{\frac{2}{\alpha}}}$. By employing a similar

method to the derivation of $M_{I_i}(s)$ in Scheme 2, we can write $M_{I_i}(s)$ for Scheme 3 as

$$M_{I_i}(s) = E_{r_i}\left[e^{-\pi\lambda_r r_i^2\left(\frac{P_I}{P_s}\right)^{\frac{2}{\alpha}}} + \sum_{t=0}^{\infty}\left(-\frac{sP_s}{\pi^{\frac{\alpha}{2}}\lambda_r^{\frac{\alpha}{2}}}\right)^t r_i^{-\alpha t} \times\left(\Gamma\left(\frac{\alpha t}{2}+1\right)-\Gamma\left(\frac{\alpha t}{2}+1,\pi\lambda_r r_i^2\left(\frac{P_I}{P_s}\right)^{\frac{2}{\alpha}}\right)\right)\right]. \quad (3.19)$$

After performing the expectation, $M_{I_i}(s)$ can be expressed as

$$M_{I_i}(s) = \frac{2\pi}{A_t}\left(\frac{e^{-\pi\lambda_r\left(\frac{P_I}{P_s}\right)^{\frac{2}{\alpha}}R_g^2}-e^{-\pi\lambda_r\left(\frac{P_I}{P_s}\right)^{\frac{2}{\alpha}}R_e^2}}{2\pi\lambda_r\left(\frac{P_I}{P_s}\right)^{\frac{2}{\alpha}}}+\sum_{t=0}^{\infty}\left(-\frac{sP_s}{\pi^{\frac{\alpha}{2}}\lambda_r^{\frac{\alpha}{2}}}\right)^t \times\left(\left(\frac{R_e^{2-\alpha t}-R_g^{2-\alpha t}}{2-\alpha t}\right)\Gamma\left(\frac{\alpha t}{2}+\right)-(\mathcal{W}(R_e,t)\mathcal{W}(R_g,t))\right)\right), \alpha>2, \quad (3.20)$$

where $\mathcal{W}(x,t)$ is given by

$$\mathcal{W}(x,t) = \frac{e^{-\pi\lambda_r x^2\left(\frac{P_I}{P_s}\right)^{\frac{2}{\alpha}}}}{\alpha t-2}\left((\pi\lambda_r)^{\frac{\alpha t}{2}-1}\left(\frac{P_I}{P_s}\right)^{t-\frac{2}{\alpha}}\left(\pi\lambda_r x^2\left(\frac{P_I}{P_s}\right)^{\frac{2}{\alpha}}+1\right) -x^{2-\alpha t}e^{\pi\lambda_r x^2\left(\frac{P_I}{P_s}\right)^{\frac{2}{\alpha}}}\Gamma\left(\frac{\alpha t}{2}+1,\pi\lambda_r x^2\left(\frac{P_I}{P_s}\right)^{\frac{2}{\alpha}}\right)\right). \quad (3.21)$$

The mean of the aggregate interference is found in a similar manner to the above schemes as

$$E[I] = \frac{2\pi\lambda_t P_s}{\pi^{\frac{\alpha}{2}}\lambda_r^{\frac{\alpha}{2}}}\left(\left(\frac{R_e^{2-\alpha}-R_g^{2-\alpha}}{2-\alpha}\right)\Gamma\left(\frac{\alpha}{2}+1\right)-(\mathcal{W}(R_e,1)-\mathcal{W}(R_g,1))\right), \alpha\neq 2. \quad (3.22)$$

Moreover, the average probability of a cognitive transmitter node being allowed to transmit is obtained using the cut-off probability as

$$q_i = 1-\frac{2\pi}{A_t}\left(\frac{e^{-\pi\lambda_r\left(\frac{P_I}{P_s}\right)^{\frac{2}{\alpha}}R_g^2}-e^{-\pi\lambda_r\left(\frac{P_I}{P_s}\right)^{\frac{2}{\alpha}}R_e^2}}{2\pi\lambda_r\left(\frac{P_I}{P_s}\right)^{\frac{2}{\alpha}}}\right) \quad (3.23)$$

### 3.3.2 Best-received-power association

This subsection develops and analyzes transmission schemes based on highest received power association.

**Scheme 5 (Best received power association and channel inversion with a cut-off power level)**

In this scheme, a transmitter first selects the receiver $\phi_{r,p\setminus i}$ with the highest instantaneous received power, and inverts the channel gain. However, this process needs the CSI and the link distance, which the transmitter utilizes to ensure an average received power of $P_s$ at the selected receiver. However, if the required transmit power exceeds the cut-off $P_c$, the transmission attempt would be aborted. The major advantage of this scheme over Scheme 2 employing nearest association and path loss inversion is that it guarantees the lowest required transmit power for any given $P_s$.

However, the analysis is complicated because of the need for the probability distribution of the distance to the receiver having the highest instantaneous received power. Similar to Scheme 2, the interference from $\phi_{t,i}$ (3.3) is written as $I_i = B_i P_i |h_i|^2 r_i^{-\alpha}$. The parameter $B_i$ is defined similar to $Q_i$ as $B_i = \text{Bernoulli}(b_i)$, where $b_i = \Pr[P_i < P_c]$.

Any given CR transmitter sees CR receivers distributed as a homogeneous PPP with intensity $\lambda_r$ in $\mathbb{R}^2$. We first show that the received power from a homogeneous PPP with intensity $\lambda_r$, path loss exponent $\alpha$ and Rayleigh fading is equivalent to that generated by a non-homogeneous PPP with a path loss exponent of 1, no fading, and having an intensity of $\lambda_{r,3}$. Here, $\lambda_{r,3}$ is expressed as

$$\lambda_{r,3}(r) = \frac{2\pi}{\alpha} \lambda_r r^{\frac{2}{\alpha}-1} \Gamma(\frac{2}{\alpha}+1), 0 < r < \infty. \tag{3.24}$$

*Proof:* The intensity function of a PPP in $\mathbb{R}^2$ can be transformed from $(x, y)$ coordinates to polar coordinates $(r, \theta)$ by using the Mapping theorem [73] (This is used to convert the 2-D PPP to a 1-D PPP) For a homogeneous PPP of intensity $\lambda$, the intensity function in polar coordinates is given by

$$\lambda^*(r, \theta) = \lambda\, r, \;\; 0 < r < \infty, 0 < \theta < 2\pi. \tag{3.25}$$

The received power from an interfering node does not depends on its angular position but on its distance to the receiver. Therefore, the PPP on $\mathbb{R}^2$ is mapped onto the positive real axis while preserving the distance distribution. Using the Mapping theorem, it can be shown that the mapped

points on the positive real axis form a PPP. The intensity of the this PPP $\lambda_{r,1}(r)$ can be obtained by integrating out $\theta$ [73]. Therefore,

$$\lambda_{r,1}(r) = \int_0^{2\pi} \lambda \, r d\theta = 2\pi\lambda r, \;\; 0 < r < \infty. \tag{3.26}$$

The received power at a receiver from a cognitive transmitter is given by $P_i r_p^{-\alpha} |h_i|^2$. In the following step, we use the Mapping theorem to obtain a new PPP which generates a received power identical to what is generated by the above PPP with intensity $\lambda_{r,1}$, but with a path loss exponent of 1. The intensity function of the new PPP $\lambda_{r,2}(r)$ can be derived as follows: Consider the mapping function $f(r) = r^\alpha$. In the mapping process, points in the line segment $(r, r + \Delta r)$ in the new PPP are from the $(r^{-\alpha}, (r + \Delta r)^{-\alpha})$ line segment of the PPP with intensity $\lambda_{r,1}(r)$. The number of points in the line segment $(r, r + \Delta r)$ of the new PPP can be written as [132]

$$N[r, r + \Delta r] = \int_{r^{-\alpha}}^{(r+\Delta r)^{-\alpha}} \lambda_{r,1}(r) dr. \tag{3.27}$$

Using the change of variable $t = r^\alpha$,

$$N[r, r + \Delta r] = \int_r^{r+\Delta r} \lambda_{r,1} \left(\frac{1}{t}\right) \frac{t^{\frac{1}{\alpha}-1}}{\alpha} dt. \tag{3.28}$$

Therefore, according to the Mapping theorem [73] the intensity of the new PPP is given by [132]

$$\begin{aligned} \lambda_{r,2}(r) &= \lambda_{r,1} \left(\frac{1}{r}\right) \frac{r^{\frac{1}{\alpha}-1}}{\alpha}, \;\; 0 < r < \infty \\ &= \frac{2\pi\lambda_r r^{\frac{2}{\alpha}-1}}{\alpha}, \;\; 0 < r < \infty. \end{aligned} \tag{3.29}$$

In the following step, we use the product space representation, the Marking theorem [73, Sec. 5.2], and the Mapping theorem to obtain a new PPP which generates the identical received power, but with a path loss exponent of 1 and no fading. The intensity function of the new PPP $\lambda_{r,3}(r)$ can be derived as [132]

$$\lambda_{r,3}(r) = E_{|h|^2} \left[ |h|^2 \lambda_{r,2}(r|h|^2) \right], \;\; 0 < r < \infty. \tag{3.30}$$

For Rayleigh fading channels (3.30) can be written as

$$\begin{aligned}\lambda_{r,3}(r) &= \frac{2\pi}{\alpha}\lambda_r r^{\frac{2}{\alpha}-1} E_{|h_i|^2}[(|h_i|^2)^{\frac{2}{\alpha}}], 0 < r < \infty. \\ &= \frac{2\pi}{\alpha}\lambda_r r^{\frac{2}{\alpha}-1}\Gamma\left(\frac{2}{\alpha}+1\right), 0 < r < \infty. \end{aligned} \tag{3.31}$$

Note that the limits of $r$ do not change because the SU-receivers are distributed in a 2-D field. This would not be the case otherwise.

Now, under this new PPP, the effects of the path loss exponent and fading have been normalized. The neighbor with the lowest distance metric of the new PPP (note that this metric is not the distance in its true sense) would be the receiver having the highest received power. Thus, the CDF of the distance to the receiver having the highest received power can easily be found using the void probability. Let $r_p$ be the distance from a transmitter to the receiver having the highest received power. Then,

$$F_{r_p}(x) = 1 - \Pr[\text{zero nodes in a line segment of length } x].$$

Using (2.14), $F_r(x)$ is found as

$$F_{r_p}(x) = 1 - e^{-\int_0^x \lambda_{r,3} dr} = 1 - e^{-\pi\lambda_r\Gamma(\frac{2}{\alpha}+1)x^{\frac{2}{\alpha}}}, 0 < x < \infty. \tag{3.32}$$

The PDF of this distribution $f_{r_p}$ becomes

$$f_{r_p}(x) = \frac{2\pi}{\alpha}\lambda_r\Gamma(\frac{2}{\alpha}+1)x^{\frac{2}{\alpha}-1}e^{-\pi\lambda_r\Gamma(\frac{2}{\alpha}+1)x^{\frac{2}{\alpha}}}, 0 < x < \infty. \tag{3.33}$$

Now, we return to our original objective of deriving the MGF of the interference from $\phi_{t,i}$ ($M_{I_i}(s)$). In order to ensure a constant receiver power of $P_s$, the transmitter transmits at a power of $P_s r_p$ (note that the path loss and fading are not present in the equation, but rather is included within $r_p$). Then,

$$b_i = \Pr[P_s r_p < P_c] = 1 - e^{-\pi\lambda_r\Gamma(\frac{2}{\alpha}+1)\left(\frac{P_c}{P_s}\right)^{\frac{2}{\alpha}}}.$$

We now write $M_{I_i}(s)$ as

$$M_{I_i}(s) = 1 - b_i + \frac{\pi}{A_t}\int_0^{\left(\frac{P_c}{P_s}\right)} \left((\mathcal{U}(R_g)-1)R_g^2-(\mathcal{U}(R_e)-1)R_e^2\right) f_{r_p}(r_p)dr_p, \quad (3.34)$$

where $\mathcal{U}(x) = {}_2F_1\left(1, \frac{2}{\alpha}; 1+\frac{2}{\alpha}, -\frac{x^\alpha}{sP_s r_p}\right)$. A final expression for $M_{I_i}(s)$ is obtained as

$$\begin{aligned} M_{I_i}(s) &= e^{-\pi\lambda_r\Gamma(\frac{2}{\alpha}+1)\left(\frac{P_c}{P_s}\right)^{\frac{2}{\alpha}}} + \frac{2\pi}{A_t}\sum_{t=0}^{\infty}\left(-\frac{sP_s}{(\pi\lambda_r\Gamma(\frac{2}{\alpha}+1))^{\frac{\alpha}{2}}}\right)^t\left(\frac{R_e^{2-\alpha t}-R_g^{2-\alpha t}}{2-\alpha t}\right) \\ &\quad\times\left(\Gamma\left(\frac{\alpha t}{2}+1\right) - \Gamma\left(\frac{\alpha t}{2}+1, \pi\lambda_r\Gamma(\frac{2}{\alpha}+1)\left(\frac{P_c}{P_s}\right)^{\frac{2}{\alpha}}\right)\right), \alpha > 2. \end{aligned} \quad (3.35)$$

The average aggregate interference $E[I]$ is derived as

$$\begin{aligned} E[I] &= 2\pi\lambda_t P_s\left(\pi\lambda_r\Gamma(\frac{2}{\alpha}+1)\right)^{-\frac{\alpha}{2}}\left(\frac{R_e^{2-\alpha}-R_g^{2-\alpha}}{2-\alpha}\right) \\ &\quad\times\left(\Gamma\left(\frac{\alpha}{2}+1\right) - \Gamma\left(\frac{\alpha}{2}+1, \pi\lambda_r\Gamma(\frac{2}{\alpha}+1)\left(\frac{P_c}{P_s}\right)^{\frac{2}{\alpha}}\right)\right), \alpha \neq 2. \end{aligned} \quad (3.36)$$

It should be noted that this scheme can be generalized where each receiver has a probability of not being available ($\beta_r$), and a transmitter attempts to connect to the $M$ receivers providing the best received power. This generalization could be done similar to Scheme 3.

**Scheme 6 (Best received power association and constant transmit power with self deactivation based on estimated cognitive receiver received power)**

This scheme selects $\phi_{r,p\backslash i}$ to associate, but avoids transmitter side power control. Instead, a constant power level of $P_T(\leq P_c)$ is utilized provided the received power of a cognitive receiver does not to fall below the required threshold of $P_s$. Otherwise, transmission is aborted.

The interference from $\phi_{t,i}$ (3.3) can be written as $I_i = V_i P_T |h_i|^2 r_i^{-\alpha}$, where $V_i = \text{Bernoulli}(v_i)$ with $v_i = \Pr[P_{rec} > P_s]$. $P_{rec}$ is the received power at the receiver having the best instantaneous received power. In order to find $v_i$, we will employ the result (3.33) in Scheme 4 obtained using PPP mapping. As such, $P_{rec}$ is written as $P_{rec} = P_T r_p^{-1}$. Then,

$$v_i = \Pr[P_T r_p^{-1} > P_s] = 1 - e^{-\pi\lambda_r\Gamma(\frac{2}{\alpha}+1)\left(\frac{P_T}{P_s}\right)^{\frac{2}{\alpha}}}.$$

The interference from a single transmitter $M_{I_i}(s)$ can be written as

$$M_{I_i}(s) = 1 - v_i + \frac{v_i \pi}{A_t}\left((\mathcal{Y}(R_g) - 1)R_g^2 - (\mathcal{Y}(R_e) - 1)R_e^2\right), \tag{3.37}$$

where $\mathcal{Y}(x) = {}_2F_1\left(1, \frac{2}{\alpha}; 1 + \frac{2}{\alpha}, -\frac{x^\alpha}{sP_T}\right)$. An expression for $M_{I_i}(s)$ can also be derived from the series summation based approach as

$$\begin{aligned} M_{I_i}(s) &= e^{-\pi\lambda_r\Gamma(\frac{2}{\alpha}+1)\left(\frac{P_T}{P_s}\right)^{\frac{2}{\alpha}}} + \left(1 - e^{-\pi\lambda_r\Gamma(\frac{2}{\alpha}+1)\left(\frac{P_T}{P_s}\right)^{\frac{2}{\alpha}}}\right) \\ &\quad \times \sum_{t=0}^{\infty}(-sP_T)^t \frac{2\pi}{A_t}\left(\frac{R_e^{2-\alpha t} - R_g^{2-\alpha t}}{2 - \alpha t}\right), \alpha > 2. \end{aligned} \tag{3.38}$$

The average aggregate interference thus becomes

$$E[I] = 2\pi\lambda_t P_T \left(1 - e^{-\pi\lambda_r\Gamma(\frac{2}{\alpha}+1)\left(\frac{P_T}{P_s}\right)^{\frac{2}{\alpha}}}\right)\left(\frac{R_e^{2-\alpha} - R_g^{2-\alpha}}{2 - \alpha}\right), \alpha \neq 2. \tag{3.39}$$

Similar to Scheme 3, a generalization is also possible for this scheme.

### 3.3.3 Transmission restrictions based on node locations

We now develop a scheme based on restricting transmissions of a secondary transmitter node based on other secondary node locations, where the scheme considers the distance to receivers. However, many other variants can be introduced by combining the schemes mentioned before.

**Scheme 7 (Nearest-$M$ association and path loss inversion with a maximum association radius)**

An area of radius $d_{CRR}$ around each cognitive transmitter is considered as the association region. The association region radius would be initially set as a system parameter taking into account the interference constraints of the primary receiver. Moreover, there would be no cut-off power level ($P_c$).

A secondary transmitter checks the presence of any receivers within the association region, and may transmit if there are one or more receivers. If there are, it would select the nearest receiver. If that receiver is available (with a probability of $\beta_r$), transmission is made. The transmit power is adjusted to ensure a constant average received power ($P_s$). However, this receiver may

not be available (with a probability of $1-\beta_r$). Then, the cognitive transmitter checks whether there are more receivers within the association region. If so, the second nearest one is selected, and an association is made if that receiver is available. This process continues for $T$ times where $T = \min((), M, \text{number of receivers})$.

Let the interference from $\phi_{t,i}$ be $I_i = S_i P_i |h_i|^2 r_i^{-\alpha}$, where $S_i = \text{Bernoulli}(s_i)$ with

$$s_i = \beta_r \sum_{k=1}^{M} (1-\beta_r)^{k-1} (1 - \sum_{i=0}^{k-1} \rho_i).$$

The parameter $\rho_{k-1}$ denotes the probability that there are exactly $k-1$ nodes within the association region given by $\rho_{k-1} = \frac{(\lambda_r \pi d_{CRR}^2)^{k-1}}{(k-1)!} e^{-\lambda_r \pi d_{CRR}^2}, \quad k = 1, 2, \ldots M$. Using this, $s_i$ can be simplified as

$$s_i = \beta_r \sum_{k=1}^{M} (1-\beta_r)^{k-1} \left(1 - \frac{\Gamma(k, \pi\lambda_r d_{CRR}^2)}{(k-1)!}\right).$$

We see that the expression for $s_i$ is analogous to the expression for $w_i$ obtained in Scheme 3, with $d_{CRR}$ replacing $\left(\frac{P_c}{P_s}\right)^{\frac{1}{\alpha}}$. This observation is logically consistent because an association region would bar transmissions to receivers farther than a certain distance. This is effectively enforcing a cut-off power level in a different way. Equations for $M_{I_i}(s)$ and $E[I]$ would thus be similar to Scheme 3, with $d_{CRR}$ instead $\left(\frac{P_c}{P_s}\right)^{\frac{1}{\alpha}}$.

This scheme is analogous to Scheme 2 (Nearest association and path loss inversion with a cut-off power level).

### 3.3.4 Iterative schemes

Iterative schemes utilize system feedback to reduce the primary outage and the probability of cognitive transmitter cut-off. Furthermore, when the primary outage is significantly low, there is room for either more SU-transmitters or for the existing SU-transmitters to be allowed to transmit at a higher power. Iterative power control schemes are suitable in this context. Considering per-user power control schemes, the best system parameter to change according to primary system requirements is the cut-off power level $P_c$. The value for $P_c$ may be calculated and disseminated by a central controller for the cognitive system, or generated by each cognitive transmitter individually.

As the cognitive users are scavenging spectrum from the primary system, the primary system's performance becomes the first priority. Therefore, only while the target for the primary receiver's performance is met, can the cognitive network's performance be increased. With this principle, the proposed iterative scheme is explained in the next paragraph.

We must ensure that the PU-receiver outage is less than a predetermined level $P_{OUT,max}$. However, while this requirement is fulfilled, the cognitive transmitter availability can be increased by increasing the cut-off power level $P_c$ in small steps. This process happens iteratively till $P_c$ is increased by the maximum amount while still keeping the PU-receiver outage below the threshold. Conversely, when the PU-receiver outage is above $P_{OUT,max}$, $P_c$ is reduced iteratively. The initial value for $P_c$ can be any reasonable value. Once the final $P_c$ has been decided through the iterations, the SU-transmitters can employ a power control scheme mentioned in the previous sections. Moreover, even after a suitable value for $P_c$ is established, the iteration process should be repeated every $T$ seconds as channel conditions may have changed.

It should be noted that for an iterative scheme to work, there should be co-ordination between the primary and CR networks. Moreover, additional resources are required for the feedback of information resulting in a more complex system.

## 3.4 Primary receiver outage analysis

We will derive the CDF of the signal to interference and noise ratio (SINR) of the PU-receiver in this section. A simple variable substitution of the CDF gives the outage probability.

The primary transmitter is located at a distance $R$ from the primary receiver (Fig. 3.1), and has a power level of $P_p$. The primary signals are also assumed to undergo Rayleigh fading and path-loss. Therefore, the received power ($P_R$) at the primary receiver can be written as [37], [88]

$$P_R = P_p R^{-\alpha} |h|^2, \tag{3.40}$$

where $|h|^2$ is the channel power gain. For a Rayleigh fading environment, $|h|^2$ is exponentially distributed. Let $\sigma_n^2$ denote the noise variance. The, SINR $\gamma$ can be written as $\gamma = \frac{P_p R^{-\alpha}|h|^2}{I+\sigma_n^2}$. It is possible to obtain the CDF of the SINR as below [117].

$$F_\gamma(x) = \Pr[\gamma \leq x].$$

We can write

$$\begin{aligned} F_{\gamma/I}(x) &= \Pr\left[\frac{P_p R^{-\alpha}|h|^2}{I+\sigma_n^2} \leq x\right] \\ &= \Pr\left[|h|^2 \leq \frac{x(I+\sigma_n^2)}{P_p R^{-\alpha}}\right] \\ &= 1 - e^{\left(-\frac{x(I+\sigma_n^2)}{P_p R^{-\alpha}}\right)}. \end{aligned}$$

After averaging with respect to $I$, we obtain

$$\begin{aligned} F_{\gamma}(x) &= 1 - e^{\left(-\frac{x\sigma_n^2}{P_p R^{-\alpha}}\right)} E_I\left[e^{-I\left(\frac{x}{P_p R^{-\alpha}}\right)}\right] \\ &= 1 - e^{\left(-\frac{x\sigma_n^2}{P_p R^{-\alpha}}\right)} M_I\left(\frac{x}{P_p R^{-\alpha}}\right), \end{aligned}$$

Substituting the required threshold SINR ($\gamma_{th}$) for $x$ yields the outage.

### 3.4.1 Primary transmitters form a PPP

The outage (3.41) was derived for a single primary transmitter at a fixed distance from the PU-receiver. However, in practice, there will be multiple primary transmitters which can be modeled as a PPP. We then extend the outage result (3.41) to this scenario. In this case, all transmitters other than the one associated with the receiver will cause interference.

When the primary transmitters form a PPP in $\mathbb{R}^2$, we assume that the PU-receiver is associated to the nearest primary transmitter. The transmitter will be employing a power control scheme to ensure a constant average received power at the PU-receiver ($P_{c,PR}$). Therefore, the received power at the PU-receiver ($P_R$) becomes $P_R = P_{c,PR}|h|^2$. The SINR is written as $\gamma = \frac{P_{c,PR}|h|^2}{I+I_p+\sigma_n^2}$, where $I_p$ is the aggregate interference from other primary transmitters. The CDF of the SINR is obtained as [117]

$$F_{\gamma}(x) = 1 - e^{\left(-\frac{x\sigma_n^2}{P_{c,PR}}\right)} M_I\left(\frac{x}{P_{c,PR}}\right) M_{I_p}\left(\frac{x}{P_{c,PR}}\right). \tag{3.41}$$

Let the field of interfering primary transmitters (apart from the associated transmitter) be $\psi_p$. Although each receiver is connected to the closest transmitter, in the perspective of the transmitter, the receiver may not be the one closest to it. Contrary to a cognitive network, the receivers would be the entities initiating a request in the primary network (note that the primary network would

be fundamentally different from the cognitive network). Moreover, as the downlink is considered, the transmitter may be connected to multiple receivers employing different multiplexing schemes. Therefore, the best option is to assume a fixed power level which will be the maximum transmit power giving a worst case scenario. Let this power level be $P_{p,PT}$, the distance to the closest primary transmitter $r_{c,p}$, the distance from the PU-receiver to the $j$-th primary transmitter be $R_j$, and the density of the primary transmitters be $\lambda_p$. Then, $I_p = \sum_{j \in \psi_p} P_{p,PT}|h_j|^2 R_j^{-\alpha}$ [117].

Using the Campbell's theorem [73], $M_{I_p}(s)$ is written as [117]

$$\begin{aligned} M_{I_p}(s) &= e^{\left(\int_{r_{c,p}}^{\infty} E\left[e^{-sP_{p,PT}|h_j|^2 R_j^{-\alpha}}-1\right] 2\pi\lambda_p R_j dR_j\right)} \\ &= e^{E_{r_{c,p}}\left[\frac{2\pi\lambda_p s P_{p,PT} r_{c,p}^{2-\alpha}\, {}_2F_1\left(1,1-\frac{2}{\alpha};2-\frac{2}{\alpha},-\frac{sP_{p,}}{r_{c,p}^{\alpha}}\right)}{2-\alpha}\right]}, \alpha \neq 2, \end{aligned} \tag{3.42}$$

where the result holds for $\alpha > 2$. The distribution of $r_{c,p}$ follows equation (3.2) with $\lambda_p$ instead of $\lambda_r$, and the expectation can be computed numerically.

## 3.5 Numerical results

This section provides numerical examples for the outage probability, mean aggregate interference, and the cognitive cut-off probability. We will use the parameters $R_g = 20$, $R_e = 100$, $R = 30$, and $\gamma_{th} = 1$. To highlight the effects of interference, the additive noise variance $\sigma_n^2$ is set to $0$. Moreover, for comparison purposes, we will use the value for $P_c$ for the transmit power of Scheme 6 ($P_T$).

### 3.5.1 Nearest association and highest-received-power association: impact of primary transmit power

We will first investigate the impact of the primary transmit power $P_p$ on the primary outage for the different power control and receiver association schemes.

Fig. 3.2 plots the PU-receiver outage as a function of primary transmit power level $P_p$ for Scheme 4. The theoretical results match perfectly with the simulation. The outage reduces with respect to $P_p$ as expected. We see that the primary outage depends inversely with $P_I$. However, with regards to $\alpha$, the performance diminishes with its increase. Although we would expect that a higher $\alpha$ would attenuate the interfering cognitive signals, it also means that the received primary power level is also low. Moreover, when $\alpha$ is high, the transmit power of a cognitive transmitter

would also increase to ensure a constant average cognitive receiver received power ($P_s$).

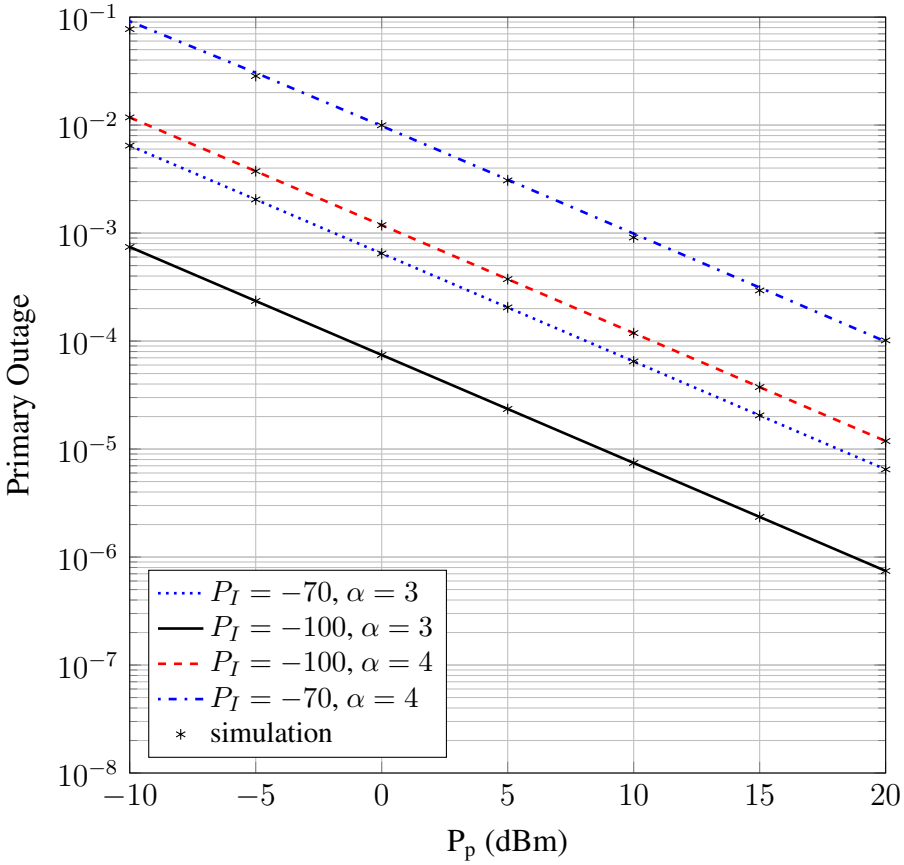


Figure 3.2: Scheme 4: The PU-receiver outage probability vs the primary power level $P_p$ for different values of $P_I$ (dBm), and $\alpha$. $\lambda_t = 5 \times 10^{-3}$, $P_s = -80$ dBm, and $\lambda_r = 2.5 \times 10^{-3}$.

The PU-receiver outage vs the primary transmit power level $P_p$ for Schemes 1, 2, 5, and 6 are plotted in Fig. 3.3. We observe that Scheme 1 results in the worst outage under the given system parameters. Scheme 6 only provides a marginally better performance. Both Schemes 2 and 5 ensure a significantly lower PU-receiver outage. Although the plots for Schemes 2 and 5 overlap, the PU-receiver outage for Scheme 5 is slightly lower. This is because although the individual cognitive transmit powers for Scheme 5 may be higher than those of Scheme 2, SU-transmitters of Scheme 5 are more likely to be cut-off from transmission (due to the cut-off power level $P_c$).

### 3.5.2 Nearest association and highest-received-power association: impact of cognitive system thresholds

We will now investigate the effect of the cut-off power threshold $P_c$ and the average received power level of a cognitive receiver ($P_s$) on the primary outage, mean $I$ on the primary receiver, and the cognitive cut-off probability.

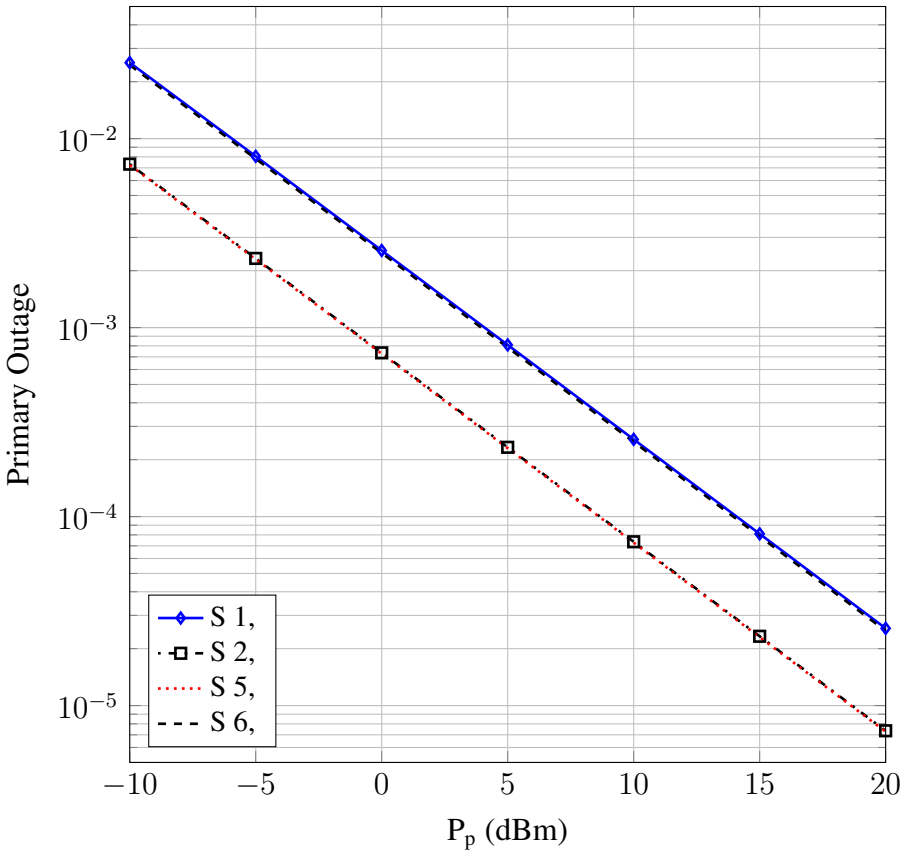


Figure 3.3: Schemes 1, 2, 5, and 6: The outage probability vs the primary power level $P_p$. $\lambda_t = 5 \times 10^{-3}$, $\lambda_r = 1 \times 10^{-3}$, $P_c = -40$ dBm, $P_s = -80$ dBm, and $\alpha = 3$.

The primary outage probability under Scheme 2 is plotted over the cognitive transmitter cut-off power threshold $P_c$ in Fig. 3.4. Naturally, we would expect the outage to increase as $P_c$ increases. However, the outage increases initially, and then flattens out. This is because at higher cut-off levels, almost all the cognitive transmit powers would fall below the threshold. Moreover, the rate of outage increase before flattening out depends on the cognitive receiver density $\lambda_r$. The cognitive transmitter density $\lambda_t$ only introduces a shift to the curves, and does not affect the shape.

Fig. 3.5 plots the mean aggregate interference power of the schemes with respect to the average received power level of a cognitive receiver ($P_s$). Scheme 1 shows a constant increase of the interference power with respect to $P_s$, and thus provides the highest interference at high $P_s$. Scheme 6 has the highest mean aggregate interference at low $P_s$. The level keeps constant initially as $P_s$ rises, but starts to drop after a certain point due to SU-transmitters getting cut-off from transmission. For Schemes 2, 4, and 5, there exists a maxima when the mean interference is at its highest. For these schemes, when the average received cognitive receiver power is low,

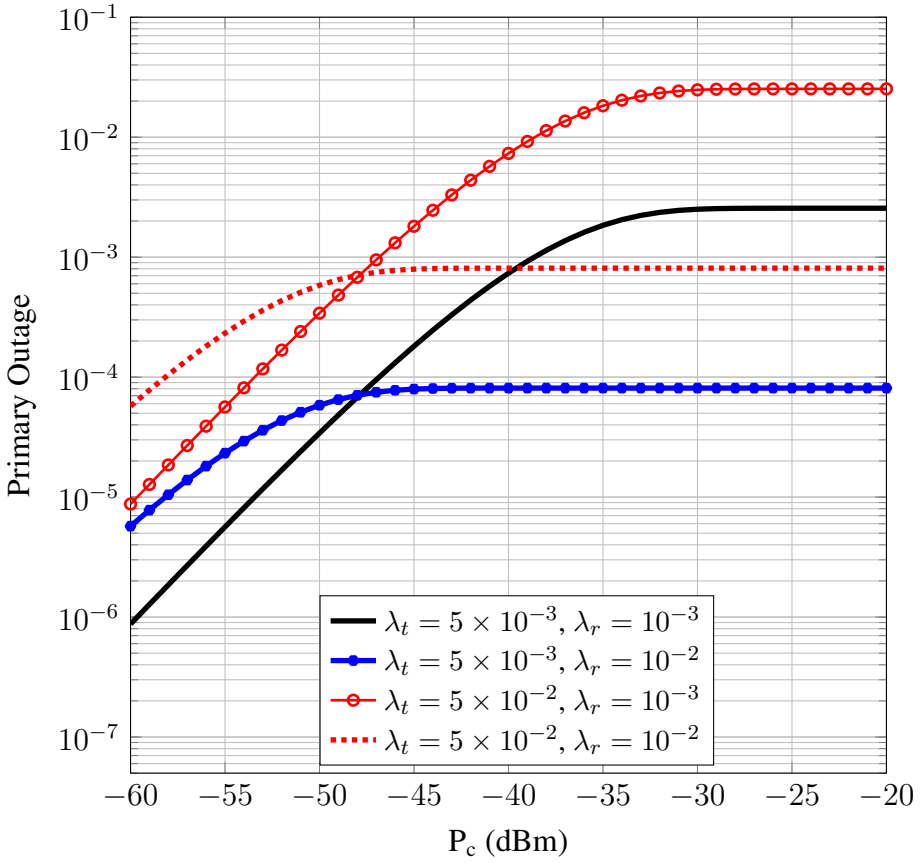


Figure 3.4: Scheme 2: The PU-receiver outage probability vs the cut-off threshold $P_c$ for different values of $\lambda_t$, and $\lambda_r$. $\alpha = 3$, $P_p = 0$ dBm, and $P_s = -80$ dBm.

the transmit powers of the SU-transmitters are low, and thus results in a low interference. When $P_s$ increases, the cognitive transmit powers would increase, and in turn the interference would increase. However, as $P_s$ increases even further, the number of SU-transmitters getting cut-off due to having a transmit power greater than the cut-off level $P_c$ would increase. Therefore, this reduction in transmitting cognitive nodes leads to a lower aggregate interference, and thus the maxima occurs. The value of $P_s$ when the maxima occurs is dependent on several factors, and can be obtained through differentiation by using the derived equations for $E[I]$. Moreover, as $P_s$ increases, Scheme 4 can generate a slightly higher mean aggregate interference to the PU-receiver compared to Schemes 2 and 5, whereas the opposite is true for lower $P_s$. Again, the curves for Schemes 2 and 5 are almost the same. However, Scheme 2 has a slightly higher aggregate interference at higher $P_s$.

It is important to gain an understanding on the impact of different power control schemes on the cognitive system. Fig. 3.6 plots the probability that a cognitive transmitter is cut-off from transmission with respect to the average received cognitive receiver power $P_s$, for Schemes 2 and

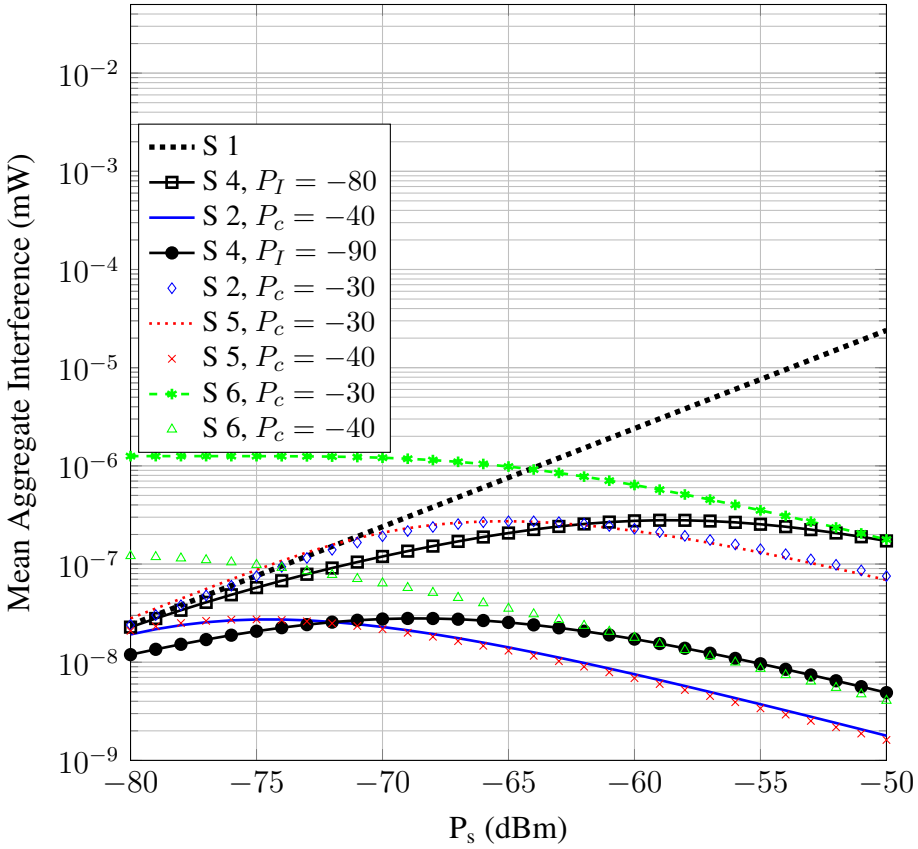


Figure 3.5: Schemes 1, 2, 4, 5, and 6: The mean aggregate interference vs the average received cognitive power $P_s$ under different $P_c$ (dBm) and $P_I$ (dBm). $\alpha = 3$, $\lambda_t = 5 \times 10^{-3}$, and $\lambda_r = 2.5 \times 10^{-3}$.

5. For Scheme 1, this probability is 0, and for Scheme 6, this probability is same as Scheme 5 (we are using the value for $P_c$ in $P_T$). For a high cognitive receiver density $\lambda_r$, the curves show a sharp drop-off under higher $P_c$ when $P_s$ is low. The cut-off probability for Scheme 2 is always lower than Scheme 5. In Fig. (3.5) and (3.3), it was observed that the mean interference and the primary outage were slightly lower for Scheme 5. Thus, a trade-off exists in the primary and cognitive performance. The curves for Scheme 4 would behave in a similar manner for appropriate values for $P_I$ instead of $P_c$. To conclude, a high cognitive receiver density, a low average received cognitive receiver power $P_s$, and a higher value for the threshold $P_c$ reduce the probability that a cognitive transmitter is cut-off from transmitting.

### 3.5.3 Nearest-$M$ association

We will now investigate the performance of Scheme 3, where the transmitter can attempt to connect with the $M$ nearest receivers. Fig. (3.7) plots the primary receiver outage vs the availability of a cognitive receiver ($\beta_r$). The base curve has parameters of $M = 10$, $\lambda_r = 1 \times 10^{-3}$, and

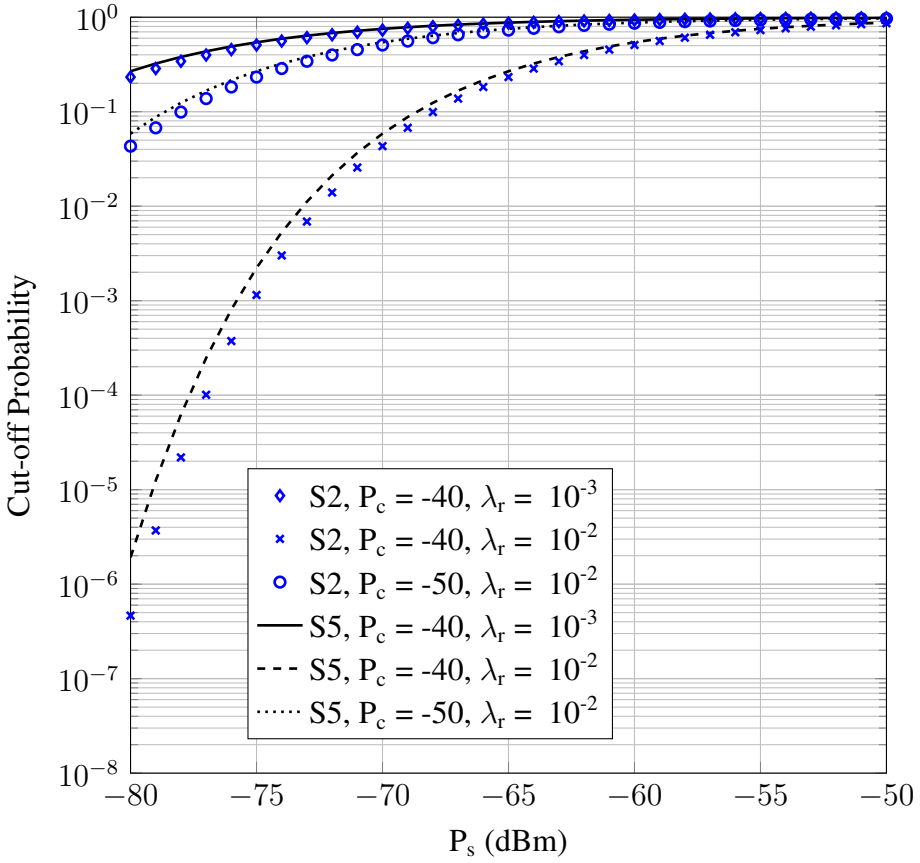


Figure 3.6: Schemes 2 and 5: The average probability of a cognitive transmitter being cut-off from transmission vs $P_s$ for different $\lambda_r$ and $P_c$ (dBm). $\alpha = 3$.

$P_s = 1 \times 10^{-7}$, and subsequent curves are plotted after varying one parameter. The PU-receiver outage for the base curve shows a gradual increase with $\beta_r$. The cut-off power level prevents transmissions to far away SU-receivers. Thus, transmissions are limited to receivers nearby, and the probability of these increases with $\beta_r$. The curve for $M = 2$ shows a similar trend. However, the PU-receiver outage is slightly less because a cognitive transmitter only has the opportunity to connect to a maximum of 2 receivers. The curves when $\lambda_r$ increases and $P_s$ decreases differ significantly from the base curve. In both of these curves, the outage increases initially, and subsequently decreases. When $P_s$ is lower and $\lambda_r$ is higher, the cut-off power would have a lower effect, and transmission is possible to receivers far away. As $\beta_r \to 1$, transmissions occur mainly to close-by receivers, and the PU-receiver outage drops. It is interesting to note that when $M = 10$, a lower $P_s$ and a higher $\lambda_r$ result in an increased outage.

The PU-receiver outage is plotted vs the cognitive transmitter cut-off power level $P_c$ for Scheme 3 in Fig. (3.8). The curves show an initial increase in outage before saturation. This occurs because the required transmit power is lower than $P_c$ most of the time. Thus, any further

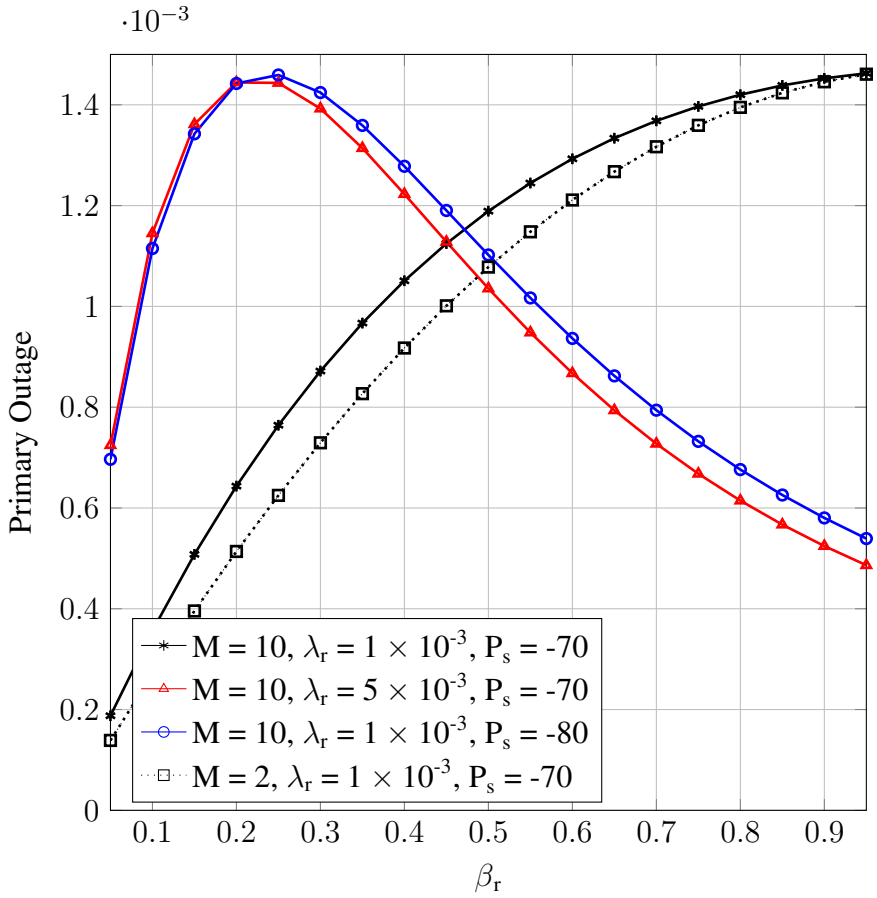


Figure 3.7: Scheme 3: Primary receiver outage probability vs the availability of a cognitive receiver $\beta_r$ for different $M$, $\lambda_r$, and $P_s$ (dBm). $P_c = -30$ dBm, $\alpha = 3$, and $\lambda_t = 0.001$.

increase in $P_c$ would have negligible effect. When the number of receivers a cognitive transmitter attempts to connect ($M$) increases, the PU-receiver outage increases because the probability of associating with a receiver increases for each cognitive transmitter. However the amount of the increase decreases with $M$. For low $P_c$, $M$ has almost no affect because transmissions to far away receivers is difficult.

### 3.5.4 Iterative scheme

Fig. (3.9) plots the probability that a cognitive transmitter is cut-off vs the target outage probability of the PU-receiver ($P_{OUT,max}$) while varying the cognitive transmitter receiver densities for the iterative scheme. From this figure, it is possible to get an insight on the required densities of the SU-transmitters and receivers to achieve a given performance target. If very low PU-receiver outages are required (below $-40$dBm), it is not possible to use the given densities meaningfully. In other words, the SU-transmitters would be cut-off most of the time they need to transmit. Intuitively, for a target $P_{OUT,max}$, the best cognitive transmitter performance is achieved when the

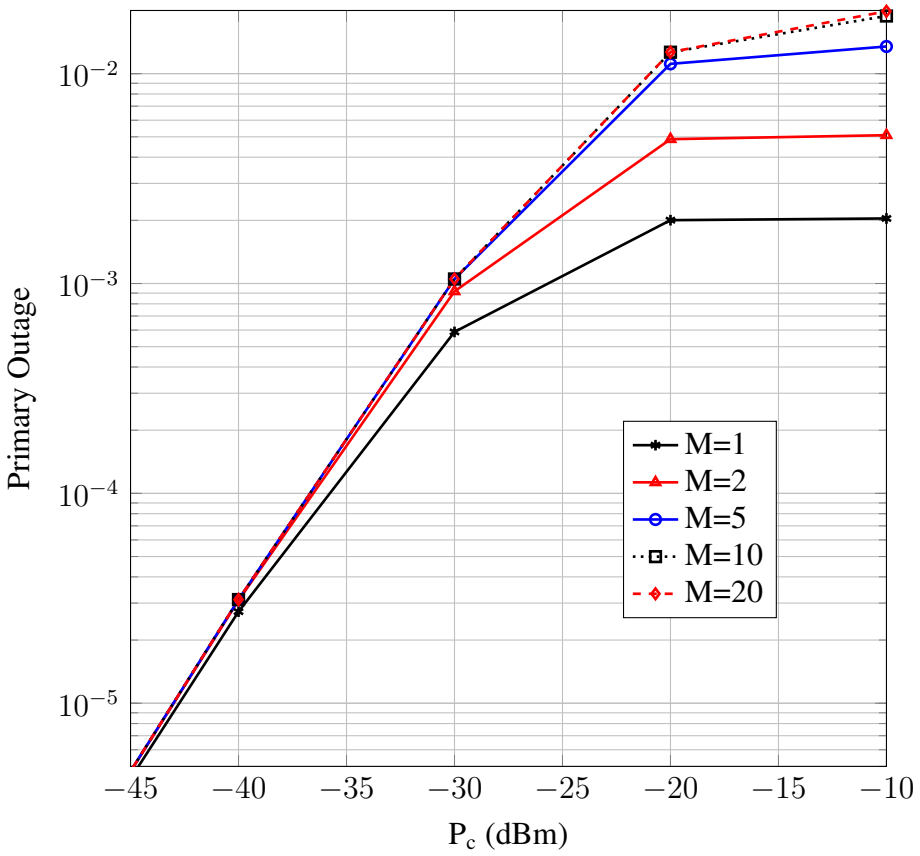


Figure 3.8: Scheme 3: Primary receiver outage probability vs the cut-off power level $P_c$ for different $M$. $\alpha = 3$, $\lambda_t = 0.001$, $\lambda_r = 0.001$, and $P_s = -70$ dBm.

cognitive transmitter density ($\lambda_t$) is low, and the cognitive receiver density $\lambda_r$ is high. It should also be noted that increasing $\lambda_r$ provides better cognitive performance than decreasing $\lambda_t$.

## 3.6 Conclusion

This chapter has investigated the aggregate $I$ from a random network of cognitive nodes which are modeled as spatially distributed independent PPPs. Multiple power control, contention control, and receiver association schemes were proposed. The MGF and mean of the aggregate $I$ of each scheme, and the PU-receiver outage probability were derived. This study provides the following main insights. First, we find that the cognitive transmission/receiver thresholds and the receiver density significantly impact the primary performance. Second, there is a trade-off in the primary and cognitive network performances. Third, having CSI information provides marginally better primary system performance while having a slightly poorer performance with respect to the cognitive transmitter cut-off probability. Fourth, feedback information from the primary system enables a higher cognitive system availability while guaranteeing a fixed primary

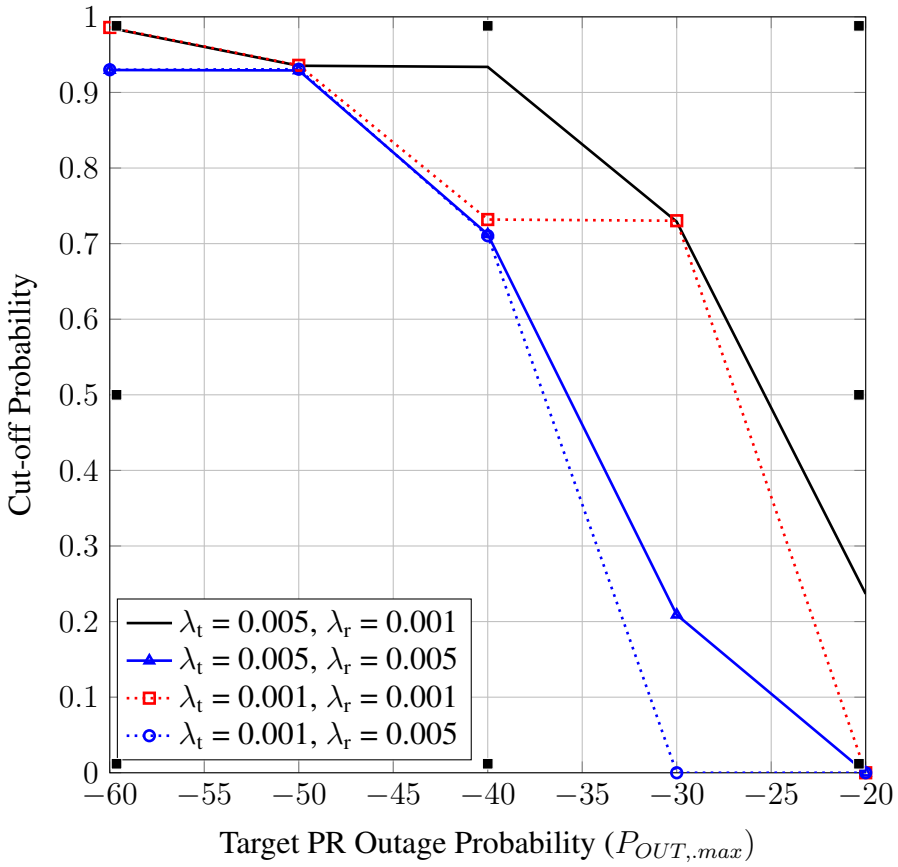


Figure 3.9: Iterative Scheme: The probability that a cognitive transmitter is cut-off from transmission vs the target outage probability of the PU-receiver ($P_{OUT,max}$). $\alpha = 3$, $P_p = -10$ dBm, and $P_s = -80$ dBm.

performance. Future research directions include considering random motion of cognitive nodes, having multiple primary receivers, and estimating the cognitive network capacity.

# Chapter 4

# Cooperative beacon sensing strategies for spatially random cognitive users

## 4.1 Introduction

The cognitive interweave mode aims to allow opportunistic access to temporary unused space-time-frequency slots (spectrum holes) [29]. However, secondary user (SU) devices must then accurately detect active PU transmissions in real time via matched filtering, cylostationarity, energy, eigenvalues, beacons or other methods [2], [35], [36], [133].

Of these, PU beacon signaling where a dedicated out-of-band channel indicates spectrum occupancy has the benefits of efficiency and simplicity [100], [103]–[105], [107], [134]. Grant or denial beacons are simply out-of-band, on-off modulated electromagnetic waves [102], proposed for IEEE 802.22.1 [106] and cognitive cellular systems [101], [102]. In this work, we focus on the problem of detecting **denial beacons** of active PU nodes. Beacon missed detection, which leads to interference on the PUs, occurs due to multipath fading, path loss, receiver uncertainty and other factors [108], [109]. Thus, a classical solution is to exploit spatial diversity. We can thus use multiple beacon measurements from spatially separated SUs and combine them into one final decision. This is an instance of cooperative sensing, which can be based on OR, AND, or majority rules [35], [135]. In this chapter, we will limit ourselves to the OR rule to determine the presence of a denial beacon, which leads to conservative spectrum access attempts (i.e., ensuring less interference but higher false alarm). The reduction in missed detection probability due to cooperative beacon sensing (CBS) depends on the number of cooperating SUs and their locations [136], which are random. Due to this spatial randomness, path loss, and fading, the expected

performance improvements of CBS may be severely compromised. To characterize such issues, a comprehensive analysis of the overall beacon missed detection probability ($P_{md}$) is necessary.

### 4.1.1 Problem statement and contribution

In this chapter, we analyze the overall $P_{md}$ and false alarm probability ($P_f$) of several CBS methods as a function of how cooperating SUs are selected, local detection methods, spatial randomness of primary and secondary nodes, channel fading, and the sharing of imperfect decisions. Specifically, we address the following questions: 1) How does a SU device locally process one or more beacons transmitted from multiple PU devices to mitigate the impact of fading and path loss? 2) How do we select a set of SUs for cooperative spectrum sensing when the beacons are sent by PU-receiver nodes or PU-transmitter nodes? What are the rules that specify a suitable set of cooperating SUs? The cooperative sensing stage will be affected by the channel propagation characteristics and spatial randomness of the cooperating SUs. The availability of channel state information (CSI) for the SU-to-SU channels affects the selection of best nodes to cooperate with. Clearly, the cooperating set should be chosen to minimize $P_{md}$, which will depend on mutual distances and fading conditions. 3) What is the overall performance of CBS?

To investigate all these questions for coexisting cellular (primary) and cognitive networks, we first ensure that the spatial randomness of nodes is fully accounted for. To this end, we use the tools from spatial geometry to model the random locations of PU and SU nodes. Specifically, we model PU-receiver nodes and SUs as Poisson Point Processes (PPPs) [73]. However, the PU-transmitters are fixed at the centers of hexagonal cells. For realistic propagation modeling, we incorporate both power-law path loss and Rayleigh fading. The beacon detection process of a SU is consisted of two distinct stages: 1) local detection, and 2) cooperation. The sharing of detection results is done via a control channel subject to fading and path-loss. Moreover, we consider beacons sent by both PU-receivers and PU-transmitters. Our main contributions in this chapter are as follows:

1. For stage one, we propose three local beacon processing schemes: 1) aggregating beacon powers, 2) separately sensing multiple beacons, and 3) detecting the best average received beacon signal (i.e. from the closest).

2. For stage two, we propose three cooperation schemes: 1) nearest scheme, 2) multiple-random scheme, and 3) best received power scheme. For beacons emitted by PU-transmitters,

we propose two additional schemes: 1) nearest SU to PU-transmitter scheme and 2) random SU to PU-transmitter scheme.

3. For all these schemes, we derive $P_{md}$ and $P_f$ from the OR rule fusion in order to characterize the performance improvement of CBS under different system parameters.

4. We derive the outage probability of a PU-receiver to characterize how its performance is affected by interference due to beacon missed detection.

### 4.1.2 Prior research

We first review papers that do not focus on beacons signaling but perform general missed detection analysis and interference characterization for CR networks [134], [137]–[142]. For brevity, we denote the aggregate interference by $I$. In [134], the distribution of $I$ is characterized in terms of sensitivity, transmit power, density of the SUs, the propagation characteristics, and cooperative spectrum sensing. In [142], the theory of truncated stable distributions and power control are studied for a CR network. Reference [137] analyzes the primary coverage probability under missed detections and false alarms, and develops an approximation and bounds for the Laplace transform of $I$. Statistics of $I$ from a secondary network with an ALOHA based medium access control, spectrum sensing, and power control is derived [138]. Moreover, [139] derives the moment generating function of $I$ for a spectrum sensing CR network, and a scheme is proposed to maximize the transmission powers of multiple active SU transmitters while satisfying $I$ constraints. This scheme leads to significantly higher capacity. Reference [141] analyzes the geometric region allowing CR transmission with the help of cooperative sensors, and finds that the shape of this region is not circular. Furthermore, reference [143] develops models for bounding interference levels by modeling SUs as a modified Matern process. Co-operating spectrum sensing methods are analyzed over correlated shadow fading environments [140]. The spatial throughput of a CR network is characterized for a two threshold based opportunistic spectrum access protocol in [105].

Several works consider spectrum sensing using beacon detection and also cooperative spectrum sensing [86], [87], [103], [144]–[146]. Reference [103] analyzes capacity-outage probability of a PU due to interference from beacon missed detection. The emission of beacons by PU-receiver nodes leads to higher capacity-outage performance. Furthermore, [144] considers three levels of cooperation under beacon transmissions from the primary users. It is shown that

cooperation is vital when the SU node density is high. Threshold based opportunistic spectrum access methods are studied in [145] under PU-transmitter and receiver pilot signals and beacons, and the spatial opportunity (probability that an arbitrary location is discovered as a spectrum hole) is derived. Furthermore, [86], [87] study the resultant aggregate interference due to missed detection in beacon based CR networks. Moreover, [146] studies the soft combination of spectrum information shared by the cooperating nodes when for multiple beacon signalling, and derives the optimal beacon sequence to reduce missed detection.

The differences among the aforementioned works and this chapter are now described. First, spatial randomness of SUs is not considered in [103] and thus the spatial densities of the nodes do not appear in their analysis. Second, the existence of multiple PU-receivers is not considered [86], [87]. Third, the control channel for sharing the sensing result has been assumed perfect [103], [144], [145]. In contrast, in this chapter we consider the effect of propagation impairments (path loss and fading) on the quality of reception of control signals. Fourth, the availability of channel state information (CSI) has not been considered for cooperating node selection [86], [87], [103], [144]–[146]. However, we differentiate CBS strategies depending on the availability of CSI. Fifth, no distinction is made between beacons emitted by PU-transmitters and those by PU-receivers [86], [87]. In contrast, this chapter derives the interference statistics of the two cases in detail. Sixth, the impact of spatial locations has not been considered [103], [144]–[146]. As such, our chapter strives to fill these gaps while investigating the missed detection probability reduction of cooperative sensing.

## 4.2 System model

### 4.2.1 Spatial distribution

We consider coexisting primary and cognitive (secondary) networks. We assume the PU network to use the same frequency block (the frequency reuse factor is $1$). The area is divided into hexagonal cells with a PU-transmitter (e.g. base-station) at the center of each (Fig. 4.1), which serves a set of spatially random PU-receivers within each cell. We refrain from using a random model for the PU network to make our analysis more mathematically tractable. The cognitive network which can be an ad-hoc network or a sensor network [147] utilizes primary spectrum holes to transmit data. To facilitate analysis, we approximate the PU hexagonal cells with circular cells having a radius of $r_{cell}$ (Fig. 4.1). The spatial randomness of SUs is also considered.

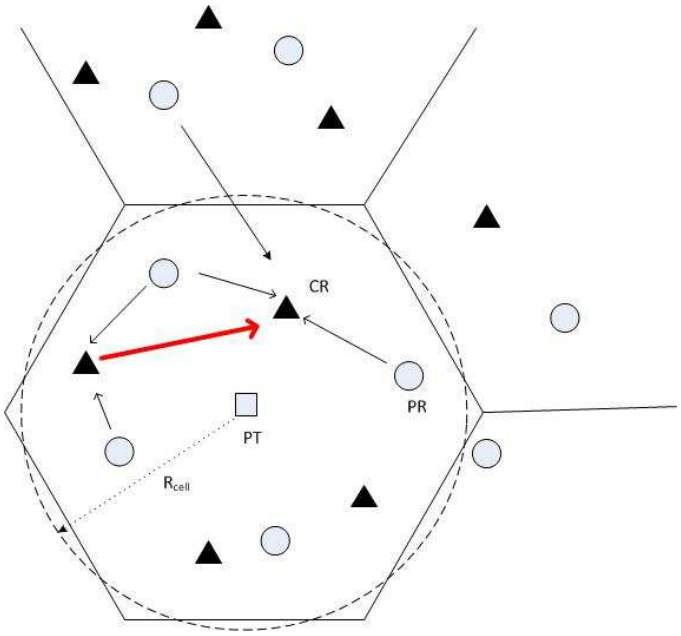


Figure 4.1: PU-receiver node emit beacons. Squares, triangles, circles, and solid arrows respectively denote the PU-transmitters, SUs, PU-receivers, and the beacon signals. Each cell is hexagonal with a PU-transmitter at the center. PU-receivers and SUs are distributed randomly in $\mathbb{R}^2$.

To model spatial randomness, we will make use of point processes. In this chapter, we model PU-receivers and SU nodes as as two independent homogeneous PPPs $\Phi_p$ and $\Phi_s$ in $\mathbb{R}^2$ with spatial densities $\lambda_p$ and $\lambda_s$. We assume that the CSI of the PU-SU links are not available to individual SUs. This assumption is reasonable and common [103] because of the general commercial and regulatory pressures that push primary and secondary networks to operate independently. However, a SU may or may not know about the CSI of links between itself and other SUs. The degree of availability of this CSI to SUs will impact the development of cooperative spectrum sensing protocols.

In this work, mobility of wireless nodes is not analyzed for two reasons. First, some PU nodes are fixed (e.g., base-stations, TV receivers and others). Second, even if the SUs move randomly (e.g. random walk or the Brownian motion), a snapshot of at any specific time generates a homogeneous PPP. Nevertheless, the impact of the mobility of nodes is a challenging, future topic.

Furthermore, we assume that SUs are always ready to transmit data upon detecting a spectrum hole and that all the PU-receivers are active. There is no loss of generality in these assumptions since activity factors ($\leq 1$) can easily be incorporated using the Coloring Theorem [73]. That is,

if nodes of a PPP $\Phi$ with intensity $\lambda$ are marked independently, and $p_t$ is the probability of a node receiving the $t$-th color, the set of $t$-th color nodes forms a PPP $\Phi_t$ with intensity $p_t\lambda$. Thus, if a PU-receiver is active with an activity factor of $q_p$, the set of active PU-receivers follows a thinned PPP with intensity $q_p\lambda_p$. The same argument holds for the SUs.

### 4.2.2 Signal propagation

The propagation effects are characterized by independent Rayleigh fading and log-distance path loss [3]. With small-scale Rayleigh fading, the channel power gain $|h|^2$ has the Exponential PDF (2.4). The log-distance path loss model in (2.11) is used. The path loss exponent is a function of carrier frequency, terrain, obstructions, antenna heights and others. The typical values range from 2 to 8 (at around 1 GHz). Note however that because $g(r) = r^{-\alpha}$ leads to analytical difficulties when $r < 1$, we will also use $g(r) = min(1, r^{-\alpha})$.

Throughout the chapter, we assume that all SUs transmit at a fixed power level [37], [88], [119]. Although SU power control methods are beyond the scope of this chapter, they can be easily incorporated if needed [84].

### 4.2.3 Local detection

As mentioned before, beacon detection process at a SU is divided into 2 stages: the local detection stage, and the cooperative stage. We assume the downlink transmission of the cellular network with denial beacons where the PU devices (either PU-transmitters or PU-receivers [102], [107]) transmit a beacon signal. This beacon will have a set number of bits indicating that $\kappa(\kappa \in (1 \dots K))$ future time-slots will be occupied by the transmitting device. Moreover, the beacon would uniquely identify the transmitting PU device, and would enable synchronization between the primary and secondary network. Beacons from different primary transmitters and receivers will use orthogonal narrow frequency bands, codes, or time slots. Furthermore, the beacon signal is transmitted before channel access by the PU device. For example, in the case of PU-transmitter beacons, the device sends the beacon signal before transmitting its data, while for PU-receiver beacons, the beacon is emitted by all active devices before they begin receiving oncoming data.

PU-receivers, which are hand-held user devices, can rapidly drain their battery life when emitting beacons. Remedially, beacon signals can be made shorter, their frequency can be reduced, or their power can be reduced. All these options may unfortunately increase the missed detection of beacons. On the other hand, when PU-transmitters emit beacons, such beacons can be used

under high power levels [103].

**PU-receiver beacons**

Without the loss of generality, we assume that all PU-receivers are active and transmit beacons. For this to work, we assume synchronization between the different PU-receivers. However, if only a subset of the PU-receiver nodes are active, this can be easily incorporated using the Coloring Theorem [73]. Note that a SU may detect a beacon from a PU-receiver in another cell (Fig. 4.1). Thus, we suggest three local beacon detection schemes. These schemes are:

1. *Aggregating all beacons in the range.*
   Each SU simply uses the aggregate beacon power received, which does not require it to differentiate among the different PU-receiver beacons. The beacons in this case are simple signals which do not need to be decoded. However, this is a conservative approach in terms of opportunistic spectrum access because the aggregate beacon power may exceed the sensing threshold even when nearby PU-receivers are inactive.

2. *Sensing beacons separately and combining them via the OR rule.*
   A SU is assumed to differentiate the beacons emitted by various PU-receivers (e.g. each one may use a different orthogonal code [148] or matched filtering may be used [145]). Thus, each distinct beacon is uniquely sensed. The beacons in this instance have limited information, and are thus not simple signals such as with the previous scheme. However, the implementation of a separate beacon sensing scheme has significant challenges. As the spatial density of PU nodes increases, this schemes requires additional processing. Moreover, longer codewords and thus longer beacons are needed to uniquely identify the different PU-receivers. On a practical point of view, only the PU-receivers within a certain radius from the SU may be considered for local detection instead of all the PU-receivers within the geographical area. The separate sensing scheme is advantageous for SUs because it allows them to access the spectrum whenever a beacon signal from a PU is less than the threshold. This is in contrast with the aggregate scheme where even if the individual beacon powers are far less than the threshold, the aggregate can still be above the threshold, barring a SU from accessing the spectrum.

3. *Sensing the beacon from the closest PU-receiver only.*

The SU must find the closest PU-receiver perhaps by measuring the average received signal power [149]. Moreover, the SU must differentiate among the beacons from different PU-receivers in order to achieve this. Thus, the beacons for this scheme also contain limited information. This scheme has the advantage of considerable less processing than the separately sensing scheme after the closest PU-receiver has been established. Moreover, it provides the best opportunities for a SU to access the spectrum among the three local detection schemes. However, because only a single PU beacon is considered, there is a high missed detection probability.

**PU-transmitter beacons**

We assume that all PU-transmitters become active at the same time. Each SU listens to its own cell's PU-transmitter for beacon signals. It should be noted that while a SU may receive a better instantaneous signal from a neighbouring cell due to a favourable channel, the PU-transmitter of its cell would also be the closest PU-transmitter to a given SU, and thus would provide the best received beacon signal power on average when shadowing is ignored. We assume that the SUs have the ability to uniquely identify its own PU-transmitter from neighbouring PU-transmitters[1]. While beacon signal reception from out-of-cell PU-transmitters can also be considered, we leave this for future work.

### 4.2.4 Co-operative sensing

In the cooperative stage, the SU will select one or more other SUs to obtain the sensing results via a single narrowband control signal. We assume that the SUs can identify each other via the use of separate orthogonal codes or time slots. In our analysis, we will consider distributed cooperation schemes without the involvement of a fusion center, information sharing via decision-fusion, and combination via the OR rule [35]. The OR rule minimizes $P_{md}$ compared to other combining rules [35], but can adversely affect the false alarm probability. Because distributed co-operating schemes are used, each individual SU keeps a dynamic database of neighbouring SUs. This database will include details about activity, distance, and CSI if available. Information for the individual databases is obtained via periodic control signals, and updated regularly. We thus propose three cooperation schemes, where the selection is based on the information within each SU's database. They are:

[1] Separately identifying PU-transmitter beacons may be achieved by using unique codes or time slots.

1. *Nearest scheme*:

   Each SU cooperates with its closest neighbor SU, which provides the best received signal power on average. To implement this, distances among the SUs are needed [83]. These distances may be obtained via a database, shared GPS information or via periodic control signals.

2. *Multiple random scheme*:

   Here, $M$ neighbouring SUs are randomly selected within a cooperation radius of $R_c$ where $R_c$ is less than the outer distance $R_e$. A SU is assumed to only cooperate with a neighbour within this radius. The signals from nodes beyond the outer distance $R_e$ are assumed to have negligible power due to high path loss. If the number of SUs within $R_c$ is less than $M$, all would be selected. The selected nodes are always available for cooperation.

3. *Best received power scheme*:

   In this scheme, each SU cooperates with the neighbouring SU providing the best instantaneous received signal power. This amounts the lowest propagation loss considering both path loss and fading. We assume that each SU knows CSI and the positions of other SUs. Moreover, we further assume that a SU can cooperate with nodes outside its own cell.

We will assume that SUs can differentiate the beacon signals from the PU-receivers and the control signals from other cooperating SUs. For example, this involves using separate orthogonal codes for different SUs and PU-receivers, using different time slots, matched filtering, or having a separate narrow band channel for SU spectrum information sharing [100], [145], [148]. This assumption is valid when there is proper co-ordination between the 2 networks. Furthermore, it should be noted that each SU shares its local detection result, but not the final decision of CBS.

With PU-transmitter beacons, we propose two additional schemes based on the intuition that SUs close to the PU-transmitter will have a better chance of correctly detecting the beacon. These schemes are:

1. *Nearest SU to PU-transmitter scheme*:

   Each SU, $x \in \Phi_s$, selects the closest SU to the PU-transmitter, which has the best probability to detect the beacon signal due to the lowest path loss. Furthermore, selection of distances to a fixed PU-transmitter may be less complex than find all SU-to-SU distance.

2. *Random SU to PU-transmitter scheme*:

   A random SU within a distance of $R_c$ from the PU-transmitter is selected. The distance constraint from the PU-transmitter which ensures the cooperating SU has a good chance of detecting the PU beacon. This scheme has the advantage over the previous scheme of not burdening a single SU (the one closest to the PU-transmitter) for sensing data.

Choosing other SU nodes to cooperate with based on distances to PU nodes is most suitable when PU-transmitters emit beacons. PU-transmitters would generally be fixed, and their locations would thus not change dynamically. As such, choosing SU nodes within a certain distance from the PU-transmitter is relatively straightforward. On the other hand, PU-receivers may be fluid in their activity, and multiple PU-receivers will be transmitting (with PU-transmitters, we assume the SU only listens to the PU-transmitter of its own cell) their beacons. As such, choosing cooperating SU nodes satisfying distance requirements from PU-receivers is more cumbersome, and such schemes are not considered in this chapter.

## 4.3 missed detection probability analysis for PU-receiver beacons

### 4.3.1 Local primary beacon detection

In this section, we analyze $P_{md}$ for the local spectrum sensing methods in Section II C.

**Aggregating beacon power**

This scheme works when the beacons are simple signals which do not bear information. Consider the SU node $x \in \Phi_s$ and the PU-receiver node $y \in \Phi_p$. The distance between them is $||x-y||$. However, as this distance becomes large, $g(||x-y||) \to 0$. As such, the beacons emitted by PU-receiver nodes $y$ such that $||x-y|| > R_e$ are considered to be negligible, where $R_e$ is an outer distance. Since $x$ and $y$ are two random points from two independent PPPs, we need the distribution of the distance $||x-y||$. However, because a homogeneous Poisson process is considered for $\Phi_p$, its points are distributed randomly. Moreover, due to the outer distance, the area of node distribution is annular. Therefore, the CDF of $||x-y||$ can be obtained as [88]

$$F_{||x-y||}(t) = \frac{t^2}{R_e^2}, \quad 0 < t < R_e. \tag{4.1}$$

Thus, $||x-y||$ is distributed with PDF $Lin(R_e)$.

All PU-receiver nodes $y \in \Phi_p$ transmit a beacon signal of constant power level $P_b$. As the SU will aggregate these beacons, the received beacon power at SU $x$ is given by

$$P_R = P_b \sum_{y \in \Phi_p} |h_{x,y}|^2 g(||x - y||), \tag{4.2}$$

where $h_{x,y}$ is the channel between nodes $x$ and $y$, and this incorporates both path loss and small scale fading. The received signal to noise ratio (SNR) $\gamma$ at SU $x \in \Phi_s$ becomes $\gamma = \frac{P_R}{\sigma_b^2}$, where $\sigma_b^2$ is the additive noise variance. A beacon is detected whenever the received beacon power $P_R > P_{th}$, where $P_{th}$ is the reception threshold.

Let $P_{md}(x)$ be the probability of PU beacon missed detection by the SU $x \in \Phi_s$ in its local-detection stage. This probability is given by

$$P_{md}(x) = \Pr[P_R < P_{th}] = F_{P_R}(P_{th}),$$

which is the CDF of $P_R$. This can be evaluated using an MGF based approach [37], [89]–[91]. Let $M_{P_R}(s)$ be the MGF of the received beacon power at $x \in \Phi_s$, which is defined as $M_{P_R}(s) = E\left[e^{-sP_R}\right]$. If $M_{P_{R,y}}(s)$ is the MGF of the received beacon power from $y \in \Phi_p$, and $N$ is a Poisson random variable with mean $\pi R_e^2 \lambda_p$, we can write $M_{P_R}(s)$ as [37], [88]

$$M_{P_R}(s) = E_N\left[(M_{P_{R,y}}(s))^N\right] = e^{\pi R_e^2 \lambda_p (M_{P_{R,y}}(s) - 1)}. \tag{4.3}$$

$M_{P_{R,y}}(s)$ is obtained as follows.

$$\begin{aligned} M_{P_{R,y}}(s) &= E\left[e^{-sP_b |h_{x,y}|^2 g(||x-y||)}\right] \\ &= \int_0^1 \frac{1}{1 + sP_b} \frac{2t}{R_e^2} dt + \int_1^{R_e} \frac{1}{1 + sP_b t^{-\alpha}} \frac{2t}{R_e^2} dt. \end{aligned} \tag{4.4}$$

A closed-form expression for the second integral (4.4) appears intractable. However, using the expansion $(1+t)^{-1} = \sum_{k=0}^{\infty} (-t)^k$, $|t| < 1$, we derive a alternate expression as

$$M_{P_{R,y}}(s) = \frac{1}{R_e^2} \left( \frac{1}{1 + sP_b} + \sum_{l=0}^{\infty} 2(-sP_b)^l \frac{R_e^{2-\alpha l} - 1}{2 - \alpha l} \right). \tag{4.5}$$

$F_{P_R}(t)$ can be obtained through the inverse Laplace transform by $F_{P_R}(t) = \mathcal{L}^{-1}\left(\frac{M_{P_R}(s)}{s}\right)$, and replacing $t$ with $P_{th}$ gives $P_{md}(x)$, $x \in \Phi_s$. Note that because a closed-form solution is not apparent for $P_{md}(x)$, where $x \in \Phi_s$, numerical techniques and approximations must be used.

Although aggregating beacon power decreases $P_{md}$, viable spectrum access opportunities are also lost due to detecting aggregated beacons even when there may not be any PU-receivers close by to be hindered by interference.

**Separately sensing primary beacons**

This scheme assumes that the beacons are structured, information bearing, and orthogonal. Missed detection occurs only when all beacon sensing outputs fall below the threshold. Thus we have $P_{md}(x) = (\Pr[P_{R,y} < P_{th}])^N$, where $x \in \Phi_s$ and $P_{R,y}$ is the beacon power from $y \in \Phi_p$ received at $x \in \Phi_s$, and $N$ is a Poisson random variable with $\mathbb{E}[N] = \lambda_p \pi R_e^2$. The missed detection of the beacon from $y \in \Phi_p$ may be written as $\Pr[P_{R,y} < P_{th}] = E_{(||x-y||)}\left[1 - e^{-\frac{P_{th}}{P_b g(||x-y||)}}\right]$. Thus, denoting $||x - y|| = t$, the local missed detection probability may be expressed as

$$P_{md}(x) = e^{-\pi R_e^2 \lambda_p \left(\frac{e^{-\frac{P_{th}}{P_b}}}{R_e^2} + \frac{2}{R_e^2}\int_1^{R_e} e^{-\frac{P_{th}}{P_b t^{-\alpha}}} t dt\right)}. \tag{4.6}$$

Because a closed-form solution for (4.6) appears impossible, we numerically evaluate this. A series summation based simplification can be used to simplify (4.6) which results in

$$P_{md}(x) = e^{-\pi R_e^2 \lambda_p \left(\frac{e^{-\frac{P_{th}}{P_b}}}{R_e^2} + \frac{2}{R_e^2}\sum_{k=0}^{\infty} \frac{\left(-\frac{P_{th}}{P_b}\right)^k}{k!}\left(\frac{R_e^{2+\alpha k}-1}{2+\alpha k}\right)\right)}. \tag{4.7}$$

However, more resources are required for separate sensing, and is invariably more complex. Furthermore, the PU-receivers need to be co-ordinated to send separately identifiable beacons. This may not be practical for certain PU-receiver types such as digital terrestrial television subscribers.

**Closest PU-receiver selection**

Each SU, $x \in \Phi_s$, senses the beacon emitted by the closest PU-receiver. The closest PU-receiver may be found in practice by measuring the average received signal power [149]. Moreover, the SU must then have the ability to differentiate among different beacons.

Let $y^* = \arg\min_{y \in \Phi_p} ||y - x||$ ($y^* \in \Phi_p$) be the nearest PU-receiver to $x \in \Phi_s$, and the distance $r^* = ||y^* - x||$. The distribution of $r^*$ is derived via the void probability of a PPP (probability of no nodes within a given radius from the origin) [126], [127], and is found out to be $Ral(\pi\lambda_p)$.

However, as the beacons from node $y \in \Phi_p$ at a distance more than $R_e$ are neglected due to path loss, there may be an occasion where there is no closet PU-receiver within $R_e$. The probability of this event is $p_0 = e^{-\pi\lambda_p R_e^2}$. Whenever this occurs, the SU $x \in \Phi_s$ will misdetect with probability 1. However, conversely, because of the high path loss in such a scenario, the interfering signals will also have a negligible effect on the primary system. Let $r_1^*$ be the truncated distance from $x$ to $y^*$ whenever $r^* < R_e$. Thus, $r_1^*$ is distributed according to $TRal(\pi\lambda_p, R_e)$.

Let $|h_{x,y*}|^2$ be the channel power gain between $x$ and $y^*$. Therefore, when a PU-receiver exists, the received beacon power ($P_R$) at $x$ from $y^*$ is given by $P_R = P_b|h_{x,y*}|^2 g(r_1^*)$, where $g(r_1^*)$ is the path-loss factor between $x$ and $y^*$.

$P_{md}(x)$ can thus be written as

$$\begin{aligned} & P_{md}(x) = e^{-\pi\lambda_p R_e^2} + (1 - e^{-\pi\lambda_p R_e^2}) \times \Pr[R_b < P_{th}] \\ = \; & e^{-\pi\lambda_p R_e^2} + (1 - e^{-\pi\lambda_p R_e^2}) \times \Pr\left[|h_{x,y*}|^2 < \frac{P_{th}}{P_b g(r_1^*)}\right] \\ = \; & e^{-\pi\lambda_p R_e^2} + (1 - e^{-\pi\lambda_p R_e^2}) \left(1 - e^{-\frac{P_{th}}{P_b}} \left(\frac{1 - e^{-\pi\lambda_p}}{1 - e^{-\pi\lambda_p R_e^2}}\right)\right. \\ & \left. - \int_1^{R_e} \frac{2\pi\lambda_p t}{1 - e^{-\pi\lambda_p R_e^2}} e^{-\frac{P_{th}}{P_b t^{-\alpha}}} e^{-\pi\lambda_p t^2} dt\right), \end{aligned} \tag{4.8}$$

and the integration in (4.8) can be performed numerically.

### 4.3.2 Co-operative spectrum sensing

In this section, we analyze $P_{md}$ when each SU employs the SU selection schemes proposed in Section II D. The total $P_{md}$ depends on both: 1) beacon missed detection, and 2) control channel missed detection.

**Nearest scheme**

Let the closest neighbour from SU $x \in \Phi_s$ be denoted as $x^*$ ($x^* \in \Phi_s$) with $x^* = \arg\min_{z \in \Phi_s} ||z - x||$ , located at a distance $\tilde{r}^*$ from $x$. Because the signals from $x^*$ with $\tilde{r}^* > R_e$ are neglected due to path loss, there may be an occasion where a node $x^*$ does not exist for cooperation. This probability $\rho_0$ is obtained as $\rho_0 = e^{-\pi\lambda_s R_e^2}$ using the void probability of a PPP. Let $\tilde{r}_1^*$ be the

distance from $x$ to $x^*$ whenever $\tilde{r}^* < R_e$. Thus $\tilde{r}_1^*$ is distributed as $TRal(\pi\lambda_s, R_e)$.

Node $x^*$ senses the presence of primary receiver beacons, and passes that information in the form of binary information in a narrow band channel using another control signal. Let $P_{b,s}$ be the power of this control signal, and $|h_{x,x^*}|^2$ be the channel power gain between $x$ and $x^*$. Therefore, if the received control signal power ($P_{R,s}$) at $x$ from $x^*$ is given by $P_{R,s} = P_{b,s}|h_{x,x^*}|^2 g(\tilde{r}_1^*)$, where $g(\tilde{r}_1^*)$ is the path loss gain between $x$ and $x^*$.

The probability of misdetecting the control signal transmitted by $x^*$, $q_{s,i}$, is obtained as

$$q_{s,i} = \Pr[P_{R,s} < P_{th}] = E_{\tilde{r}_1^*}\left[1 - e^{-\frac{P_{th}}{P_{b,s}\, g(\tilde{r}_1^*)}}\right]. \tag{4.9}$$

After performing the averaging with respect to $\tilde{r}_1^*$, the simplified expression for $q_{s,i}$ is

$$\begin{aligned} q_{s,i} &= 1 - e^{-\frac{P_{th}}{P_{b,s}}}\left(\frac{1 - e^{-\pi\lambda_s}}{1 - e^{-\pi\lambda_s R_e^2}}\right) \\ &- \int_1^{R_e} \frac{2\pi\lambda_s t}{1 - e^{-\pi\lambda_s R_e^2}} e^{-\frac{P_{th}}{P_b t^{-\alpha}}} e^{-\pi\lambda_s t^2} dt \end{aligned} \tag{4.10}$$

Let $P_{md}^1$ be the final missed detection probability of $x$ when cooperating with its closest neighbor. We will assume that $x$ uses an OR rule [103] where $P_{md}^1$ becomes the product of the separate primary beacon and secondary control signal misdetecting probabilities. However, the probability that there is no SU within $R_e$ must be considered. $P_{md}^1$ is composed of the following events: (1) $x^*$ does not exist, and $x$ misdetects, (2) $x^*$ does exist, but both $x^*$ and $x$ misdetect the primary beacons, and (3) $x^*$ does exist, and detects the primary beacon correctly, but $x$ misdetects both the primary system beacons and the control signal from $x^*$. After combining these three events, we can write $P_{md}^1$ as

$$\begin{aligned} P_{md}^1 &= P_{md}(x)\left(e^{-\pi\lambda_s R_e^2} + \left(1 - e^{-\pi\lambda_s R_e^2}\right)\right. \\ &\times \left.\left(P_{md}(x) + (1 - P_{md}(x))\, q_{s,i}\right)\right). \end{aligned} \tag{4.11}$$

We have used the fact that correct secondary control signal reception due to double errors ( $x^*$ misdetects the primary beacons but $x$ detects a secondary control signal when it's not present) are negligible. Moreover, spatial correlations have not been taken into account in the derivation of (4.11).

**Multiple random scheme**

Let $x_r$ ($x_r \in \Phi_s$) be any SU within a cooperating distance of $R_c$ from $x$, and $r_r$ be the distance from $x$ to $x_r$. Using similar arguments as the derivation of $||x-y||$, the distribution of $r_r$ is shown to be distributed according to $Lin(R_c)$.

Similar to the nearest scheme, whenever an $x_r$ detects the primary beacons, this information is sent via a control signal to $x$. We assume that $x$ can differentiate the control signals coming from the $M$ associated SUs, which can be easily achieved via orthogonal codes serving as an identifier of each SU within $\Phi_s$. If $|h_{x,x_r}|^2$ and $g(r_r)$ are the small scale channel gain and path loss gain between $x_r$ and $x$, the received signal power $P_{R,s}$ from $x_r$ is given by $P_{R,s} = P_{b,s}|h_{x,x_r}|^2 g(r_r)$.

If $q_{s,i}$ is the probability of $x$ misdetecting the control signal from $x_r$, it is obtained as

$$\begin{aligned} q_{s,i} &= 1 - \frac{e^{-\frac{P_{th}}{P_{b,s}}}}{R_c^2} - \frac{2}{R_c^2}\int_1^{R_c} e^{-\frac{P_{th}}{P_{b,s}t^{-\alpha}}} t dt \\ &= 1 - \frac{e^{-\frac{P_{th}}{P_{b,s}}}}{R_c^2} + \frac{2}{\alpha} E_{1-\frac{2}{\alpha}}\left(\frac{P_{th}R_c^{\alpha}}{P_{b,s}}\right). \end{aligned} \tag{4.12}$$

Let $P_{md}^2$ be the final missed detection probability of $x \in \Phi_s$. Although $M$ is fixed beforehand, due to spatial randomness, the available number of SUs may be less than $M$. Thus, $P_{md}^2$ is the sum of several probability components corresponding to the number of cooperating nodes. Let $q$ be the probability of missed detection arising from a single cooperating node (sum of the primary beacon missed detection probability by $x_r$ and the probability that the control signal of $x_r$ is misdetected by $x$ when $x_r$ correctly detects the primary beacons). It can be written as $q = (P_{md}(x) + (1 - P_{md}(x))\, q_{s,i})$. Whenever a given $k(\leq M)$ cooperating nodes are present, the final misdetecting probability of $x \in \Phi_s$ becomes $P_{md}(x)q^k$. As such, $P_{md}^2 = E_k[P_{md}(x)q^k]$, where $0 \leq k \leq M$. After averaging with respect to $k$ using (2.14), $P_{md}^2$ becomes

$$P_{md}^2 = P_{md}(x)\left(e^{-\pi\lambda_s R_c^2(1-q)}\frac{\Gamma(M,\pi\lambda_s R_c^2 q)}{\Gamma(M)} + \left(1 - \frac{\Gamma(M,\pi\lambda_s R_c^2)}{\Gamma(M)}\right)q^M\right). \tag{4.13}$$

**Best received power scheme**

Let the neighbouring SU of $x \in \Phi_s$ having the best instantaneous received signal power be denoted as $x_h$. In order to evaluate the secondary control signal missed detection probability

($q_{s,i}$), the Mapping theorem [73] is used on the PPP $\Phi_s$. Furthermore, for convenience, we will use the path loss function $g(r_h) = r_h^{-\alpha}$ where $r_h = ||x - x_h||$ is the distance between $x$ and $x_h$. Moreover, we denote the channel gain between $x$ and $x_h$ as $|h_{x,x_h}|^2$. The mapping procedure is as follows. With respect to $x \in \Phi_s$, the process of SUs is homogeneous in $\mathbb{R}^2$ with it at the center. It is shown that an inhomogeneous PPP $\Phi_{s,h}$ with intensity $\lambda_{s,h}$, an exponential path loss with a path loss exponent of 1 and no fading generates the equivalent received power to that from a homogeneous PPP, and exponential path loss with an exponent $\alpha$ and Rayleigh fading [132], where $\lambda_{s,h}$ is written as (3.24)

$$\lambda_{s,h} = \frac{2\pi}{\alpha}\lambda_s r_{s,h}^{\frac{2}{\alpha}-1}\Gamma(\frac{2}{\alpha}+1), 0 < r_{s,h} < \infty. \tag{4.14}$$

Note that $r_{s,h}$ is a distance based metric of the PPP and not any physical distance. In $\Phi_{s,h}$, the node having the smallest distance metric from $x$ is $x_h$. Thus, using (4.14), the PDF of the distance metric to $x_h$ (denoted by $r_h^*$) can be obtained as

$$f_{r_h^*}(t) = \frac{2\pi}{\alpha}\lambda_s\Gamma(\frac{2}{\alpha}+1)t^{\frac{2}{\alpha}-1}e^{-\pi\lambda_s\Gamma(\frac{2}{\alpha}+1)t^{\frac{2}{\alpha}}}, 0 < t < \infty. \tag{4.15}$$

With these results, the received secondary control signal power at $x$ is written as $P_{R,s} = P_{b,s}(r_h^*)^{-1}$. Thus, $q_{s,i}$ is obtained as

$$\begin{aligned} q_{s,i} &= \Pr[P_{b,s}(r_h^*)^{-1} < P_{th}] \\ &= e^{-\pi\lambda_s\Gamma(\frac{2}{\alpha}+1)\left(\frac{P_{b,s}}{P_{th}}\right)^{\frac{2}{\alpha}}}. \end{aligned} \tag{4.16}$$

The final missed detection probability of $\phi_{s,i}$ ($P_{md}^3$) is composed of two components. First $x$ and $x_h$ may both misdetect the primary beacon. Second, while $x_h$ detects the primary beacon, $x$ may misdetect the control channel between $x$ and $x_h$. Thus, $P_{md}^3$ is obtained as

$$P_{md}^3 = P_{md}(x)(P_{md}(x) + (1 - P_{md}(x))q_{s,i}). \tag{4.17}$$

## 4.4 missed detection probability analysis for PU-transmitter beacons

This case is depicted in Fig. 4.2. In primary cellular networks where the transmitter is a base station, and receivers are user equipment, this approach provides wide benefits as base stations are not power limited and avoids PU-receiver power drain.

### 4.4.1 Local primary beacon detection

Each SU ($x \in \Phi_s$) listens for the beacon of the PU-transmitter ($v$) of its cell. Let $R_{cell}$ be the cell radius, and $P_{b,p}$ be power level of the beacon. Let $r_{x,v} = ||x - v|$. This is the distance between a fixed point and a random point from $\Phi_s$. The $r_{x,v}$ will be distributed as $Lin(R_{cell})$ (we assume that $R_{cell} << R_e$). If $|h_{x,v}|^2$ and $g(r_{x,v})$ are the small scale channel gain and path loss gain between $x$ and $v$, the received beacon power at $x$ ($P_R$) is given by $P_R = P_{b,p}|h_{x,v}|^2 g(r_{x,v})$. Whenever it falls below the threshold, the detection fails. Thus, the probability of missed detection is given by

$$\begin{aligned} & P_{md}(x) = \Pr[P_{b,p}|h_{x,v}|^2 g(r_{x,v}) < P_{th}] \\ = \; & 1 - \frac{e^{-\frac{P_{th}}{P_{b,p}}}}{R_{cell}^2} - \frac{2}{R_{cell}^2} \int_1^{R_{cell}} e^{-\frac{P_{th}}{P_{b,p} t^{-\alpha}}} t dt \\ = \; & 1 - \frac{e^{-\frac{P_{th}}{P_{b,p}}}}{R_{cell}^2} + \frac{2}{\alpha} E_{1-\frac{2}{\alpha}} \left( \frac{P_{th} R_{cell}^{\alpha}}{P_{b,p}} \right). \end{aligned} \tag{4.18}$$

### 4.4.2 Co-operative sensing

For PU-transmitter emitted beacons, we will now analyze the two additional schemes proposed.

**Nearest SU to PU-transmitter scheme**

Let $x_{cv}$ be the closest SU ($\in \Phi_s$) to $v$ ($x_{cv} = \arg\min_{z \in \Phi_s} ||z - v||$), with $r_{v,cv} = ||v - x_{cv}||$ and $r_{x,cv} = ||x - x_{cv}||$. If $r_{v,cv} > R_{cell}$, a cooperating node does not exist. The probability of this scenario occurring ($\rho_1$) is given by $\rho_1 = e^{-\pi \lambda_s R_{cell}^2}$. Thus, the variable $r_{v,cv}$ is distributed according to $TRal(\pi\lambda_s, R_{cell})$. This distribution is obtained by removing $x$ from $\Phi_s$. This removal does not significantly affect the statistics of $\Phi_s$.

We now need to find the probability that $x_{cv}$ misdetects the PU-transmitter's beacon ($P_{md}(x_{cv})$) for this scenario. Let $|h_{v,cv}|^2$ and $g(r_{v,cv})$ be the small scale channel gain and path loss gain between $v$ and $x_{cv}$. The received beacon power at $x_{cv}$ ($P_{R,s}$) is given by $P_{R,s} = P_{b,p}|h_{v,cv}|^2 g(r_{v,cv})$.

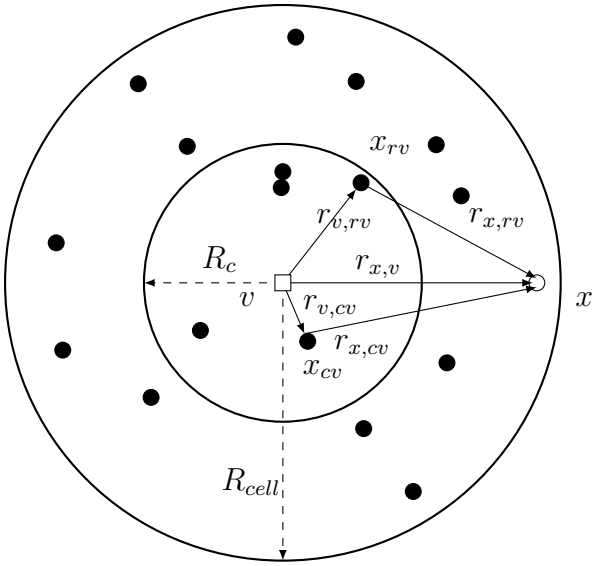


Figure 4.2: The PU-transmitter $v$ located at (0,0) sends the beacon. The cell radius is denoted by $R_{cell}$, the cooperating radius is denoted by $R_c$, while the black dots denote the SUs. The SU $x$ located at a distance $r_{x,v}$ from $v$ can cooperate with either the closest SU to $v$ ($x_{cv}$), or cooperate with a random SU within a distance of $R_c$ from $v$ ($x_{rv}$).

$P_{md}(x_{cv})$ is thus obtained as

$$P_{md}(x_{cv}) = 1 - e^{-\frac{P_{th}}{P_{b,p}}} \left( \frac{1 - e^{-\pi\lambda_s}}{1 - e^{-\pi\lambda_s R_{cell}^2}} \right) - \int_1^{R_{cell}} \frac{2\pi\lambda_s t}{1 - e^{-\pi\lambda_s R_{cell}^2}} e^{-\frac{P_{th}}{P_{b,p} t^{-\alpha}}} e^{-\pi\lambda_s t^2} dt. \tag{4.19}$$

We now derive the probability that $x \in \Phi_s$ misdetects secondary control signal from $x_{cv}$ whenever it ($x_{cv}$) detects the PU transmitter's beacon. The small scale channel gain and path loss gain between $x$ and $x_{cv}$ are denoted by $|h_{x,cv}|^2$ and $g(r_{x,cv})$ respectively. The received power of the secondary control at $x \in \Phi_s$ is given by $P_{R,s} = P_{b,s}|h_{x,cv}|^2 g(r_{x,cv})$, and the probability of $x$ misdetecting the control signal ($q_{s,i}$) is then given by

$$\begin{aligned} q_{s,i} &= \Pr[P_{R,s} < P_{th}] \\ &= E_{r_{x,cv}} \left[ 1 - e^{-\frac{P_{th}}{P_{b,s} g(r_{x,cv})}} \right]. \end{aligned} \tag{4.20}$$

In order to evaluate this, the distribution of $r_{x,cv}$ is needed. From the cosine rule, $r_{x,cv}$ can be written as $r_{x,cv} = \sqrt{r_{v,cv}^2 + r_{x,v}^2 - 2r_{x,v}r_{v,cv}\cos\theta}$, where $\theta$ is a uniform between 0 and $2\pi$, with $f_\theta(x) = \frac{1}{2\pi},\ 0 \leq x < 2\pi$. Furthermore, for mathematical convenience, we will take

$g(r_{x,cv}) = r_{x,cv}^{-\alpha}$. Thus, $q_{s,i}$ becomes

$$\begin{aligned} q_{s,i} &= 1 - \int_0^{R_{cell}} \int_0^{R_{cell}} \int_0^{2\pi} e^{-\frac{P_{th}}{P_{b,s}(r_{v,cv}^2 + r_{x,v}^2 - 2r_{x,v}r_{v,cv}\cos\theta)^{-\frac{\alpha}{2}}}} \\ &\times \frac{2\lambda_s r_{x,v} r_{v,cv}}{R_{cell}^2\left(1 - e^{-\pi\lambda_s R_{cell}^2}\right)} e^{-\pi\lambda_s r_{v,cv}^2} d\theta dr_{v,cv} dr_{x,v}. \end{aligned} \tag{4.21}$$

Let $P_{md}^4$ be the overall missed detection probability of $x \in \Phi_s$. Similar to the previous analysis, it is necessary to consider probability of no cooperating node ($\rho_1$). Thus, $P_{md}^4$ is composed of three events: (1) $x$ misdetects beacon and no cooperating node exists, (2) $x$ and $x_{cv}$ both misdetect beacon, and (3) $x$ misdetects the beacon and $x_{cv}$ detects it but $x$ misdetects the control signal from $x_{cv}$. Considering these three events, we can write

$$\begin{aligned} P_{md}^4 &= P_{md}(x)\left(e^{-\pi\lambda_s R_{cell}^2} + \left(1 - e^{-\pi\lambda_s R_{cell}^2}\right)\right. \\ &\times \left.\left(P_{md}(x_{cv}) + \left(1 - P_{md}(x_{cv})\right) q_{s,i}\right)\right). \end{aligned} \tag{4.22}$$

**Random SU to PU-transmitter scheme**

Let the randomly selected SU be $x_{rv}$, its distance from $v$ be $r_{v,rv}$, and its distance from $x$ be $r_{x,rv}$. We assume that $R_c < \min\left(()\, R_{cell}, R_e\right)$. If no such SU exists within a distance of $R_c$ of $v$, no cooperation occurs. The probability of it is $\rho_2 = e^{-\pi\lambda_s R_c^2}$.

The probability that $x_{rv}$ misdetects the beacon from $v$ is obtained next. We denote this probability as $P_{md}(x_{rv})$, and the small scale channel gain and path loss gain between $v$ and $x_{rv}$ respectively as $|h_{v,rv}|^2$ and $g(r_{v,rv})$. The received beacon power at $x_{rv}$ ($P_{R,s}$) is given by $P_{R,s} = P_{b,p}|h_{v,rv}|^2 g(r_{v,rv})$. We can now write $P_{md}(x_{rv})$ as

$$\begin{aligned} &P_{md}(x_{rv}) = \Pr\left[P_{b,p}|h_{v,rv}|^2 g(r_{v,rv}) < P_{th}\right] \\ &= 1 - \frac{e^{-\frac{P_{th}}{P_{b,p}}}}{R_c^2} - \frac{2}{R_c^2}\int_1^{R_c} e^{-\frac{P_{th}}{P_{b,p}t^{-\alpha}}} t dt \\ &= 1 - \frac{e^{-\frac{P_{th}}{P_{b,p}}}}{R_c^2} + \frac{2}{\alpha} E_{1-\frac{2}{\alpha}}\left(\frac{P_{th}R_c^\alpha}{P_{b,p}}\right). \end{aligned} \tag{4.23}$$

We will now derive the the probability that $x$ misdetects the secondary control signal from $x_{rv}$ (denoted by $q_{s,i}$), whenever a secondary control signal is transmitted. The small scale channel

gain and path loss gain between $x$ and $x_{rv}$ are respectively denoted as $|h_{x,rv}|^2$ and $g(r_{x,rv})$. Similar to the previous scheme, we will use $g(r_{x,rv}) = r_{x,rv}^{-\alpha}$ for mathematical convenience. Using the cosine rule, $r_{x,rv}$ is written as $r_{x,rv} = \sqrt{r_{v,rv}^2 + r_{x,v}^2 - 2r_{x,v}r_{v,rv}\cos\theta}$. Thus, $q_{s,i}$ is written as

$$\begin{aligned} q_{s,i} &= \Pr[P_{b,s}|h_{x,rv}|^2 r_{x,rv}^{-\alpha} < P_{th}] \\ &= 1 - \int_0^{R_{cell}} \int_0^{R_c} \int_0^{2\pi} e^{-\frac{P_{th}}{P_{b,s}(r_{v,rv}^2 + r_{x,v}^2 - 2r_{x,v}r_{v,rv}\cos\theta)^{-\frac{\alpha}{2}}}} \\ &\times \frac{2}{\pi R_c^2 R_{cell}^2} r_{x,v} r_{v,rv} d\theta dr_{v,rv} dr_{x,v}. \end{aligned} \tag{4.24}$$

The final missed detection probability of $x$ (denoted as $P_{md}^5$) is comprised of 3 terms as the previous scheme (Nearest SU to PU-transmitter scheme). Thus, $P_{md}^5$ is obtained as

$$\begin{aligned} P_{md}^5 &= P_{md}(x)\left(e^{-\pi\lambda_s R_c^2} + \left(1 - e^{-\pi\lambda_s R_c^2}\right)\right. \\ &\times \left.\left(P_{md}(x_{rv}) + (1 - P_{md}(x_{rv}))\, q_{s,i}\right)\right). \end{aligned} \tag{4.25}$$

This scheme can be generalized where a cooperates with up to $M$ SUs within a distance of $R_c$ from the PU-transmitter.

## 4.5 False alarm probability Analysis

For completeness, we will conduct an analysis of the false alarm probability $P_f$. First, we will analyze $P_f$ for the different local detection schemes for PU-receiver and PU-transmitter beacons.

### 4.5.1 False alarm probability for local detection schemes

#### Aggregating beacon power

A false alarm occurs when the SU detects the presence of a beacon when none are present. In this scenario, the received power is purely composed of noise. Thus

$$P_R = w, \tag{4.26}$$

where $w = \mathcal{N}(0, \sigma^2)$, and $sigma^2$ is the noise variance (it should be noted that because a narrowband channel is used for beacons and control signals, $sigma^2$ is very small). Let $P_f(x)$ be the probability of falsely detecting PU beacons by the SU $x \in \Phi_s$ in its local detection stage. $P_f$

can be written as $P_f = \Pr[P_R > P_{th}]$. As such

$$P_f(x) = Q\left(\frac{P_{th}}{\sigma}\right), \tag{4.27}$$

and $Q(\cdot)$ is the $Q$ function.

**Separately sensing primary beacons**

When separately detecting primary beacons, a false alarm can occur even if a single stream from a PU is detected in error. Thus, we have

$$P_f(x) = \mathbb{E}[1 - (\Pr[P_R < P_{th}])^N] = \mathbb{E}[1 - \left(1 - Q\left(\frac{P_{th}}{\sigma}\right)\right)^N]. \tag{4.28}$$

After averaging with respect to $N$,

$$P_f(x) = 1 - e^{-\pi R_e^2 \lambda_p Q\left(\frac{P_{th}}{\sigma}\right)}. \tag{4.29}$$

**Closest PU-receiver selection**

$P_f(x)$ for this scenario is identical to (4.27), and $P_f(x) = Q\left(\frac{P_{th}}{\sigma}\right)$.

**PU-transmitter beacons**

As each SU ($x \in \Phi_s$) listens to the beacon of the primary transmitter of its own cell, $P_f(x)$ is simply written similar to (4.27) as $P_f(x) = Q\left(\frac{P_{th}}{\sigma}\right)$.

### 4.5.2 False alarm probability after co-operation

Using the local false alarm probabilities derived above, we now derive the final false alarm probability after co-operation for the different schemes.

**PU-receiver beacons: Nearest scheme**

For this scheme, false alarm occurs even if one of the following cases occur: 1) $x$ falsely detect beacons, 2) $x$ properly detects beacons, the nearest neighbour $x^*$ properly detects, but $x$ improperly detects the control channel, and 3) $x$ properly detects beacons, the nearest neighbour $x^*$ falsely detects, and $x$ detects the control channel. After combining these events, we can write $P_f^1$ as

$$P_f^1 = P_f(x) + (1 - P_f(x))((1 - P_f(x))P_f(x) + P_f(x)(1 - q_{s,i})). \tag{4.30}$$

It should be noted that the probability of falsely detecting the control channel also follows (4.27), and that $q_{s,i}$ follows (4.10).

**PU-receiver beacons: Multiple random scheme**

In this scheme, even a single false alarm from one of the co-operating nodes triggers a false alarm after combination. Let $p$ be the probability that there is **no** false alarm from a co-operating node $x_r$. $p$ can be written as $p = (1-P_f(x))(1-P_f(x))+P_f(x)(q_{s,i})$. The final false alarm probability can thus be written as $P_f^2 = 1-(1-P_f(x))p^k$, for a given $k(\leq M)$. Averaging with respect to $k$ (2.14) results in

$$\begin{aligned} P_f^2 &= 1-(1-P_f(x))\left(e^{-\pi\lambda_s R_c^2(1-p)}\frac{\Gamma(M,\pi\lambda_s R_c^2 p)}{\Gamma(M)}\right. \\ &+ \left.\left(1-\frac{\Gamma(M,\pi\lambda_s R_c^2)}{\Gamma(M)}\right)p^M\right). \end{aligned} \tag{4.31}$$

**PU-receiver beacons: Best received power scheme**

The final false alarm probability $P_f$ for this scheme follows (4.30) with $q_{s,i}$ following (4.16).

**PU-transmitter beacons: Nearest SU to PU-transmitter scheme**

The final $P_f$ for this scheme follows (4.30) with $q_{s,i}$ following (4.21).

**PU-transmitter beacons: Random SU to PU-transmitter scheme**

The final $P_f$ for this scheme also follows (4.30) with $q_{s,i}$ following (4.24).

## 4.6 Primary system performance

The missed detection of beacons by a set of SUs will cause interference, which will degrade the received SINR, $\gamma_{p,y}$, at PU-receiver $y \in \Phi_p$. Thus, let $I$ be the aggregate interference from the SUs, $P_{R,p}$ be the received primary signal power at $y \in \Phi_p$, and $\sigma_n^2$ be the noise power spectral density at the PU-receiver. We assume that different PU-transmitters use orthogonal codes, and do not pose significant interference to PU-receivers within other cells. $P_{R,p}$ is written as $P_{R,p} = P_p|h_{v,y}|^2 g(r_{v,y})$, where $P_p$, $|h_{v,y}|$ and $r_{v,y}$ are respectively the PU transmit power, channel power gain and distance between the PU-transmitter $v$ and $y$. We can thus write the SINR as $\gamma_y = \frac{P_{R,p}}{I+\sigma_n^2}$. An outage occurs whenever $\gamma_y < \gamma_{th}$ where $\gamma_{th}$ is a threshold. Note that we are more interested in the SINR falling below a threshold for the primary signals as opposed to the received signal

falling below a threshold used for beacon detection. The primary signals would be transmitting data whereas the beacon signals only indicate the channel occupation for which the received signal level was sufficient. Thus, the outage probability of $\gamma_y$ may be written as

$$P_{Out,y} = \Pr[\gamma_y < \gamma_{th}].$$

We can write

$$\begin{aligned} P_{Out,y/I,r_{v,y}}(x) &= \Pr\left[\frac{P_p|h_{v,y}|^2 g(r_{v,y})}{I+\sigma_n^2} \leq \gamma_{th}\right] \\ &= \Pr\left[|h_{v,y}|^2 \leq \frac{\gamma_{th}(I+\sigma_n^2)}{P_p g(r_{v,y})}\right] \\ &= 1 - e^{\left(-\frac{\gamma_{th}(I+\sigma_n^2)}{P_p g(r_{v,y})}\right)}. \end{aligned}$$

$P_{Out,y/I,r_{v,y}}(x)$ can be further averaged with respect to $I$ as

$$\begin{aligned} P_{Out,j/r_{v,y}}(x) &= 1 - e^{\left(-\frac{\gamma_{th}\sigma_n^2}{P_p g(r_{v,y})}\right)} E_I\left[e^{-I\left(\frac{\gamma_{th}}{P_p g(r_{v,y})}\right)}\right] \\ &= 1 - e^{\left(-\frac{\gamma_{th}\sigma_n^2}{P_p g(r_{v,y})}\right)} M_I\left(\frac{\gamma_{th}}{P_p g(r_{v,y})}\right). \end{aligned} \tag{4.32}$$

Equation (4.32) provides the outage probability of node $y$ given $r_{v,y}$ is known. However, if averaging over all PU-receivers is needed, we need the PDF of $r_{v,y}$, which is the distance from a fixed point to a random point from $\Phi_p$, which can be shown to be $Lin(R_{cell})$. Thus, the average outage can be expressed as

$$\begin{aligned} P_{Out,y}(x) = 1 &- \frac{e^{\left(-\frac{\gamma_{th}\sigma_n^2}{P_p}\right)}}{R_{cell}^2} M_I\left(\frac{\gamma_{th}}{P_p}\right) \\ - &\int_1^{R_{cell}} 2\frac{t}{R_{cell}^2} e^{\left(-\frac{\gamma_{th}\sigma_n^2}{P_p t^{-\alpha}}\right)} M_I\left(\frac{\gamma_{th}}{P_p t^{-\alpha}}\right) dt. \end{aligned} \tag{4.33}$$

To evaluate this, the MGF of the aggregate interference at $y$ ($M_I(s)$) needs to be obtained. However, the exact expressions for interference is a function of each individual cooperating scheme, and thus complex. But, for completion, we suggest the following approximate approach. $M_I(s)$ is written as $M_I(s) = E[e^{-sI}]$. Let $r_{x,y} = ||x-y||$ for any interfering SU $x \in \Phi_s$, which is

distributed as $Lin(R_e)$. Note that similar to Section III, we do not consider the interference from $x$ whenever $r_{x,y} > R_e$. When $P_{md}(x)$ is the final missed detection probability of $x \in \Phi_s$ with CBS, the Coloring theorem [73] suggests that the intensity of the interfering SUs is $P_{md}(x)\lambda_s$. $M_I(s)$ is thus obtained as

$$M_I(s) = e^{\pi R_e^2 P_{md}(x)\lambda_s (M_{I_x}(s)-1)}, \tag{4.34}$$

where $M_{I_x}(s)$ is the MGF of the interference from $x$. It is given by $M_{I_x}(s) = E[e^{-sP_s|h_{x,y}|^2 g(r_{x,y})}]$, where $P_s$ is the SU transmit power, and $|h_{x,y}|^2$ and $g(r_{x,y})$ are respectively the small scale channel gain and the path loss gain between $y$ and $x$. $M_{I_x}(s)$ is derived as

$$M_{I_x}(s) = \frac{1}{R_e^2}\left(\sum_{k=0}^{\infty}(-sP_s)^k + \sum_{l=0}^{\infty} 2(-sP_s)^l \frac{R_e^{2-\alpha l}-1}{2-\alpha l}\right). \tag{4.35}$$

## 4.7 Numerical results

We will first provide numerical results on the total missed detection probability for different cooperation and local primary beacon detection schemes. Subsequently, we will have a brief look at the false alarm probability of the different schemes. We used MATLAB for the simulation, with $10^4$ topologies, and $10^4$ transmissions for each topology; thus $10^8$ simulations for each plot point. Note that because simulation results match with the theoretical results, we have not used separate marker styles.

### 4.7.1 Beacons emitted by PU-receiver nodes

We will first investigate the case of PU-receiver beacons. The parameters are $R_e = 1500$, $R_c = 500$, $\alpha = 3$, $P_{b,s} = -40$ dBm, and $P_b = -50$ dBm. The low power of $P_{b,s}$ and $P_b$ is due to the fact that the PU receivers and CR nodes in practice are power-limited devices. Moreover, $P_{th}$ is chosen as $-110$ dBm, which is the minimum signal reception thresholds for several mobile standards [150].

Fig. 4.3 plots the total missed detection probability $P_{md}$ (eqs. 4.13, 4.17, and 4.11) and the false alarm probability $P_{md}$ with respect to the CU detection threshold ($P_{th}$). While the performance improvement due to CBS is slight for higher $P_{th}$, it is significant when $P_{th}$ is small. For example, when $P_{th} = -120$ dBm and using multiple random cooperation with 10 nodes, $P_{md}$ decreases by a $10^4$ fold. This decrease is even higher for best received power cooperation

when separately detecting all PU-receiver beacons. Furthermore, the latter performs better than sensing the beacon from the closest PU-receiver. However, as mentioned before, this comes at the cost of additional complexity and resources. It is also interesting to note that while the nearest scheme performs better than the multiple random scheme when $P_{th}$ is higher, the converse is true for lower $P_{th}$. Moreover, while the best received power cooperation scheme always has better performance than the nearest scheme, the difference is only slight when detecting the closest PU-receiver's beacon. Contrary to the missed detection probability, the false alarm probability is very high for low $P_{th}$ values and drops sharply as $P_{th}$ increases. As expected, co-operation slightly increases the false alarm probability. The multiple random scheme with PU-receiver beacons has the worst performance because this scheme takes input from multiple CUs; even a single false alarm from one CU makes the final decision a false alarm. Moreover, the nearest and best received power co-operation schemes show almost identical performance with respect to the false alarm probability. It should also be noted that as unlicensed users, CUs should err in the side of false alarm rather than missed detection.

The behaviour of $P_{md}$ for the multiple random scheme (eq. 4.13) is investigated in Fig. 4.4 under different values of $M$ and primary node density $\lambda_p$. For both separate and closest methods of primary beacon detection, the missed detection probability approaches $1$ when $\lambda_p$ is low. Increasing the number of cooperating nodes $M$ does not help significantly. However, when $\lambda_p$ increases to $10^{-3}$, increasing $M$ has some effect. Furthermore, the performance gap between these two methods becomes apparent. Moreover, all curves flatten out indicating that the effect of $\lambda_s$ becomes negligible beyond $-40$ dB.

### 4.7.2 Beacons emitted by PU-transmitter nodes

We now focus on nearest CU-to-PU and random CU-to-PU schemes (eqs. 4.22 and 4.25). Parameter values of $\alpha = 3$ and $P_{b,p} = -20$ dBm are used. The latter reflects the fact that the PU-transmitters can manage high power levels. Fig. 4.5 shows how $P_{md}$ and $P_f$ of the two CBS schemes varies with the detection threshold $P_{th}$. The effect of cooperation is more pronounced for low $P_{th}$ values in terms of missed detection. The impact of the control channel is also seen. For example, a $10$ dB increase in the control power $P_{b,s}$ results in order of magnitude reduction of missed detection. For both $P_{b,s}$ values, the nearest CU to PU-transmitter scheme has a slightly lower missed detection probability compared with the random CU to PU-transmitter scheme. In

terms of false alarm, co-operation slightly increases $P_f$, and both co-operation schemes show very similar performance. When $P_{th}$ increases beyond $-100$ dBm, there is a sudden drop in the false alarm probability. Furthermore, as expected, when the control channel power increases, the false alarm probability is slightly higher as erroneous information is more readily received from co-operating devices.

In Fig. 4.6, we study the impact of the cell size; $P_{md}$ (eqs. 4.22 and 4.25) versus cell radius $R_{cell}$ is plotted. The most important insight from this graph is that the effect of cooperation decreases as cell radius increases when other parameters are kept constant, and that both CBS schemes converge in performance. This is due to a high $R_{cell}$ outweighing the effect from other parameters, and the overall performance gain diminishing. With a high $R_{cell}$ and a low cooperation radius $R_c$, the distance from the given CU to its cooperating node is high irrespective of the cooperation scheme causing similar secondary control channel missed detection probabilities. As expected, increasing the CU node spatial density $\lambda_s$ decreases $P_{md}$. This is especially important for the nearest CU to PU-transmitter scheme. For the random CU to PU-transmitter scheme, increasing $\lambda_s$ ensures that there is a CU available for cooperation within $R_c$. The effect of increasing $\lambda_s$ are mainly seen for lower cell radius values. Furthermore, the nearest CU to PU-transmitter scheme shows a slightly better performance than the random CU to PU-transmitter scheme for both $\lambda_s$ values. However, the performance increase is higher when $\lambda_s = 10^{-3}$.

The effect of the cooperation radius $R_c$ on the missed detection for the random CU to PU-transmitter scheme (4.25) is investigated in Fig. 4.7 for various levels of control signal power, $P_{b,s}$. A best-case cooperation radius can be observed, which ensures the lowest missed detection probability. When the cooperation radius approaches $0$, random cooperation approaches converge no cooperation as expected. However, as $R_c$ increases, the missed detection probability drops steeply to the best-case value. Furthermore, it is observed that the steepness of this reduction increases with the control signal power. Subsequent increases in $R_c$ up to $R_{cell}$ only result in a gradual increase in missed detection.

## 4.8 Conclusion

This chapter investigated the overall missed detection and false alarm probabilities of an interweave SU using several cooperative beacon sensing strategies. We captured the spatial randomness of PU and SU nodes via independent PPPs. The propagation effects included path loss

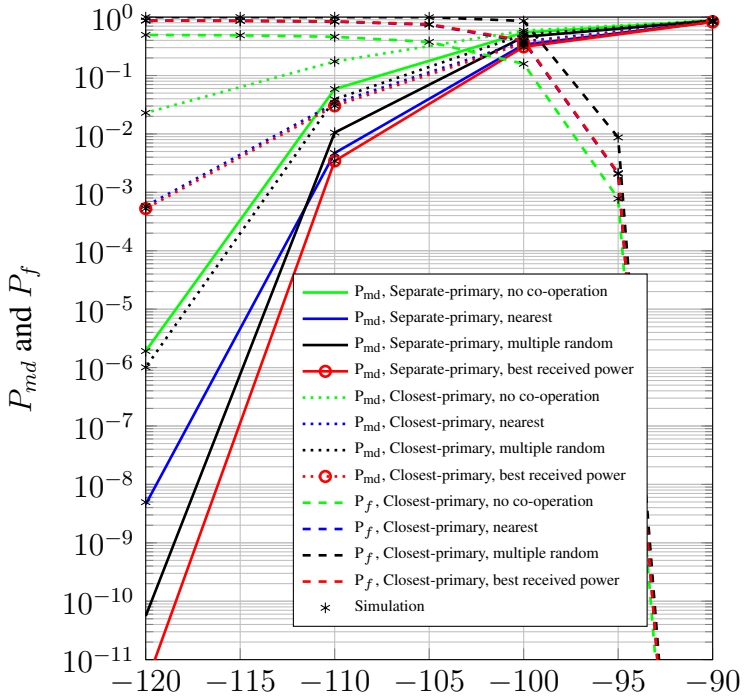


Figure 4.3: $P_{md}$ and $P_f$ for PU-receiver beacons as a function of $P_{th}$ for different cooperation schemes. $\lambda_p = 0.0001$, $\sigma^2 = 10^{-10}$, $\lambda_s = 0.0001$, and $M = 10$.

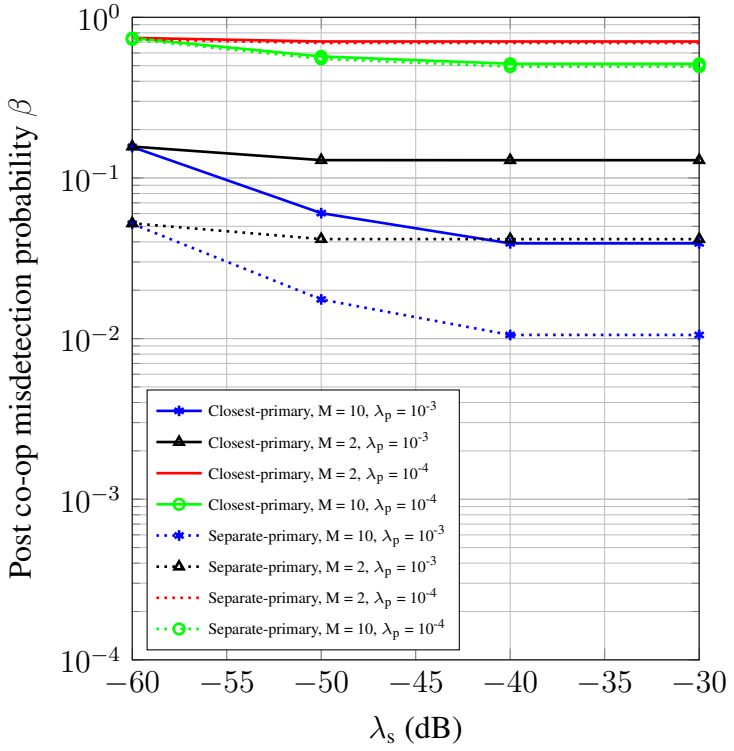


Figure 4.4: $P_{md}$ for PU-receiver beacons as a function of CU receiver density $\lambda_s$ for multiple random cooperation. $P_{th} = -110$ dBm.

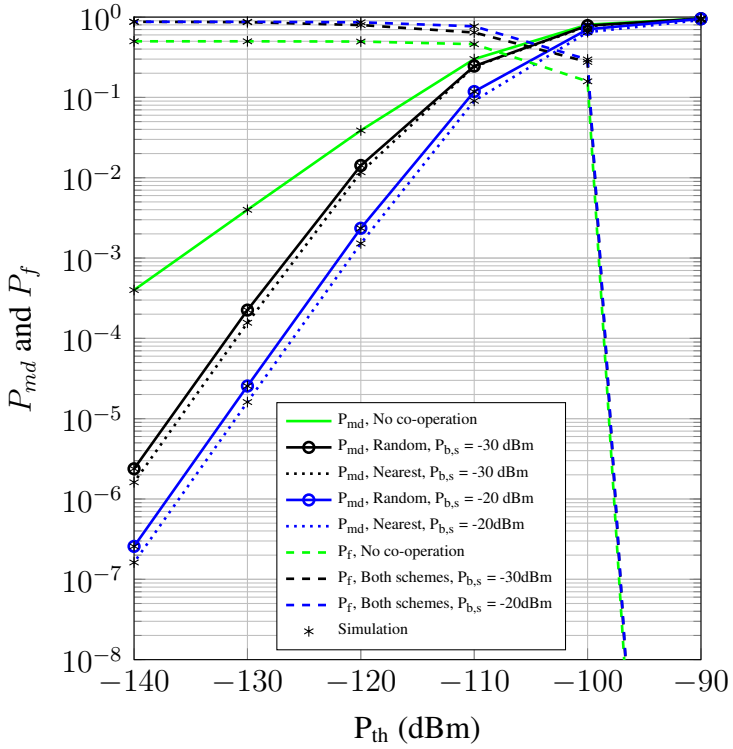


Figure 4.5: $P_{md}$ and $P_f$ as a function of $P_{th}$ for PU-transmitter beacons. $\lambda_s = 0.0001$, $R_{cell} = 1000$, $R_c = 500$, $\sigma^2 = 10^{-10}$ and $P_{b,p} = -20$ dBm.

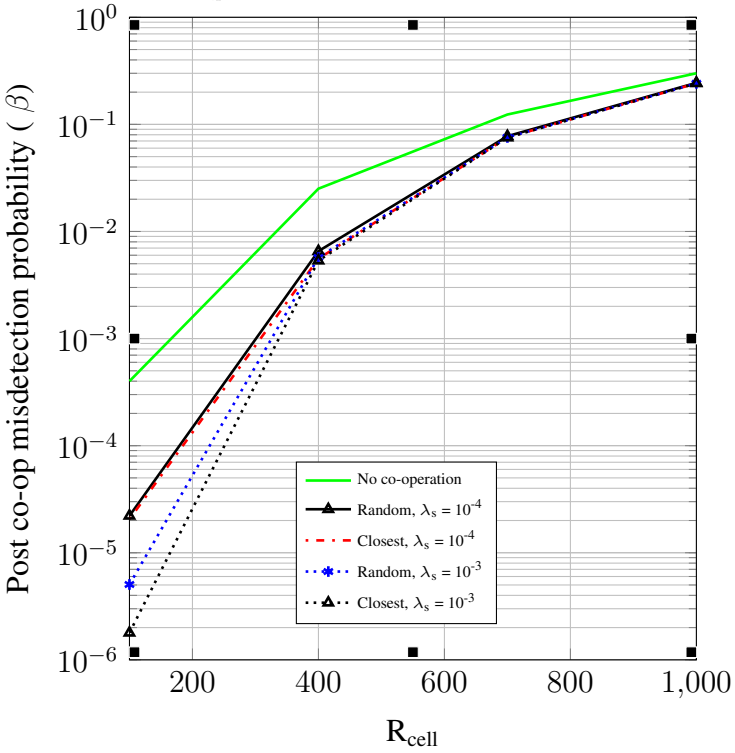


Figure 4.6: $P_{md}$ for PU-transmitter beacons as a function of $R_{cell}$. $R_c = 100$, $P_{b,p} = -20$ dBm, $P_{b,s} = -30$ dBm, and $P_{th} = -110$ dBm.

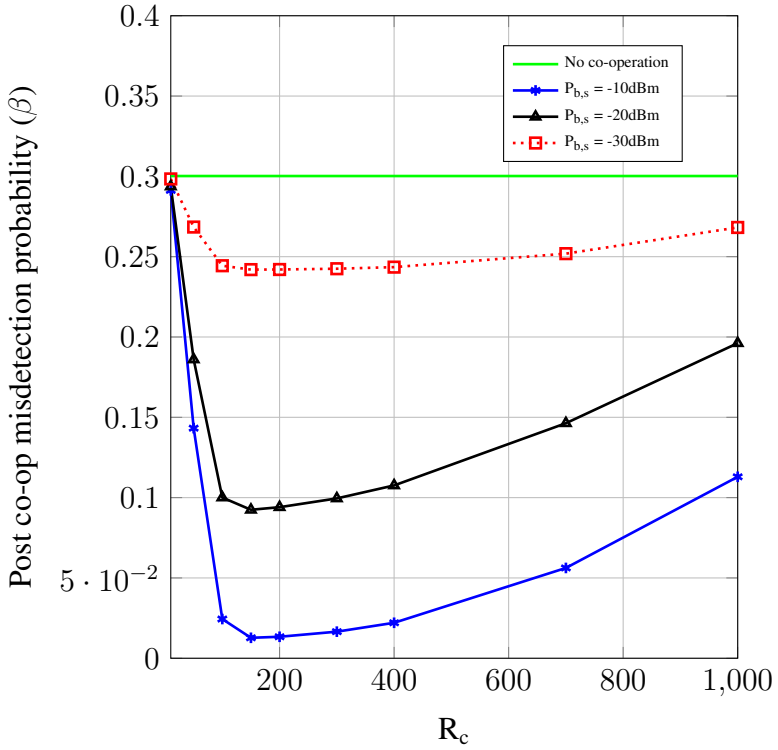


Figure 4.7: $P_{md}$ for PU-transmitter beacons as a function of $R_c$ for random cooperation. $R_{cell} = 1000$, $P_{b,p} = -20$ dBm, and $P_{th} = -110$ dBm.

and Rayleigh fading. Moreover, beacons emitted by both PU-receivers and PU-transmitters were considered. For the former, when sensing beacons emitted by the closest PU-receiver, multiple random CBS performs better when the reception threshold $P_{th}$ is lower; e.g., missed detection decreases by $10^4$ fold for thresholds as low as $-120$ dBm. However, the best received power scheme works slightly better for higher $P_{th}$. Moreover, the spatial density of PU-receiver nodes varies inversely with detection performance. Furthermore, the best received power scheme outperforms the nearest and multiple random cooperation schemes significantly when SUs sense primary beacons separately. When PU-transmitters send the beacons, a 10 dB increase in $P_{b,s}$ decreases the missed detection probability by 10 fold for both cooperation schemes. Furthermore, the effect of cooperation decreases for higher cell radii, and there exists a best case cooperation distance $R_c$ which provides the lowest missed detection probability for random cooperation. For PU-transmitter beacons, nearest cooperation provides slightly better results than random cooperation. In addition, it was seen that co-operation slightly increases the false alarm probability. Future research ideas extending this work include considering spatial and temporal correlation, considering other detection rules at the SU, and investigating the energy efficiency of cooperation

schemes for CR networks.

# Chapter 5

# Interference characterization for massive MIMO enabled transmitters in a cellular network

## 5.1 Introduction

The aggregate interference on the receiver of a secondary (unlicensed) user (SU) is one of the most fundamental performance limiting factors. The interference will reduce the achievable data rate and reliability (e.g., increasing outage). However, it is the direct result of allowing simultaneous spectrum access for both primary users (PUs) and SUs. But this is the fundamental premise of the underlay paradigm[31], a candidate for future fifth generation (5G) wireless systems, device-to-device (D2D) communications, sensor networks, and cognitive femtocells in heterogeneous networks [8], [9], [151]. Since cognitive radio (CR) underlay networks operate on an interference tolerant basis [8], [133], mitigating the interference on PU nodes via exclusion regions around PU receivers [93], maximum underlay transmit power thresholds, and interference temperature based channel access is the primary research focus of many works. In contrast, the aggregate interference on a SU receiver from PU and other SU transmissions has not been analyzed in detail.

This aggregate interference on a SU receiver constitutes two main parts (i) PU-to-SU interference and (ii) SU-to-SU interference. Both these interference terms depend on how transmitting nodes control their power, their receiver association policies, and their random locations. The interference depends on both large-scale and small-scale fading as well. Can this interference on a SU receiver be controlled by using spatial degrees of freedom? To this end, massive multiple input multiple output (MIMO) systems, with extremely large antenna arrays, provide exciting

prospects [46]. For instance, the integration of CR and massive MIMO cancels interference via the use of excessive spatial degrees of freedom, provides simultaneous service to a large number of users, increases spectral and energy efficiencies, and negates the effects of small scale fading and noise [8]. However, the successful integration faces technical challenges. The fundamental challenge of massive MIMO is the need for extensive channel state information (CSI) for the different transmitter-receiver links. In a time domain duplexing (TDD) set-up, channel reciprocity is exploited, and the CSI is commonly obtained via periodic uplink pilot transmissions. However, the length of the pilots are practically constrained by the channel coherence time[1] and the acceptable pilot overhead[2]. Therefore, the number of orthogonal pilots are limited, and pilot reuse by different base stations in both primary and SU networks leads to pilot contamination which generates focused interference to the links using the same pilot sequence. Pilot contamination is a fundamental bottleneck in massive MIMO systems, which limits the potential spectral and throughput gains [46]. Overall, all these factors and in turn the aggregate interference tightly depends on spatial randomness of the nodes, which must be modeled via stochastic geometry tools. Thus, statistical characterization of the aggregate interference on a SU receiver using stochastic geometry approaches is the focus of this chapter.

### 5.1.1 Problem statement and contribution

In this chapter, we derive the statistics of the aggregate interference on a SU receiver node due to both PU and SU transmissions, and investigate its impact on the performance. We will incorporate pilot contamination (when base stations employ massive MIMO), spatial randomness of nodes, power control and receiver association procedures, and channel imperfections.

Our study is motivated by a number of questions. While interference issues in underlay CR networks have been extensively investigated, for analytical tractability, it is not uncommon to ignore power control and receiver association schemes, and omitting spatial randomness [121], [153]–[156]. How do these assumptions affect of the overall interference levels? Moreover, how do we characterize the aggregate interference when there are massive MIMO enabled base stations with power control techniques? Furthermore, how do we incorporate a network of PU and SU nodes where the locations and numbers of transmitter/receiver nodes are random without

[1]This is the time period in which the channel response can be assumed to be constant. For standards like LTE and UMTS, this is practically in the range of 1-2 ms [152].

[2]The proportion of symbols within the coherence time used for pilot transmissions is an overhead because it does not lead to any effective data transfer.

restricting the system model to a single PU transmitter receiver pair or a single cell with one massive MIMO enabled base station?

To further investigate such questions, in this chapter, we begin by representing PU nodes (transmitters and receivers) with two independent homogeneous Poisson point processes in $\mathbb{R}^2$ (Fig. 5.1). We will consider two models for the underlay system: 1) a Matern cluster process with the underlay base stations representing the cluster heads distributed as a homogeneous Poisson point process, and 2) underlay base stations and receivers distributed in $\mathbb{R}^2$ as independent homogeneous Poisson point process. The Matern cluster process is considered because certain practical network configurations tend to be clustered. The PU receiver nodes have exclusion zones around them. When a SU transmitter falls within this zone, it has to stay silent.

The base stations are either single antenna or equipped with massive MIMO, with CSI being obtained via uplink pilots. Log distance path loss and independent Rayleigh fading are assumed for all channels. Furthermore path loss inversion based power control is considered. While channel inversion or feedback based power control schemes exist [157], they are beyond the scope. PU receivers associate with their closest base station. For the underlay system, we consider three association schemes: 1) a transmitter initiates a connection with the closest receiver, 2) a receiver initiates an association with the closest transmitter, and 3) the receiver associates with the base station at the cluster head. We characterize the performance of an associated SU receiver by deriving the moment generating function (MGF) of the aggregate interference for the single antenna case, and the MGF, mean, and variance of the normalized aggregate interference for the massive MIMO case along with the outage probability.

### 5.1.2 Prior research

Extensive interference characterization and modelling of underlay networks includes developing analytical results based on the MGF, moments, cumulants, outage, and coverage. For instance, [38] develops interference models considering power control, contention control, and hybrid power-contention control schemes. The success probability, spatial average rate, and area spectral efficiency are derived for cellular and underlay D2D users under Rician fading [158], and it is shown that these measures depend on user density, channel propagation parameters, and spectrum occupancy ratios. The authors in [158] further propose a centralized opportunistic access control scheme as well as a mode selection mechanism to reduce cross tier interference. An

analytical framework to characterize the area spectral efficiency of a large Poisson underlay SU network is proposed in [159]. The authors highlight shaping medium access and transmit power as available degrees of freedom in designing the SU network, and shows that an area spectral efficiency wall exists. Furthermore, [80] proposes an adaptive power control scheme for SU systems in a Rayleigh fading channel which maximizes the output signal to noise ratio (SNR) and the interference, and shows that this scheme can achieve up to a 3 dB SNR gain. Reference [160] proposes a limited feedback based underlay spectrum sharing scheme for Poisson cognitive networks, with the benefit that the secondary area spectral efficiency increases with the secondary outage constraint. Moreover, interference on a PU receiver is characterized [119] by considering constraints on a secondary (underlay) transmitter from both primary and secondary systems.

The integration of massive MIMO and underlay CR is an emerging research area. Thus, interference issues in randomly deployed massive MIMO base stations are investigated in [153], [161]–[165]. For example, the interference from massive MIMO enabled cellular networks to D2D networks is studied in [164] under perfect and imperfect CSI at the receivers. With perfect CSI, it is observed that underlay contamination arises in addition to pilot contamination. The trade-offs between the average sum rate and energy efficiency is studied in [165], and in order for these parameters to improve from the high number of antennas, the number of cellular users should be a function of the number of base station antennas. Moreover, in order for massive MIMO and underlay D2D to coexist, the density of D2D users must be low. Reference [163] derives closed-form expressions for the base station density bounded by the maximum outage probability and concludes that the base station density must be below a certain bound to fulfill coverage requirements, while [153] obtains signal-to-interference-ratio expressions for both uplink and downlink under orthogonal and non-orthogonal pilot sequences and shows that the downlink signal to interference ratio is limited by the inverse of the total pilot correlation. Furthermore, the uplink of a wireless network using linear minimum mean square error spatial processing is analyzed in [161], and the distribution of the spectral efficiency in the interference limited regime is derived. Moreover, [162] analyzes the coverage probability and area spectral efficiency for a heterogeneous network showing that significant throughput gains can be achieved by interference nulling and co-ordination among the tiers.

There are two main differences between our work and previous literature. First, most of the work involving massive MIMO do not consider a stochastic set-up, and thus do not consider

the dynamics of association policies and path loss. Second, while some works -notably [153]- consider a PPP of base stations, they assumed a fixed transmit power level. While this assumption lends itself to a simpler analysis, transmit power control procedures are part and parcel of modern systems, and thus need to be considered in a meaningful analysis.

## 5.2 System model and assumptions

### 5.2.1 Spatial model

This section describes the spatial distribution of primary and underlay nodes.

**Primary network**

A single class of PU transmitters (base stations) distributed randomly in $\mathbb{R}^2$ is considered. Although node locations in actuality are not purely random (e.g. base station locations are planned), a point process can accurately approximate even planned node placements while providing analytical tractability [12], [14]. The Poisson point process model has thus been extensively used to model node locations [37], [38], [67], [142] for cognitive, D2D, and heterogeneous networks. Thus, to develop a general analysis and to avoid special cases, we assume homogeneous Poisson point processes for both PU transmitters and receivers.

Let the PU transmitters be distributed as a stationary homogeneous Poisson point process $\Phi_{p,t}$ with intensity $\lambda_{p,t} > 0$. Due to the homogeneity of $\Phi_{p,t}$, $\lambda_{p,t}$ is a constant over all $\mathbb{R}^2$. The PU receivers are also modeled similarly and denoted by $\Phi_{p,r}$ with spatial intensity $\lambda_{p,r} > 0$. $\Phi_{p,r}$ and $\Phi_{p,t}$ are considered to be independent, stationary, and motion invariant. Moreover, the PU receiver locations are independent of PU transmitters. It should be noted that the Matern Cluster model [68] which will be employed for modelling the underlay network can also be used for the PU network.

One significant aspect of underlay networks is the guard (exclusion) region [37], [121]. We will assume that a guard region exists around each PU receiver having a constant radius of $R_G$, and that the SUs perfectly know it.

**Underlay network**

For this, we will consider two separate configurations. For both configurations, it is assumed that the SU devices are spatially independent from the primary transmitters and receivers.

- *Cluster model*:

In this configuration, we will model this network as a Matern cluster process [68]–[70]. This model consists of multiple node clusters centered around underlay base stations [69]. The Matern Cluster process is formally defined as follows [70]. Let $\Phi_{u,t} = \{a_1, a_2, a_3...\}$ be a homogeneous Poisson point process representing cluster centers with intensity $\lambda_{u,t} > 0$, and $B_i$ is a set of Poisson point processes conditional on $\Phi_{u,t}$ centred on $a_i$ $(\forall i)$ where each $B_i$ is independent of each other and stationary. The resulting cluster process $\Phi_{u,r} = \cup_i B_i$ is a Matern cluster process if $B_i$ is uniformly distributed within a ball $b(a_i, d_l)$ with density $\lambda_{u,r}$ centred at $a_i$ and having a radius $\frac{d_l}{2}$. The cluster centers correspond to base stations while the daughter processes correspond to the receivers. The cluster radii, admission of receivers, and scheduling within the clusters are dependent on the specific network parameters. A wireless local area network or a nano/pico cell base station are examples where clustering could occur [70] for the SU network.

- *Voronoi model*:

  Here, the SU base stations and receivers are distributed randomly in $\mathbb{R}^2$ as two independent and stationary homogeneous PPPs $\Phi_{u,t}$ and $\Phi_{u,r}$ with spatial densities $\lambda_{u,t}$ and $\lambda_{u,r}$. The Voronoi model is useful for analyzing wireless ad-hoc networks and dual macro-micro cell networks. Moreover, this model is also useful whenever a set of wireless local area and pico cell base stations belonging to the same network cover a particular area.

### 5.2.2 Signal model

We assume universal frequency re-use within the primary network. All channel power gains are independent and identically distributed and are independent of the underlying point processes. While the path loss is power-law, small scale fading is modelled as Rayleigh. The channel power gain $|h|^2$ is thus distributed as (2.4). From the simplified path loss model [3], the received power $P_R$ at a distance $r$ from the transmitter is $P_R = Pg(r)$ with $g(r) = r^{-\alpha}$, where $P$ is the transmit power level and $\alpha$ is the path loss exponent. Practically, $\alpha$ can range from around $2 - 6$, and the special case of $\alpha = 2$ occurs when the propagation is through free space [76]. However, $\alpha$ values slightly less than 2 may occur in tunnels due to the wave guide effect. But, having $g(r) = r^{-\alpha}$ creates analytical complications when $r < 1$. Thus, for tractability, we will also use $g(r) = min(1, r^{-\alpha})$ [74] where necessary. Since spatial densities are small, the probability of having a device within 1m is negligible, and both forms of $g(r)$ will yield the same results.

**Multiple antenna case**

SU and PU receivers are single antenna devices while PU transmitters and SU transmitters have $M$ and $N$ antennas respectively, which are constant. $M$ and $N$ have the relationship $M = \kappa N$. A time division duplex (TDD) scheme is assumed for both primary and underlay networks [153].

Both primary and SU networks utilize pilots in the uplink channel to estimate CSI for the downlink. The pilots are of length $L$, and are mutually orthogonal. That is, pilot sequences satisfy $x_a^* x_b = 0$ whenever $a \neq b$, where $x_a, x_b \in \mathbb{C}^{L\times 1}$ are pilot sequences. We assume a set of $q$ orthogonal pilots used by all primary and underlay base stations [153]. We assume that the training phase for all base stations occur simultaneously regardless of whether they are part of the primary or underlay network [153]. These assumptions lead to the maximum level of pilot contamination. Furthermore, the channel gains are static between the training phase and the downlink data transmission phase.

### 5.2.3 Power control and transmitter-receiver association

Both primary and SU transmitters employ path loss inversion based power control to ensure a fixed average power[3] at their receivers [38]. Note however that the instantaneous received power fluctuates due to small scale fading. Thus, the transmit power $P_T$ becomes $P_T = P_* r^\alpha$, where $r$ is the transmitter-receiver distance, $\alpha$ is the path loss exponent, and $* \in \{u, p, \{p, u\}, \{p, p\}\}$ denote underlay, primary, underlay pilots, and primary pilots. This form of power control ensures that all receivers reach the same received power, where receivers close to the transmitters are not at an unfair advantage. Moreover, for the multiple antenna case, power scaling is employed by the primary and underlay base stations where the downlink transmitted signal is scaled by $\frac{1}{\sqrt{M}}$ and $\frac{1}{\sqrt{N}}$ respectively to compensate for the number of transmitter antennas. The inverse of the square root of the number of antennas has been shown to be an appropriate scaling factor for Rayleigh fading and imperfect CSI [166].

In the primary network, the PU receiver associates with the closest PU transmitter (base station). It should be noted that if the number of users within a PU transmitter's cell exceeds $q$, some users will not be served. Such association provides the best average received power. With this scheme, the PU transmitters form Voronoi cells[4] (shown in Fig. 5.1), and associate with

[3]This power level can either be the receiver sensitivity or the receiver sensitivity plus an appropriate fade margin.

[4]A Voronoi tessellation divides an area of $\mathbb{R}^2$ into different regions depending on the distance to a specific set of nodes. For each node, its corresponding Voronoi cell consists of points which are closer to it than to any other node

intra-cell receivers.

For the underlay network, we consider several association schemes. These are categorized according to the number of antennas at a SU transmitter:

- *Single antenna case*

  Here, we consider 2 different association policies for the Voronoi model: 1) the receiver initiates communication and selects the closest available transmitter, and 2) the transmitter initiates the communication and selects the closest available receiver. These policies are valid for networks such as ad-hoc and D2D networks (Case 1 corresponds with a typical cellular mobile or digital TV user while case 2 corresponds with an ad-hoc or sensor network). We assume that all available transmitters (with a density of $\bar{\lambda}_{u,t}$) are associated with receivers, and occurrences of multiple transmitters associating with a single receiver are permissible. For both aforementioned schemes, the selection of transmitters and receivers only occurs whenever they are within a distance of $D$ from the initiating receiver or transmitter. The maximum allowable distance $D$ ensures that the transmit power level would not increase beyond the maximum possible power level, and is analogous to having a maximum cut-off power level.

  For the cluster model, the receivers associate with their cluster head (parent node).

- *Multiple antenna case*

  Underlay association schemes for the multiple antenna case are as follows. With a cluster model, the associated base station is the cluster head, while with a Voronoi model, the receivers associate with the closest base station similar to the association policy of the primary network. In a scenario where the transmitter has a large number of antennas, it is a fully fledged base station, and not part of an ad-hoc network. Therefore, situations where transmitters initiate the communication procedure in the downlink are rare, and transmitters would have sufficient power which makes the maximum allowable distance irrelevant.

## 5.3 Outage analysis for the single antenna case

Within this section, we derive the outage probability of an active SU receiver along with the MGF of the interference. We assume that the receiver is associated with a transmitter successfully.

Let $r$ be the distance between the SU receiver and the associated transmitter. The received power $P_R$ may be written as $P_R = P_u r^{\alpha} r^{-\alpha} |h|^2 = P_u |h|^2$. Thus, given that an association

has occurred, neither the association policy for the underlay network nor $r$ play any role in the received power. However, other SU and all PU transmissions generate interference. Let $I_p$, $I_u$, and $\sigma^2$ be the interference from the primary and underlay networks, and the noise variance respectively. The signal to interference and noise ratio (SINR) at the SU receiver ($\gamma$) is written as $\gamma = \frac{P_u|h|^2}{I_p+I_u+\sigma^2}$. The CDF of the SINR ($F_\gamma(x)$) can be obtained as (See Chapter 3.4)

$$F_\gamma(x) = 1 - e^{(-\frac{x\sigma^2}{P_u})} M_{I_p}\left(\frac{x}{P_u}\right) M_{I_u}\left(\frac{x}{P_u}\right). \tag{5.1}$$

Substituting the required SINR threshold ($T$) instead of $x$ gives us the outage probability. However, in order to evaluate this, the MGFs of $I_p$ and $I_u$ are needed, which will be derived next. The MGF can also be used to calculate additional statistics of the interference such as thoughput and bit error rate [89]–[91].

### 5.3.1 Interference from the primary network

The primary interference on the SU receiver can be written as $I_p = \sum_{i\in\Phi_{p,t}} I_{p,i}$, where $I_{p,i}$ is the interference from the $i$-th PU transmitter. We can write $I_{p,i}$ as $I_{p,i} = P_P|h|^2 r_p^{-\alpha}$, where $P_P$ is the transmit power of a PU transmitter and $r_p$ is its distance to the SU receiver in question. Without loss of generality, we consider this SU receiver to be at the origin. A useful trick is mapping the intensity function from 2-D to 1-D to provide better mathematical tractability. Therefore, using the Mapping Theorem [73], the 1-D intensity of the PU transmitters with respect to the SU receiver ($\tilde{\lambda}_{p,t}$) can be written as $\tilde{\lambda}_{p,t} = 2\pi\lambda_{p,t} r_p$.

The MGF of $I_p$ is defined as $M_{I_p}(s) = \mathbb{E}[e^{-sI_p}]$. By the Campbell's theorem [73], $M_{I_p}(s)$ is written as

$$M_{I_p}(s) \;=\; e^{\left(\int_0^\infty \mathbb{E}\left[e^{-sP_P|h|^2 r_p^{-\alpha}}-1\right] 2\pi\lambda_{p,t} r_p dr_p\right)}, \tag{5.2}$$

where the expectation is with respect to $|h|^2$ and $P_P$. The evaluation of (5.2) requires the distribution of $P_P$. However, due to the distance dependent power control, $P_P = P_p r_{p,tx}^{\alpha}$, where the distance between a PU transmitter, and the associated receiver is $r_{p,tx}$. Thus, the problem is to find the distribution of $r_{p,tx}$.

However, finding the exact distribution of $r_{p,tx}$ is difficult, and thus we will approximate it. We assume that $r_{p,tx}$ is independent from the distances to other PU transmitters. However, as the

PU network forms Voronoi cells and because each Voronoi cell has only a single PU transmitter as its nucleus, coupling is introduced between the cells [167]. As such $r_{p,tx}$ is correlated with corresponding transmitter-receiver distances within other Voronoi cells. Furthermore, the probability that there are no receivers associated with a given transmitter is greater than zero. However, this probability is negligible when the primary receiver density is much larger than the primary transmitter density ($\lambda_{p,r} >> \lambda_{p,t}$), which is the case in practice.

Thus, using the distribution of the nearest node from a point within a PPP [126], the distance $r_{p,tx}$ is approximately distributed with the PDF $f_{r_{p,tx}}(x) = 2\pi\lambda_{p,t}xe^{-\pi\lambda_{p,t}x^2}$ which is given by $Ral(\pi\lambda_{p,t})$.

The 1-D intensity of PU receivers with respect to a PU transmitter ($\tilde{\lambda}_{p,r}$) is $\tilde{\lambda}_{p,r} = 2\pi\lambda_{p,r}r, 0 < r < \infty$. Let $\nu$ be the probability that any PU receiver has the PU transmitter concerned as the closest PU transmitter. We assume $\nu$ is independent for each PU receiver. Using the Coloring Theorem [73], we can perform independent thinning on the process of PU receivers to obtain the intensity of the process of PU receivers which have the given PU transmitter as the closest ($\bar{\lambda}$). $\bar{\lambda}$ is given by $\bar{\lambda} = \nu\tilde{\lambda}$. To find $\nu$, we need to use the void probability for PPPs. In other words, there should be 0 PU transmitters within an annular area of radius $r$. The probability of having $n$ nodes within a given area $A$ is [65] $P(n) = \frac{(\lambda_{p,t}A)^n}{n!}e^{-\lambda_{p.t}A}$. Therefore, $\nu$ is obtained as $\nu = e^{-\pi\lambda_{p,t}r^2}$, and $\bar{\lambda}$ is derived as $\bar{\lambda} = 2\pi\lambda_{p,r}r_{p,tx}e^{-\pi\lambda_{p,t}r_{p,tx}^2}$, where $r_{p,tx}$ was substituted for $r$. The CDF of $r_{p,tx}$ is given by

$$F_{r_{p,tx}}(x) = \frac{\int_{r_{p,tx}=0}^{x}\bar{\lambda}dr}{\int_{r_{p,tx}=0}^{\infty}\bar{\lambda}dr} = 1 - e^{-\pi\lambda_{p,t}x^2}. \tag{5.3}$$

Differentiating (5.3) gives the PDF.

Coming back to the original objective of finding $M_{I_p}(s)$, we can perform the expectation on (5.2) with respect to $|h|^2$ and obtain $M_{I_p}(s) = e^{\left(\int_0^\infty \mathbb{E}\left[\frac{1}{1+sP_p r_{p,tx}^{\alpha} r_p^{-\alpha}}-1\right]2\pi\lambda_{p,t}r_p dr_p\right)}$, where the remaining expectation is with respect to $r_{p,tx}$. When $\alpha > 2$, changing the order of integration and averaging results in

$$M_{I_p}(s) = e^{\left(-\frac{2\pi^2\lambda_{p,t}}{\alpha}\frac{(sP_p)^{\frac{2}{\alpha}}}{\sin\left(\frac{2\pi}{\alpha}\right)}\mathbb{E}\left[r_{p,tx}^2\right]\right)} = e^{\left(-\frac{2\pi}{\alpha}\frac{(sP_p)^{\frac{2}{\alpha}}}{\sin\left(\frac{2\pi}{\alpha}\right)}\right)}. \tag{5.4}$$

The mean interference $\mathbb{E}[I_p]$ is another important performance measure. $\mathbb{E}[I_p]$ can be used to

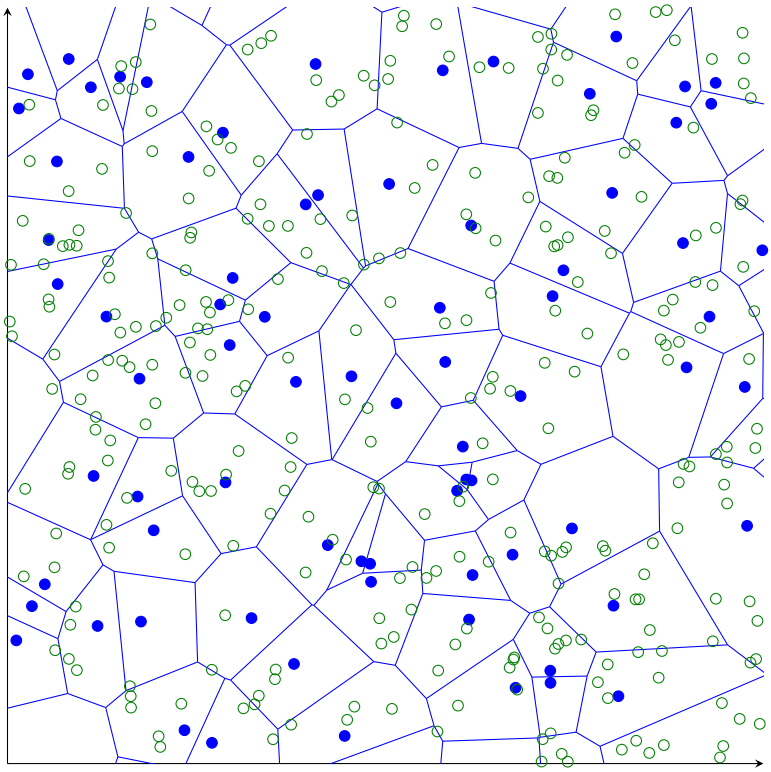

Figure 5.1: Primary network layout: blue circles = PU transmitters, and green circles = PU receivers. The PU transmitters and receivers are distributed as independent homogeneous Poisson point processes. The receivers within each Voronoi cell connect to the corresponding transmitter. Note that underlay nodes are not shown.

gauge the severity of interference affecting a particular device. Furthermore, $\mathbb{E}[I_p]$ is also vital when approximating the interference to another well-known distribution, or when simplifying the interference component when calculating an approximation for the outage. From the Campbell's theorem [73], we can write

$$\mathbb{E}[I_p] \quad = \quad \int_0^{\infty} \mathbb{E}_{|h|^2, r_{p,tx}} \left[ P_p |h|^2 r_{p,tx}^{\alpha} r_p^{-\alpha} \right] 2\pi\lambda_{p,t} r_p dr_p. \tag{5.5}$$

The integration in (5.5) does not necessarily converge because the simplified path loss model does not hold when $r_p < 1$, and thus we take $g(r) = min(1, r^{-\alpha})$ as illustrated in Section II B. Moreover, in practical channels $\alpha > 2$. Using these facts and breaking the integration in (5.5) into two separate parts, we obtain $\mathbb{E}[I_p]$ in closed-form as

$$\mathbb{E}[I_p] = 2P_p \frac{\Gamma(\frac{\alpha}{2}+1)}{(\pi\lambda_{p,t})^{\frac{\alpha}{2}-1}} \left( \frac{1}{\alpha-2} + \frac{1}{2} \right). \tag{5.6}$$

It should be noted that 5.6 does not hold when $\alpha \leq 2$.

### 5.3.2 Interference from the underlay network

In addition to the interference from the primary network, a given SU receiver will experience interference from other unassociated SU transmitters. We will now consider this interference $I_u$.

As mentioned in Section II, because SU nodes must not transmit whenever they are within the guard region of a PU receiver, the active SU transmitters actually form a Poisson hole process [121], which is defined as follows. When $\Phi_A$ and $\Phi_B$ are independent homogeneous PPPs, and $\forall x \in \Phi_A$, points from $\Phi_B$ are removed within a radius $b$ from $x$, the remaining points of $\Phi_B$ form a Poisson hole process [121]. However, the Poisson hole processes is not mathematically tractable, and its probability generating functional is not known [121]. Instead, we can approximate the active SU transmitters as an independently thinned PPP using the coloring theorem [73]. If $\bar{\lambda}_{u,t}$ is the density of the active SU transmitters, it can be written as $\bar{\lambda}_{u,t} = \delta\lambda_{u,t}$, where $\delta$ is the probability that any particular transmitter doesn't fall within the guard region of a PU receiver. Using the void probability, $\delta$ is obtained as $\delta = e^{-\pi\lambda_{p,r}R_G^2}$, and $\bar{\lambda}_{u,t} = \lambda_{u,t}e^{-\pi\lambda_{p,r}R_G^2}$. However, recent research has established tight bounds for the interference from Poisson hole processes which performs better than the independent thinning approximation [168]. But, the mathematical tractability is less.

We will now derive the MGF of $I_u$ for the two different system models for the underlay network.

#### Voronoi model

When the Voronoi model is considered for the underlay network, we will consider two cases of association where : 1) the receiver selects the closest transmitter, and 2) the transmitter initiates communication and selects the closest receiver. The first scheme is more prevalent in traditional mobile networks for the downlink and wireless LAN while the second scheme is more suitable for ad-hoc and sensor networks.

- *Receiver selects the closest transmitter*

  In this scheme, a receiver selects the closest transmitter to associate. Let the available SU transmitters be denoted as the PPP $\bar{\Phi}_{u,t}$. If the receiver is connected to the SU transmitter $z \in \bar{\Phi}_{u,t}$, the total interference from the underlay network is written as $I_u = \sum_{i\in\bar{\Phi}_{u,t}\setminus z} I_{u,i}$, where $I_{u,i}$ is the interference from the $i$-th SU transmitter. $I_{u,i}$ is written

as $I_{u,i} = \mathcal{B}P_s|h|^2 r_s^{-\alpha}$, where $P_s$ is the transmit power of a SU transmitter defined as $P_s = P_u r_{u,tx}^{\alpha}$ and $r_{u,tx}$ is the distance between a SU transmitter and the associated receiver. $r_s$ is the distance from an interfering SU transmitter to the SU receiver in question, and $\mathcal{B}$ is a Bernoulli random variable taking on the value 1 when $r_{u,tx} < D$, and 0 otherwise.

Using the same technique used to obtain the distribution of $r_{p,tx}$, the distribution of $r_{u,tx}$ can be shown to have the approximate PDF $Ral(\pi\bar{\lambda}_{u,t})$. Let $\beta$ be the probability that $r_{u,tx} < D$. Then, $\beta = 1 - e^{-\pi\bar{\lambda}_{u,t}D^2}$.

Using the Campbell's theorem, we can write $M_{I_u}(s)$ as

$$M_{I_u}(s) = e^{\left(\int_r^{\infty} \mathbb{E}_{r_{u,tx}}\left[1-\beta+\frac{\beta}{1+sP_u r_{u,tx}^{\alpha} r_s^{-\alpha}}-1\right] 2\pi\bar{\lambda}_{u,t} r_s dr_s\right)}, \tag{5.7}$$

where $r(< D)$ is the distance between the receiver in question and the associated transmitter. For any given associated receiver, $r$ is deterministic. A closed-form solution for (5.7) is not apparent, and can be solved using numerical techniques. A simplified equation for $M_{I_u}(s)$ obtained after some manipulations and a series expansion when $sP_u r_{u,tx}^{\alpha} r_s^{-\alpha} < 1$ as

$$M_{I_u}(s) \quad =\approx \quad e^{\left(2\pi\bar{\lambda}_{u,t}\sum_{k=1}^{\infty}\frac{(-sP_u)^k}{(\alpha k-2)(\pi\bar{\lambda}_{u,t})^{\frac{\alpha k}{2}}} r^{2-\alpha k}\left(\Gamma\left(\frac{\alpha k}{2}+1\right)-\Gamma\left(\frac{\alpha k}{2}+1,\pi\bar{\lambda}_{u,t}D^2\right)\right)\right)}, sP_u << 1 \tag{5.8}$$

This method works when $s << \frac{1}{P_u}$, and this condition is satisfied for practical system parameters. Furthermore, the mean interference $\mathbb{E}[I_u]$ can be derived as

$$\mathbb{E}[I_u] \quad \approx \quad \frac{(2\pi\bar{\lambda}_{u,t}P_u}{(\alpha-2)(\pi\bar{\lambda}_{u,t})^{\frac{\alpha}{2}}} r^{2-\alpha}\left(\Gamma\left(\frac{\alpha}{2}+1\right)-\Gamma\left(\frac{\alpha}{2}+1,\pi\bar{\lambda}_{u,t}D^2\right)\right), sP_u << 1 \tag{5.9}$$

For the special case when we do not take $r$ to be deterministic, we need the distribution of $r$. It is obtained by conditioning the distance distribution from any SU receiver to its active closest SU transmitter (given as $Ral(\pi\bar{\lambda}_{u,t})$) by the condition that the maximum allowable distance is $D$ (the distance from any SU receiver to its active closest SU transmitter should not exceed $D$, and this event occurs with a probability of $1 - e^{-\pi\bar{\lambda}_{u,t}D^2}$). As such, we can write $f_r(x) = \frac{Ral(\pi\bar{\lambda}_{u,t})}{1-e^{-\pi\bar{\lambda}_{u,t}D^2}}$, which is expressed for notational simplicity as $TRal(\pi\bar{\lambda}_{u,t}, D)$.

Therefore, if (5.8) is written as $M_{I_u}(s) = e^{\mathcal{W}}$, $M_{I_u}(s)$ for non-deterministic $r$ becomes $M_{I_u}(s) = e^{\mathbb{E}_r[\mathcal{W}]}$. However, $\mathbb{E}_r[\mathcal{W}]$ does not necessarily converge for $k > 1$. But, when $sP_u << 1$ and $\alpha < 4$, the summation in (5.8) can be accurately approximated by the first term. As such, the MGF can be written as

$$M_{I_u}(s) \approx e^{\left(\frac{-2sP_u}{(\alpha-2)(1-e^{-\pi\bar{\lambda}_{u,t}D^2})}\left(\Gamma\left(\frac{\alpha}{2}+1\right)-\Gamma\left(\frac{\alpha}{2}+1,\pi\bar{\lambda}_{u,t}D^2\right)\right)\left(\Gamma\left(2-\frac{\alpha}{2}\right)-\Gamma\left(2-\frac{\alpha}{2},\pi\bar{\lambda}_{u,t}D^2\right)\right)\right)}, sP_u << 1, \quad (5.10)$$

- *Transmitter selects the closest receiver*

  Here, the association attempt is initiated by the SU transmitter corresponding to a situation where those nodes are the data generators. Within this scheme, an available SU transmitter ($\in \bar{\Phi}_{u,t}$) selects the nearest SU receiver to associate with.

  Let the SU receiver for which performance is analyzed be connected to the SU transmitter $z \in \bar{\Phi}_{u,t}$. The total interference from the underlay network is written similar to the previous scheme as $I_u = \sum_{i\in\bar{\Phi}_{u,t}\setminus z} I_{u,i}$. $I_{u,i}$ is written as $I_{u,i} = \mathcal{C}P_s|h|^2 r_s^{-\alpha}$, where $P_s$ is the transmit power of a SU transmitter defined as $P_s = P_u r_{s,rx}^{\alpha}$. $r_{s,rx}$ is the distance between a SU transmitter and the closest receiver and $\mathcal{C}$ is a Bernoulli random variable taking on the value 1 when $r_{s,rx} < D$, and 0 otherwise. Using the void probability of a PPP [73], the distance $r_{s,rx}$ can be shown to have the PDF $Ral(\pi\lambda_{s,r})$. Let $\zeta$ be the probability that $r_{s,rx} < D$. Then, $\zeta = 1 - e^{-\pi\lambda_{s,r}D^2}$.

  Unlike the previous scheme, a complication arises when evaluating the MGF of $I_u$. Although a transmitter selects its closest receiver node, from the point of the SU receiver for which performance is evaluated, transmitter $z$ is not the closest transmitter in general. As such, we will approximate $I_u$ as $I_u \approx \sum_{i\in\bar{\Phi}_{u,t}} I_{u,i}$. In effect, our approximation gives an upper bound on the interference and thus the outage.

  With the Campbell's theorem, the MGF of the interference from underlay nodes $M_{I_u}(s)$ is written as $M_{I_u}(s) \approx e^{\left(\int_0^\infty \mathbb{E}_{r_s,rx}\left[1-\zeta+\frac{\zeta}{1+sP_u r_{s,rx}^{\alpha} r_s^{-\alpha}}-1\right]2\pi\bar{\lambda}_{u,t}r_s dr_s\right)}$. When $\alpha > 2$, the MGF becomes

$$M_{I_u}(s) \approx e^{\left(-\frac{2\pi\bar{\lambda}_{u,t}e^{-\pi\lambda_{s,r}D^2}}{\alpha\lambda_{s,r}}\frac{(sP_u)^{\frac{2}{\alpha}}}{\sin\left(\frac{2\pi}{\alpha}\right)}\left(e^{\pi\lambda_{s,r}D^2}-\pi\lambda_{s,r}D^2-1\right)\right)}. \quad (5.11)$$

The mean interference $\mathbb{E}[I_u]$ does not converge while using the simplified path loss model, and thus we will use $g(r_s) = \min((), 1, r_s^{-\alpha})$. Using this, $E[I_u]$ can be obtained as

$$\mathbb{E}[I_u]=\frac{\pi\alpha\bar{\lambda}_{u,t}P_u}{(\alpha-2)(\pi\lambda_{s,r})^{\frac{\alpha}{2}}}\left(\Gamma\left(\frac{\alpha}{2}+1\right)-\Gamma\left(\frac{\alpha}{2}+1,\pi\lambda_{s,r}D^2\right)\right). \tag{5.12}$$

**Cluster model**

Here, each SU receiver associates with its cluster head. We assume that all cluster heads (SU transmitters) outside the guard regions of PU receivers are available for association, and thus potentially active (with a density of $\bar{\lambda}_{u,t}$). If this assumption is not true, our analysis yields a worst-case performance benchmark. Let these available SU transmitters be denoted by the Poisson point process $\bar{\Phi}_{u,t}$, and the particular receiver node whose performance is analyzed is connected with the $z$-th cluster head where $z \in \bar{\Phi}_{u,t}$. The interference from SU transmitters $I_u$ is written as $I_u = \sum_{i\in\bar{\Phi}_{u,t}\setminus z} I_{u,i}$, where the interference from the $i$-th SU transmitter is given by $I_{u,i} = P_s|h|^2 r_{sc}^{-\alpha}$. $P_s$ is the transmit power of a SU transmitter, and $r_{sc}$ and $|h|^2$ are the distance and channel power gain between an underlay cluster head, and the SU receiver whose performance is analyzed. The transmit power of the SU transmitter is given by $P_s = P_u r_{c,tx}^{\alpha}$, where $r_{c,tx}$ is the distance between the $i$-th SU transmitter and its associated receiver. Due to the SU receivers within a cluster forming a homogeneous PPP, they are uniformly distributed spatially. Therefore, the CDF of $r_{c,tx}$ can be obtained by considering the number of nodes within a distance $x$ from the $i$-th SU transmitter as [88]

$$F_{r_{c,tx}}(x) = \frac{x^2}{\left(\frac{d_l}{2}\right)^2}, 0 < x < \frac{d_l}{2}. \tag{5.13}$$

Thus, the PDF of $r_{c,tx}$ is simply obtained by differentiating (5.13), and is expressed as $f_{r_{c,tx}}(x) = \frac{2x}{(d_l 2)^2}, 0 < x < \frac{d_l}{2}$, which is $Lin(\frac{d_l}{2})$.

Even though all SU transmitters outside guard regions should be active, if a SU receiver requiring association does not exist, the given SU transmitter remains inactive. Let $\rho$ be the probability that the cluster head is actually associated with a receiver. Thus $\rho$ is the probability that at least a single SU receiver exists within the cluster given by $\rho = 1 - e^{-\pi\lambda_{u,r}\left(\frac{d_l}{2}\right)^2}$. By using independent thinning [73], the density of active SU transmitters is obtained as $\rho\bar{\lambda}_{u,t}$. Moreover, for a given receiver, its cluster head may or may not be the closest transmitter, which is especially

true for the receivers towards the cluster's edge. This is because different clusters may spatially overlap. Now, using Slivnyak's theorem [74], [153], the interfering underlay base stations may be approximated as a homogeneous PPP.

Therefore, using the Campbell's theorem, $M_{I_u}(s)$ can be written as

$$M_{I_u}(s) = e^{\left(\int_0^\infty \mathbb{E}_{r_{c,tx}}\left[\frac{1}{1+sP_u r_{c,tx}^{\alpha} r_{sc}^{-\alpha}}-1\right] 2\pi\rho\bar{\lambda}_{u,t} r_{sc} dr_{sc}\right)}. \tag{5.14}$$

When $\alpha > 2$, we obtain a closed form expression for $M_{I_u}(s)$ as

$$\begin{aligned} M_{I_u}(s) &= e^{\left(-\frac{2\pi^2\rho\bar{\lambda}_{u,t}}{\alpha}\frac{(sP_u)^{\frac{2}{\alpha}}}{\sin\left(\frac{2\pi}{\alpha}\right)}\mathbb{E}\left[r_{c,tx}^2\right]\right)} \\ &= e^{\left(-\frac{\pi^2\rho\bar{\lambda}_{u,t}}{\alpha}\frac{(sP_u)^{\frac{2}{\alpha}}\left(\frac{d_l}{2}\right)^2}{\sin\left(\frac{2\pi}{\alpha}\right)}\right)}. \end{aligned} \tag{5.15}$$

Using $g(r) = \min\left(()\,1, r_{sc}^{-\alpha}\right)$, we find the mean interference $\mathbb{E}[I_u]$ to be

$$\begin{aligned} \mathbb{E}[I_u] &= \int_0^\infty \mathbb{E}_{|h|^2, r_{c,tx}}[P_u|h|^2 r_{c,tx}^{\alpha} r_{sc}^{-\alpha}] 2\pi\rho\bar{\lambda}_{u,t} r_{sc} dr_{sc} \\ &= \frac{2\pi\rho P_u \bar{\lambda}_{u,t}\alpha\left(\frac{d_l}{2}\right)^2}{(\alpha-2)(\alpha+2)}. \end{aligned} \tag{5.16}$$

## 5.4 Outage analysis with massive MIMO enabled base stations

### 5.4.1 Channel estimation

Both primary and underlay base stations estimate the downlink channel, via an initial uplink training phase. During which, the PU and SU receivers transmit pilot sequences to their serving base stations.

#### Primary system

We now consider the set of pilot signals using the $a$-th ($a \in \{1, ...q\}$) pilot sequence arriving at a primary base station. However, only a subsection of the primary and underlay base stations will use the $a$-th pilot sequence. As such, those active primary and underlay base stations are denoted by $\bar{\Phi}_{p,t}$ and $\bar{\Phi}_{u,t}$ respectively. Let $\phi_{pr,la}$ and $\phi_{ur,wa}$ respectively be the PU receiver using the $a$-th pilot sequence connected to $\bar{\phi}_{p,t,l}$ and the SU receiver using the $a$-th pilot sequence connected to

$\bar{\phi}_{u,t,w}$, where $\bar{\phi}_{p,t,l}$ is the $l$-th PU transmitter $\in \bar{\Phi}_{p,t}$ and $\bar{\phi}_{u,t,w}$ is the $w$-th SU transmitter $\in \bar{\Phi}_{u,t}$.

The received signal $y_k$ at the $k$-th primary base station ($\bar{\phi}_{p,t,k} \in \bar{\Phi}_{p,t}$) will be comprised of all pilot signals using different pilot sequences from all associated PU receivers and SU receivers. However, as orthogonal pilots are used, we restrict our attention to the signals containing the $a$-th pilot sequence without the loss of generality. Let $\bar{y}_{ka}$ denote the received signal corresponding to the $a$-th pilot sequence. Then, $\bar{y}_k$ is written as

$$\bar{y}_{ka} = \sum_{l=1}^{\infty} \mathbf{h}_{kla} r_{kla}^{\frac{-\alpha}{2}} b_a^T \sqrt{P_{p,p}} r_{la}^{\frac{\alpha}{2}} + \sum_{w=1}^{\infty} \mathbf{h}_{kwa} r_{kwa}^{\frac{-\alpha}{2}} b_a^T \sqrt{P_{p,u}} r_{wa}^{\frac{\alpha}{2}} + \mathbf{w}_k, \tag{5.17}$$

where $\mathbf{h}_{kla}$ and $r_{kla}$ are the channel gain and distance between $\bar{\phi}_{p,t,k}$ and $\phi_{pr,la}$, $\mathbf{h}_{kwa}$ and $r_{kwa}$ are the channel gain and distance between $\bar{\phi}_{p,t,k}$ and $\phi_{ur,wa}$, $r_{la}$ is the distance between $\phi_{pr,la}$ and $\bar{\phi}_{p,t,l}$, $r_{wa}$ is the distance between $\phi_{ur,wa}$ and $\bar{\phi}_{u,t,w}$, and $\mathbf{w}_k$ is the received noise. The received signal $\bar{y}_{ka} \in \mathbb{C}^{M \times L}$, $\mathbf{w}_k \in \mathbb{C}^{M \times L}$, and $\mathbf{h}_{kla}, \mathbf{h}_{kwa} \in \mathbb{C}^{M \times 1}$.

The objective of $\bar{\phi}_{p,t,k}$ is to estimate the channel gain between it and $\phi_{pr,ka}$, where $\phi_{pr,ka} \in \Phi_{p,r}$ is the PU receiver using the $a$-th pilot sequence associated with $\bar{\phi}_{p,t,k}$. If this channel gain is denoted as $\mathbf{h}_{kka}$, the estimated channel gain $\hat{\mathbf{h}}_{kka}$ may be expressed as

$$\begin{aligned} \hat{\mathbf{h}}_{kka} &= \frac{\bar{y}_{ka} b_a}{\sqrt{P_{p,p}}} \\ &= \mathbf{h}_{kka} + \sum_{l=1\backslash k}^{\infty} \mathbf{h}_{kla} r_{kla}^{\frac{-\alpha}{2}} r_{la}^{\frac{\alpha}{2}} + \sum_{w=1}^{\infty} \mathbf{h}_{kwa} r_{kwa}^{\frac{-\alpha}{2}} \sqrt{\frac{P_{p,u}}{P_{p,p}}} r_{wa}^{\frac{\alpha}{2}} + \frac{\mathbf{w}_k b_a}{\sqrt{P_{p,p}}}. \end{aligned} \tag{5.18}$$

**Underlay system**

Within this subsection, we derive the estimated channel gain between the $z$-th underlay base station $\bar{\phi}_{u,t,z} \in \bar{\Phi}_{u,t}$ and its associated SU receiver using the $a$-th pilot sequence $\phi_{ur,za}$. If $\bar{y}_{za} \in \mathbb{C}^{N \times L}$ is the received signal at $\bar{\phi}_{u,t,z}$ corresponding to the $a$-th pilot sequence,

$$\begin{aligned} \bar{y}_{za} &= \sum_{l=1}^{\infty} \mathbf{h}_{zla} r_{zla}^{\frac{-\alpha}{2}} b_a^T \sqrt{P_{p,p}} r_{la}^{\frac{\alpha}{2}} \\ &+ \sum_{w=1}^{\infty} \mathbf{h}_{zwa} r_{zwa}^{\frac{-\alpha}{2}} b_a^T \sqrt{P_{p,u}} r_{wa}^{\frac{\alpha}{2}} + \mathbf{w}_z, \end{aligned} \tag{5.19}$$

where the notation is analogous to the previous subsection. The estimated channel gain $\mathbf{h}_{zza}$ is obtained in a similar way to (5.18) as

$$\begin{aligned}\hat{\mathbf{h}}_{zza} &= \frac{\bar{y}_{za} b_a}{\sqrt{P_{p,u}}} \\ &= \mathbf{h}_{zza} + \sum_{w=1\backslash z}^{\infty} \mathbf{h}_{zwa} r_{zwa}^{\frac{-\alpha}{2}} r_{wa}^{\frac{\alpha}{2}} + \sum_{l=1}^{\infty} \mathbf{h}_{zla} r_{zla}^{\frac{-\alpha}{2}} \sqrt{\frac{P_{p,p}}{P_{p,u}}} r_{la}^{\frac{\alpha}{2}} + \frac{\mathbf{w}_z b_a}{\sqrt{P_{p,u}}}. \end{aligned} \tag{5.20}$$

### 5.4.2 Downlink transmission

#### Interference from PU transmitters

A PU transmitter will estimate the channel and then transmit the data symbols to its associated receivers in the downlink after performing matched-filter precoding. The downlink transmissions to the receivers using the $a$-th pilot sequence occurs simultaneously. That is, the base stations operate synchronously. This assumption allows us to characterize the maximum level of interference due to pilot contamination.

Each base station $\bar{\phi}_{p,t,j} \in \bar{\Phi}_{p,t}$ uses a precoding scheme where the transmit symbol to $\phi_{pr,ja}$ is precoded with the estimated channel gain $\hat{\mathbf{h}}_{jja}$. This process occurs for all associated receivers, and the summation of the precoded signals are transmitted [153].

Our objective is to obtain the received signal at a typical SU receiver utilizing the $a$-th pilot signal. Let $\phi_{ur,za}$ denote this node which is associated with the $z$-th underlay base station $\bar{\phi}_{u,t,z}$. The received interference from primary base stations at $\phi_{ur,za}$ is written as

$$Y_{za,p} = \sum_{j=1}^{\infty} \mathbf{h}_{jza}^{*} r_{jza}^{\frac{-\alpha}{2}} x_j, \tag{5.21}$$

where $\mathbf{h}_{jza}^{*}$ and $r_{jza}^{\frac{-\alpha}{2}}$ are the channel gain and path loss between $\bar{\phi}_{p,t,j}$ and $\phi_{ur,za}$, and $x_j$ is the transmit symbol by $\bar{\phi}_{p,t,j}$. $\mathbf{h}_{jza}^{*}$ is the reciprocal of the channel gain between $\phi_{ur,za}$ and $\bar{\phi}_{p,t,j}$ because a TDD system is considered. The transmitted symbol vector after matched-filter precoding $(x_j)$ is expressed as

$$x_j = \sum_{\nu=1}^{q_j} \hat{\mathbf{h}}_{jj\nu} \sqrt{\frac{P_p}{M}} r_{jj\nu}^{\frac{\alpha}{2}} d_{j\nu}, \tag{5.22}$$

where $q_j (< q)$ is the number of associated PU receivers of $\bar{\phi}_{p,t,j}$, $\hat{\mathbf{h}}_{jj\nu}$ and $r_{jj\nu}$ are the estimated

uplink channel and distance between $\bar{\phi}_{p,t,j}$ and $\phi_{pr,j\nu}$, and $d_{j\nu}$ is the data symbol intended for $\phi_{pr,j\nu}$. After scaling $Y_{za,p}$ with respect to $\sqrt{M}$, the asymptotic received interference signal from primary base stations is written as

$$\begin{aligned}\tilde{Y}_{za,p} &= \lim_{M\to\infty} \frac{Y_{za,p}}{\sqrt{M}} \\ &= \lim_{M\to\infty} \frac{1}{M} \sum_{j=1}^{\infty} \mathbf{h}^{*}_{jza} r_{jza}^{\frac{-\alpha}{2}} \sqrt{P_p} \sum_{\nu=1}^{q_j} r_{jj\nu}^{\frac{\alpha}{2}} d_{j\nu} \times \\ &\left( \mathbf{h}_{jj\nu} + \sum_{l=1\setminus j}^{\infty} \mathbf{h}_{jl\nu} r_{jl\nu}^{\frac{-\alpha}{2}} r_{l\nu}^{\frac{\alpha}{2}} + \sum_{w=1}^{\infty} \mathbf{h}_{jw\nu} r_{jw\nu}^{\frac{-\alpha}{2}} \sqrt{\frac{P_{p,u}}{P_{p,p}}} r_{w\nu}^{\frac{\alpha}{2}} + \frac{\mathbf{w}_j b_\nu}{\sqrt{P_{p,p}}} \right). \end{aligned} \tag{5.23}$$

However, $\lim_{M\to\infty} \frac{\mathbf{h}^{*}_{jza}\mathbf{h}_{jl\nu}}{M} \to 0, \forall j, \nu, l$ because independent and identically distributed channel gains are considered for different links, and $\lim_{M\to\infty} \frac{\mathbf{h}^{*}_{jza}\mathbf{w}_j b_\nu}{M} \to 0, \forall j$. Furthermore, $\lim_{M\to\infty} \frac{\mathbf{h}^{*}_{jza}\mathbf{h}_{jw\nu}}{M} \to 1$ whenever $w = z, \nu = a$. Thus, $\tilde{Y}_{za,p}$ can be expressed as

$$\tilde{Y_{za,p}} = \sum_{j=1}^{\infty} \sqrt{\frac{P_p P_{p,u}}{P_{p,p}}} r_{jza}^{-\alpha} r_{jja}^{\frac{\alpha}{2}} r_{za}^{\frac{\alpha}{2}} d_{ja}. \tag{5.24}$$

**Downlink signal from SU transmitters**

Similar to the downlink transmission from primary base stations, each underlay base station $\bar{\phi}_{u,t,i} \in \bar{\Phi}_{u,t}$ precodes its symbol to $\phi_{ur,ia}$ with the estimated channel gain $\hat{h}_{iia}$. We will assume that downlink transmissions from all SU transmitters occur at the same time. The received signal from underlay base stations at $\phi_{ur,za}$ is thus written as

$$Y_{za,u} = \sum_{i=1}^{\infty} \mathbf{h}^{*}_{iza} r_{iza}^{\frac{-\alpha}{2}} x_i, \tag{5.25}$$

where $x_i$ is defined by

$$x_j = \sum_{\nu=1}^{q_i} \hat{\mathbf{h}}_{ii\nu} \sqrt{\frac{P_u}{N}} r_{ii\nu}^{\frac{\alpha}{2}} d_{i\nu}. \tag{5.26}$$

The number of associated SU receivers of $\bar{\phi}_{u,t,i}$ is denoted by $q_i(< q)$. After scaling $Y_{za,u}$ with respect to $\sqrt{M}$, the signal from the underlay base stations is written as

$$\begin{aligned}
\tilde{Y}_{za,u} &= \lim_{M\to\infty} \frac{Y_{za,u}}{\sqrt{M}} \\
&= \lim_{N\to\infty} \frac{1}{\sqrt{\kappa}N} \sum_{i=1}^{\infty} \mathbf{h}^{*}_{iza} r_{iza}^{\frac{-\alpha}{2}} \sqrt{P_u} \sum_{\nu=1}^{q_i} r_{ii\nu}^{\frac{\alpha}{2}} d_{i\nu} \times \\
&\left( \mathbf{h}_{ii\nu} + \sum_{w=1\setminus i}^{\infty} \mathbf{h}_{iw\nu} r_{iw\nu}^{\frac{-\alpha}{2}} r_{w\nu}^{\frac{\alpha}{2}} + \sum_{l=1}^{\infty} \mathbf{h}_{il\nu} r_{il\nu}^{\frac{-\alpha}{2}} \sqrt{\frac{P_{p,p}}{P_{p,u}}} r_{l\nu}^{\frac{\alpha}{2}} + \frac{\mathbf{w}_i b_\nu}{\sqrt{P_{p,u}}} \right) \\
&= \frac{\sqrt{P_u}}{\sqrt{\kappa}} + \sum_{i=1\setminus z}^{\infty} \frac{\sqrt{P_u}}{\sqrt{\kappa}} r_{iza}^{-\alpha} r_{iia}^{\frac{\alpha}{2}} r_{za}^{\frac{\alpha}{2}} d_{ia}. \qquad (5.27)
\end{aligned}$$

The first term of (5.27) represents the desired signal to $\phi_{ur,za}$ while the second term represents the interference from SU transmitters.

**Interfering base station density**

In the previous subsections, we expressed the interference to $\phi_{ur,za}$ from primary and SU transmitters using the $a$-th pilot sequence (namely $\bar{\Phi}_{p,t}$ and $\bar{\Phi}_{u,t}$). This subsection derives the densities of these processes.

- *Density of* $\bar{\Phi}_{p,t}$

  We will first derive the density of density of $\bar{\Phi}_{p,t}$ denoted as $\bar{\lambda}_{p,t}$. To this end, we approximate $\bar{\Phi}_{p,t}$ as a thinned PPP [73] where the density $\bar{\lambda}_{p,t} = \eta\lambda_{p,t}$. The factor $\eta$ is the probability that a particular base station uses the $a$-th ($a \in \{1, ...q\}$) pilot sequence.

  We will consider a typical primary base station $\phi_{p,t,k} \in \Phi_{p,t}$. The number of users associated with $\phi_{p,t,k}$ is a random variable depending on the area of its Voronoi cell ($S$). However, the exact distribution of the area of a Voronoi cell is not known. Consequently, a two parameter gamma empirical approximation [169] has been shown to fit the exact size distribution. Thus, the normalized cell size $\tilde{S} = S/\bar{S}$ is distributed as follows:

$$f_{\tilde{S}}(y) \approx \frac{\beta^{\mu}}{\Gamma(\mu)} y^{\mu-1} e^{-\beta y}, 0 \leq y < \infty, \qquad (5.28)$$

  where $\mu = 3.61$, $\beta = 3.57$, and $\bar{S}$ is the average size of a cell given by $\bar{S} = \frac{1}{\lambda_{p,t}}$.

Let $\omega_1$ be the number of associated users with $\phi_{p,t,k}$. When $\omega_1 \geq q$, all the pilot sequences will be used whereas when $\omega_1 < q$ there exists a probability that the $a$-th pilot sequence is not used by any user associated with $\phi_{p,t,k}$. Thus, we can write $\eta$ as

$$\begin{aligned}\eta &= \Pr[\omega_1 \geq q] + \Pr[\omega_1 < q]\frac{\mathbb{E}_{\omega_1 \setminus \omega_1 < q}[\omega_1]}{q} \\ &= \mathbb{E}_S\left[\sum_{n=q}^{\infty}\frac{(\lambda_{p,r}S)^n}{n!}e^{-\lambda_{p,r}S} + \frac{1}{q}\sum_{\omega_1=1}^{q-1}\frac{(\lambda_{p,r}S)^{\omega_1}}{\omega_1 - 1!}e^{-\lambda_{p,r}S}\right]. \end{aligned} \tag{5.29}$$

Substituting $S = \tilde{S}\bar{S}$ and performing the expectation with respect to (5.28) we obtain

$$\begin{aligned}\eta &= \frac{\beta^\mu}{\Gamma(\mu)}\sum_{n=q}^{\infty}\frac{\Gamma(\mu+n)}{n!(\beta+\frac{\lambda_{p,r}}{\lambda_{p,t}})^{\mu+n}}\left(\frac{\lambda_{p,r}}{\lambda_{p,t}}\right)^n \\ &+ \frac{1}{q}\frac{\beta^\mu}{\Gamma(\mu)}\sum_{\omega_1=1}^{q-1}\frac{\Gamma(\mu+\omega_1)}{(\omega_1-1)!(\beta+\frac{\lambda_{p,r}}{\lambda_{p,t}})^{\mu+\omega_1}}\left(\frac{\lambda_{p,r}}{\lambda_{p,t}}\right)^{\omega_1}. \end{aligned} \tag{5.30}$$

- *Density of* $\bar{\Phi}_{u,t}$ for the cluster model

  We now derive the density of $\bar{\Phi}_{u,t}$ for the cluster model denoted as $\bar{\lambda}_{u,t}$. Similar to before, $\bar{\Phi}_{u,t}$ can be obtained by applying independent thinning on $\Phi_{u,t}$. Therefore, $\bar{\lambda}_{u,t} = \theta\hat{\lambda}_{u,t}$, and $\theta$ is the probability that a particular underlay base station uses the $a$-th pilot sequence while $\hat{\lambda}_{u,t}$ is given by $\hat{\lambda}_{u,t} = \tilde{\theta}\lambda_{u,t}$, where $\tilde{\theta}$ is the probability that a SU transmitter is not inside the guard region of a PU receiver given by $\tilde{\theta} = e^{-\pi\lambda_{p,r}R_G^2}$.

  Let $\phi_{u,t,z} \in \Phi_{u,t}$ be a typical active SU transmitter. Although the cluster area of $\phi_{u,t,z}$ is fixed, the number of receivers associated with it ($\omega_2$) is still a random variable. We can thus write $\theta$ as

$$\begin{aligned}\theta &= \Pr[\omega_2 > q] + \Pr[\omega_2 < q]\frac{\mathbb{E}_{\omega_2 \setminus \omega_2 < q}[\omega_2]}{q} \\ &= \sum_{n=q}^{\infty}\frac{(\lambda_{u,r}\frac{\pi d_l^2}{4})^n}{n!}e^{-\lambda_{u,r}\frac{\pi d_l^2}{4}} \\ &+ \frac{1}{q}\sum_{\omega_2=1}^{q-1}\frac{(\lambda_{u,r}\frac{\pi d_l^2}{4})^{\omega_2}}{\omega_2 - 1!}e^{-\lambda_{u,r}\frac{\pi d_l^2}{4}}. \end{aligned} \tag{5.31}$$

- *Density of* $\bar{\Phi}_{u,t}$ for the Voronoi model

The density of $\bar{\Phi}_{u,t}$ for the Voronoi model (denoted as $\bar{\lambda}_{u,t}$) is written similar to the cluster model as $\bar{\lambda}_{u,t} = \theta\hat{\lambda}_{u,t}$, where $\hat{\lambda}_{u,t} = \tilde{\theta}\lambda_{u,t}$ and $\tilde{\theta} = e^{-\pi\lambda_{p,r}R_G^2}$. However, $\theta$ is analogous to $\eta$ and is written as

$$\begin{aligned}\theta &= \frac{\beta^{\mu}}{\Gamma(\mu)}\sum_{n=q}^{\infty}\frac{\Gamma(\mu+n)}{n!(\beta+\frac{\lambda_{u,r}}{\hat{\lambda}_{u,t}})^{\mu+n}}\left(\frac{\lambda_{u,r}}{\hat{\lambda}_{u,t}}\right)^{n} \\ &+ \frac{1}{q}\frac{\beta^{\mu}}{\Gamma(\mu)}\sum_{\omega_1=1}^{q-1}\frac{\Gamma(\mu+\omega_1)}{(\omega_1-1)!(\beta+\frac{\lambda_{u,r}}{\hat{\lambda}_{u,t}})^{\mu+\omega_1}}\left(\frac{\lambda_{u,r}}{\hat{\lambda}_{u,t}}\right)^{\omega_1}. \end{aligned} \tag{5.32}$$

### 5.4.3 Interference characterization

We now characterize the interference at $\phi_{ur,za}$ and obtain the outage probability. Using (5.24) and (5.27), the aggregate interference ($I$) scaled with respect to $\sqrt{M}$ can be written as $I = I_p + I_u$, where $I_p = \sum_{j=1}^{\infty}\frac{P_pP_{p,u}}{P_{p,p}}r_{jza}^{-2\alpha}r_{jja}^{\alpha}r_{za}^{\alpha}$ and $I_u = \sum_{i=1\setminus z}^{\infty}\frac{P_u}{\kappa}r_{iza}^{-2\alpha}r_{iia}^{\alpha}r_{za}^{\alpha}$. Without the loss of generality, we assume that $d_{ja}^2, d_{ia}^2 = 1$. The SIR[5] ($\gamma$) at $\phi_{ur,za}$ is written as $\gamma = \frac{P_u}{\kappa(I_p+I_u)}$, and the outage probability is expressed as

$$P_O = \Pr[\gamma < T] = \Pr[I > \frac{P_u}{\kappa T}], \tag{5.33}$$

where $T$ is the threshold SIR required at a SU receiver. In order to evaluate $P_O$, the distribution of $I$ is required.

To this end, we will first evaluate the MGF of $I$. However, because $I_p$ and $I_u$ are independent, $M_I(s)$ becomes $M_I(s) = \mathbb{E}[e^{-sI_p}]\mathbb{E}[e^{-sI_u}] = M_{I_p}(s)M_{I_u}(s)$. Using the Campbell's theorem [73], $M_{I_p}$ is expressed as

$$M_{I_p}(s) = e^{\left(\int_0^{\infty}\mathbb{E}\left[e^{-s\frac{P_pP_{p,u}}{P_{p,p}}r_{jza}^{-2\alpha}r_{jja}^{\alpha}r_{za}^{\alpha}}-1\right]2\pi\bar{\lambda}_{p,t}r_{jza}dr_{jza}\right)}, \tag{5.34}$$

where the expectation is with respect to $r_{jja}$ and $r_{za}$. Therefore, in order to evaluate (5.34), the distributions of $r_{jja}$ and $r_{za}$ are needed.

[5]Note that SIR is equal to the SINR (signal to interference and noise ratio) because the noise power approaches zero when scaled by $\sqrt{M}$.

**Cluster model**

The variable $r_{jja}$ can be interpreted as the distance from a primary base station to any associated receiver. However, the receiver can be located at any point within the Voronoi cell of $\bar{\phi}_{p,t,j}$. It has been shown in [170] that $r_{jja}$ has the approximate PDF given by $Ral(\pi\lambda_{p,t})$. However, it is worth emphasizing that this is not the exact PDF due to correlations and dependence induced by the structure of the Voronoi tessellation. On the contrary, $r_{za}$ which can be interpreted as the distance between a cluster head and a random daughter node in the cluster has an exact simple PDF given by $Lin(\frac{d_l}{2})$.

Using the PDFs for $r_{za}$ and $r_{jja}$, and replacing $r_{jza}$ with $r$ for clarity, we can simplify (5.34) as

$$\begin{aligned} M_{I_p}(s) &= e^{\left(\int_0^\infty \mathbb{E}_{r_{jja},r_{za}}\left[\sum_{v=1}^\infty \frac{\left(-s\frac{P_pP_{p,u}}{P_{p,p}} r^{-2\alpha} r_{jja}^{\alpha} r_{za}^{\alpha}\right)^v}{v!}\right] 2\pi\bar{\lambda}_{pt} r dr\right)} \\ &= e^{\left(\sum_{v=1}^\infty \frac{\pi\bar{\lambda}_{pt}}{v!}\left(\frac{-sP_pP_{p,u}}{P_{p,p}}\right)^v \left(\frac{\alpha v d_l^{\alpha v}\Gamma(\frac{\alpha v}{2}+1)}{(\alpha v-1)2^{\alpha v-1}(\alpha v+2)(\pi\lambda_{p,t})^{\frac{\alpha v}{2}}}\right)\right)}. \end{aligned} \tag{5.35}$$

From (5.35), it is possible to obtain the first and second order statistics of $I_p$[6] as $\mathbb{E}[I_p] = \frac{\eta P_pP_{p,u}\alpha d_l^{\alpha}\Gamma(\frac{\alpha}{2}+1)}{P_{p,p}(\alpha-1)2^{\alpha-1}(\alpha+2)(\pi\lambda_{p,t})^{\frac{\alpha}{2}-1}}$ and $Var[I_p] = \frac{\eta(P_pP_{p,u})^2\alpha d_l^{2\alpha}\Gamma(\alpha+1)}{P_{p,p}^2(2\alpha-1)2^{2\alpha-1}(\alpha+1)(\pi\lambda_{p,t})^{\alpha-1}}$.

We now focus our attention $I_u$. Using the Slivnyak's theorem [74], [153], the interfering underlay base stations ($\bar{\Phi}_{u,t}\backslash z$) can be taken as forming a homogeneous PPP. Therefore, using Campbell's theorem [73], $M_{I_u}(s)$ is written as

$$M_{I_u}(s) = e^{\left(\int_0^\infty \mathbb{E}\left[e^{-s\frac{P_u}{\kappa} r_{iza}^{-2\alpha} r_{iia}^{\alpha} r_{za}^{\alpha}} - 1\right] 2\pi\bar{\lambda}_{u,t} r_{iza} dr_{iza}\right)}, \tag{5.36}$$

where the expectation is with respect to $r_{iia}$ and $r_{za}$. However, $r_{iia}$ follows the distribution of $r_{za}$ as all clusters have similar dimensions. Therefore, we can simplify (5.36) as

$$M_{I_u}(s) = e^{\left(\sum_{v=1}^\infty \frac{\pi\bar{\lambda}_{u,t}\alpha v}{v!(\alpha v-1)}\left(\frac{-sP_u}{\kappa}\right)^v \left(\frac{d_l^{\alpha v}}{2^{\alpha v-1}(\alpha v+2)}\right)^2\right)}. \tag{5.37}$$

The expectation and variance of $I_u$ are obtained from the moments of (5.37) as $\mathbb{E}[I_u] = \frac{\pi\bar{\lambda}_{u,t}\alpha P_u d_l^{2\alpha}}{\kappa(\alpha-1)(2^{\alpha-1}(\alpha+2))^2}$ and $Var[I_u] = \frac{\pi\bar{\lambda}_{u,t}\alpha P_u^2 d_l^{4\alpha}}{\kappa^2(2\alpha-1)(2^{2\alpha}(\alpha+1))^2}$.

[6]The singularities at $\alpha = 0.5, 1$ are irrelevant as those values do not occur in practical systems.

**Voronoi model**

We now derive the MGFs of $I_p$ and $I_u$ under the Voronoi model for the underlay nodes. Under this model, the distributions of $r_{za}$ and $r_{iia}$ are different. $r_{za}$ has an approximate PDF obtained using similar arguments to $r_{jja}$ which is given by $Ral(\pi\hat{\lambda}_{u,t})$. Now, we can simplify (5.34) as

$$M_{I_p}(s)=e^{\left(\sum_{v=1}^{\infty}\frac{\pi\bar{\lambda}_{pt}}{v!}\left(\frac{-sP_pP_{p,u}}{P_{p,p}}\right)^v\left(\frac{\alpha v(\Gamma(\frac{\alpha v}{2}+1))^2}{(\alpha v-1)(\pi\lambda_{p,t})^{\frac{\alpha v}{2}}(\pi\hat{\lambda}_{u,t})^{\frac{\alpha v}{2}}}\right)\right)}. \tag{5.38}$$

The mean and variance of $I_p$ are obtained for the Voronoi model as $\mathbb{E}[I_p]=\frac{\eta P_pP_{p,u}\alpha(\Gamma(\frac{\alpha}{2}+1))^2}{P_{p,p}(\alpha-1)(\pi\lambda_{p,t})^{\frac{\alpha}{2}-1}(\pi\hat{\lambda}_{u,t})^{\frac{\alpha}{2}}}$ and $Var[I_p]=\frac{2\eta(P_pP_{p,u})^2\alpha(\Gamma(\alpha+1))^2}{P_{p,p}^2(2\alpha-1)(\pi\lambda_{p,t})^{\alpha-1}(\pi\hat{\lambda}_{u,t})^{\alpha}}$.

When deriving $M_{I_u}(s)$, the distribution of $r_{iia}$ is need. However, this follows the same distribution as $r_{za}$ as both involve SU receivers selecting the nearest SU transmitter. Thus, this PDF is given by $Ral(\pi\hat{\lambda}_{u,t})$. With this, we can simplify (5.36) as

$$M_{I_u}(s)=e^{\left(\sum_{v=1}^{\infty}\frac{\pi\bar{\lambda}_{u,t}\alpha v}{v!(\alpha v-1)}\left(\frac{-sP_u}{\kappa}\right)^v\left(\frac{\Gamma(\frac{\alpha v}{2}+1)}{(\pi\hat{\lambda}_{u,t})^{\frac{\alpha v}{2}}}\right)^2\right)}. \tag{5.39}$$

Furthermore, the mean and variance of $I_u$ are obtained as $\mathbb{E}[I_u]=\frac{\theta\alpha P_u(\Gamma(\frac{\alpha}{2}+1))^2}{\kappa(\alpha-1)(\pi\hat{\lambda}_{u,t})^{\alpha-1}}$ and $Var[I_u]=\frac{2\theta\alpha P_u^2(\Gamma(\alpha+1))^2}{\kappa^2(2\alpha-1)(\pi\hat{\lambda}_{u,t})^{2\alpha-1}}$.

Now, in order to evaluate (5.33), $I$ will be approximated as a gamma distribution using first and second order moment matching [88]. The resulting gamma distribution has shape and scale parameters of $\frac{(\mathbb{E}[I_u]+\mathbb{E}[I_p])^2}{Var[I_u]+Var[I_p]}$ and $\frac{Var[I_u]+Var[I_p]}{\mathbb{E}[I_u]+\mathbb{E}[I_p]}$ respectively. The outage probability of a SU receiver is finally expressed as

$$P_O=1-\frac{1}{\Gamma\left(\frac{(\mathbb{E}[I_u]+\mathbb{E}[I_p])^2}{Var[I_u]+Var[I_p]}\right)}\gamma\left(\frac{(\mathbb{E}[I_u]+\mathbb{E}[I_p])^2}{Var[I_u]+Var[I_p]},\frac{\frac{P_u}{\kappa T}}{\frac{Var[I_u]+Var[I_p]}{\mathbb{E}[I_u]+\mathbb{E}[I_p]}}\right). \tag{5.40}$$

## 5.5 Numerical results

This section provides numerical outage probability of a SU receiver. We first investigate the single antenna case, followed by the massive MIMO case.

### 5.5.1 Single antenna

For this case, we use the parameters $\lambda_{u,t} = 1 \times 10^{-5}$, $\lambda_{p,t} = 1 \times 10^{-5}$, $r = 50$, $R_G = 20$, $P_u = 1 \times 10^{-8}$, and $\sigma^2 = 0$ [37], [157]. The noise variance is set to zero in order to highlight the effect of interference. We will denote the underlay association scheme where the transmitter selects the closest receiver as Scheme 1, and the receiver selects the closest transmitter as Scheme 2.

Fig. 5.2 plots the outage probability of a SU receiver with respect to the required SINR threshold. Although the outage probabilities differ significantly for different $\alpha$ when the threshold ($T$) is low, they converge to 1 as expected when $T$ increases. The outage increase for higher $\alpha$ occurs primarily due to the power control procedures which require an inversion of the path loss. Although the outage of Scheme 2 is higher, the difference is not significant because the main source of interference is the primary network.

The SU receiver outage is plotted vs. the required PU receiver power level $P_p$ in Fig. 5.3. The plots diverge for lower $P_p$ due to interference from the primary network playing a less dominant role. The outage probabilities drop significantly when the primary and SU receiver densities are increased. For Scheme 1, this is due to the guard region surrounding each PU receiver. For Scheme 2, in addition to this reason, the distance from an interfering SU transmitter to its associated receiver reduces; causing the transmit power to reduce, which in turn reduces interference. Moreover, when the maximum allowable transmit distance $D$ increases, the outage increases because more associations (requiring higher transmit power) are successful. It is also interesting to note that Scheme 1 shows a worse outage performance compared to Scheme 2 when $D = 200$ and $\lambda_{p,r} = \lambda_{s,r} = 1 \times 10^{-3}$.

We now investigate the performance of the cluster model. Fig. 5.4 plots the underlay outage with respect to the threshold SINR level. The outage increases significantly when the path loss exponent $\alpha$ increases. Moreover, the rate of outage decrease vs. the threshold is inversely proportional to $\alpha$. Furthermore, for each value of $\alpha$, increasing the cluster radius $d_l$ further increases outage. This is due to higher transmit power requirements for SU transmitters. When the threshold increases, the effect of $\alpha$ decreases, and $d_l$ plays a bigger role. For example, above $-28$ dB, having a cluster radius of 50 and $\alpha = 4$ provides a lower outage than a cluster radius of 500 and $\alpha = 3$.

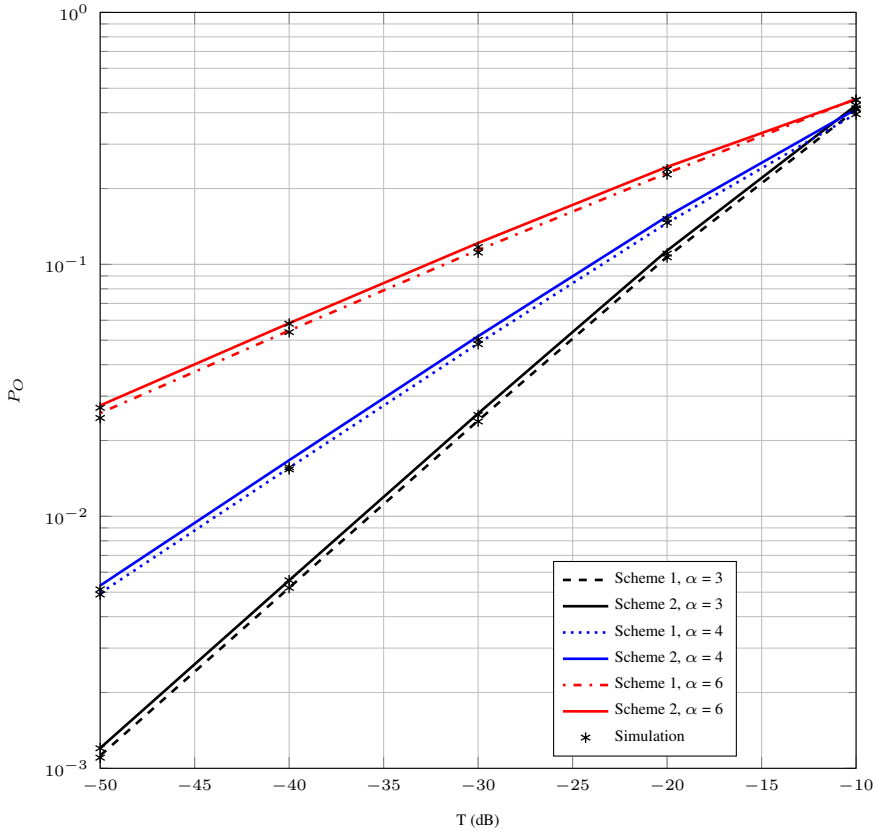


Figure 5.2: Outage probability vs. the required SINR threshold $T$ under different path loss exponents $\alpha$ for the two underlay association schemes. $D = 100$, $P_p = 1 \times 10^{-8}$, $\lambda_{p,r} = 1 \times 10^{-4}$, and $\lambda_{s,r} = 1 \times 10^{-4}$.

### 5.5.2 Massive MIMO

This provides numerical results on the outage probability of a SU receiver for different system parameters with massive MIMO base stations. The parameter values are $P_{p,p} = -80$ dBm, $P_{p,u} = -80$ dBm, $P_u = -70$ dBm, $q = 64$, $T = 1$, $R_G = 20$, $M = 500$, and $\kappa = 1$ unless stated otherwise [37], [153], [171], [172].

We first investigate the cluster model for underlay nodes. As mentioned in Section II, the cluster model is useful for sets of independent pico cells or wireless local area networks underlayed within a cellular network or a terrestrial television network. Fig. 5.5 plots the variation of the outage probability $P_O$ with respect to the path loss exponent $\alpha$. As $\alpha$ increases, $P_O$ reduces for all values of $P_p$ and $d_l$. However, the rate of decline varies slightly with $\alpha$. Moreover, while having a higher outage probability when other parameter values remain the same, a higher $d_l$ also provides a greater outage variation when $P_p$ is varied.

In Fig. 5.6, the outage probability is plotted with respect to the PU receiver density $\lambda_{p,r}$.

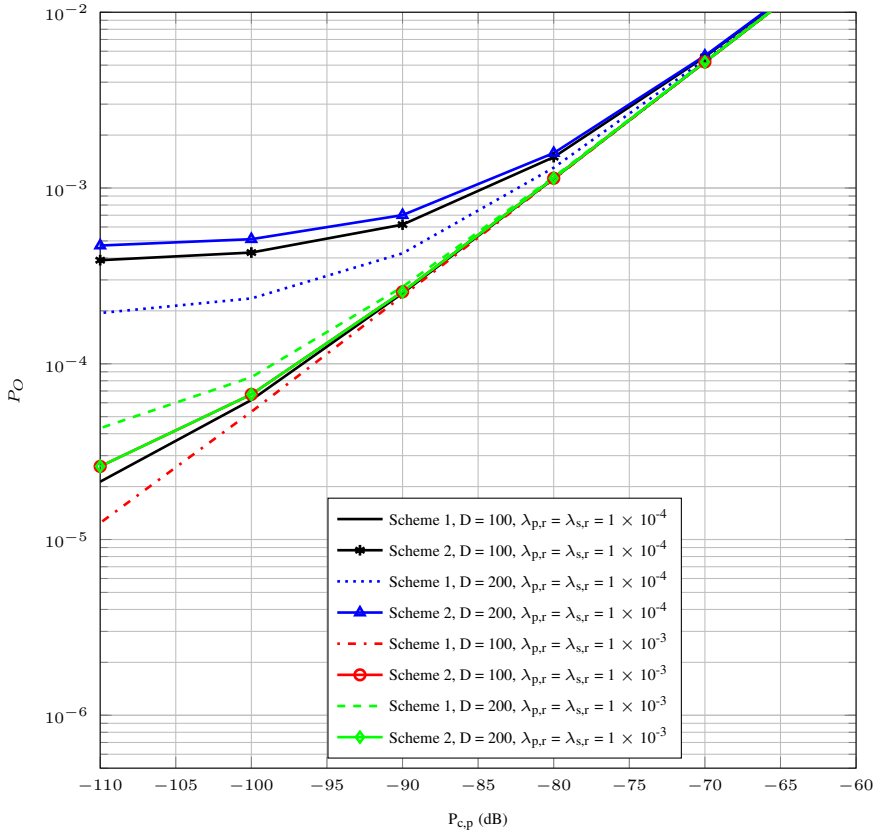


Figure 5.3: Outage probability vs. $P_p$ under different $\lambda_{p,r}$, $\lambda_{s,r}$, and $D$ for the two underlay association schemes. $\alpha = 3$, and $T = 0.0001$.

The plot shows a complex relationship without a clear trend. However, a higher cluster radius $d_l$ always provides a higher outage. It is interesting to note that at $\lambda_{p,r} \approx -25$ dB, all curves roughly show a similar outage. However, it should be noted that they do not coincide at the same exact value. For very low PU receiver densities, each set of values approach a steady state outage without significant deviation when $\lambda_{p,r}$ changes. However, when $\lambda_{p,r}$ is high, the curves under $\lambda_{p,t} = 10^{-3}$ shows a slight increase before decreasing while all other curves show a sharp decrease. The total interference is due to the sum of primary and underlay interference. When $\lambda_{p,r}$ is increased, two contradictory effects occur. First, as the area under guard regions increase, there would be less underlay transmitters, and thus less underlay interferers. Second, the proportion of idle primary transmitters with which no receiver is associated with decrease, and thus primary interference is increased. However, for this second effect to be significant, the primary interference should have played a significant role in the first place. Therefore, it is not seen within the curves with $\lambda_{p,t} = 10^{-4}$ for which the underlay interference is the main contributor to the outage. However, when the primary transmitter density is sufficiently high

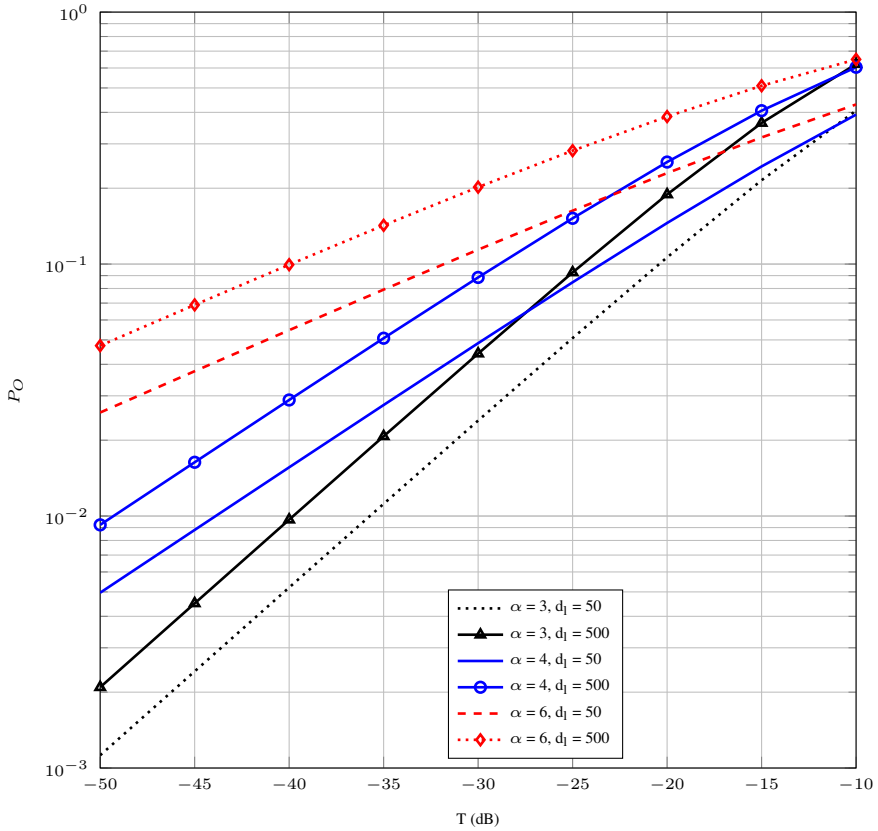


Figure 5.4: Outage probability vs. the required SINR threshold $T$ under different path loss exponents $\alpha$ and cluster radii. $P_p = 1 \times 10^{-8}$, $\lambda_{p,r} = 1 \times 10^{-4}$, and $\lambda_{s,r} = 1 \times 10^{-4}$.

($\lambda_{p,t} = 10^{-3}$), the primary interference still imparts a considerable impact on the outage, and thus the second effect initially occurs as seen with the increased outage. However, the first effect predominates as $\lambda_{p,r}$ is increased further, and the outage drops.

We now move our attention to the Voronoi model for the SU network, which is useful when multiple pico or wireless local area network base stations belonging to the same network cover a particular geographical area. Fig. 5.7 plots the outage vs. the path loss exponent. While increasing $\alpha$ reduces the outage, the rate of decrease changes with $\alpha$, and this in turn depends on the specific $P_p$ and $P_u$ values. Furthermore, for high $P_u$ and low $P_p$ values, the outage is significantly lower at low $\alpha$. Conversely, for low $P_u$ and high $P_p$, the outage is significantly higher due to the primary interference being comparatively higher with respect to the desired signal power. We can observe that when $P_p = P_u$, the outage does not depend on the actual value of $P_p$ or $P_u$.

Fig. 5.8 plots the outage with respect to the SU transmitter density $\lambda_{u,t}$. For all values of $\lambda_{u,r}$, there exists a $\lambda_{u,t}$ value where the outage peaks. Moreover, increasing $\lambda_{p,t}$ pushes the location of

the maxima to the right; making it occur at a higher $\lambda_{u,t}$. The reason behind the outage peak is as follows. When the SU transmitter density $\lambda_{u,t}$ increases, the interference increases initially as the number of concurrent transmissions increase, and a rise in the outage occurs. However, when $\lambda_{u,t}$ increases further, the additional SU transmitters will not have an associated receiver. Moreover, an increased $\lambda_{u,t}$ means a lower average cell size, and thus due to the path loss inversion based power control, the transmit power of a SU transmitter reduces. Therefore, even the interference from associated SU transmitters would reduce. The outage peak is significant when $\lambda_{u,r} = 10^{-2}$ while it is insignificant for $\lambda_{u,r} = 10^{-3}$. This is because having a higher $\lambda_{u,r}$ means that the additional SU transmitters would be associated to a receiver, creating interference. Conversely, when $\lambda_{u,r}$ is lower, only a small amount of the additional SU transmitters cause interference. As such, the best way to reduce the outage peak is by having a lower SU receiver density.

We now investigate the effect of the ratio between PU and SU transmitter antennas $\kappa$ on the outage in Fig. 5.9. When $\kappa$ is increased from $1$ to $20$, the change in outage is not very significant. However, the trends of the change show significant differences with respect to the PU and SU transmitter densities. While showing similar trends, $\lambda_{p,t} = \lambda_{u,t} = 10^{-3}$ has a lower outage than $\lambda_{p,t} = \lambda_{u,t} = 10^{-4}$. Because the PU and SU receiver densities are comparable at $10^{-3}$, the additional transmitters do not get associated with a receiver. Furthermore, the shrinking of cell size causes the transmit power to drop, reducing interference.

## 5.6 Conclusion

This chapter analyzed the aggregate interference on a SU receiver from primary and other underlay base stations when the interfering base stations are single antenna type or massive MIMO. We considered a path loss inversion based power control scheme for transmitting the pilot signals as well as the primary and underlay data signals. The PU transmitters and receivers were modeled as homogeneous PPPs in $\mathbb{R}^2$ while the underlay network was modeled in two ways: 1) as a Matern cluster process with the cluster centres representing base stations, and 2) as homogeneous PPPs in $\mathbb{R}^2$. All processes were assumed to be stationary. Moreover, two underlay association schemes were analyzed and exclusion regions around the PU receivers were considered.

The MGF of the aggregate interference on a SU receiver and its outage probability were derived for both single antenna scenarios and massive MIMO scenarios under pilot contamination. For the single antenna case, the interference from the primary system was shown to be indepen-

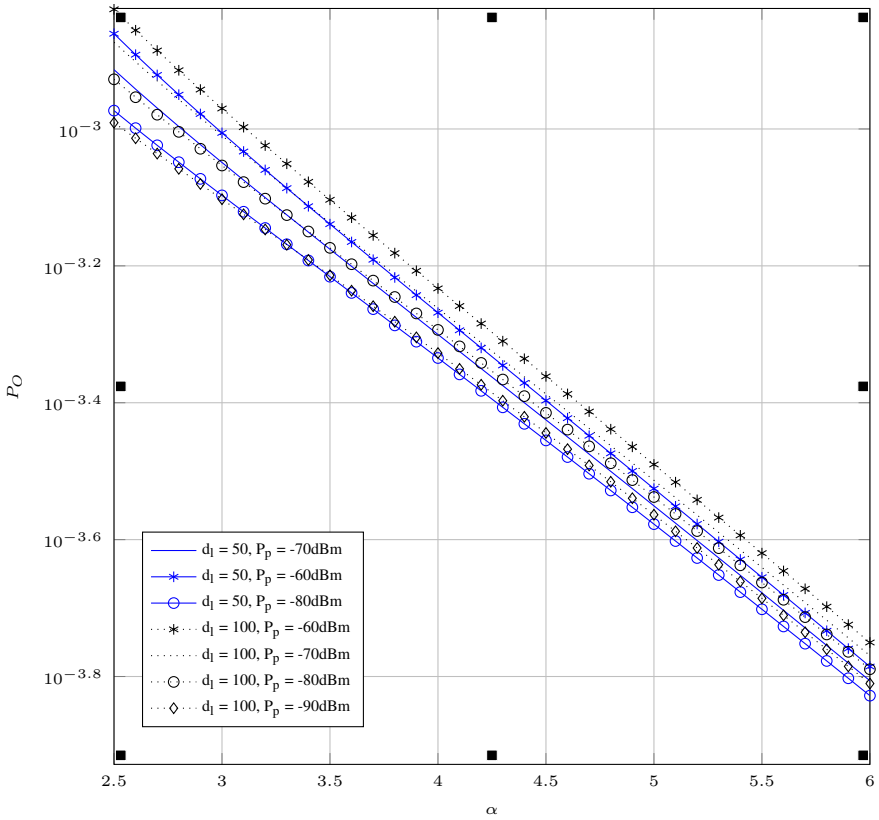


Figure 5.5: Outage probability vs. the path loss exponent ($\alpha$) under the cluster model for different values of $d_l$ and $P_p$. $\lambda_{p,t} = 10^{-4}$, $\lambda_{u,t} = 10^{-4}$, $\lambda_{p,r} = 10^{-2}$, $\lambda_{u,r} = 10^{-2}$.

dent of the node densities. Furthermore, when the required power threshold for the PU receiver ($P_p$) is comparative with the required underlay threshold ($P_u$), interference from the primary system dominates, and the path loss exponent greatly affects the outage. However, when $P_p < P_u$, the outage is significantly affected by the receiver densities and the maximum allowable underlay transmit distance. Moreover, increasing the cluster radius significantly increases the outage. For the massive MIMO case, it was observed that while an increased path loss exponent reduced the outage, the rate of decrease varied with threshold power levels and system parameters. Furthermore, transmitter densities of both networks significantly affected the outage characteristics, and a specific SU transmitter density maximizes the outage probability. Furthermore, when the thresholds $P_p$ and $P_u$ are equal, the outage does not depend on the exact value of either.

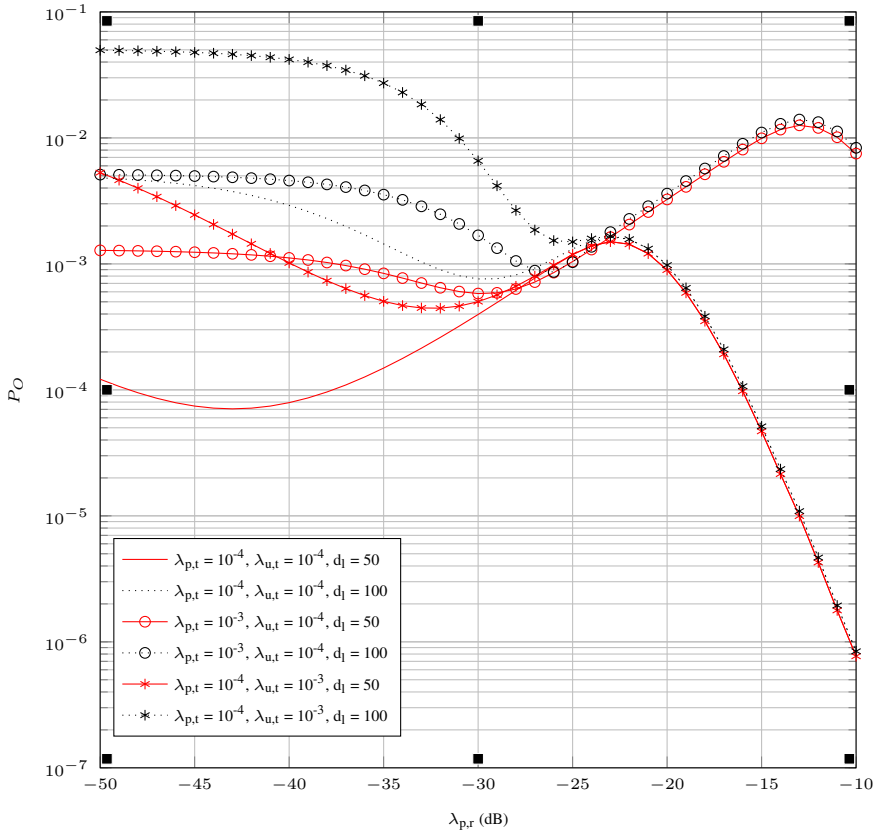


Figure 5.6: Outage probability vs. the PU receiver density ($\lambda_{p,r}$) under different values of $\lambda_{p,t}$, $\lambda_{u,t}$, and $d_l$ for the cluster model. $\alpha = 3$, $P_p = -70$ dBm, and $\lambda_{u,r} = 10^{-2}$.

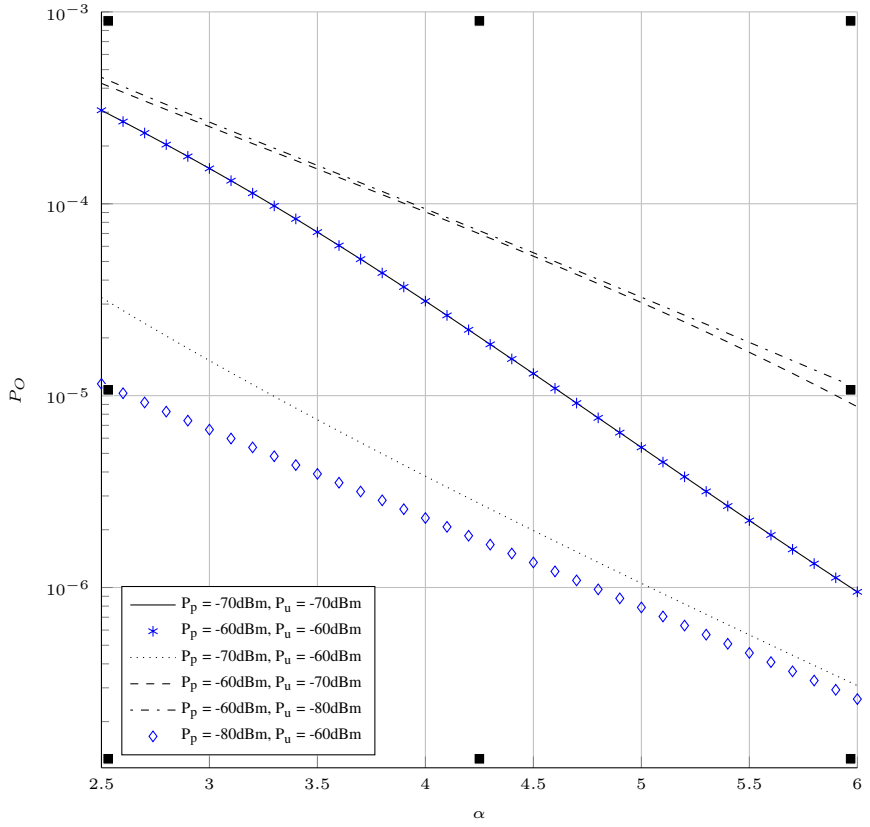


Figure 5.7: Outage probability vs. the path loss exponent ($\alpha$) for different values of $P_u$ and $P_p$ for the Voronoi model. $\lambda_{p,t} = 10^{-4}$, $\lambda_{u,t} = 10^{-4}$, $\lambda_{p,r} = 10^{-3}$, and $\lambda_{u,r} = 10^{-2}$.

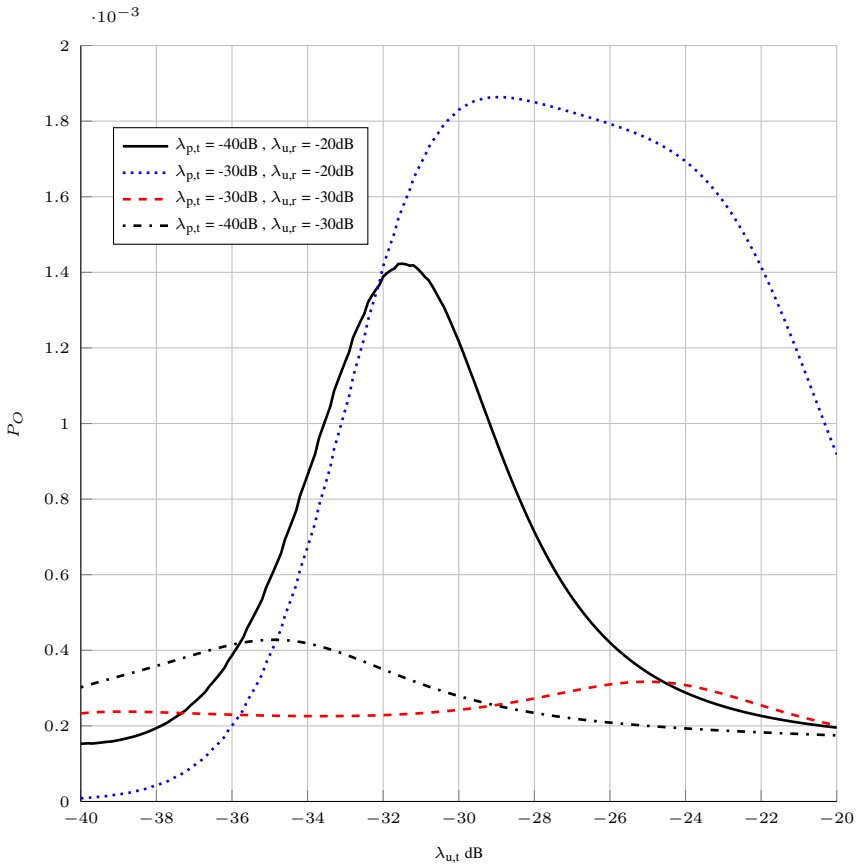


Figure 5.8: Outage probability vs. the SU transmitter density ($\lambda_{u,t}$) under different values of $\lambda_{p,t}$ and $\lambda_{u,r}$ for the Voronoi model. $\alpha = 3$, $P_p = -70$ dBm, and $\lambda_{p,r} = 10^{-3}$.

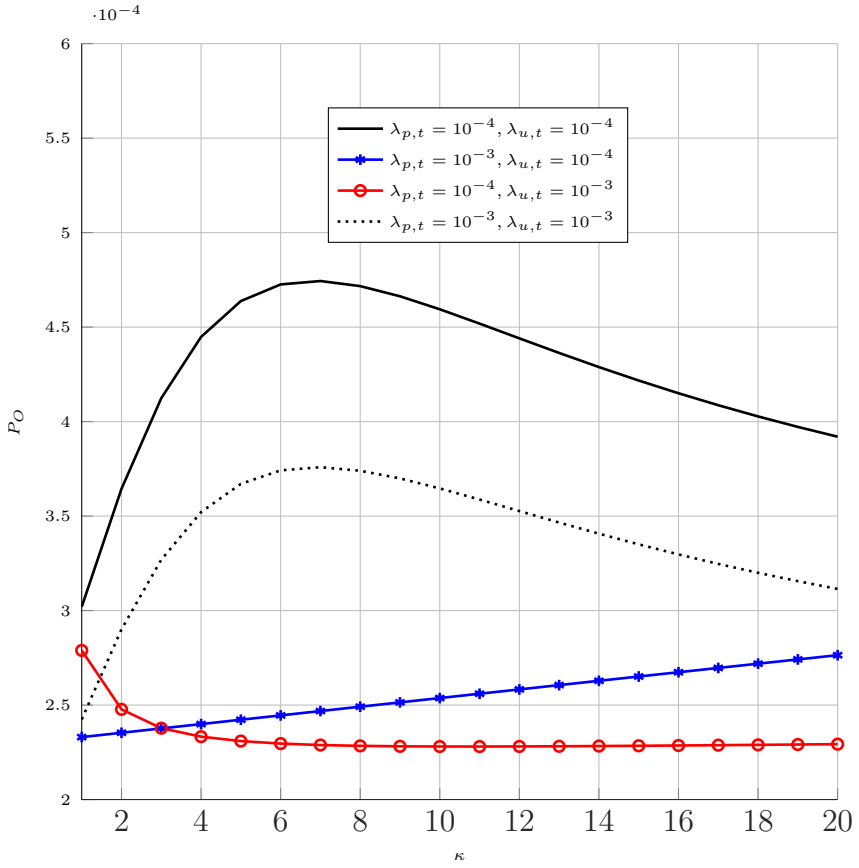


Figure 5.9: Outage probability vs. the ratio between PU and SU transmitter antennas ($\kappa$) under different values of $\lambda_{p,t}$ and $\lambda_{u,t}$ for the Voronoi model. $\alpha = 3$, $P_p = -70$ dBm, $\lambda_{p,r} = 10^{-3}$, and $\lambda_{u,r} = 10^{-3}$.

# Chapter 6

# Performance characterization of spatially random energy harvesting underlay D2D networks with transmit power control

## 6.1 Introduction

D2D networks are a special case of underlay cognitive radio (CR) networks which allow simultaneous spectrum access for primary and secondary users in an interference tolerant basis [173], [174]. The concept of multi-channel cognitive cellular networks, where macro base stations (BSs) are underlaid with cognitive femtocell BS [2], provides an idea that D2D technology can also be used to underlay the existing cellular networks [3]. However, D2D interference on the primary network must be managed, and hence the enforcement of exclusion regions and transmit power constraints may hinder the throughput of the D2D network.

In principle, D2D nodes can harvest energy and spend that energy in order to power their transmissions. Harvested powers of $3.5\,\text{mW}$ and $1\,\mu\text{W}$ have been achieved at $0.6\,\text{m}$ and $11\,\text{m}$ respectively [120]. Moreover, it was shown in [175] that a ambient power of $-25\,\text{dBm}$ can be observed in an environment with $800\,\text{MHz}$ cellular base stations and that conversion efficiencies of up to $19\%$ were achievable. However, the uncertainty of energy harvests and interference from other co-channel transmissions are significant challenges. While initial attention was directed towards extracting energy from natural sources, radio frequency (RF) energy harvesting has received heightened attention [176]. For example, this process allows D2D nodes to improve their energy efficiency [177]–[181]. Although current harvesting circuits have limited capability, only

low power is needed by underlaid D2D nodes in order to limit their interference on the primary network. Thus, such nodes may survive on energy harvesting. However, spatial randomness of radio nodes, transmit power control and propagation effects make the amount of harvested energy stochastic [182], [183]. Thus, the power levels and frequency of transmissions of D2D nodes may not be viable at times. Overall, proper design of energy harvesting schemes is vital to ensure a reasonable performance.

### 6.1.1 Motivation and contributions

In this chapter, we investigate the energy harvesting process of a typical underlaid D2D node, $\mathcal{D}_t$ from the down-link transmissions of a multi-channel primary cellular network. The amount of energy harvested, say, $E_h$ depends on the distances from $\mathcal{D}_t$ to the set of primary base-stations, transmit power control and channel conditions. Having collected energy $E_h$, which is random, $\mathcal{D}_t$ goes on to transmit to its associated D2D receiver. Note that $E_h$ may not be sufficient for D2D transmissions depending on the receiver distance and sensitivity. In order to reduce this risk, we can consider energy harvests spanning multiple harvesting periods. An important factor is PLI transmit power control, which is employed by both cellular and D2D transmitters. It will affect both aggregate interference and link performance. Another critical question is to find suitable harvesting schemes which ensure regularity of transmission and sufficient energy harvests.

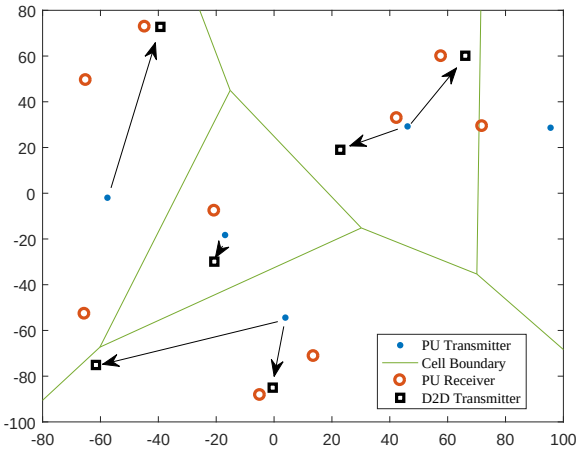


Figure 6.1: System model.

The specific problem investigated in this chapter can be explained as follows. In Fig. 6.1, D2D nodes and cellular devices (both users and base stations) share the same spectrum, and D2D nodes harvest the RF energy from cellular downlink transmissions. Each cell has $K$ down-link

channels and all base-stations are synchronous at network level. Our goal is to analyze the cumulative effects of all spatial, channel, and power control effects on the amount of energy extracted by a typical D2D node ($\mathcal{D}_t$) and to develop suitable harvesting schemes. While the interference on primary cellular users from D2D transmissions is also a critical concern, we will leave this for a future work. To study the impact of spatial randomness in $\mathbb{R}^2$, we model primary transmitters, primary receivers and D2D transmitters as three independent homogeneous Poisson point processes (Fig. 6.1) , where primary receivers associate with their closest primary transmitters and each D2D transmitter is associated with a corresponding receiver randomly distributed within a given distance from it. To model propagation effects, log distance path loss and Rayleigh fading are assumed. The primary spectrum is divided in to multiple sub-bands. All transmitters use path-loss inversion based power control. Furthermore, an exclusion region prohibiting D2D transmissions is enforced around every primary receiver. The D2D transmitters harvest ambient RF energy from the primary system and transmit their data within a single sub-band. Our contributions can be summarized as follows:

1. The aggregate ambient RF power at a typical $\mathcal{D}_t$ is the critical quantity. By using stochastic geometry, we derive its moment generating function (MGF), mean and variance, and model it as a Gamma random variable using moment matching. The derivation of the MGF is complicated by the fact that $K$ sub-bands are used by each base station, and because separated power control schemes are employed for each sub-band by every base station. As an auxiliary result, we also derive the probability of a primary transmitter using a particular sub-band when cellular users are assigned any of the $K$ sub-bands randomly without any specific priority.

2. We propose four energy harvesting protocols for a typical D2D transmitter node $\mathcal{D}_t$:

   (a) Single time-slot harvest - $\mathcal{D}_t$ harvests for one period and then transmits irrespective of the harvested energy.

   (b) Multi slot harvest - $\mathcal{D}_t$ continues till the harvested energy satisfies transmission requirements.

   (c) $\mathcal{N}$ slot harvesting scheme - $\mathcal{D}_t$ harvests for $\mathcal{N}$ slots before it transmits.

   (d) Hybrid harvesting - $\mathcal{D}_t$ can harvest energy for a maximum of $\mathcal{N}$ slots, and harvesting

process stops whenever extracted energy satisfies the transmission requirements.

The detailed descriptions of these can be found Section II.D.

3. We derive the probability of a successful energy harvest and being ready to transmit for the four aforementioned schemes. Because temporal dynamics are at play, we utilize Markov chains to model state transitions. Furthermore, we analyze the steady state probability of being within the desired states.

4. We characterize the D2D link coverage performance for a channel assignment protocol where each D2D transmitter selects a random sub-band for its transmission, for the four proposed energy harvesting schemes. In deriving this, we consider the interference from other D2D nodes and the cellular transmissions using the same sub-band.

### 6.1.2 Related work

Investigating energy harvesting by D2D nodes within a cellular setup has received the interest of researchers. As the most relevant work, the authors in [112] investigate the feasibility of energy harvesting for a multi-channel cellular system model similar to our work, and the D2D nodes are found to be able to harvest sufficient energy to allow for their own transmissions. However, the authors do not consider power control procedures, which will significantly alter the ambient RF power. Moreover, while [112] focuses more on sub-channel assignment policies, our work focuses on different energy harvesting protocols.

While other works also consider energy harvesting based networks, they do not necessarily consider either power control, a multi-channel cellular setup, temporal correlations, or a combination of these criteria. For example the fundamental trade-offs between the number of D2D transmissions and the harvesting period, and the optimum spectrum partitioning factor are characterized in [184]. Similarly, [185] investigates the resource management problem of energy harvesting for an uplink cellular set-up. Moreover, [186] analyzes the network performance when user-equipment relays harvest energy, and the authors develop an analytical framework and model the status of the harvested energy as a Markov chain. In [187] the authors investigate the effects of allowing multiple hops for transmission when the harvested energy of a D2D node is insufficient, and it is shown that two hop D2D communication outperforms single hop communication. Reference [57] analyzes a set of random primary and secondary nodes which

communicate with their receivers located a fixed distance away, and derives the optimal transmit power and secondary user density to achieve maximum throughput. Moreover, a novel energy field model is introduced in [188] and the coverage probability of a cellular network powered by energy harvesting is characterized, while a tractable $K$-tier heterogeneous model with energy harvesting base stations is introduced in [189]. In addition, [190] proposes dynamic spectrum and power allocation schemes, while [191] incorporates massive MIMO nodes in characterizing the efficiency of energy harvesting D2D networks.

## 6.2 System model

This section introduces the spatial distribution of primary and D2D nodes, the wireless channel model, receiver selection schemes, and power control procedures.

### 6.2.1 Spatial distribution

The network is broadly divided into primary and D2D nodes. We assume that both these networks are co-located but separate. In other words, we assume that primary receivers do switch to be a D2D node and vice-versa.

**Primary network distribution**

In this chapter, we will thus model primary nodes and D2D transmitters as homogeneous Poisson point processes [12], [38], [93], [192], [193], where the intensity of the process (average node density) does not depend on the location. While non-homogeneous processes perhaps suit actual real-world scenarios better, they are not amenable to more general analysis. As such, we model the primary transmitters (e.g., base stations) and receivers with two such processes $\Phi_{pt}$ and $\Phi_{pr}$ with intensities $\lambda_{pt}(> 0)$ and $\lambda_{pr}(> 0)$. Furthermore, since a base station typically serves multiple receivers, we further assume that $\lambda_{pt} < \lambda_{pr}$. Moreover, it is assumed that $\Phi_{pt}$ and $\Phi_{pr}$ are stationary, and mutually independent. All these assumptions are extremely common in the literature.

The primary network employs universal frequency reuse [94], [112]. The frequency band which is used for the downlink is divided into $K > 1$ sub-channels where each can accommodate a different primary receiver [112]. In practical terms, these sub-channels are resource blocks associated with modern cellular networks such as LTE (Long Term Evolution) systems [194].

**D2D network**

This consists of transmitter and receiver pairs, and are distributed in $\mathbb{R}^2$. We model the D2D transmitters as homogeneous Poisson point process $\Phi_{d2d}$ with intensity $\lambda_{d2d}(> 0)$. On the other hand, the D2D receivers are distributed uniformly in an annular area of radius $d_l$ centered on each D2D transmitter. Without the loss of generality, each D2D transmitter is associated with a unique receiver with probability one. However, if this probability is less than one, say, $\kappa$, then Colouring Theorem [73] shows that the associated D2D transmitters follow a thinned homogeneous Poisson process whose intensity is $\hat{\lambda}_{d2d} = \kappa\lambda_{d2d}$[1].

### 6.2.2 Channel model

The propagation model incorporates power-law path loss and small scale fading. We assume the simplified path loss model [3] where the received power follows (2.11). The value of $\alpha$ is assumed to be constant within the $k$ sub-bands. However, this model does not hold whenever $r \to 0$ as the received power $P_R \to \infty$. Therefore, we assume $P_R = P_T \left(\max(\delta, r)\right)^{-\alpha}$ where $\delta = 1$ is the reference distance. Because the probability of event $\{r \leq \delta\}$ is very small, this alteration does not significantly affect the overall statistics [157]. The small-scale fading follows the Rayleigh fading model. Consequently, the channel power gain $|h|^2$ follows (2.4). The fading gains of different links are mutually independent.

### 6.2.3 Power control and transmitter-receiver association

Both primary and D2D transmitters employ PLI power control scheme in order to ensure a fixed received power level on average. The level is called the receiver sensitivity[2]. If the sensitivities of the primary and D2D receivers are respectively $\rho_p$ and $\rho_{d2d}$, and the receiver distance is $r$, the transmit power can be written as $P_T = \rho_* r^\alpha$, where $* \in \{p, d2d\}$ [83]. Although PLI power control can potentially lead to excessive transmit powers, this difficulty is alleviated in our system model due to two reasons. First, primary transmitters are grid-connected base stations and are not peak-power constrained. Second, the association distance between a D2D transmitter and receiver is less than the radius $d_l$, which naturally lends to the limiting of peak-power requirements, as the maximum possible transmit power requirement is $\rho_{d2d} d_l^\alpha$.

[1]Here is an equivalent alternative interpretation. The D2D transmitters and receivers form separate independent Poisson point processes, and each transmitter randomly selects a receiver within a distance $d_l$, where a receiver can be connected to multiple transmitters concurrently.

[2]Note that the instantaneous received power may still vary depending on small scale fading

The general association rule for primary network is the closest association rule [157]. This rule may be implemented with the help of GPS information, location databases, or periodic fixed-power pilot sequences [195]. In general, the closest receiver link provides the best received power on average. With such an association policy, we can divide the coverage area into Voronoii cells surrounding each primary transmitter. In each cell, all primary receivers associate with the primary transmitter. We assume that out-of-cell associations do not take place. Accordingly, the associated distance between a primary receiver and transmitter relates to the void probability of a Poisson point process, and follows the Rayleigh distribution with [73]

$$f_X(x) = 2\pi\lambda_{pt} x e^{-\pi\lambda_{pt}x^2}, 0 < x < \infty. \tag{6.1}$$

Without any loss of generality, we assume that all primary receivers connect with a primary transmitter, and that no receiver is idle unless all the sub-bands of the transmitter are occupied. The Colouring theorem [73] can be easily employed if only a subset of the primary receivers need to be serviced at any given time.

For the D2D network, the association rule is simple where each transmitter connects with its paired receiver. The transmitter-receiver distance is obtained as follows. With respect to any transmitter, the receiver can be uniformly located within an annular region of radius $d_l$ [112]. Thus, the CDF of the transmitter-receiver distance $X$ becomes $F_X(x) = \frac{\pi x^2}{\pi d_l^2}$, $0 < x < d_l$. Differentiating this CDF yields the PDF which follows a linear distribution

$$f_X(x) = \frac{2x}{d_l^2}, 0 < x < d_l. \tag{6.2}$$

Similar to the primary network, without loss of generality, each D2D transmitter has data to be disseminated at any given time instant.

Because D2D transmissions may occur simultaneously with those of primary network, guard regions must be employed [120]. These are D2D-free zones around the primary users, and clearly limit the potential interference. The guard regions can be broadcast dynamically through periodic control sequences from the primary users [37], [157]. There are two placement options for the guard zones: (1) around primary receivers or (2) around primary transmitters. We assume option one, but not two. This assumption is due to several reasons. First, what is needed in the underlay mode is the interference temperature at each primary receiver is below a threshold. Thus, main

requirement to limit interference on primary receivers. Second, if option two is adopted, the primary receivers outside or close to the cell edge may not be detected by sensing algorithm and will suffer interference. Third, as energy must be harvested from primary transmissions, the close proximity of D2D nodes to primary transmitters reduces the path loss and increases the energy harvest , but option two prevents that.

The guard regions are assumed to be annular regions with a radius of $d_g$. Let $\Phi_{pr}$ be denoted by the set of points $\{x_1, x_2, ...\}$, and $\phi_{pr,i}$ be the primary receiver located at $x_i, (x_i \in \Phi_{pr})$. The guard region encircling $\phi_{pr,i}$ is thus denoted as $b(x_i, d_g)$. Therefore, if $\Phi_{d2d}$ is represented by $\{y_1, y_2, ...\}$, and node $\mathcal{D}_t$ is a typical D2D transmitter located at $y_j$ ($j \in \Phi_{d2d}$), it is precluded from transmitting if $y_j \in \mathcal{A}_{\mathcal{G}}$. Here, $\mathcal{A}_{\mathcal{G}} \in \mathbb{R}^2$ is the area of all the guard regions given by $\mathcal{A}_{\mathcal{G}} = \bigcup_{i \in \Phi_{pr}} b(x_i, d_g)$. Now, let the process of D2D transmitters outside $\mathcal{A}_{\mathcal{G}}$ be denoted as $\tilde{\Phi}_{d2d}$. $\tilde{\Phi}_{d2d}$ is non-homogeneous, and forms what is termed a Poisson hole process. Let $\nu$ be the probability that node $\mathcal{D}_t$ lies outside $\mathcal{A}_{\mathcal{G}}$, and alternatively is the probability that no primary receiver falls within a distance $d_g$ from node $\mathcal{D}_t$. We can thus obtain $\nu$ from (2.14) as $\nu = e^{-\pi \lambda_{pr} d_g^2}$.

### 6.2.4 D2D network operation

The D2D transmitters power their circuits with the energy harvested from ambient primary RF emissions. We assume that the power conversion circuits have an efficiency of $\beta(< 1)$, and that energy is harvested in the downlink phase from all sub-bands. Moreover, we assume that each D2D transmitter is always ready to transmit. Let a primary downlink time slot have length $T$. If the D2D transmitter requires additional energy at the beginning of a time slot, it will allocate the entire time slot for energy harvesting. Therefore, even in the best case scenario when the required energy is harvested in each time slot, data transfer is performed only on $50\%$ of the time slots.

Energy harvesting is subject to inherent unreliability because the harvested amount may not be enough to ensure that the receiver sensitivity is met [112]. Moreover, if harvesting time increases, the fraction of time available for data transfer will decrease, increasing delay and reducing spectral efficiency. To balance such conflicting requirements, we next propose four different energy harvesting schemes for a typical D2D transmitter (i.e., node $\mathcal{D}_t$ for brevity). The four schemes are subject to two common conditions. First, $\mathcal{D}_t$ uses up all harvested energy for its own transmissions and returns to the zero power state after each transmission. An extended work which removes this assumption is found in [196]. Second, the transmission of $\mathcal{D}_t$ are subject to

the guard zones around primary receivers (i.e., there are no transmissions).

1. Single-slot harvesting

   - Energy is harvested in slot 1. Let the power level associated with this energy be $P_{EH}$ (The energy harvesting process is explained in detail in the subsequent sections). $P_{EH} = \beta PT$ where the ambient RF power at node $\mathcal{D}_t$ is $P$.
   - If $P_{EH} < P_{TT}$, node $\mathcal{D}_t$ transmits at $P_{EH}$ during the subsequent time slot as long as it's outside the guard region $\mathcal{A}_{\mathcal{G}}$. Here, $P_{TT}$ is the required transmit power to ensure the receiver's sensitivity with PLI power control given by $P_{TT} = \rho_{d2d} r_{d2d}^{\alpha} T$, where the distance between node $\mathcal{D}_t \in \Phi_{d2d}$ and its receiver is denoted as $r_{d2d}$.
   - If $P_{EH} > P_{TT}$, node $\mathcal{D}_t$ transmits at $P_{TT}$ during the subsequent time slot.
   - If node $\mathcal{D}_t$ is within $\mathcal{A}_{\mathcal{G}}$, no transmission occurs.

   It's worth noting that the data transmission occurs irrespective of the harvested energy level. However, the transmit power could vary. If enough power is harvested, PLI power control ensures that node $\mathcal{D}_t$ has enough to satisfy the receiver's sensitivity requirement. But, if this is not satisfied, the transmission occurs using the harvested energy without any power control procedure. This scheme is most appropriate when the D2D users must transfer time critical data to because a transmission is guaranteed every two time slots subject to node $\mathcal{D}_t$ being outside a guard region.

2. Multi-slot harvesting

   Node $\mathcal{D}_t$ waits multiple time slots till the harvested energy is greater than the required transmission energy to ensure the receiver's sensitivity requirement through PLI power control. The specific protocol is as follows.

   - Energy is harvested in slot 1.
   - If $P_{EH} < P_{TT_m}$, energy harvesting occurs at the subsequent time slot. This process continues till $P_{EH} > P_{TT_m}$, where $P_{TT_m}$ is the maximum energy required to transmit, given by $P_{TT_m} = \rho_{d2d} d_l^{\alpha} T$.

- Whenever $P_{EH} > P_{TT_m}$, node $\mathcal{D}_t$ transmits at $P_{TT_m}$ during the subsequent time slot as long as $\mathcal{D}_t$ is outside $\mathcal{A}_{\mathcal{G}}$.
- If node $\mathcal{D}_t$ is within $\mathcal{A}_{\mathcal{G}}$, no transmission occurs.

However, if this sensitivity requirement is high or if the ambient RF energy from the primary system is low, it can take a significant amount of time slots for node $\mathcal{D}_t$ to charge fully, which reduces its ability to transmit at the start of a given time slot. On the flip side, the eventual transmission has a high probability of success to ensure that receiver sensitivity requirements are met. This scheme is most suitable under one or more of the following conditions: the data is not time critical and the data generation is irregular and infrequent.

3. $\mathcal{N}$-slot harvesting

This is an extension of the single slot harvesting scheme to $\mathcal{N}$ slots, and the protocol can be summarized as below.

- Energy is harvested by node $\mathcal{D}_t$ in slots 1 to $\mathcal{N}$.
- If $P_{EH} < P_{TT}$, node $\mathcal{D}_t$ transmits at $P_{EH}$ during the subsequent time slot ($\mathcal{N} + 1$).
- If $P_{EH} > P_{TT}$, node $\mathcal{D}_t$ transmits at $P_{TT}$ during the subsequent time slot.
- If the D2D transmitter is within $\mathcal{A}_{\mathcal{G}}$, no transmission occurs.

While keeping the regularity of single slot harvesting, $\mathcal{N}$ slot harvesting attempts to harvest more energy before the transmission is conducted so that the resulting transmission is successful. Moreover, similar to single slot harvesting, transmission occurs irrespective of the harvested energy after $\mathcal{N}$ harvesting slots. With this scheme, the selection of $\mathcal{N}$ must be performed judiciously. While a small $\mathcal{N}$ provides regular transmission opportunities, it also constrains the harvested power.

4. Hybrid harvesting

Hybrid harvesting is a cross between $\mathcal{N}$ slot harvesting and multi slot harvesting. Within this scheme, node $\mathcal{D}_t$ can harvest energy for a maximum of $\mathcal{N}$ slots. However, if the harvested energy exceeds $P_{TT}$ before the $\mathcal{N}$ slots are up, node $\mathcal{D}_t$ aborts the harvesting and transmits within the subsequent slot. In other words, the hybrid harvesting scheme is multi slot harvesting with a cap of $\mathcal{N}$ harvesting slots. If the harvested energy is still lower than $P_{TT}$ after $\mathcal{N}$ time slots, node $\mathcal{D}_t$ has no option other than transmitting using the harvested energy as long as it is outside the guard region $\mathcal{A}_{\mathcal{G}}$. This scheme keeps the predictability of the $\mathcal{N}$ slot harvesting scheme by forcing a transmission after a pre-determined period. But it goes a step further by providing the flexibility to cease energy harvesting if the required energy amount is harvested before $\mathcal{N}$ periods. The specific protocol can be summarized as below.

- Energy is harvested in slot $1$.
- If $P_{EH} < P_{TT}$, energy harvesting ocurs at the subsequent time slot. This process continues till either $P_{EH} > P_{TT}$ or till the $\mathcal{N}$-th time slot.
- Whenever $P_{EH} > P_{TT}$, node $\mathcal{D}_t$ transmits at $P_{TT}$ during the subsequent time slot as long as it's outside the guard region $\mathcal{A}_{\mathcal{G}}$.
- If $P_{EH} < P_{TT}$ even after the $\mathcal{N}$-th time slot, node $\mathcal{D}_t$ transmits at $P_{EH}$ during the subsequent time slot as it's outside the guard region $\mathcal{A}_{\mathcal{G}}$.
- If the D2D transmitter is within $\mathcal{A}_{\mathcal{G}}$, no transmission occurs.

As mentioned before, the D2D transmitters use one of the $K > 1$ different sub-bands for their transmissions. The selected sub-band determines the resultant interference on both the primary and D2D receivers. To limit this, we will consider the random selection of a sub-band by each D2D transmitter. This protocol reduces lower intra-D2D interference as the different D2D transmissions may occur in different sub-bands. However, on the downside, as no particular band is free from a potential D2D access, all primary transmissions may be adversely effected. An alternative is to restrict all D2D transmissions to a particular sub-band $q \in \{1, \ldots, K\}$ which has the lowest usage by the primary system. Such a protocol lowers inter-network interference when the number of primary receivers within a cell falls below $K$. However, it incurs disadvantages of

high intra-D2D interference and high interference on primary receivers on band $q$. Moreover, it needs substantial amount of prior network information, and thus will not be analyzed.

## 6.3 Energy harvesting

In this section, we will derive total harvested energy in each of the four harvesting schemes and the probability of a successful energy harvest within the harvesting period.

In many cases, since exact distributions of random variables are generally intractable, MGF (moment generating function) is widely used [88]–[94]. The MGF can be obtained relatively easily when there is a sum of independent variables [88], [93].

Let $P$ be the received ambient RF power (i.e., $\beta PT$ is the harvested energy) at node $\mathcal{D}_t$, which we place at the origin without the loss of generality. Ambient power $P$ emanates from all primary transmitters, hence we write $P = \sum_{l\in\Phi_{pt}} P_l$, where $P_l$ is the ambient RF power from the $l$-th primary transmitter $\phi_{pt,l}$. $P_l$ is written as $P_l = \sum_{k=1}^{K} C_{k,l}\rho_p \hat{r}_{k,l}^{\alpha}|h_l|^2 g(r_l)$, where the term $\rho_p \hat{r}_{k,l}^{\alpha}$ is the transmit power from $\phi_{pt,l}$ to the primary receiver using the $k$-th sub-band located at a distance of $\hat{r}_{k,l}$ from it. Quantities $|h_l|^2$ and $g(r_l) = \min\left(()\,1, r_l^{-\alpha}\right)$ are respectively small-scale channel power gain and the path loss between $\phi_{pt,l}$ and $\mathcal{D}_t$, and $C_{k,l}$ is the probability that the $k$-th ($1 \le k \le K$) sub-band is in occupation during the specific harvesting time-slot.

To conduct further analysis with $P$, we will evaluate its MGF, which is defined as $M_P(s) = \mathbb{E}[e^{-sP}]$. Using Campbell's Theorem [73], we can write $M_P(s)$ as

$$M_P(s) = e^{\int_0^\infty \mathbb{E}\left[e^{-s\sum_{k=1}^{K} C_{k,l}\rho_p \hat{r}_{k,l}^{\alpha}|h_l|^2 g(r_l)}-1\right]2\pi\lambda_{pt} r_l dr_l}. \tag{6.3}$$

Using the fact that $\frac{1}{1+x} = \sum_{v=0}^{\infty}(-x)^v$, and averaging with respect to $|h_l|^2$ and $r_l$ we can simplify $M_P(s)$ as

$$M_P(s) \;=\; e^{\left(\sum_{v=1}^{\infty} \frac{\pi\lambda_{pt}\alpha v}{\alpha v-2}(-sC_{k,l}\rho_p)^v \mathbb{E}[(\sum_{k=1}^{K}\hat{r}_{k,l}^{\alpha})^v]\right)}. \tag{6.4}$$

Because $P$ and its MGF are of complicated forms, it is advantageous to approximate $P$ with a well known random variable. It has been shown that the received power from a random field of base stations follows a skewed $\alpha$-stable distribution, which can be closely modeled as a Gamma r.v. with hape and scale parameters $k_P$ and $\theta_P$ respectively [88]. For this, we can match actual moments of $P$ are with those of the Gamma r.v. To this end, we use MGF to derive the moments

of $P$, where the $n$-th moment is given by $\mathbb{E}[P^n] = (-1)^n \left[\frac{d^n}{ds^n} M_P(s)\right]_{s=0}$. Therefore, we can find $\mathbb{E}[P]$ and $\mathbb{VAR}[P]$ when $\alpha > 2$ as follows:

$$\mathbb{E}[P] = \frac{\Gamma\left(\frac{\alpha}{2}+1\right)\alpha K C_{k,l}\rho_p}{(\pi\lambda_{pt})^{\frac{\alpha}{2}-1}(\alpha-2)}, \tag{6.5}$$

$$\mathbb{VAR}[P] = \frac{\alpha(C_{k,l}\rho_p)^2 K}{(\pi\lambda_{pt})^{\alpha-1}(\alpha-1)}\left(\Gamma(\alpha+1) - \left(\Gamma\left(\frac{\alpha}{2}+1\right)\right)^2(1-K)\right). \tag{6.6}$$

Via moment matching, shape and scale parameters $k_P$ and $\theta_P$ are obtained as $k_P = \frac{(\mathbb{E}[P])^2}{\mathbb{VAR}[P]}$ and $\theta_P = \frac{\mathbb{VAR}[P]}{\mathbb{E}[P]}$.

### 6.3.1 Derivation of the probability of sub-band occupation

All $K$ sub-bands used by the primary transmitter $\phi_{pt,l}$ have equal probabilities to be assigned for communication with a primary receiver, and thus $C_{k,l}$ remains constant $\forall k \in \{1, 2, ..., K\}$. From intuition, $C_{k,l}$ depends on the number of primary receivers associated with $\phi_{pt,l}$, which is itself dependent on the area of its Voronoii cell. However, the area of a Voronoii cell has no exact distribution. But, an accurate approximation can be made using the Gamma distribution [169]. If $\mathcal{B}$ and $\bar{\mathcal{B}}$ are the cell area and average cell area, the normalized area $\tilde{\mathcal{B}} = \frac{B}{\bar{\mathcal{B}}}$ of a Voronoii cell is given by $f_{\tilde{\mathcal{B}}}(x) = \frac{\beta_v^{\mu_v}}{\Gamma(\mu_v)} x^{\mu_v - 1} e^{-\beta_v x}$, where $\beta_v = 3.57$, $\mu_v = 3.61$, and $\bar{\mathcal{B}} = \frac{1}{\lambda_{pt}}$.

If the number of primary receivers associated with $\phi_{pt,l}$ is $Z$, $C_{k,l}$ can be expressed as

$$C_{k,l} \backslash z = \Pr[Z \geq K] + \sum_{z=1}^{K-1} \Pr[Z = z]\frac{z}{K}. \tag{6.7}$$

Using (2.14) for a given area $\mathcal{B}$ and subsequent averaging by the distribution of $f_{\tilde{\mathcal{B}}}(x)$ results in

$$C_{k,l} = \frac{\beta_v^{\mu_v}}{\Gamma(\mu_v)}\left(\sum_{z=K}^{\infty}\frac{\Gamma(\mu_v+z)\eta^z}{z!(\beta_v+\eta)^{\mu_v+z}} + \sum_{z=1}^{K-1}\frac{\Gamma(\mu_v+z)\eta^z}{K(z-1)!(\beta_v+\eta)^{\mu_v+z}}\right), \tag{6.8}$$

where $\eta = \frac{\lambda_{pr}}{\lambda_{pt}}$.

## 6.4 D2D transmission probability

In this section, we derive the transmission probability of a D2D transmitter for four energy harvesting schemes. For all four schemes, we assume that the energy level drops to $0$ after a transmission. Moreover, we assume that each D2D transmitter has data to be transmitted at the start of a given time slot.

### 6.4.1 Single slot harvest

This scheme is described in Page 136, where node $\mathcal{D}_t$ attempts a transmission irrespective of the energy harvest provided $\mathcal{D}_t$ lies outside the guard region. The distance between the node $\mathcal{D}_t \in \Phi_{d2d}$ and its receiver, $r_{d2d}$, is distributed as (6.2). If the harvested energy $\beta PT > \rho_{d2d} r_{d2d}^{\alpha} T$, the transmitted power $P_{\mathcal{D}_t} = \rho_{d2d} r_{d2d}^{\alpha}$. However, whenever $\beta PT < \rho_{d2d} r_{d2d}^{\alpha} T$, $P_{\mathcal{D}_t} = \beta P$. Therefore, $\tau = \Pr[P_{\mathcal{D}_t} = \beta P]$ can be obtained as

$$\begin{aligned} \tau &= \Pr\left[P < \frac{\rho_{d2d} r_{d2d}^{\alpha}}{\beta}\right] \\ &= \int_0^{d_l} \frac{2x}{d_l^2 \Gamma(k_P)} \gamma\left(k_P, \frac{\rho_{d2d} x^{\alpha}}{\beta \theta_P}\right) dx, \end{aligned} \tag{6.9}$$

where (10) is obtained after first evaluating $\tau$ conditioned on $r_{d2d}$, and then averaging over (6.2).

Let $p^{ss}$ be the probability that $\mathcal{D}_t$ is ready to transmit at the start of a time slot at steady state. Due to the temporal effects, we use a two state Markov chain: charged (state $1$) and uncharged (state $0$). While $\mathcal{D}_t$ always transitions from the uncharged state to the charged state at the start of the next time slot, it only transitions from the charged state to the uncharged state if it lies outside the guard region $\mathcal{A}_{\mathcal{G}}$. The state transition matrix $Q$ can be written as

$$Q = \begin{bmatrix} 0 & 1 \\ \nu & 1-\nu \end{bmatrix}.$$

Let $\Omega = [\omega_0 \ \omega_1]$ be the vector comprising steady state probabilities of $Q$. During steady state, $\Omega = \Omega Q$, and we can derive $p^{ss} = \omega_1 = \frac{1}{1+\nu}$. Thus, the probability of conducting a transmission at the start of a time slot is $\nu p^{ss}$.

### 6.4.2 Multi-slot harvest

As mentioned in Section II, under multi-slot harvesting, node $\mathcal{D}_t$ harvests energy in multiple time slots until the total harvested energy $\beta PT$ is greater than the maximum energy required to transmit, which is $\rho_{d2d} d_l^{\alpha} T$. While the harvested energy at the end of a time slot does not confine to discrete levels, for mathematical convenience, we divide the energy levels into $M+1$ discrete states where $M$ can be increased arbitrarily to better reflect the non-discrete nature of the energy level. The $0$-th and $M$-th states respectively denotes the uncharged and fully charged levels. Let

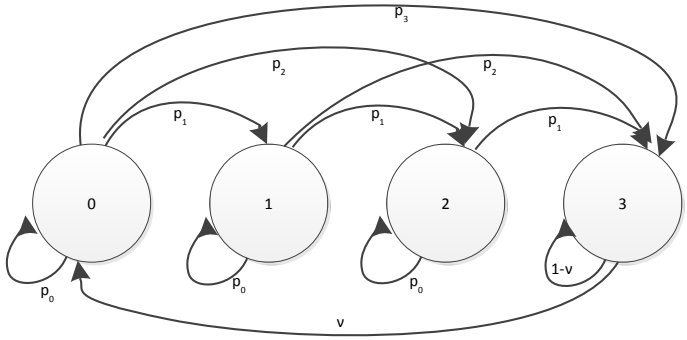


Figure 6.2: Markov chain model for multi-slot harvesting with $M = 3$.

the power level of the $\delta$-th state ($0 < \delta < M$) be denoted as $E_\delta$. If $\mathcal{D}_t$ was initially in state $0$, it would transition to state $\delta$ whenever $E_\delta \leq \beta PT < E_{\delta+1}$, remain at state $0$ if $\beta PT < E_1$, and reach state $M$ if $\beta PT \geq E_M$. Similarly, whenever $\mathcal{D}_t$ is initially at state $\delta$, the transitioned state increases correspondingly.

The state transition diagram is in Fig. 6.2, and the state transition matrix $Q$ (with the vector of steady state probabilities being $\Omega = [\omega_0\ \omega_1\ ..\ \omega_M]$) is expressed as follows.

$$Q = \begin{bmatrix} p_0 & p_1 & p_2 & . & p_{M-1} & 1-\sum_{g=0}^{M-1} p_g \\ 0 & p_0 & p_1 & . & p_{M-2} & 1-\sum_{g=0}^{M-2} p_g \\ 0 & 0 & p_0 & . & p_{M-3} & 1-\sum_{g=0}^{M-3} p_g \\ . & . & . & . & . & . \\ 0 & 0 & 0 & . & p_0 & 1-p_0 \\ \nu & 0 & 0 & . & 0 & 1-\nu \end{bmatrix}.$$

Here $p_g (g \in \{1, 2, 3, ..., M-1\})$ refers to the probability of transitioning $g$ states higher from the initial state, and can be expressed as

$$\begin{aligned} p_g &= \Pr\left[\frac{g\rho_{d2d} d_l^\alpha}{\beta M} \leq P < \frac{(g+1)\rho_{d2d} d_l^\alpha}{\beta M}\right] \\ &= \frac{1}{\Gamma(k_P)}\left(\gamma\left(k_P, \frac{(g+1)\rho_{d2d} d_l^\alpha}{\beta M \theta_P}\right) - \gamma\left(k_P, \frac{g\rho_{d2d} d_l^\alpha}{\beta M \theta_P}\right)\right). \end{aligned} \tag{6.10}$$

Let $p^{ms}$ be the probability that $\mathcal{D}_t$ is ready to transmit at the start of a time slot, which is also the steady state probability of being at state $M$. We can obtain $p^{ms}$ as

$$p^{ms} = \omega_M = \frac{1}{1 + \sum_{g=0}^{M-1} \mathcal{D}_g}. \tag{6.11}$$

Here, $\mathcal{D}_0 = \frac{-\nu}{p_0 - 1}$, and $\mathcal{D}_g = \frac{-1}{p_0 - 1}(\sum_{h=0}^{g-1} p_{g-h}\mathcal{D}_h)$ for $1 \leq g \leq M-1$. It can be easily seen that (6.11) reduces to $p^{ss}$ when $M = 1$ and $p_0 = 0$. The probability of conducting a transmission at the start of any time slot is thus $\nu p^{ms}$.

### 6.4.3 $\mathcal{N}$ slot harvest

Let $\beta P_{T,\mathcal{N}} T$ be the harvested energy at the end of $\mathcal{N}$ time slots. $P_{T,\mathcal{N}} T$ is written as

$$P_{T,\mathcal{N}} = P_1 + P_2 + \cdots + P_{\mathcal{N}}, \tag{6.12}$$

where $P_w, w \in \{1, 2, \ldots, \mathcal{N}\}$ is the ambient power available to be harvested during the $w$-th time slot. It should be noted that $P_w \ \forall w$ are independent and identically distributed random variables having the distribution of $P$ (Gamma with shape and scale parameters $k_P$ and $\theta_P$). As such, $P_{T,\mathcal{N}}$ is also Gamma distributed with shape and scale parameters $\mathcal{N}k_P$ and $\theta_P$ respectively.

Whenever the harvested energy $\beta P_{T,\mathcal{N}} T > \rho_{d2d} r_{d2d}^{\alpha} T$, the transmit power $P_{\mathcal{D}_t} = \rho_{d2d} r_{d2d}^{\alpha}$. But, when $\beta P_{T,\mathcal{N}} T < \rho_{d2d} r_{d2d}^{\alpha} T$, $P_{\mathcal{D}_t} = \beta P_{T,\mathcal{N}}$ because transmission occurs after $\mathcal{N}$ slots irrespective of the harvested energy. Thus, we can write $\tau = \Pr[P_{\mathcal{D}_t} = \beta P_{T,\mathcal{N}}]$ as

$$\begin{aligned} \tau &= \Pr[P_{T,\mathcal{N}} < \frac{\rho_{d2d} r_{d2d}^{\alpha}}{\beta}] \\ &= \int_0^{d_l} \frac{2x}{d_l^2 \Gamma(\mathcal{N}k_P)} \gamma\left(\mathcal{N}k_P, \frac{\rho_{d2d} x^{\alpha}}{\beta \theta_P}\right) dx. \end{aligned} \tag{6.13}$$

We now require the probability that a typical D2D transmitter $\mathcal{D}_t$ is ready to transmit at the start of a given time slot, which is denoted by $p^{\mathcal{N}s}$. Similar to the previous schemes, we will use a Markov chain in order to account for the temporal effects. This chain will have $\mathcal{N}+1$ states, where the $\delta$-th state ($0 \leq \delta \leq \mathcal{N}$) corresponds to the state after charging for $\delta$ time slots. As such, the 0-th state is the uncharged state while the $\mathcal{N}$-th state is the state where transmission is conducted. While the current state $\delta < \mathcal{N}$, transition always occurs to the subsequent state $(\delta+1)$ after charging for a time slot. When the current state is $\mathcal{N}$, transmission can occur whenever $\mathcal{D}_t$ is outside the guard region $\mathcal{A}_{\mathcal{G}}$, and a transition occurs to the 0-th state. Conversely, whenever $\mathcal{D}_t$ is located within $\mathcal{A}_{\mathcal{G}}$, no transmission occurs and the state remains at $\mathcal{N}$. This can be written as a

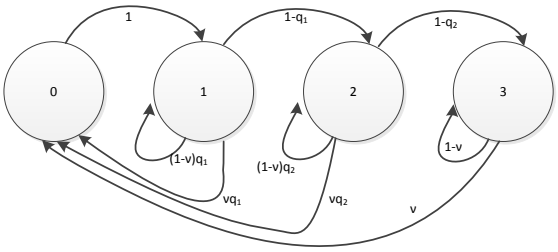


Figure 6.3: Markov chain model for hybrid harvesting with $\mathcal{N} = 3$.

state transition matrix $Q$ where

$$Q = \begin{bmatrix} 0 & 1 & 0 & . & 0 & 0 \\ 0 & 0 & 1 & . & 0 & 0 \\ . & . & . & . & . & . \\ 0 & 0 & 0 & . & 1 & 0 \\ 0 & 0 & 0 & . & 0 & 1 \\ \nu & 0 & 0 & . & 0 & 1-\nu \end{bmatrix}.$$

If $\Omega = [\omega_0\ \omega_1 \ldots \omega_{\mathcal{N}}]$ be the steady state probability vector. $p^{\mathcal{N}s}$ is thus equivalent to $\omega_{\mathcal{N}}$, which is the steady state probability of being at state $\mathcal{N}$. Thus we can obtain $p^{\mathcal{N}s}$ as

$$p^{\mathcal{N}s} = \frac{1}{1+\mathcal{N}\nu}. \tag{6.14}$$

It can be observed that $p^{\mathcal{N}s}$ reduces to $p^{ss}$ whenever $\mathcal{N} = 1$. The probability of $\mathcal{D}_t$ conducting a transmission at the start of any time slot is thus $\nu p^{\mathcal{N}s}$.

### 6.4.4 Hybrid harvest

The state transition diagram for this harvesting scheme is shown in Fig. 6.3. It should be noted that while the states of Fig. 6.2 represented distinct levels of energy, the states in Fig. 6.3 represent the states after particular time slots. Similar to the $\mathcal{N}$ slot harvesting scheme, the Markov chain will have $\mathcal{N}+1$ states. While the $\delta$-th state ($0 \leq \delta \leq \mathcal{N}$) corresponds to the state after charging for $\delta$ time slots similar to the $\mathcal{N}$ slot harvesting scheme, there are some notable differences as well. If the D2D transmitter is fully charged at the $\delta$-th state, it either remains within that state if it's within the guard region $\mathcal{A}_{\mathcal{G}}$ or transmits and transitions back to the $0$-th uncharged state if outside $\mathcal{A}_{\mathcal{G}}$.

Let the harvested energy after $w$ time slots ($0 < w \leq \mathcal{N}$) be $\beta P_{T,w} T$. As described in the previous subsection (Section III C), $P_{T,w}$ follows a Gamma distribution with shape and scale parameters of $wk_P$ and $\theta_P$. If $q_w$ is the probability that the D2D transmitter harvests sufficient energy after $w$ time slots, $q_w$ can be expressed as follows.

$$\begin{aligned} q_w &= \Pr\left[\beta P_{T,w} T > \rho_{d2d} r_{d2d}^{\alpha} T\right] \\ &= 1 - \int_0^{d_l} \frac{2x}{d_l^2 \Gamma(wk_P)} \gamma\left(wk_P, \frac{\rho_{d2d} x^{\alpha}}{\beta \theta_P}\right) dx. \end{aligned} \tag{6.15}$$

Now, we will evaluate the probability that the transmit power of node $\mathcal{D}_t$ $P_{\mathcal{D}_t} \neq \rho_{d2d} r_{d2d}^{\alpha}$. After $\mathcal{N}$ time slots, transmission occurs irrespective of the harvested energy. Therefore, if $\mathcal{D}_t$ harvests energy for the full $\mathcal{N}$ time slots, and if the harvested energy $\beta P_{T,\mathcal{N}} T < \rho_{d2d} r_{d2d}^{\alpha} T$, $P_{\mathcal{D}_t} = \beta P_{T,\mathcal{N}}$. Thus, we can express $\tau = \Pr[P_{\mathcal{D}_t} = \beta P_{T,\mathcal{N}}]$ as

$$\tau = \prod_{w=1}^{\mathcal{N}} (1 - q_w), \tag{6.16}$$

where $q_w$ is given in (6.15).

The state transition matrix $Q$ is written as

$$Q = \begin{bmatrix} 0 & 1 & 0 & . & 0 & 0 \\ \nu q_1 & (1-\nu) q_1 & 1 - q_1 & . & 0 & 0 \\ . & . & . & . & . & . \\ \nu q_{\mathcal{N}-2} & 0 & 0 & . & q_{\mathcal{N}-1} & 0 \\ \nu q_{\mathcal{N}-1} & 0 & 0 & . & (1-\nu) q_{\mathcal{N}-1} & 1 - q_{\mathcal{N}-1} \\ \nu & 0 & 0 & . & 0 & 1 - \nu \end{bmatrix}.$$

Let $\Omega = [\omega_0 \ \omega_1 \ldots \omega_{\mathcal{N}}]$ be the steady state probability vector. During steady state, $\Omega = \Omega Q$. After solving this expression for different $\omega_\delta (\delta \in \{0, 1, \ldots, \mathcal{N}\})$, we obtain

$$\omega_\delta = \begin{cases} \frac{1}{(1-(1-\nu)q_1)} \omega_0 & , \delta = 1 \\ \frac{\prod_{g=1}^{\delta-1}(1-q_g)}{\prod_{h=1}^{\delta}(1-(1-\nu)q_h)} \omega_0 & , \delta = 2, 3, \ldots, \mathcal{N}-1 \\ \frac{\prod_{g=1}^{\delta-1}(1-q_g)}{\nu \prod_{h=1}^{\delta-1}(1-(1-\nu)q_h)} \omega_0 & , \delta = \mathcal{N} \end{cases}, \tag{6.17}$$

$$\omega_0 = \frac{1}{1 + \frac{1}{(1-(1-\nu)q_1)} + \sum_{\delta=2}^{\mathcal{N}-1} \frac{\prod_{g=1}^{\delta-1}(1-q_g)}{\prod_{h=1}^{\delta}(1-(1-\nu)q_h)} + \frac{\prod_{g=1}^{\mathcal{N}-1}(1-q_g)}{\nu \prod_{h=1}^{\mathcal{N}-1}(1-(1-\nu)q_h)}} \tag{6.18}$$

where $\omega_0$ is given in (6.18).

Let $p^{hs}$ be the probability that $\mathcal{D}_t$ is ready to transmit at the beginning of a particular time slot under the hybrid harvesting scheme. This probability is composed of multiple components where each component comprises the ready-to-transmit probability after each harvesting slot. Thus, we may write $p^{hs}$ as

$$p^{hs} = \sum_{\delta=1}^{\mathcal{N}-1} \omega_\delta q_\delta + \omega_{\mathcal{N}}, \mathcal{N} \geq 2. \tag{6.19}$$

Whenever $\mathcal{N} = 1$, the hybrid harvesting scheme reduces to the single slot harvesting scheme. The probability of the D2D transmitter $\mathcal{D}_t$ actually conducting a transmission is therefore written as $\nu p^{hs}$.

## 6.5 D2D receiver performance

Here we analyze the coverage performance of a D2D receiver where each D2D transmitter randomly selects a sub-band $k (k \in \{1, 2, ..., K\})$ when it is ready to transmit. If $\gamma_{d2d}$ is the SINR at the D2D receiver associated with $\mathcal{D}_t$, we can write it as $\gamma_{d2d} = \frac{P_{d2d,j}}{I_P + I_{d2d} + \sigma_n^2}$, where $P_{d2d,j}$ is the received power from $\mathcal{D}_t$, $I_P$ is the interference from primary signals within the $k$-th sub band, $I_{d2d}$ is the interference from other D2D transmissions, and $\sigma_n^2$ is the noise power.

Coverage occurs if $\gamma_{d2d} > \gamma_T$, where $\gamma_T$ is a threshold SINR level. Coverage probability $\mathbb{P}_C = \Pr[\gamma_{d2d} > \gamma_T]$ may thus be expressed as

$$\begin{aligned} \mathbb{P}_C &= \tau \Pr\left[\frac{\beta P |h_{d2d}| r_{d2d}^{-\alpha}}{I_P + I_{d2d} + \sigma_n^2} > \gamma_T\right] \\ &+ (1-\tau) \Pr\left[\frac{\rho_{d2d} |h_{d2d}|}{I_P + I_{d2d} + \sigma_n^2} > \gamma_T\right], \end{aligned} \tag{6.20}$$

where $\tau$ is defined in (6.9). Note that for the multi slot harvesting scheme $\tau = 0$, and the first term of (6.20) vanishes. After several mathematical manipulations and ignoring the negligible interference from D2D transmitters when a full charge does not occur (for the single slot scheme), we can express $\mathbb{P}_C$ as (6.21) where the remaining integrals must be performed numerically. However,

$$\mathbb{P}_C = \int_{r_{d2d}=0}^{d_l} \int_{P=0}^{\frac{\rho_{d2d} r_{d2d}^{\alpha}}{\beta}} e^{\frac{-\sigma_n^2 \gamma_T r_{d2d}^{\alpha}}{\beta P}} M_{I_p}\left(\frac{\gamma_T r_{d2d}^{\alpha}}{\beta P}\right) \frac{P^{k_P-1} e^{-\frac{P}{\theta_P}}}{\Gamma(k_P)\theta_P} \frac{2 r_{d2d}}{d_l^2} dP dr_{d2d}$$
$$+ \quad (1-\tau) e^{\frac{-\sigma_n^2 \gamma_T}{\rho_{d2d}}} M_{I_p}\left(\frac{\gamma_T}{\rho_{d2d}}\right) M_{I_{d2d}}\left(\frac{\gamma_T}{\rho_{d2d}}\right) \tag{6.21}$$

---

in order to evaluate (6.21), the MGFs of $I_p$ and $I_{d2d}$ are needed.

The interference from primary network is composed of signals from $k$-th sub band primary transmitters. Thus, these interfering primary transmitters form a thinned homogeneous Poisson point process with density $C_{k,l}\lambda_{pt}$, where $C_{k,l}$ follows (6.8), and the interference from a single primary transmitter $\phi_{pt,l}$ is written as $I_{P,l} = \rho_p \hat{r}_{k,l}^{\alpha} |h_{l,r}| g(r_{l,r})$, where $|h_{l,r}|$ and $g(r_{l,r}) = r_{l,r}^{-\alpha}$ are respectively the channel power gain and path loss between the $l$-th interfering primary transmitter and the receiver associated with $\mathcal{D}_t$. Thus, making use of Slyvniak's and Campbell's theorems, we can write $M_{I_p}(s) = e^{\left(\int_0^{\infty} \mathbb{E}\left[e^{-s\rho_p \hat{r}_{k,l}^{\alpha} |h_{l,r}| r_{l,r}^{-\alpha}} - 1\right] 2\pi C_{k,l}\lambda_{pt} r_{l,r} dr_{l,r}\right)}$. After first averaging with respect to $|h_{l,r}|$, performing the integral, and finally averaging with respect to $\hat{r}_{k,l}$ we get

$$M_{I_p}(s) = e^{\left(-\frac{2\pi^2 C_{k,l}\lambda_{p,t}(s\rho_p)^{\frac{2}{\alpha}}}{\alpha sin\left(\frac{2\pi}{\alpha}\right)} \mathbb{E}[\hat{r}_{k,l}^2]\right)} = e^{\left(-\frac{2\pi C_{k,l}(s\rho_p)^{\frac{2}{\alpha}}}{\alpha sin\left(\frac{2\pi}{\alpha}\right)}\right)}. \tag{6.22}$$

We now focus our attention on deriving the MGF of $I_{d2d}$. $I_{d2d}$ is composed of the interference from other D2D transmitters occupying the $k$-th sub band. For interference to occur from the $jj$-th D2D transmitter, it must be ready to transmit, be outside guard regions, and must choose the $k$-th sub band. As these conditions occur independently from other D2D transmitters within $\Phi_{d2d}$, the interfering D2D transmitters can be approximated by a thinned homogeneous Poisson point process with a density of $\frac{\nu p^* \lambda_{d2d}}{K}$, where $* \in \{ss, ms\}$. Now the interference from the $jj$-th D2D transmitter can be written as $I_{d2d,jj} = P_{jj}|h_{jj,r}|g(r_{jj,r})$, where $|h_{jj,r}|$ and $g(r_{jj,r}) = r_{jj,r}^{-\alpha}$ are the channel power gain and path loss between the $jj$-th interfering D2D transmitter and the receiver associated with $\mathcal{D}_t$, while $P_{jj}$ is the transmit power of the $jj$-th interfering D2D transmitter. Using a similar method to the derivation of (6.22), we can write $M_{I_{d2d}}$ as

$$M_{I_{d2d}} = e^{\left(-\frac{2\pi^2 \nu p^* \lambda_{d2d} s^{\frac{2}{\alpha}}}{\alpha K sin\left(\frac{2\pi}{\alpha}\right)} \mathbb{E}[P_{jj}^{\frac{2}{\alpha}}]\right)}. \tag{6.23}$$

The expectation $\mathbb{E}[P_{jj}^{\frac{2}{\alpha}}]$ can be expressed as

$$\mathbb{E}[P_{jj}^{\frac{2}{\alpha}}] \quad = \quad \tau\mathbb{E}[\beta^{\frac{2}{\alpha}}P^{\frac{2}{\alpha}}] + (1-\tau)\mathbb{E}[\rho_{d2d}^{\frac{2}{\alpha}}r_{d2d}^{2}], \tag{6.24}$$

where the first and second expectations are respectively with respect to $P|P < \frac{\rho_{d2d}r_{d2d}^{\alpha}}{\beta}$ and $r_{d2d}$. It should be noted that for the multi slot harvesting scheme $\tau = 0$, and the first term will disappear. Thus, after some mathematical modifications, we obtain

$$\mathbb{E}[P_{jj}^{\frac{2}{\alpha}}] = \int_{0}^{d_l} \frac{2x(\beta\theta_P)^{\frac{2}{\alpha}}}{\Gamma(k_P)d_l^2}\gamma\left(k_P+\frac{2}{\alpha},\frac{\rho_{d2d}x^{\alpha}}{\beta\theta_P}\right)dx+(1-\tau)\frac{\rho_{d2d}^{\frac{2}{\alpha}}d_l^2}{2}. \tag{6.25}$$

**Probability of a successful transmission**

The final probability of a successful transmission during a given time slot ($\mathbb{P}_{C,Total}$) depends on three factors. First, the D2D transmitter should be in the charged state at the start of the time slot. Second, it should not be inside any guard region. Third, if a transmission occurs, the D2D receiver should be within coverage. Considering all three conditions, we can write

$$\mathbb{P}_{C,Total} = p^{*}\nu\mathbb{P}_{C}. \tag{6.26}$$

## 6.6 Numerical results

Within this section, we investigate the probability of being able to transmit at the start of a particular time slot and the successful transmission probability ($\mathbb{P}_{C,Total}$) of an energy harvesting D2D transmitter. The parameter values are $K = 10$, $\lambda_{d2d} = 10^{-3}$, $\alpha = 2.5$, $\rho_p = -100\,\text{dBm}$ , $d_g = 10$, $M = 5$, $\beta = 0.5$, $\gamma_T = -30\,\text{dB}$ unless otherwise mentioned.

First, we plot the probability of each D2D transmitter being able to transmit ($p$, $p \in \{p^{ss}, p^{ms}, p^{\mathcal{N}s}, p^{hs}\}$) vs. the primary receiver density $\lambda_{pr}$ for all the energy harvesting schemes in Fig. 6.4. Because energy is harvested during a single time slot, the single slot harvesting scheme has the highest probability of being able to transmit, and thus $p^{ss}$ is the highest. The $\mathcal{N}$ slot and hybrid harvesting schemes follow next with the hybrid scheme showing a slightly higher probability which is not easily identifiable within the figure. When $\lambda_{pr}$ increases, $p^{ss}$, $p^{\mathcal{N}s}$, and $p^{hs}$ approach 1. Counter intuitively, this is due to the actual transmission probability ($\nu p$) getting lower because of the larger area getting earmarked as guard regions. Thus, the probability that a D2D transmitter gets

stuck being able to transmit, but without being allowed to transmit is higher. From the figure, it is evident that the the multi slot harvesting scheme fares the worst in terms of $p$. However, as we will see in the subsequent plots, it will have better total coverage under certain conditions. Moreover, as $\lambda_{pr}$ increases beyond $-40\,\text{dB}$, $p^{ms}$ keeps relatively constant, which is contrary to the other three schemes. The different performance trend of the multi slot scheme is due to it being a scheme based on the harvested energy level as opposed to the number of harvesting slots.

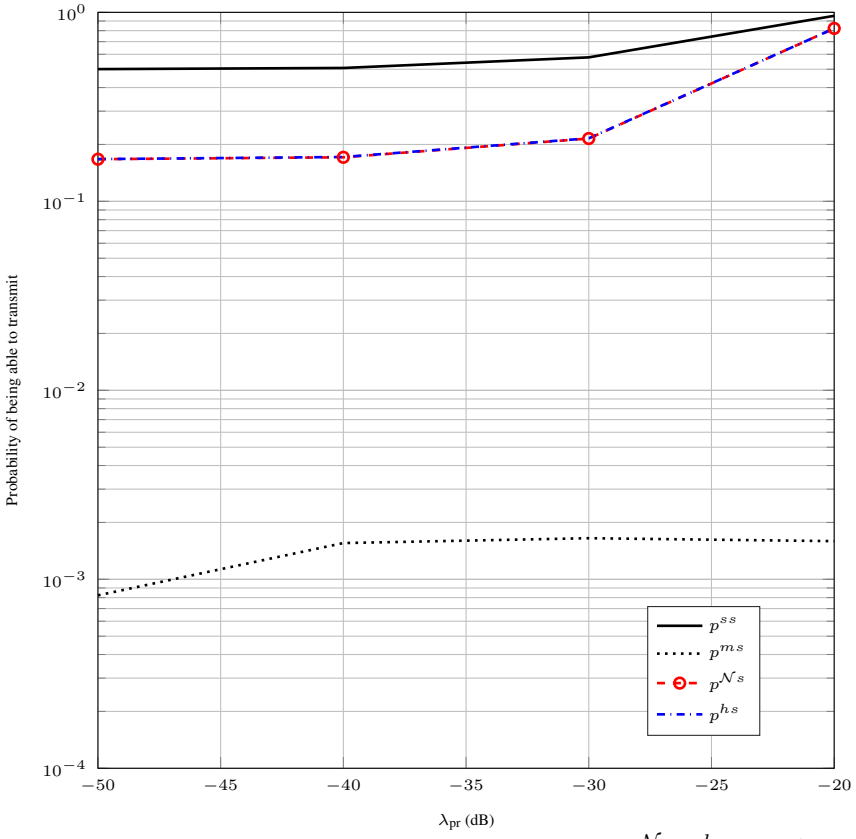


Figure 6.4: The probability of being able to transmit ($p^{ss}, p^{ms}, p^{\mathcal{N}s}, p^{hs}$) vs. $\lambda_{pr}$ for the different energy harvesting schemes. $\rho_{d2d} = -100\,\text{dBm}$, $\mathcal{N} = 5$, $d_l = 100$, and $\lambda_{pt} = 10^{-5}$.

In the subsequent figures, we investigate how different system parameters effect the total coverage probability $\mathbb{P}_{C,Total}$. To this end, we plot $\mathbb{P}_{C,Total}$ vs. the threshold SINR level $\gamma_T$ in Fig. 6.5. Except when $\gamma_T = -50\,\text{dB}$, single slot harvesting has the lowest total coverage. Increasing the number of harvesting time slots ($\mathcal{N}$) to 5 with $\mathcal{N}$ slot harvesting significantly increases the performance. Moreover, the performance increases further when hybrid harvesting is employed for $\mathcal{N} = 5$. Furthermore, while the rate of coverage drop as $\gamma_T$ increases is similar for the single slot and $\mathcal{N}$ slot harvesting, hybrid harvesting has a lower rate of decrease. The multi slot harvesting scheme shows a different trend compared to the other three schemes. While

it has the worst performance for very low $\gamma_T$, its relative performance compared to the other schemes increases as $\gamma_T$ is increased. For high $\gamma_T$, the total coverage is mostly affected by the transmitted signal falling below the SINR threshold. Because multi slot harvesting ensures that a sufficient power is harvested before transmission, the resultant transmission is more likely to be successful. However, the other schemes do not ensure a sufficient power harvest, and thus are adversely effected when $\gamma_T$ increases.

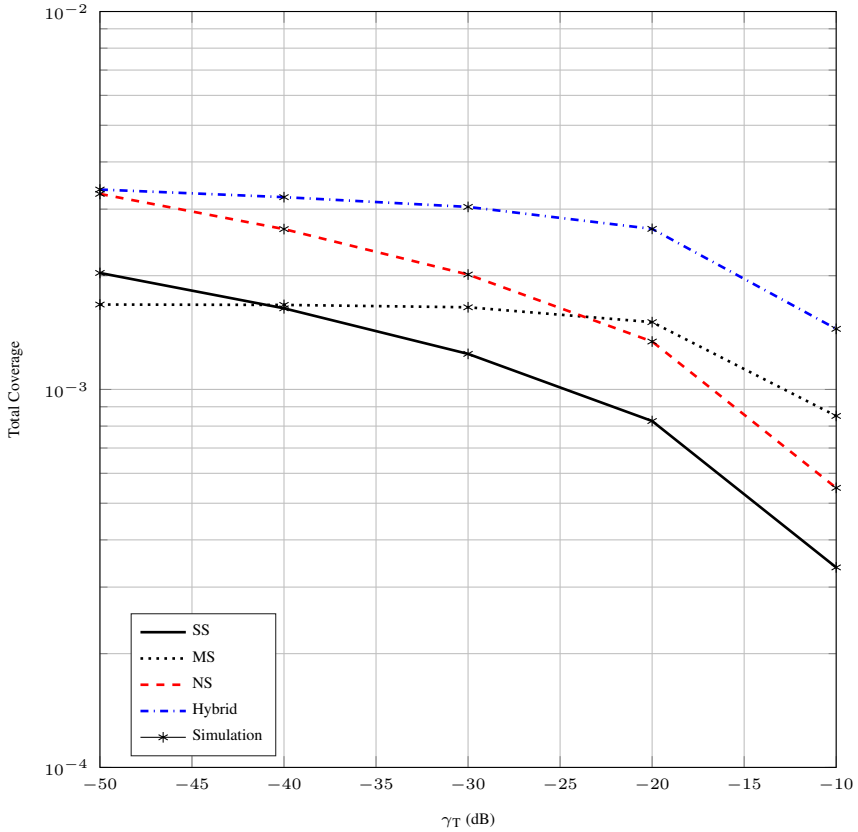


Figure 6.5: $\mathbb{P}_{C,Total}$ vs. $\gamma_T$ for the different energy harvesting schemes. $\rho_{d2d} = -100$ dBm, $d_l = 100$, $\lambda_{pr} = 10^{-3}$, $\mathcal{N} = 5$ and $\lambda_{pt} = 10^{-5}$.

In Fig. 6.6, we plot the total coverage probability $\mathbb{P}_{C,Total}$ with respect to the path loss exponent $\alpha$. $\mathbb{P}_{C,Total}$ drops as $\alpha$ increases for all harvesting schemes. However, the rate of decrease reduces with $\alpha$ as well. $\mathcal{N}$ slot harvesting with $\mathcal{N} = 5$ has a significant better coverage than single slot harvesting, and hybrid harvesting with $\mathcal{N} = 5$ has even better coverage performance. While $\mathcal{N}$ slot has a lower probability of being able to transmit compared to single slot harvesting, the resulting transmissions are more successful due to more energy being harvested. Moreover, hybrid harvesting improves on $\mathcal{N}$ slot harvesting by having a higher probability of being able to transmit. Similar to previous figures, multi slot harvesting shows a different trend; the rate of

coverage decrease is lower compared to other schemes. Thus, for very high path loss exponents, multi slot harvesting has the best coverage performance.

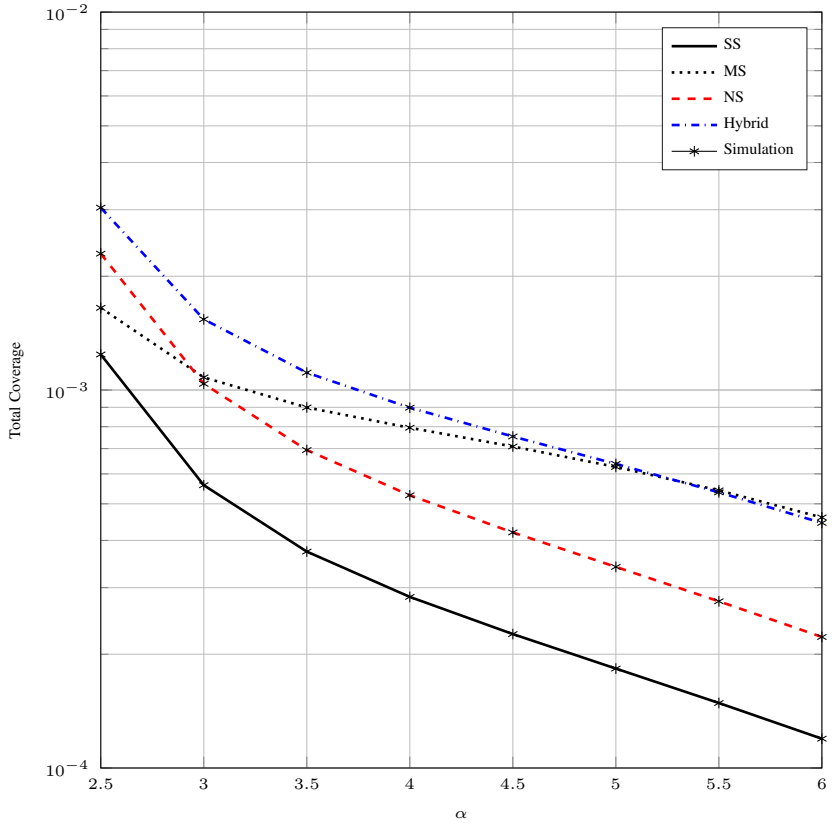


Figure 6.6: $\mathbb{P}_{C,Total}$ vs. $\alpha$ for the different energy harvesting schemes. $\rho_{d2d} = -100$ dBm, $d_l = 100$, $\lambda_{pr} = 10^{-3}$, $\mathcal{N} = 5$ and $\lambda_{pt} = 10^{-5}$.

Fig. 6.7 plots $\mathbb{P}_{C,Total}$ vs. the D2D receiver sensitivity $\rho_{d2d}$ for the single slot and multi slot harvesting schemes. While $\mathbb{P}_{C,Total}$ increases and keeps constant with $\rho_{d2d}$ for single slot harvesting, the trend is drastically different for multi slot harvesting where $\mathbb{P}_{C,Total}$ initially increases and then drops sharply. The initial increase in $\mathbb{P}_{C,Total}$ is due to the increase of $\mathbb{P}_C$ because the desired signal power increases. For single slot harvesting, further increasing $\rho_{d2d}$ is counter productive because the probability of acquiring the increased energy is low. However, for multi slot harvesting, increasing $\rho_{d2d}$ significantly reduces $p^{ms}$ as this scheme always ensures that the required power is harvested before a transmission. Moreover, it is interesting to note that while reducing the primary receiver density increases $\mathbb{P}_{C,Total}$ for single slot harvesting, the trend is different for multi slot harvesting. While reducing $\lambda_{pr}$ increases $\mathbb{P}_{C,Total}$ for low $\rho_{d2d}$, the opposite is true for high $\rho_{d2d}$.

$\mathbb{P}_{C,Total}$ is plotted against the D2D transmitter-receiver distance $d_l$ in Fig. 6.8 for the single

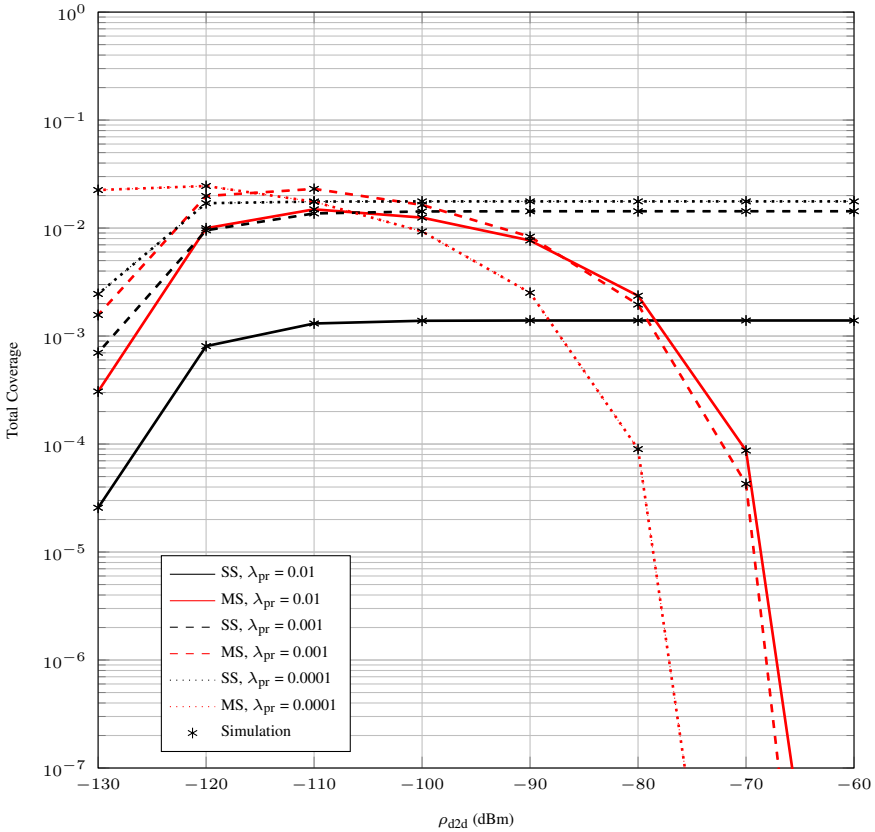


Figure 6.7: $\mathbb{P}_{C,Total}$ vs. $\rho_{d2d}$ for SS and MS energy harvesting. $d_l = 100$, $\lambda_{pr} = 10^{-3}$, and $\lambda_{pt} = 10^{-4}$.

slot and multi slot harvesting schemes. While increasing $d_l$ reduces $\mathbb{P}_{C,Total}$ as expected, the rate of decrease varies significantly for different primary transmitter densities and the energy harvesting scheme. When $\lambda_{pt} = 1 \times 10^{-5}$, the multi slot harvesting scheme always outperforms the single slot scheme, and the successful transmission probability is consistently low. When $\lambda_{pt} = 1 \times 10^{-4}$, the coverage performance increases, for both energy harvesting schemes. However, while the multi slot scheme performs better when $d_l$ is lower, the opposite is true for higher $d_l$. When $\lambda_{pt}$ is increased further to $1 \times 10^{-5}$, the single slot scheme performs better under all $d_l$ values. Moreover, the performance of the multi slot energy harvesting drops drastically as $d_l$ increases. With a higher $d_l$, a higher power is required for transmission, and with the MS scheme, the D2D transmitter must wait till fully charged before it can transmit. However, because $\lambda_{pt}$ is high, the powers of the primary transmitters are low due to lower transmitter receiver distances, which means smaller amounts of energy available for harvesting during each time slot. As such, $p^{ms}$ drops significantly, and thus $\mathbb{P}_{C,Total}$ as well.

We now investigate the effects of different $\mathcal{N}$ on $\mathcal{N}$ slot and hybrid harvesting schemes. To

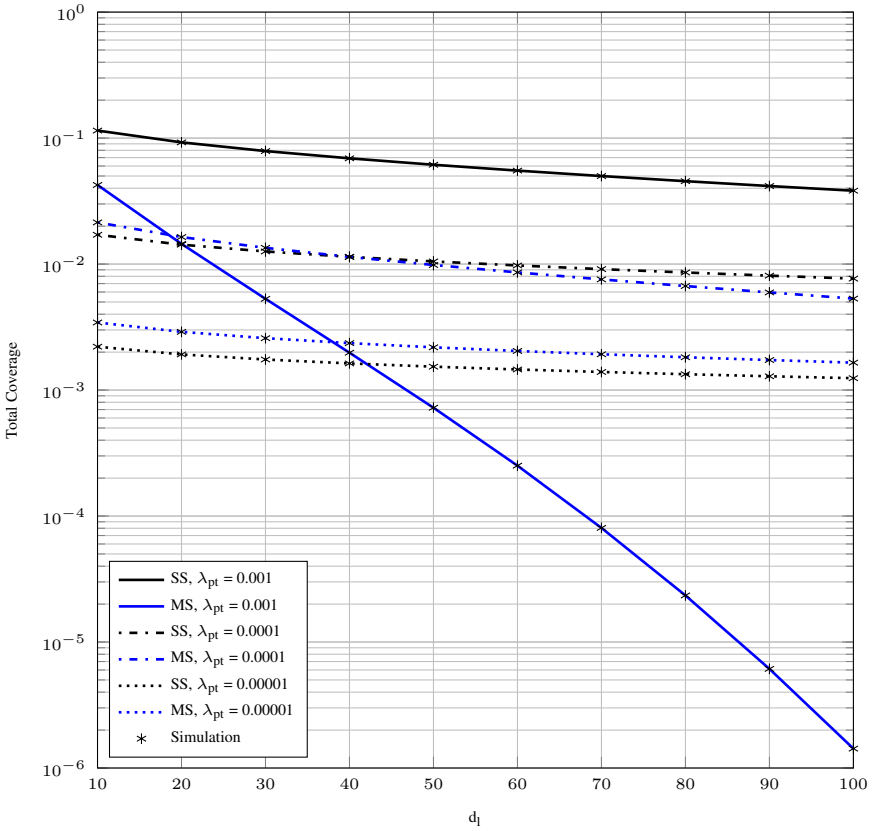


Figure 6.8: $\mathbb{P}_{C,Total}$ vs. $d_l$ for SS and MS harvesting. $\rho_{d2d} = -100$ dBm, and $\lambda_{pr} = 10^{-3}$.

this end, we plot $\mathbb{P}_{C,Total}$ vs. $\rho_p$ in Fig. 6.9. For the corresponding $\mathcal{N}$ value, hybrid harvesting always has better coverage than $\mathcal{N}$ slot harvesting. Moreover, as $\mathcal{N}$ increases, the coverage increases for both schemes. As $\rho_p$ increases, all curves are relatively flat or show a slight increase in coverage till approximately $-80$ dBm. However, after this value, the coverage drops steadily. When $\rho_p$ increases two affects occur which have contrasting effects on the coverage. First, as the transmit energy of primary transmitters increase to ensure primary receiver sensitivities are met, there is more power to be harvested. Second, the increased primary transmit power causes interference to the D2D transmissions. While the two effects roughly cancel each other out initially, the second effect takes precedence as $\rho_p$ increases. After enough power is harvested to ensure that D2D receiver sensitivities are met, having additional ambient power is not useful for the D2D network because power controlling takes place.

## 6.7 Conclusion

This chapter analyzed the performance of random energy harvesting D2D networks. It considered four energy harvesting schemes and a channel selection protocol where each D2D transmitter selects a sub-band randomly. Random fields of primary transmitters and receivers alongside

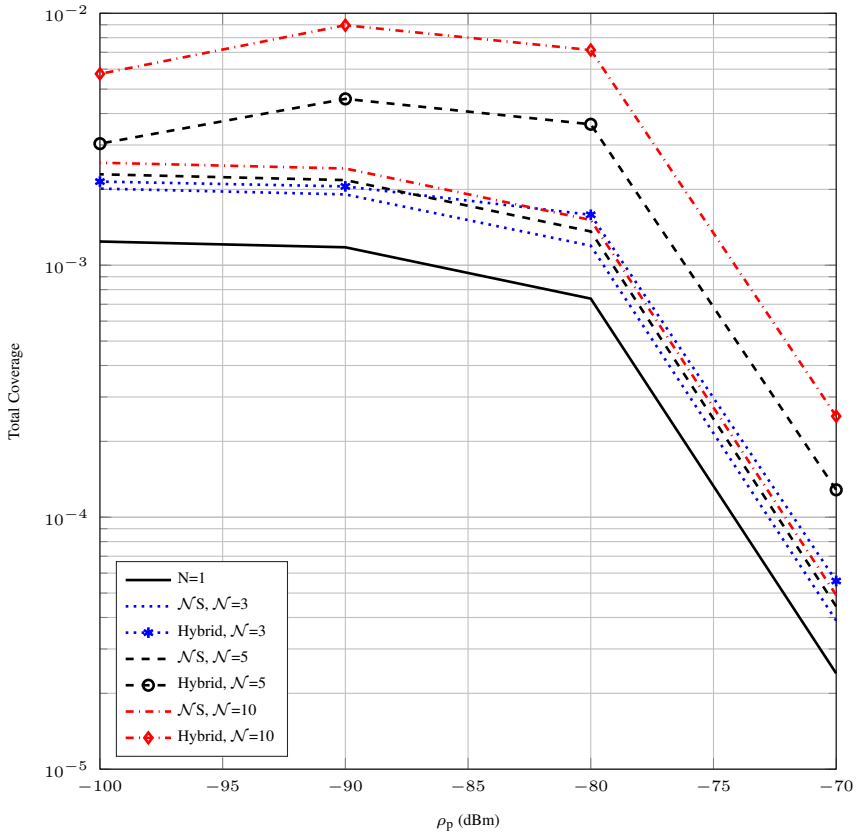


Figure 6.9: $\mathbb{P}_{C,Total}$ vs. $\rho_p$ for the $\mathcal{N}$ slot and hybrid harvesting schemes. $\rho_{d2d} = -100$ dBm, $d_l = 100$, $\lambda_{pr} = 10^{-3}$, and $\lambda_{pt} = 10^{-5}$.

D2D transmitter-receiver pairs distributed as independent stationary homogeneous Poisson point processes were considered. Multiple sub-channels for primary transmitter-receiver communication, log-distance path loss and Rayleigh fading were assumed. The MGF and other statistics of the ambient RF power at a D2D transmitter were derived and subsequently approximated by a Gamma distribution. Single slot, multi slot, $\mathcal{N}$ slot, and hybrid energy harvesting schemes were proposed, and the probability of successful transmissions were derived for each using a Markov chain based approach incorporating temporal correlations. Moreover, the coverage performance of a D2D link was characterized for 2 sub-band selection protocols. Overall, the hybrid harvesting scheme has the best performance among the four proposed schemes. Compared to the other schemes, the multi slot harvesting scheme has different performance trends. It performs better for lower D2D receiver sensitivities, higher SINR thresholds, and higher path loss exponents. Moreover, an optimum performance occurs when $\rho_{d2d}$ is between $-120$ dBm and $-100$ dBm. Furthermore, the primary transmitter and receiver densities along with reception thresholds significantly affect the total coverage probability of energy harvesting D2D nodes.

# Chapter 7

# Random D2D networks under millimeter-wave channels

## 7.1 Introduction

Due to the scarcity of unallocated spectrum within the conventional microwave bands, millimeter-wave communication in the $30 - 300$ GHz band has emerged as one of the most promising technologies for the fifth generation (5G) of cellular communication [197], [198]. Standardization has already occurred under IEEE 802.15.3c and IEEE 802.11ad for the $60$ GHz band [4]. However, high path loss, the sensitivity to blockages, atmospheric absorption, and high noise powers provide significant challenges to successfully incorporating millimeter-wave frequencies. On another note, device-to-device (D2D) networks underlaying the cellular network enable transmissions between neighbouring devices for certain applications which saves transmission power and network resources [8]. Thus, integrating millimeter-wave with D2D networking is an exciting prospect [199], [200]. However, underlaying D2D onto a cellular network provides challenges with respect to interference management, and the peculiarities of the millimeter-wave channel exemplify the challenge regarding coverage.

### 7.1.1 Related work

Research on millimeter-wave cellular networks has received significant attention in the recent years. Reference [201] considers the possibility of base station downlink co-operation to reduce the outage probability, and concludes that co-operation significantly improves the performance in dense networks without small scale fading. However, the authors show that the performance improvement is minimal in less dense networks with Rayleigh fading. A general framework to

evaluate the coverage and rate in millimeter-wave networks is proposed in [4], [202], and the case of dense networks is investigated further in [4] where the line of sight region is approximated with a ball. It is concluded that dense networks achieve similar coverage and significantly higher data rates with respect to conventional cellular networks. In contrast, [202] proposes a mathematical framework which accounts for the interference from other cells in ultra-dense deployments.

The research on millimeter-wave networks has also incorporated D2D networks. Reference [203] considers stochastic geometry to analyze wearable D2D networks within a finite region, and concludes that millimeter-wave frequencies provide significant throughput gain even with omni-directional antennas. Furthermore [204] proposes an efficient scheduling scheme for millimeter-wave small cells while exploiting D2D links for efficiency while [205] studies the spatial heterogeneity of outdoor users via the coefficient of variation. Moreover, [206] proposes a resource allocation scheme for underlaid D2D networks within the E-band, and shows that the proposed solution increases throughput while reducing interference.

### 7.1.2 Motivation and contribution

In this work, we aim to characterize the outage performance of a D2D network underlaid upon a millimeter-wave cellular network. While millimeter-wave frequencies will present lower interference due to directionality, there would be degradation to the desired signal due to blockages. Moreover, how log-distance path loss and peak power constraints affect the performance under millimeter-wave frequencies are open issues. In addition, ubiquitous networks are increasingly irregular. As such, stochastic models incorporating spatial randomness need to be taken into account.

In this work, we model the cellular base stations and users as independent homogeneous Poisson point processes and the D2D network as a Matern cluster process in $\mathbb{R}^2$ to incorporate spatial randomness. A simplified Boolean blockage model is assumed, and line-of-sight (LOS) and non-line-of-sight (NLOS) conditions are modelled separately with different log-distance path loss exponents and Nakagami fading parameters. Moreover, directional antenna patterns are assumed for all devices, and antenna alignment takes place before any data transmission attempt. Each cellular user is assumed to connect to its nearest base station while a D2D receiver connects with the transmitter corresponding to the cluster head. We assume a path loss and antenna gain inversion based power control model where the D2D network is also peak power constrained.

Our main contributions of this chapter are listed below:

- The moment generating function (MGF) of the interference to a D2D receiver from other D2D transmitters and cellular base stations is derived using stochastic geometry based tools. More precisely, the Mapping and Marking theorems relating to Poisson point processes are used to transform the process of interfering base stations into an equivalent inhomogeneous process which incorporates blockage, antenna gains, transmit power, fading, and path loss variations.

- The outage performance of a D2D receiver is derived in closed-form while taking into account the constraints due to peak power constraints and random blockages.

## 7.2 System model and assumptions

This section introduces the system parameters and models used throughout the rest of the chapter.

### 7.2.1 Spatial distribution and blockages

We consider four separate types of nodes: 1) cellular base stations, 2) cellular users, 3) D2D transmitters, and 4) D2D receivers. While the D2D transmitters/receivers in principle can also be cellular users, we differentiate them in this research for the ease of analysis. The cellular base stations and users are modelled as two independent, stationary homogeneous Poisson point processes in $\mathbb{R}^2$. As such, the processes of cellular base stations and users are respectively denoted as $\Phi_{c,b}$ and $\Phi_{c,u}$ having densities of $\lambda_{c,b}$ and $\lambda_{c,u}$ respectively.

The D2D network is modelled as a Matern cluster process [69]. Within a Matern cluster process, multiple clusters exist in $\mathbb{R}^2$ where the cluster centers are distributed as a homogeneous Poisson point process and each cluster center is encircled by a daughter process existing within a ball of radius $R$ from it[1]. The daughter processes are homogeneous within their respective annular regions and independent of each other. In our case the cluster centers having a density of $\lambda_{d,t}$ model the D2D transmitters and the daughter nodes having a density of $\lambda_{d,r}$ model the D2D receivers[2].

An important factor to consider in millimeter-wave networks is the signal blockage from random objects which significantly impacts the received signal characteristics. We will model

[1]Note that this system model is analogous to a homogeneous Poisson point process of D2D receivers where the transmitters only select a receiver within a given radius.

[2]We assume that each daughter process has the same constant density.

the blockages stochastically using a rectangular Boolean scheme [207], and the blockages are assumed to be stationary and isotropic. With these assumptions, the probability of a link of length $r$ with no blockage (LOS link) is given by $e^{-\beta r}$, where $\beta$ is a constant relating to the size and density of the blockages. Similarly, the probability of a NLOS link is given by $1 - e^{-\beta r}$. It is readily observed that a link is more susceptible to blockage as its length increases. Moreover, for mathematical tractability, we assume that the effect of blockage on different links is independent. Note that the different types of nodes have a chance of falling within the environs of a blocking object. However, although we omit such a scenario, it can be readily incorporated to our analysis through independently thinning the different processes of nodes [4].

### 7.2.2 Channel model and antenna pattern

The cellular system is assumed to employ universal frequency reuse, and the same set of cellular frequencies are also used by D2D users. For mathematical tractability, we assume that the channel gains are independent of the underlying spatial process of nodes. We consider path loss and small scale fading for all the links. However, the parameters of these vary depending on the LOS or NLOS nature of the link.

From the model [208], we write the general path loss for a millimeter-wave link of distance $r$ as $PL(r) = c_s r^{\alpha_s}$, where $s \in \{L, N\}$, and $L, N$ correspond to LOS and NLOS links. The parameter $\alpha_s$ is the path loss exponent while $c_s$ is the intercept. The small fading is assumed to be Nakagami. Thus, the channel power gain ($|h_s|^2$) is distributed as [76], [90]

$$f_{|h_s|^2}(x) = \frac{m_s^{m_s}}{\Gamma(m_s)} x^{m_s - 1} e^{-m_s x}, 0 \leq x < \infty, 0.5 < m < \infty, \tag{7.1}$$

where the Nakagami parameter $m_s (s \in \{L, N\})$ is an indicator of fading severity where $m_s \to \infty$ indicates no fading while $m_s = 1$ indicates Rayleigh fading. As LOS links would have very few scatterers in millimeter-wave frequencies, $m_L$ would tend to be higher while the NLOS parameter $m_N$ would be lower.

Under millimeter-wave frequencies, large numbers of antenna elements can be packed within a small area which enables directional beamforming. All different types of nodes are assumed to be capable of performing directional beamforming. Moreover, the antenna patterns of cellular users and D2D transmitters/receivers are assumed to be similar while cellular base stations have a different pattern. To keep the analysis concise, we consider a sectored antenna model [113]

where the antenna gain pattern is divided into discrete regions based on the angle off the boresight direction. Thus, the antenna gain ($G_*(* \in \{cb, u\})$ where $cb$ and $u$ respectively denote cellular base stations and all other types of nodes) can be expressed as follows:

$$G_* = \begin{cases} M_* & , |\theta| \leq \frac{\omega_*}{2} \\ m_* & , \text{otherwise} \end{cases}, \tag{7.2}$$

where $\omega_*$ is the antenna beamwidth, $\theta$ is the angle off the boresight direction, $M_*$ is the main lobe gain, and $m_*$ is the gain from the side and back lobes. While this gain pattern can be generalized for different side and back lobe gains, and angle dependent main lobe gains, we defer it for future work.

The transmitters and receivers in both cellular and D2D networks perform a beam sweeping process initially in order to estimate the angle of arrival, and we assume that perfect estimation takes place. As such, the combined antenna gains of intended cellular and D2D links are $M_{cb}M_u$ and $M_uM_u$ respectively. The gains of all other links vary randomly depending on the angle off boresight.

### 7.2.3 User association and power control

For the cellular network, each user associates with its closest base station. While other association schemes such as highest received power association may be more favourable, they come at the cost of added complexity and processing power. Moreover, the closest base station is the least likely to suffer from blockages, and thus the most likely to provide the best received signal power. Furthermore, we assume that there only exists at most a single associated user for each base station within a given time-frequency block. Under these assumptions, if the distance between the $i$-th cellular base station $\phi^i_{c,b} \in \Phi_{c,b}$ and its associated receiver $\phi^i_{c,u} \in \Phi_{c,u}$ is $r_c$, it has a Rayleigh distribution given by [94]

$$f_{r_c}(x) = 2\pi\lambda_{c,b}xe^{-\pi\lambda_{c,b}x^2}, 0 < x < \infty. \tag{7.3}$$

In the D2D network, each receiver associates with the corresponding transmitter within its cluster. If this distance is $r_{d2d}$, its distribution can be expressed as [94]

$$f_{r_{d2d}}(x) = \frac{2x}{R^2}, 0 < x < R. \tag{7.4}$$

Both cellular and D2D transmitters employ power control which inverts path loss and antenna gains. If $P_T$ is the transmit power, the transmit power to a receiver at distance $r$ can be expressed as $P_T = \frac{\rho c_s r^{\alpha_s}}{M_* M_u}$, where $s \in \{L, N\}$, $* \in \{cb, u\}$, and $\rho$ is the receiver sensitivity. While we assume that that both cellular and D2D receivers have the same sensitivity, different sensitivities can be readily incorporated. Furthermore, we assume that the D2D transmitters are peak power constrained. As such, a D2D transmitter will abort whenever $P_T > P_{d2d}$ where $P_{d2d}$ is the maximum allowable transmit power. The cellular base stations are not assumed to be peak power constrained as they are part of the network infrastructure.

## 7.3 Outage performance

We consider a typical D2D receiver located at a distance of $r_{d2d}$ from its respective transmitter. Without the loss of generality, we consider that this receiver is located at the origin. The outage probability ($P_O$) is defined as $P_O = \Pr[\gamma < \gamma_{th}]$, where $\gamma$ is the signal to interference and noise ratio (SINR) at the D2D receiver while $\gamma_{th}$ is the SINR reception threshold of the receiver. The SINR can be written as

$$\gamma = \frac{P_s |h_s|^2 M_u^2 c_s^{-1} r_{d2d}^{-\alpha_s}}{I_c + I_{d2d} + N}, \tag{7.5}$$

where $P_s$ is the transmit power, $I_c$ is the interference from cellular base stations, $I_{d2d}$ is the interference from other D2D transmitters, and $N$ is the noise power. It is clearly seen that $\gamma$ varies with the LOS and NLOS nature of the link. Therefore, we can separate the LOS and NLOS cases and express $P_O$ as

$$\begin{aligned} P_O &= \mathbb{E}[a_l P_{O,L} + a_N P_{O,N}] \\ &= \frac{2P_{O,L}}{\beta^2 R^2}\left(1 - e^{-\beta R}(\beta R + 1)\right) \\ &+ P_{O,N}\left(1 - \frac{2}{\beta^2 R^2}\left(1 - e^{-\beta R}(\beta R + 1)\right)\right), \end{aligned} \tag{7.6}$$

where $a_l = e^{-\beta r_{d2d}}$ is the probability of the link being LOS, $a_N = 1 - e^{-\beta r_{d2d}}$ is the probability of the link being NLOS, while $P_{O,L}$ and $P_{O,N}$ are respectively the outages given LOS and NLOS links.

**Deriving** $P_{O,L}$

When a LOS link exists between the D2D transmitter and receiver given a certain $r_{d2d}$, we can express $P_{O,L}$ as

$$P_{O,L} = \Pr\left[\frac{P_L |h_L|^2 M_u^2 c_L^{-1} r_{d2d}^{-\alpha_L}}{I_c + I_{d2d} + N} < \gamma_{th}\right]. \tag{7.7}$$

The transmit power $P_L$ is given by

$$P_L = \begin{cases} \frac{\rho c_L r_{d2d}^{\alpha_L}}{M_u^2} & , \frac{\rho c_L r_{d2d}^{\alpha_L}}{M_u^2} < P_{d2d} \\ 0 & , \text{otherwise} \end{cases}. \tag{7.8}$$

Let $\tau_L$ be the probability that $P_L = \frac{\rho c_L r_{d2d}^{\alpha_L}}{M_u^2}$. Thus, we can express $\tau_L = \Pr\left[r_{d2d} < \left(\frac{P_{d2d} M_u^2}{\rho c_L}\right)^{\frac{1}{\alpha_L}}\right]$ as

$$\tau_L = \begin{cases} \frac{1}{R^2}\left(\frac{P_{d2d} M_u^2}{\rho c_L}\right)^{\frac{2}{\alpha_L}} & , \text{if } \left(\frac{P_{d2d} M_u^2}{\rho c_L}\right)^{\frac{1}{\alpha_L}} < R \\ 1 & , \text{if } \left(\frac{P_{d2d} M_u^2}{\rho c_L}\right)^{\frac{1}{\alpha_L}} > R \end{cases}. \tag{7.9}$$

Now, getting back to the objective of deriving $P_{O,L}$, we can express (7.7) for integer $m_l$ as

$$\begin{aligned} P_{O,L} &= 1 - \tau_L + \tau_L \Pr\left[|h_L|^2 < \frac{\gamma_{th}(I_c + I_{d2d} + N)}{\rho}\right] \\ &= 1 - \tau_L \mathbb{E}\left[\frac{\Gamma\left(m_L, m_L \frac{\gamma_{th}(I_c + I_{d2d} + N)}{\rho}\right)}{\Gamma(m_L)}\right] \\ &= 1 - \tau_L \mathbb{E}_I\left[\frac{1}{\Gamma(m_L)} \int_{\frac{m_L \gamma_{th}(I_c + I_{d2d} + N)}{\rho}}^{\infty} y^{m_L - 1} e^{-y} dy\right] \\ &= 1 - \tau_L \mathbb{E}_I\left[e^{-\frac{m_L \gamma_{th}(I_c + I_{d2d} + N)}{\rho}} \sum_{\nu=0}^{m_L - 1} \frac{1}{\nu!}\left(\frac{m_L \gamma_{th}(I_c + I_{d2d} + N)}{\rho}\right)^{\nu}\right] \\ &= 1 - \tau_L e^{-\frac{m_L \gamma_{th} N}{\rho}} \sum_{\nu=0}^{m_L - 1} \frac{1}{\nu!}\left(\frac{m_L \gamma_{th}}{\rho}\right)^{\nu} \sum_{\mu=0}^{\nu} \binom{\nu}{\mu} N^{\nu - \mu} \end{aligned}$$

$$\times \quad \sum_{\kappa=0}^{\mu} \binom{\mu}{\kappa} \mathbb{E}_{I_c}\left[I_c^{\kappa} e^{-\frac{m_L \gamma_{th} I_c}{\rho}}\right] \mathbb{E}_{I_{d2d}}\left[I_{d2d}^{\mu-\kappa} e^{-\frac{m_L \gamma_{th} I_{d2d}}{\rho}}\right]$$

$$= \; 1 - \tau_L e^{-\frac{m_L \gamma_{th} N}{\rho}} \sum_{\nu=0}^{m_L-1} \frac{1}{\nu!} \left(\frac{m_L \gamma_{th}}{\rho}\right)^{\nu} \sum_{\mu=0}^{\nu} \binom{\nu}{\mu} N^{\nu-\mu} \sum_{\kappa=0}^{\mu} \binom{\mu}{\kappa}$$

$$\times \quad (-1)^{\kappa} M_{I_c}^{(\kappa)}\left(s\big|_{s=\frac{m_L \gamma_{th}}{\rho}}\right) (-1)^{\mu-\kappa} M_{I_{d2d}}^{(\mu-\kappa)}\left(s\big|_{s=\frac{m_L \gamma_{th}}{\rho}}\right).$$

**Deriving $P_{O,N}$**

In a similar way to $P_{O,L}$, $P_{O,N}$ can be derived as

$$\begin{aligned} P_{O,N} &= 1 - \tau_N e^{-\frac{m_N \gamma_{th} N}{\rho}} \sum_{\nu=0}^{m_N-1} \frac{1}{\nu!} \left(\frac{m_N \gamma_{th}}{\rho}\right)^{\nu} \\ &\times \sum_{\mu=0}^{\nu} \binom{\nu}{\mu} N^{\nu-\mu} \sum_{\kappa=0}^{\mu} \binom{\mu}{\kappa} (-1)^{\kappa} M_{I_c}^{(\kappa)}\left(s\big|_{s=\frac{m_N \gamma_{th}}{\rho}}\right) \\ &\times (-1)^{\mu-\kappa} M_{I_{d2d}}^{(\mu-\kappa)}\left(s\big|_{s=\frac{m_N \gamma_{th}}{\rho}}\right), \end{aligned} \tag{7.10}$$

where $\tau_N$ is given by

$$\tau_N = \begin{cases} \frac{1}{R^2}\left(\frac{P_{d2d} M_u^2}{\rho c_N}\right)^{\frac{2}{\alpha_N}} & \text{, if } \left(\frac{P_{d2d} M_u^2}{\rho c_N}\right)^{\frac{1}{\alpha_N}} < R \\ 1 & \text{, if } \left(\frac{P_{d2d} M_u^2}{\rho c_N}\right)^{\frac{1}{\alpha_N}} > R \end{cases}. \tag{7.11}$$

## 7.4 Interference characteristics

In this section, we derive the MGFs of the interference from both cellular and other D2D transmitters $M_{I_c}$ and $M_{I_{d2d}}$. For both cellular and D2D networks, we assume that all transmitters/base stations are actively engaged in transmission. This assumption is valid since they have a significantly lower spatial density compared to the relevant receivers. Moreover, independent thinning can be easily used to remove non-active base stations/transmitters.

### 7.4.1 Interference from cellular transmitters

The interference from transmitting cellular base stations $I_c$ can be divided into two separate terms composed of LOS and NLOS cellular base stations using the thinning property [73]. If $I_{c,L}$ and $I_{c,N}$ denote these two terms, $I_c = I_{c,L} + I_{c,N}$. Moreover, $M_{I_c} = M_{I_{c,L}} M_{I_{c,N}}$ due to the

independence of thinned Poisson point processes [73].

**Deriving $M_{I_{c,L}}$**

In order to derive $M_{I_{c,L}}$ we first transform the process of interfering LOS base stations to an equivalent inhomogeneous Poisson point process which incorporates the path loss exponent, antenna gains, transmit power, and fading. Let $r$ be the distance from the $i$-th cellular base station $\phi^i_{c,b}$ to the considered D2D receiver. While the field of cellular base stations $\Phi_{c,b}$ exists in $\mathbb{R}^2$ as a homogeneous Poisson point process, it can be mapped to an equivalent 1-D inhomogeneous Poisson point process [73] with density $\tilde{\lambda}_{c,b}$ where

$$\tilde{\lambda}_{c,b} = 2\pi\lambda_{c,b}r, 0 < r < \infty. \tag{7.12}$$

The cellular base station $\phi^i_{c,b}$ is LOS from the D2D receiver with a probability of $e^{-\beta r}$. While this probability depends on $r$, it is independent from the positions of other cellular base stations. As such, the Colouring Theorem [73] can be used to perform independent thinning of $\Phi_{c,b}$ to obtain the process of LOS cellular base stations as an inhomogeneous Poisson point process with density $\tilde{\lambda}_{c,bL} = e^{-\beta r}\tilde{\lambda}_{c,b} = 2\pi\lambda_{c,b}e^{-\beta r}r$.

Using the Mapping Theorem further [73], this thinned 1-D Poisson process can be mapped to an equivalent 1-D Poisson process in terms of interference statistics where the path loss exponent is 1 [157]. The density of the resultant process $\hat{\lambda}_{c,bL}$ is given by

$$\hat{\lambda}_{c,bL} = \frac{2\pi\lambda_{c,b}e^{-\beta r^{\frac{1}{\alpha_L}}}r^{\frac{2}{\alpha_L}-1}}{\alpha_L}, 0 < r < \infty. \tag{7.13}$$

Next, we go one step further and incorporate the transmit power of $\phi^i_{c,b}$, the antenna gains of $\phi^i_{c,b}$ and the D2D receiver, and the fading between $\phi^i_{c,b}$ and the D2D receiver to the process of LOS cellular base stations [157]. Thus, the resultant process has a density $\bar{\lambda}_{c,bL}$ which can be expressed as

$$\begin{aligned}\bar{\lambda}_{c,bL} &= \mathbb{E}_{P_{cL}G_{cb}G_u|h_{cL}|^2}\left[P_{cL}|h_{cL}|^2\hat{\lambda}_{c,bL}(P_{cL}G_{cb}G_u|h_{cL}|^2 r)\right] \\ &= \frac{2\pi\lambda_{c,b}r^{\frac{2}{\alpha_L}-1}}{\alpha_L}\sum_{k=0}^{\infty}\frac{(-\beta r^{\frac{1}{\alpha_L}})^k}{k!}\end{aligned}$$

$$\times \quad \mathbb{E}\left[P_{cL}^{\frac{2+k}{\alpha_L}}\right]\mathbb{E}\left[G_{cb}^{\frac{2+k}{\alpha_L}}\right]\mathbb{E}\left[G_{u}^{\frac{2+k}{\alpha_L}}\right]\mathbb{E}\left[\left(|h_{cL}|^2\right)^{\frac{2+k}{\alpha_L}}\right], \tag{7.14}$$

where $P_{cL}$ is the transmit power of the base station $\phi_{c,b}^i$, $G_{cb}$ is the gain of $\phi_{c,b}^i$, $G_u$ is the gain of the D2D receiver, and $|h_{cL}|^2$ is the small scale fading channel gain between $\phi_{c,b}^i$ and the D2D receiver.

In order to evaluate (7.14), the distribution of $P_{cL}$ is required, which in turn depends on whether the associated cellular user to $\phi_{c,b}^i$ is within LOS or not. The associated receiver $\phi_{c,u}^i$ is LOS to $\phi_{c,b}^i$ with probability $e^{-\beta r_c}$, and NLOS with probability $1-e^{-\beta r_c}$, where $r_c$ is the distance between $\phi_{c,u}^i$ and $\phi_{c,b}^i$. These probabilities are independent from whether $\phi_{c,b}^i$ and the D2D receiver are LOS or not. Thus, $P_{cL}$ can be expressed as follows:

$$P_{cL} = \begin{cases} \frac{\rho c_L r_c^{\alpha_L}}{M_U M_{cb}} & , \phi_{c,u}^i \text{ and } \phi_{c,b}^i \text{ are LOS} \\ \frac{\rho c_N r_c^{\alpha_N}}{M_U M_{cb}} & , \phi_{c,u}^i \text{ and } \phi_{c,b}^i \text{ are NLOS} \end{cases}. \tag{7.15}$$

After substituting $\mathbb{E}_{|h_{cL}|^2}\left[\left(|h_{cL}|^2\right)^{\frac{2+k}{\alpha_L}}\right]$ and $\mathbb{E}_{P_{cL}}\left[P_{cL}^{\frac{2+k}{\alpha_L}}\right]$ to (7.14), we obtain the final expression for $\bar{\lambda}_{c,bL}$ as

$$\bar{\lambda}_{c,bL} = \sum_{k=0}^{\infty} \frac{2\pi\lambda_{c,b}(-\beta)^k r^{\frac{2+k}{\alpha_L}-1}}{\alpha_L k!}\mathbb{U}_{c,L}, 0<r<\infty, \tag{7.16}$$

where $\mathbb{U}_{c,L}$ is

$$\begin{aligned}
\mathbb{U}_{c,L} = {} & \frac{\rho^{\frac{2+k}{\alpha_L}}\Gamma\left(m_L+\frac{2+k}{\alpha_L}\right)}{4\pi^2\Gamma(m_L)m_L^{-\frac{2+k}{\alpha_L}}(M_u M_{cb})^{\frac{2+k}{\alpha_L}}}\left(\theta_{cb}M_{cb}^{\frac{2+k}{\alpha_L}}+(2\pi-\theta_{cb})m_{cb}^{\frac{2+k}{\alpha_L}}\right)\left(\theta_u M_u^{\frac{2+k}{\alpha_L}}+(2\pi-\theta_u)m_u^{\frac{2+k}{\alpha_L}}\right) \\
& \times\left(\frac{c_L^{\frac{2+k}{\alpha_L}}}{(\pi\lambda_{c,b})^{\frac{3+k}{2}}}\left(\sqrt{\pi\lambda_{c,b}}\Gamma\left(\frac{k+2}{2}\right){}_1\mathcal{F}_1\left(\frac{k+2}{2};\frac{1}{2};\frac{\beta^2}{4\pi\lambda_{c,b}}\right)-\beta\Gamma\left(\frac{k+5}{2}\right){}_1\mathcal{F}_1\left(\frac{k+5}{2};\frac{3}{2};\frac{\beta^2}{4\pi\lambda_{c,b}}\right)\right)\right. \\
& + \frac{c_N^{\frac{2+k}{\alpha_L}}}{(\pi\lambda_{c,b})^{\frac{\alpha_L+\alpha_N(2+k)}{2\alpha_L}}}\left(-\sqrt{\pi\lambda_{c,b}}\Gamma\left(1+\frac{(2+k)\alpha_N}{2\alpha_L}\right)\left({}_1\mathcal{F}_1\left(1+\frac{(2+k)\alpha_N}{2\alpha_L};\frac{1}{2};\frac{\beta^2}{4\pi\lambda_{c,b}}\right)-1\right)\right. \\
& \left.\left. + \beta\Gamma\left(\frac{3}{2}+\frac{(2+k)\alpha_N}{2\alpha_L}\right){}_1\mathcal{F}_1\left(\frac{3}{2}+\frac{(2+k)\alpha_N}{2\alpha_L};\frac{3}{2};\frac{\beta^2}{4\pi\lambda_{c,b}}\right)\right)\right).
\end{aligned} \tag{7.17}$$

We now return to our origin objective of deriving $M_{I_{c,L}} = \mathbb{E}[e^{-sI_{c,L}}]$. Due to the mapping, the

interference power from a single cellular base station $\phi^i_{c,b}$ within the resultant process reduces to $(c_L r)^{-1}$. Note that the path loss exponent has reduced to 1 while the gains, fading, and transmit powers are absent. Thus, using the Campbell's Theorem [73], $M_{I_{c,L}}$ is expressed as

$$\begin{aligned} M_{I_{c,L}} &= e^{\left(\int_0^\infty \left(e^{-s(c_L r)^{-1}}-1\right)\bar{\lambda}_{c,bL}dr\right)} \\ &= e^{\sum_{k=0}^{\infty} \frac{2\pi\lambda_{c,b}(-\beta)^k}{\alpha_L k!}\left(\frac{s}{c_L}\right)^{\frac{2+k}{\alpha_L}}\Gamma\left(-\frac{2+k}{\alpha_L}\right)\mathbb{U}_{c,L}}. \end{aligned} \tag{7.18}$$

**Deriving** $M_{I_{c,N}}$

Using similar arguments as with the derivation of $M_{I_{c,L}}$, $M_{I_{c,N}}$ ca be written as

$$M_{I_{c,N}} = e^{\sum_{k=1}^{\infty} -\frac{2\pi\lambda_{c,b}(-\beta)^k}{\alpha_N k!}\left(\frac{s}{c_N}\right)^{\frac{2+k}{\alpha_N}}\Gamma\left(-\frac{2+k}{\alpha_N}\right)\mathbb{U}_{c,N}}, \tag{7.19}$$

where $\mathbb{U}_{c,N}$ is

$$\begin{aligned} \mathbb{U}_{c,N} = &\frac{\rho^{\frac{2+k}{\alpha_N}}\Gamma\left(m_N+\frac{2+k}{\alpha_N}\right)}{4\pi^2\Gamma(m_N)m_N^{-\frac{2+k}{\alpha_N}}(M_u M_{cb})^{\frac{2+k}{\alpha_N}}}\left(\frac{c_L^{\frac{2+k}{\alpha_N}}}{(\pi\lambda_{c,b})^{\frac{\alpha_N+\alpha_L(2+k)}{\alpha_N}}}\left(\sqrt{\pi\lambda_{c,b}}\Gamma\left(\frac{(k+2)\alpha_L}{2\alpha_N}\right)\right.\right. \\ \times\quad & {}_1\mathcal{F}_1\left(\frac{(k+2)\alpha_L}{2\alpha_N};\frac{1}{2};\frac{\beta^2}{4\pi\lambda_{c,b}}\right)-\beta\Gamma\left(\frac{3}{2}+\frac{(2+k)\alpha_L}{2\alpha_N}\right){}_1\mathcal{F}_1\left(\frac{3}{2}+\frac{(2+k)\alpha_L}{2\alpha_N};\frac{3}{2};\frac{\beta^2}{4\pi\lambda_{c,b}}\right)\Bigg) \\ + \quad & \frac{c_N^{\frac{2+k}{\alpha_N}}}{(\pi\lambda_{c,b})^{\frac{3+k}{2}}}\left(-\sqrt{\pi\lambda_{c,b}}\Gamma\left(1+\frac{2+k}{2}\right)\left({}_1\mathcal{F}_1\left(1+\frac{2+k}{2};\frac{1}{2};\frac{\beta^2}{4\pi\lambda_{c,b}}\right)-1\right)\right. \\ + \quad & \left.\left.\beta\Gamma\left(\frac{k+5}{2}\right){}_1\mathcal{F}_1\left(\frac{k+5}{2};\frac{3}{2};\frac{\beta^2}{4\pi\lambda_{c,b}}\right)\right)\right)\left(\theta_{cb}M_{cb}^{\frac{2+k}{\alpha_N}}+(2\pi-\theta_{cb})m_{cb}^{\frac{2+k}{\alpha_N}}\right)\left(\theta_u M_u^{\frac{2+k}{\alpha_N}}+(2\pi-\theta_u)m_u^{\frac{2+k}{\alpha_N}}\right) \end{aligned} \tag{7.20}$$

### 7.4.2 Interference from other D2D transmitters

The interference from other D2D transmitters on the D2D receiver in question can be decomposed into LOS ($I_{d2d,L}$) and NLOS ($I_{d2d,N}$) components with $I_{d2d} = I_{d2d,L} + I_{d2d,N}$ and $M_{I_{d2d}} = M_{I_{d2d,L}} M_{I_{d2d,N}}$.

**Deriving** $M_{I_{d2d,L}}$

While the derivation of $M_{I_{d2d,L}}$ is similar to $M_{I_{c,L}}$ and $M_{I_{c,N}}$, a complication arises while obtaining the $\frac{2+k}{\alpha}$-th moment of the transmit power of a D2D transmitter ($P_{dL}$). If $r_d$ is the distance from

a D2D transmitter to the associated receiver, $P_{dL}$ takes $\frac{\rho c_L r_d^{\alpha_L}}{M_u^2}$ with probability $e^{-\beta r_d}\tau_L$, $\frac{\rho c_N r_d^{\alpha_N}}{M_u^2}$ with probability $(1-e^{-\beta r_d})\tau_N$, and 0 with probability $e^{-\beta r_d}(1-\tau_L)+(1-e^{-\beta r_d})(1-\tau_N)$ after considering blockages and peak power constraints. Moreover, while $\tau_L$ (7.9) and $\tau_N$ (7.11) can take multiple combinations as evident from their expressions, we consider the case where $\max\left(\left(\frac{P_{d2d}M_u^2}{\rho c_N}\right)^{\frac{1}{\alpha_N}}, \left(\frac{P_{d2d}M_u^2}{\rho c_L}\right)^{\frac{1}{\alpha_L}}\right) < R$ for this chapter.

After using the Slivnyak's theorem [73] to remove the desired transmitter from the field of interferers, $M_{I_{d2d,L}}$ is expressed as

$$M_{I_{d2d,L}} = e^{\sum_{k=0}^{\infty} \frac{2\pi\lambda_{d,t}(-\beta)^k}{\alpha_L k!}\left(\frac{s}{c_L}\right)^{\frac{2+k}{\alpha_L}}\Gamma\left(-\frac{2+k}{\alpha_L}\right)\mathbb{U}_{d,L}}, \tag{7.21}$$

where $\mathbb{U}_{d,L}$ is given in

$$\begin{aligned}
\mathbb{U}_{d,L} &= \frac{1}{2\pi^2 R^2}\left(\frac{\rho}{M_u^2}\right)^{\frac{2+k}{\alpha_L}} \frac{\Gamma\left(m_L+\frac{2+k}{\alpha_L}\right)}{\Gamma(m_L)m_L^{-\frac{2+k}{\alpha_L}}}\left(\frac{c_L^{\frac{2+k}{\alpha_L}}}{\beta^{4+k}}\left(\Gamma(4+k)-\Gamma\left(4+k,\beta\left(\frac{P_{d2d}M_u^2}{c_L\rho}\right)^{\frac{1}{\alpha_L}}\right)\right)\right. \\
&+ \frac{c_N^{\frac{2+k}{\alpha_L}}}{(2\alpha_L+(2+k)\alpha_N)\beta^{\frac{2\alpha_L+(2+k)\alpha_N}{\alpha_L}}}\left(\alpha_L\left(\beta\left(\frac{P_{d2d}M_u^2}{c_N\rho}\right)^{\frac{1}{\alpha_N}}\right)^{\frac{2\alpha_L+(2+k)\alpha_N}{\alpha_L}}\right. \\
&- \left.\left.(2\alpha_L+(2+k)\alpha_N)\left(\Gamma\left(\frac{2\alpha_L+(2+k)\alpha_N}{\alpha_L}\right)-\Gamma\left(\frac{2\alpha_L+(2+k)\alpha_N}{\alpha_L},\beta\left(\frac{P_{d2d}M_u^2}{c_N\rho}\right)^{\frac{1}{\alpha_N}}\right)\right)\right)\right) \\
&\times \left(\theta_u M_u^{\frac{2+k}{\alpha_L}}+(2\pi-\theta_u)m_u^{\frac{2+k}{\alpha_L}}\right)^2.
\end{aligned} \tag{7.22}$$

**Deriving** $M_{I_{d2d,N}}$

The expression for $M_{I_{d2d,N}}$ is obtained as

$$M_{I_{d2d,N}} = e^{\sum_{k=1}^{\infty} -\frac{2\pi\lambda_{d,t}(-\beta)^k}{\alpha_N k!}\left(\frac{s}{c_N}\right)^{\frac{2+k}{\alpha_N}}\Gamma\left(-\frac{2+k}{\alpha_N}\right)\mathbb{U}_{d,N}}, \tag{7.23}$$

where

$$\begin{aligned}
\mathbb{U}_{d,N} &= \frac{1}{2\pi^2 R^2}\left(\frac{\rho}{M_u^2}\right)^{\frac{2+k}{\alpha_N}} \frac{\Gamma\left(m_N+\frac{2+k}{\alpha_N}\right)}{\Gamma(m_N)m_N^{-\frac{2+k}{\alpha_N}}}\left(\frac{c_L^{\frac{2+k}{\alpha_N}}}{\beta^{\frac{2\alpha_N+(2+k)\alpha_L}{\alpha_N}}}\left(\Gamma\left(\frac{2\alpha_N+(2+k)\alpha_L}{\alpha_N}\right)\right.\right.
\end{aligned}$$

$$- \quad \Gamma\left(\frac{2\alpha_N + (2+k)\alpha_L}{\alpha_N}, \beta\left(\frac{P_{d2d}M_u^2}{c_L\rho}\right)^{\frac{1}{\alpha_L}}\right)\right) + \frac{c_N^{\frac{2+k}{\alpha_N}}}{(4+k)\beta^{4+k}}\left(\left(\beta\left(\frac{P_{d2d}M_u^2}{c_N\rho}\right)^{\frac{1}{\alpha_N}}\right)^{4+k}\right.$$

$$\left. - \quad (4+k)\left(\Gamma(4+k) - \Gamma\left(4+k, \beta\left(\frac{P_{d2d}M_u^2}{c_N\rho}\right)^{\frac{1}{\alpha_N}}\right)\right)\right)\left(\theta_u M_u^{\frac{2+k}{\alpha_N}} + (2\pi - \theta_u)m_u^{\frac{2+k}{\alpha_N}}\right)^2 \quad (7.24)$$

## 7.5 Numerical results

We next present performance trends of millimeter-wave D2D networks for several system parameter configurations. The details of the simulation setup are as follows. A $100$MHz bandwidth is considered (with a resultant noise power of $-94$ dBm) in the $28$ GHz band along with intercepts $cL = cN = 10^5$, and path loss exponents $\alpha_L = 2.1$ and $\alpha_N = 4.1$. Moreover, $\lambda_{c,b} = 10^{-4}$, $\theta_c = \theta_u = \frac{\pi}{10}$, $M_c = 20$ dB, $m_c = m_u = -10$ dB, $\rho = -80$ dBm, and $\beta = 0.001$.

Fig. 7.1 plots the outage probability with respect to the SINR threshold $\gamma_{th}$. It is clearly seen that D2D operation is infeasible when $\gamma_{th} > 20$ dB. For millimeter-wave D2D networks, four major factors affect the overall outage of a D2D receiver: interference from cellular base stations, interference from other D2D transmitters, thermal noise due to the high bandwidth, and the outage due to the associated transmitter being cut-off due to the peak power constraint. When $M_u = 10$ dB, increasing the cluster radius $R$ generally increases the outage probability. This is due to two reasons. First, a higher radius causes other D2D transmitters to transmit at a higher power level, increasing interference. This effect is amplified due to the fact that the probability of a NLOS link increases with the cell radius. Second, as the cell radius increases, the desired link itself has an increased tendency to be NLOS, resulting in more severe fading and being cut-off due to the required power exceeding the peak power threshold. However, when $M_u$ is increased to $20$ dB, the trend is unclear. As $R$ is increased, the outage roughly drops and then increases again. This is due to two competing effects occurring for a $M_u$ value; the desired link would have a lower probability to get cut-off due to the lower transmit power needed, and the intra-D2D interference increases because a lesser number of interfering D2D transmitters get cut-off. At a certain radius, the effect of the latter outweighs the former, and the outage increases. Moreover, it is important to note that the $R$ and $M_u$ pair providing the best performance also depends on the specific SINR threshold $\gamma_{th}$.

The outage probability is plotted against the D2D transmitter density $\lambda_{d,t}$ in Fig. 7.2. While

a higher $\lambda_{d,t}$ causes the outage to approach $1$ due to intra-D2D interference, reducing $\lambda_{d,t}$ causes the outage to first drop abruptly, and then flatten out towards a value determined by noise and inter-network interference. Interestingly, note that the outage probability increases when $m_L$ is increased from $2$ to $4$. While this may seem counter-intuitive, this phenomenon occurs due to the intra-D2D interference being less severely faded. However, the change in the outage when $m_N$ changes is negligible, and the curves for $m_N = 1$ and $m_N = 2$ almost overlap. Moreover, it's interesting to note that while a lower $P_{d2d}$ provides a lower outage at very low $\lambda_{d,t}$ values, the converse is true when $\lambda_{d,t}$ increases. As $P_{d2d}$ is lower, more D2D transmitters requiring additional power to transmit due to the increased radius get cut-off; thus reducing interference. However, under this scenario, the desired link also has an increased cut-off probability, which becomes more prominent when $\lambda_{d,t}$ is high. This is because for high $\lambda_{d,t}$, its contribution to the interference outweighs the interference reduction caused by a lower $P_{d2d}$.

We investigate the effect of the peak D2D transmit power $P_{d2d}$ on the outage in Fig. 7.3. While $P_{d2d}$ increases, the outage first drops, and then approaches $1$. As such, there is an optimum $P_{d2d}$ which gives the best performance. Furthermore, it is observed that a change in the receiver sensitivity $\rho$ does not significantly change the performance characteristics except shifting the location of the minimum outage; a higher $\rho$ provides the best performance at a higher $P_{d2d}$ and vice-versa.

## 7.6 Conclusion

The performance of a random D2D network underlaying a millimeter-wave cellular network was characterized within this chapter. Homogeneous Poisson processes were considered for the cellular base stations and users while a Matern cluster process was considered for the D2D network nodes. Sectored antenna patterns and random blockages were considered alongside different path loss exponents and Nakagami fading indexes depending on the LOS or NLOS nature of a link. The cellular users were assumed to connect with their closest base station while D2D receivers within a cluster connect with the transmitter represented by the cluster head. Moreover, path loss and antenna gain inversion based power control, varying upon the LOS or NLOS nature is employed by both networks while D2D transmitters are also peak power constrained. The MGFs of interference to a D2D receiver device from the cellular base stations and other D2D transmitters are derived in closed-form, and are used to obtain the outage probability of a D2D receiver. It is observed that the outage has a complex relationship with the D2D cluster radius and antenna

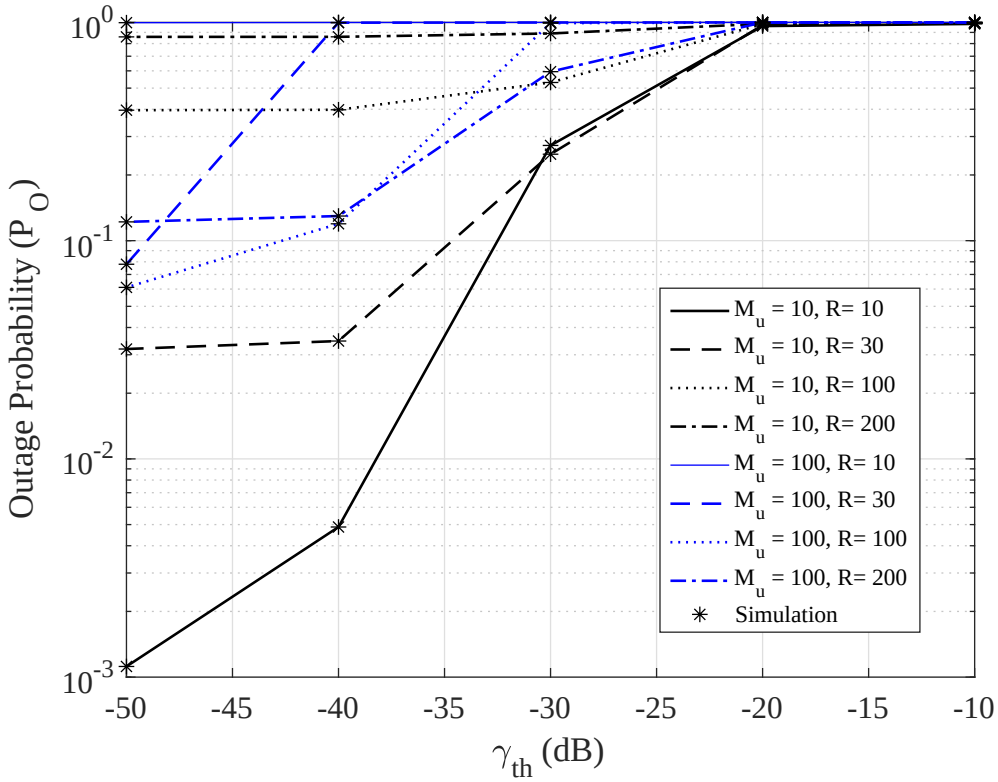


Figure 7.1: The outage probability ($P_O$) vs. $\gamma_{th}$ in dB for different D2D cell radii ($R$) and $M_u$. $\lambda_{d,t} = 10^{-4}$, $m_L = 4$, $m_N = 2$, and $P_{d2d} = -10$ dBm.

gains. Furthermore, a minima of the outage is occurs for a specific D2D peak power threshold, while a higher LOS fading severity (lower $m_L$) also reduces the outage. Extensions of the work include considering alternate transmitter-receiver association schemes and power control schemes.

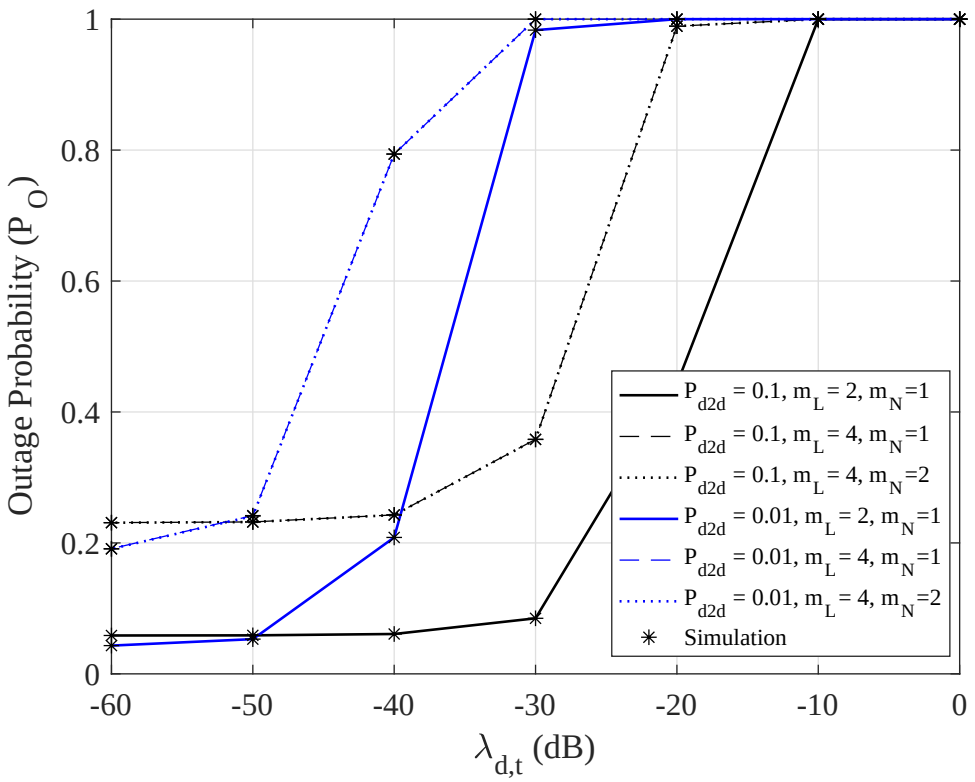


Figure 7.2: The outage probability ($P_O$) vs. the D2D transmitter density $\lambda_{d,t}$ in dB under varying $m_L$, $m_N$, and $P_{d2d}$. $\gamma_{th} = 10^{-3}$, $R = 20$, and $M_u = 10$ dB.

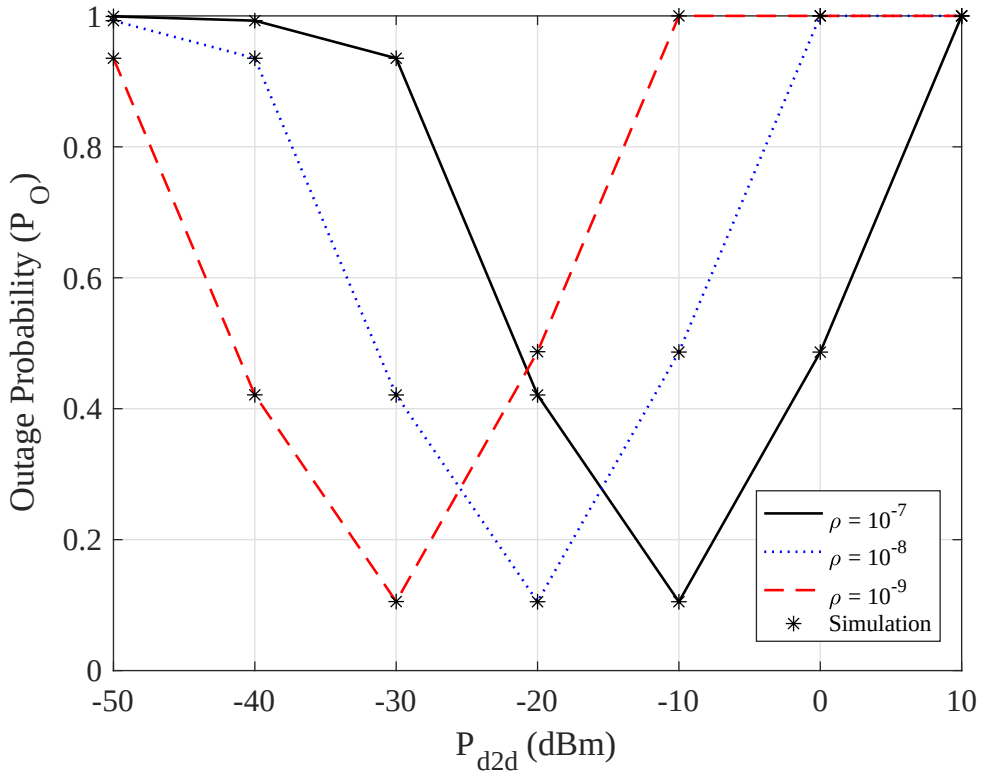


Figure 7.3: The outage probability ($P_O$) vs. the peak D2D power level $P_{d2d}$ under different receiver thresholds $\rho$. $\gamma_{th} = 10^{-3}$, $R = 100$, and $M_u = 20\,\text{dB}$, $m_L = 2$, $m_N = 1$, and $\lambda_{d,t} = 10^{-4}$.

# Chapter 8

# Conclusions and future research directions

## 8.1 Conclusions

This thesis considered several novel technologies which have been proposed for 5G networks and analyzed their performance using PPPs.

Chapter 3 characterized the aggregate interference from a finite annular field of underlay CR devices on a single PU receiver. Multiple power control schemes and receiver association schemes were considered. For each of these schemes, the MGF of the aggregate interference, the average interference, and the outage probability were derived. It was shown that CR power thresholds and node densities significantly affect the primary user performance.

In Chapter 4, the beacon-misdetection probability and the false-alarm probability were analyzed for multiple beacon detection and co-operation schemes. Beacon-emitter placement at both PU receivers and PU transmitters was considered. Three local detection schemes and several sensed information sharing schemes were considered. Several mechanisms for selecting co-operating CUs were proposed and analyzed. Co-operative beacon sensing was found out to reduce the misdetection probability by a factor of $10^4$.

The outage performance of a secondary network was analyzed in Chapter 5 for both single antenna and massive MIMO enabled base stations. Significant reductions in outage were observed. Moreover, a higher path loss exponent was found out to reduce outage under massive MIMO whereas this was the opposite for single antenna base stations.

Chapter 6 analyzed the energy harvesting process of a D2D node while considering temporal dynamics. Three independent PPPs were considered for the cellular base stations, cellular users,

and the D2D users. Moreover, log-distance path loss, Rayleigh fading, and path loss inversion based power control were incorporated. The ambient energy available for harvest at a typical D2D user was derived. In addition, multiple energy harvesting protocols were proposed: single slot harvesting, multi slot harvesting, $\mathcal{N}$ slot harvesting, and multi slot harvesting. Temporal effects were analyzed using a Markov chain based approach. The optimum parameter ranges and environments for the different harvesting schemes were derived.

Chapter 7 develops a characterization of D2D networks at millimeter wave frequencies. Blockages due to random objects, antenna gain patterns, log distance path loss, Nakagami-$m$ fading are considered along with antenna gain inversion based power control and peak power constraints. Closed-form expressions are obtained for the MGF of the aggregate interference on a D2D node and the outage probability. System parameters such as D2D cluster radii, peak power thresholds and node densities significantly affect the D2D performance under millimeter wave channels.

## 8.2 Future research directions

The work in this thesis can be enhanced and improved along the following lines of research

- **Non-homogeneous cases and medium access**

  This thesis assumes homogeneous sets of independent PPPs for the locations of users and base stations. While this leads to analytical tractability, it may not be applicable in some cases. For example, sets of users may be highly congregated around the base stations. In such cases, the Poisson cluster process can be used. Moreover, when CR and D2D devices communicate, medium access control can be considered where a particular device may refrain from transmitting if a nearby co-channel device is active. For this, hardcore point processes where a minimum distance exists between nodes can be used.

- **Mobility of nodes**

  Throughout the thesis, the mobility of nodes has not been considered. All devices (base stations and users) were assumed to be static. While this assumption holds true for base stations, it may not be ideal for user devices. Most hand held devices have the potential to be mobile. As a result, mobility models such as the random walk, random waypoint

model, or Brownian motion can be incorporated into the framework. Such an analysis would provide better understanding on the overall performance. Moreover, issues such as handover which were not addressed in this thesis can be analyzed.

- **Receiver association schemes in millimeter wave**

  D2D millimeter-wave systems were analyzed in Chapter 7. The nearest association scheme between a transmitter and a receiver was considered. However, because blocking, path loss, and other parameters are significantly different for line-of-sight and non-lone-of-sight conditions, the nearest association scheme may not be the best. For example, the nearest base station may be blocked, and an association to it may give a worse performance than an association with a line-of-sight base station at a further distance. Therefore, more suitable association schemes can be proposed and analyzed as a future work.

- **Millimeter wave under massive MIMO**

  Millimeter-wave systems (Chapter 7) were limited to single-antenna transmitters. However, as smaller antenna sizes are possible at high frequencies, these systems will incorporate massive MIMO. As such, research on how these two technologies interplay with and complement each other is needed. However, challenges exist dealing with channel estimation considering the sparsity of millimeter wave scatterers.

- **Internet of things**

  The work in this thesis can be applied for an application specific scenario such as IoT. The concepts relating to D2D devices, energy harvesting, and millimeter wave communication can be readily applied to an IoT environment. Moreover, IoT can be readily modelled using stochastic geometry models.

$\sim$

# References


[1] "Cisco visual networking index: Global mobile data traffic forecast update, 2014–2019." Tech. Rep., 2015.

[2] S. Kusaladharma, P. Herath, and C. Tellambura, "An overview of cognitive radio networks," in *To appear in Wiley Encyclopedia of Electrical and Electronics Engineering*.

[3] A. Goldsmith, *Wireless Communications*. Cambridge University Press, 2005.

[4] T. Bai and R. W. Heath, "Coverage and rate analysis for millimeter-wave cellular networks," *IEEE Trans. Wireless Commun.*, vol. 14, no. 2, pp. 1100–1114, Feb 2015.

[5] I. Gradshteyn and I. Ryzhik, *Table of integrals, Series, and Products*, 7th ed. Academic Press, 2007.

[6] J. Andrews, S. Buzzi, W. Choi, S. Hanly, A. Lozano, A. Soong, and J. Zhang, "What will 5g be?" *IEEE J. Sel. Areas Commun.*, vol. 32, no. 6, pp. 1065–1082, June 2014.

[7] T. Rappaport, S. Sun, R. Mayzus, H. Zhao, Y. Azar, K. Wang, G. Wong, J. Schulz, M. Samimi, and F. Gutierrez, "Millimeter wave mobile communications for 5g cellular: It will work!" *IEEE Access*, vol. 1, pp. 335–349, 2013.

[8] C.-X. Wang, F. Haider, X. Gao, X.-H. You, Y. Yang, D. Yuan, H. Aggoune, H. Haas, S. Fletcher, and E. Hepsaydir, "Cellular architecture and key technologies for 5g wireless communication networks," *IEEE Commun. Magazine*, vol. 52, no. 2, pp. 122–130, February 2014.

[9] A. Gupta and R. Jha, "A survey of 5g network: Architecture and emerging technologies," *IEEE Access*, vol. 3, pp. 1206–1232, 2015.

[10] M. Di Renzo, "Stochastic geometry modeling and analysis of multi-tier millimeter wave cellular networks," *Wireless Communications, IEEE Transactions on*, vol. 14, no. 9, pp. 5038–5057, Sept 2015.

[11] M. Haenggi, J. Andrews, F. Baccelli, O. Dousse, and M. Franceschetti, "Stochastic geometry and random graphs for the analysis and design of wireless networks," *Selected Areas in Communications, IEEE Journal on*, vol. 27, no. 7, pp. 1029–1046, September 2009.

[12] H. Dhillon, R. Ganti, F. Baccelli, and J. Andrews, "Modeling and analysis of k-tier downlink heterogeneous cellular networks," *IEEE J. Sel. Areas Commun.*, vol. 30, no. 3, pp. 550–560, April 2012.

[13] P. C. Pinto and M. Z. Win, "Communication in a Poisson field of interferers–part I: Interference distribution and error probability," *IEEE Trans. Wireless Commun.*, vol. 9, no. 7, pp. 2176–2186, Jul. 2010.

[14] E. Salbaroli and A. Zanella, "Interference analysis in a Poisson field of nodes of finite area," *IEEE Trans. Veh. Technol.*, vol. 58, no. 4, pp. 1776–1783, May 2009.

[15] Y. Dhungana and C. Tellambura, "Outage probability of underlay cognitive relay networks with spatially random nodes," in *2014 IEEE Global Communications Conference*, Dec 2014, pp. 3597–3602.

[16] J. Chen, M. Ding, and Q. Zhang, "Interference statistics and performance analysis of mimo ad hoc networks in binomial fields," *IEEE Trans. Veh. Technol.*, vol. 61, no. 5, pp. 2033–2043, Jun. 2012.

[17] T. Nechiporenko, P. Kalansuriya, and C. Tellambura, "Performance of optimum switching adaptive-qam for amplify-and-forward relays," *IEEE Transactions on Vehicular Technology*, vol. 58, no. 5, pp. 2258–2268, 2009.

[18] G. Amarasuriya, M. Ardakani, and C. Tellambura, "Output-threshold multiple-relay-selection scheme for cooperative wireless networks," *IEEE Transactions on Vehicular Technology*, vol. 59, no. 6, pp. 3091–3097, 2010.

[19] S. P. Herath, N. Rajatheva, and C. Tellambura, "Unified approach for energy detection of unknown deterministic signal in cognitive radio over fading channels," in *2009 IEEE International Conference on Communications Workshops*. IEEE, 2009, pp. 1–5.

[20] D. T. Ngo, C. Tellambura, and H. H. Nguyen, "Efficient resource allocation for ofdma multicast systems with spectrum-sharing control," *IEEE Transactions on Vehicular Technology*, vol. 58, no. 9, pp. 4878–4889, 2009.

[21] X. Gong, S. A. Vorobyov, and C. Tellambura, "Joint bandwidth and power allocation with admission control in wireless multi-user networks with and without relaying," *IEEE Transactions on Signal Processing*, vol. 59, no. 4, pp. 1801–1813, 2011.

[22] Qualcomm. (2011) The visible light communications motivation. [Online]. Available: http://visiblelightcomm.com/the-visible-light-communications-motivation/

[23] S. Haykin, "Cognitive radio: brain-empowered wireless communications," *IEEE J. Sel. Areas Commun.*, vol. 23, no. 2, pp. 201–220, Feb. 2005.

[24] H. S. Shahraki, "Opportunistic usage of television white space with respect to the long term evolution-advanced parameters," *IET Commun.*, vol. 9, no. 9, pp. 1240–1247, 2015.

[25] M. T. Masonta, M. Mzyece, and N. Ntlatlapa, "Spectrum decision in cognitive radio networks: A survey," *IEEE Commun. Surveys Tuts.*, vol. 15, no. 3, pp. 1088–1107, March 2013.

[26] J. Mitola, "Cognitive radio for flexible mobile multimedia communications," in *Proc. IEEE Int. Workshop MoMuC*, Nov 1999, pp. 3–10.

[27] L. Gavrilovska, D. Denkovski, V. Rakovic, and M. Angjelichinoski, "Medium access control protocols in cognitive radio networks: Overview and general classification," *IEEE Commun. Surveys Tuts.*, vol. 16, no. 4, pp. 2092–2124, Fourthquarter 2014.

[28] M. Matinmikko, M. Palola, H. Saarnisaari, M. Heikkil?, J. Prokkola, T. Kippola, T. H?nninen, M. Jokinen, and S. Yrj?l?, "Cognitive radio trial environment: First live authorized shared access-based spectrum-sharing demonstration," *IEEE Veh.Tech. Mag.*, vol. 8, no. 3, pp. 30–37, Sept 2013.

[29] I. F. Akyildiz, W.-Y. Lee, M. C. Vuran, and S. Mohanty, "Next generation/dynamic spectrum access/cognitive radio wireless networks: A survey," *Computer Networks*, vol. 50, no. 13, pp. 2127–2159, 2006. [Online]. Available: http://www.sciencedirect.com/science/article/pii/S1389128606001009

[30] R. Menon, R. Buehrer, and J. Reed, "Outage probability based comparison of underlay and overlay spectrum sharing techniques," in *Proc. IEEE DYSPAN 2005*, Nov. 2005, pp. 101–109.

[31] S. Srinivasa and S. Jafar, "Cognitive radios for dynamic spectrum access - the throughput potential of cognitive radio: A theoretical perspective," *IEEE Commun. Mag.*, vol. 45, no. 5, pp. 73–79, May 2007.

[32] E. Hossain, D. Niyato, and Z. Han, *Dynamic Spectrum Access and Management in Cognitive Radio Networks*. Cambridge University Press, 2009.

[33] B. Wang and K. Liu, "Advances in cognitive radio networks: A survey," *IEEE J. Sel.Topics Signal Process.*, vol. 5, no. 1, pp. 5–23, Feb. 2011.

[34] S. K. Sharma, T. E. Bogale, S. Chatzinotas, B. Ottersten, L. B. Le, and X. Wang, "Cognitive radio techniques under practical imperfections: A survey," *IEEE Commun. Surveys Tuts.*, vol. 17, no. 4, pp. 1858–1884, Fourthquarter 2015.

[35] S. Atapattu, C. Tellambura, and H. Jiang, "Energy detection based cooperative spectrum sensing in cognitive radio networks," *IEEE Trans. Wireless Commun.*, vol. 10, no. 4, pp. 1232–1241, April 2011.

[36] A. Al-Dulaimi, J. Cosmas, and A. Mohammed, *Self-Organization and Green Applications in Cognitive Radio Networks*. IGI Global, 2013.

[37] L. Vijayandran, P. Dharmawansa, T. Ekman, and C. Tellambura, "Analysis of aggregate interference and primary system performance in finite area cognitive radio networks," *IEEE Trans. Commun.*, vol. 60, no. 7, pp. 1811–1822, July 2012.

[38] Z. Chen, C.-X. Wang, X. Hong, J. Thompson, S. Vorobyov, X. Ge, H. Xiao, and F. Zhao, "Aggregate interference modeling in cognitive radio networks with power and contention control," *IEEE Trans. Commun.*, vol. 60, no. 2, pp. 456–468, Feb. 2012.

[39] A. Rabbachin, T. Q. S. Quek, H. Shin, and M. Z. Win, "Cognitive network interference," *IEEE J. Sel. Areas Commun.*, vol. 29, no. 2, pp. 480–493, Feb. 2011.

[40] C. han Lee and M. Haenggi, "Delay analysis of spatio-temporal channel access for cognitive networks," in *Proc. IEEE ICC*, June 2011, pp. 1–5.

[41] A. Goldsmith, S. Jafar, I. Maric, and S. Srinivasa, "Breaking spectrum gridlock with cognitive radios: An information theoretic perspective," *Proc. IEEE*, vol. 97, no. 5, pp. 894–914, 2009.

[42] M. Tehrani, M. Uysal, and H. Yanikomeroglu, "Device-to-device communication in 5g cellular networks: challenges, solutions, and future directions," *IEEE Commun. Magazine*, vol. 52, no. 5, pp. 86–92, May 2014.

[43] X. Shen, "Device-to-device communication in 5g cellular networks," *IEEE Network*, vol. 29, no. 2, pp. 2–3, March 2015.

[44] J. Qiao, X. Shen, J. Mark, Q. Shen, Y. He, and L. Lei, "Enabling device-to-device communications in millimeter-wave 5g cellular networks," *IEEE Commun. Magazine*, vol. 53, no. 1, pp. 209–215, January 2015.

[45] M. Usman, A. Gebremariam, U. Raza, and F. Granelli, "A software-defined device-to-device communication architecture for public safety applications in 5g networks," *IEEE Access*, vol. 3, pp. 1649–1654, 2015.

[46] V. Jungnickel, K. Manolakis, W. Zirwas, B. Panzner, V. Braun, M. Lossow, M. Sternad, R. Apelfro?jd, and T. Svensson, "The role of small cells, coordinated multipoint, and massive mimo in 5g," *Communications Magazine, IEEE*, vol. 52, no. 5, pp. 44–51, May 2014.

[47] F. Boccardi, R. Heath, A. Lozano, T. Marzetta, and P. Popovski, "Five disruptive technology directions for 5g," *IEEE Commun. Magazine*, vol. 52, no. 2, pp. 74–80, February 2014.

[48] Z. Gao, L. Dai, D. Mi, Z. Wang, M. Imran, and M. Shakir, "Mmwave massive-mimo-based wireless backhaul for the 5g ultra-dense network," *IEEE Wireless Commun.*, vol. 22, no. 5, pp. 13–21, October 2015.

[49] A. Khansefid and H. Minn, "On channel estimation for massive MIMO with pilot contamination," *IEEE Commun. Lett.*, vol. 19, no. 9, pp. 1660–1663, Sept 2015.

[50] X. Zhu, Z. Wang, L. Dai, and C. Qian, "Smart pilot assignment for massive MIMO," *IEEE Commun. Lett.*, vol. 19, no. 9, pp. 1644–1647, Sept 2015.

[51] J.-C. Shen, J. Zhang, and K. Letaief, "Downlink user capacity of massive MIMO under pilot contamination," *IEEE Trans. Wireless Commun.*, vol. 14, no. 6, pp. 3183–3193, June 2015.

[52] L. You, X. Gao, X. gen Xia, N. Ma, and Y. Peng, "Pilot reuse for massive MIMO transmission over spatially correlated rayleigh fading channels," *IEEE Trans. Wireless Commun.*, vol. 14, no. 6, pp. 3352–3366, June 2015.

[53] J. Nam, J.-Y. Ahn, A. Adhikary, and G. Caire, "Joint spatial division and multiplexing: Realizing massive mimo gains with limited channel state information," in *Proc. IEEE CISS*, March 2012, pp. 1–6.

[54] P. Wang, Y. Li, L. Song, and B. Vucetic, "Multi-gigabit millimeter wave wireless communications for 5g: from fixed access to cellular networks," *IEEE Commun. Magazine*, vol. 53, no. 1, pp. 168–178, January 2015.

[55] T. Bai, A. Alkhateeb, and R. Heath, "Coverage and capacity of millimeter-wave cellular networks," *IEEE Commun. Magazine*, vol. 52, no. 9, pp. 70–77, September 2014.

[56] M. Peng, C. Wang, J. Li, H. Xiang, and V. Lau, "Recent advances in underlay heterogeneous networks: Interference control, resource allocation, and self-organization," *IEEE Commun. Surveys Tuts.*, vol. 17, no. 2, pp. 700–729, Secondquarter 2015.

[57] S. Lee, R. Zhang, and K. Huang, "Opportunistic wireless energy harvesting in cognitive radio networks," *IEEE Trans. Wireless Commun.*, vol. 12, no. 9, pp. 4788–4799, September 2013.

[58] P. Kamalinejad, C. Mahapatra, Z. Sheng, S. Mirabbasi, V. Leung, and Y. L. Guan, "Wireless energy harvesting for the internet of things," *IEEE Commun. Magazine*, vol. 53, no. 6, pp. 102–108, June 2015.

[59] S. Kim, R. Vyas, J. Bito, K. Niotaki, A. Collado, A. Georgiadis, and M. Tentzeris, "Ambient rf energy-harvesting technologies for self-sustainable standalone wireless sensor platforms," *Proc. IEEE*, vol. 102, no. 11, pp. 1649–1666, Nov 2014.

[60] M. Simon and M. S. Alouini, *Digital Communications over fading channels, 2nd edition*. Wiley, 2004.

[61] M. Nakagami, "The m-distribution, a general formula for intensity distribution of rapid fading," *Statistical Methods in RadioWave Propagation*, pp. 3–36, 1960.

[62] I. Trigui, A. Laourine, S. Affes, and A. Stephenne, "Outage analysis of wireless systems over composite fading/shadowing channels with co-channel interference," in *Proc. IEEE WCNC*, Apr. 2009, pp. 1–6.

[63] P. Bithas, N. Sagias, P. Mathiopoulos, G. Karagiannidis, and A. Rontogiannis, "On the performance analysis of digital communications over generalized-k fading channels," *IEEE Commun. Lett.*, vol. 10, no. 5, pp. 353–355, May 2006.

[64] S. Atapattu, C. Tellambura, and H. Jiang, "A mixture gamma distribution to model the snr of wireless channels," vol. 10, no. 12, pp. 4193 –4203, Dec. 2011.

[65] D. Stoyan, W. S. Kendall, and J. Mecke, *Stochastic Geometry and Its Applications*. Wiley, 1996.

[66] A. Baddeley, I. Barany, R. Schneider, and W. Weil, *Spatial Point Processes and their Applications*. Springer, 2007.

[67] S.-R. Cho and W. Choi, "Coverage and load balancing in heterogeneous cellular networks with minimum cell separation," *IEEE Trans. Mobile Computing*, vol. 13, no. 9, pp. 1955–1966, Sept 2014.

[68] N. Deng, W. Zhou, and M. Haenggi, "Heterogeneous cellular network models with dependence," *IEEE J. Sel. Areas Commun.*, vol. 33, no. 10, pp. 2167–2181, Oct 2015.

[69] Y. Liu, C. Yin, J. Gao, and X. Sun, "Transmission capacity for overlaid wireless networks: A homogeneous primary network versus an inhomogeneous secondary network," in *Proc. IEEE ICCCAS*, vol. 1, Nov 2013, pp. 154–158.

[70] Y. Zhou, Z. Zhao, Q. Ying, R. Li, X. Zhou, and H. Zhang, "Two-tier spatial modeling of base stations in cellular networks," in *Proc. IEEE PIMRC*, Sept 2014, pp. 1570–1574.

[71] G. Alfano, M. Garetto, and E. Leonardi, "New directions into the stochastic geometry analysis of dense csma networks," *IEEE Trans. Mobile Computing*, vol. 13, no. 2, pp. 324–336, Feb 2014.

[72] B. Matern, *Spatial Variation*. Springer Lecture Notes in Statistics, 2nd ed., 1986.

[73] J. F. Kingman, *Poisson Processes*. Oxford University Press, 1993.

[74] M. Haenggi and R. K. Ganti, *Interference in Large Wireless Networks*. Now Publishers, 2009.

[75] P. Mach and Z. Becvar, "QoS-guaranteed power control mechanism based on the frame utilization for femtocells," *EURASIP Journal on Wireless Communications and Networking*, vol. 2011, 2011.

[76] A. Molisch, *Wireless Communications*. Wiley-IEEE Press, 2011.

[77] J. Jang and K.-B. Lee, "Transmit power adaptation for multiuser OFDM systems," *IEEE J. Sel. Areas Commun.*, vol. 21, no. 2, pp. 171–178, 2003.

[78] D. Qiao, S. Choi, and K. Shin, "Interference analysis and transmit power control in IEEE 802.11a/h wireless LANs," *IEEE/ACM Trans. Networking*, vol. 15, no. 5, pp. 1007–1020, 2007.

[79] S. Gong, P. Wang, Y. Liu, and W. Zhuang, "Robust power control with distribution uncertainty in cognitive radio networks," *IEEE J. Sel. Areas Commun.*, vol. 31, no. 11, pp. 2397–2408, 2013.

[80] C. Sun, Y. Alemseged, H.-N. Tran, and H. Harada, "Transmit power control for cognitive radio over a Rayleigh fading channel," *IEEE Trans. Veh. Technol.*, vol. 59, no. 4, pp. 1847–1857, 2010.

[81] D. Senaratne, C. Tellambura, and H. A. Suraweera, "Performance analysis of MIMO channel inversion in rayleigh fading," *IEEE Transactions on Vehicular Technology*, vol. 61, no. 3, pp. 1188–1196, 2012.

[82] N. Hoven and A. Sahai, "Power scaling for cognitive radio," in *Proc. IEEE WNCMC*, vol. 1, 2005, pp. 250–255 vol.1.

[83] S. Kusaladharma, P. Herath, and C. Tellambura, "Impact of transmit power control on aggregate interference in underlay cognitive radio networks," in *Proc. IEEE ICC*, June 2014, pp. 1–6.

[84] ——, "Impact of transmit power control and receiver association on interweave network interference," in *Proc. IEEE VTC*, Sept 2014, pp. 1–5.

[85] ——, "Underlay interference analysis of power control and receiver association schemes," *IEEE Trans. Veh. Technol.*, vol. 65, no. 11, pp. 8978–8991, Nov 2016.

[86] ——, "Aggregate interference analysis for interweave cognitive networks," in *Proc. IEEE VTC*, Sept 2014, pp. 1–5.

[87] S. Kusaladharma and C. Tellambura, "Impact of beacon misdetection on aggregate interference for hybrid underlay-interweave networks," *IEEE Wireless Commun. Lett.*, vol. 17, no. 11, pp. 2052–2055, November 2013.

[88] ——, "Aggregate interference analysis for underlay cognitive radio networks," *IEEE Wireless Commun. Lett.*, vol. 1, no. 6, pp. 641–644, 2012.

[89] C. Tellambura, A. J. Mueller, and V. K. Bhargawa, "Analysis of M-ary phase-shift keying with diversity reception for land-mobile satellite channels," *IEEE Transactions on Vehicular Technology*, vol. 46, no. 4, pp. 910–922, Nov 1997.

[90] C. Tellambura, A. Annamalai, and V. K. Bhargava, "Closed form and infinite series solutions for the MGF of a dual-diversity selection combiner output in bivariate Nakagami fading," *IEEE Transactions on Communications*, vol. 51, no. 4, pp. 539–542, April 2003.

[91] C. Tellambura, "Evaluation of the exact union bound for trellis-coded modulations over fading channels," *IEEE Transactions on Communications*, vol. 44, no. 12, pp. 1693–1699, Dec 1996.

[92] S. Kusaladharma, P. Herath, and C. Tellambura, "Secondary user interference characterization for underlay networks," in *Proc. IEEE VTC*, Sept 2015, pp. 1–5.

[93] S. Kusaladharma and C. Tellambura, "On approximating the cognitive radio aggregate interference," *IEEE Wireless Commun. Lett.*, vol. 2, no. 1, pp. 58–61, 2013.

[94] ——, "Massive MIMO based underlay networks with power control," in *Proc. IEEE ICC*, May 2016, pp. 1–6.

[95] M. Hanif, M. Shafi, P. Smith, and P. Dmochowski, "Interference and deployment issues for cognitive radio systems in shadowing environments," in *Proc. IEEE ICC*, Jun. 2009, pp. 1–6.

[96] A. Babaei and B. Jabbari, "Interference modeling and avoidance in spectrum underlay cognitive wireless networks," in *Proc. IEEE ICC*, May 2010, pp. 1–5.

[97] K. Woyach, P. Grover, and A. Sahai, "Near vs. far field: Interference aggregation in tv whitespaces," in *Proc. IEEE GLOBECOM*, Dec. 2011, pp. 1–5.

[98] X. Hong, C.-X. Wang, and J. Thompson, "Interference modeling of cognitive radio networks," in *Proc. IEEE VTC*, May 2008, pp. 1851–1855.

[99] S. Kusaladharma and C. Tellambura, "A multiple-ring model for cognitive radio aggregate interference," *IEEE Commun. Lett.*, vol. 18, no. 4, pp. 596–599, April 2014.

[100] A. M. Wyglinski, M. Nekovee, and T. Hou, *Cognitive Radio Communications and Networks: Principles and Practice*. Elsevier, 2010.

[101] F. Paisana, N. Marchetti, and L. DaSilva, "Radar, TV and cellular bands: Which spectrum access techniques for which bands?" *IEEE Commun. Surveys and Tut.*, vol. 16, no. 3, pp. 1193–1220, Third 2014.

[102] L. Barlemann and S. Mangold, *Cognitive Radio and Dynamic Spectrum Access*. Wiley, 2009.

[103] M. Derakhshani and T. Le-Ngoc, "Aggregate interference and capacity-outage analysis in a cognitive radio network," *IEEE Trans. Veh. Technol.*, vol. 61, no. 1, pp. 196–207, Jan. 2012.

[104] K. Bian, J.-M. Park, L. Chen, and X. Li, "Addressing the hidden terminal problem for heterogeneous coexistence between tdm and CSMA networks in white space," *IEEE Trans. Veh. Technol.*, vol. 63, no. 9, pp. 4450–4463, Nov 2014.

[105] X. Song, C. Yin, D. Liu, and R. Zhang, "Spatial throughput characterization in cognitive radio networks with threshold-based opportunistic spectrum access," *IEEE J. Sel. Areas Commun.*, vol. 32, no. 11, pp. 2190–2204, November 2014.

[106] Z. Lei and F. Chin, "A reliable and power efficient beacon structure for cognitive radio systems," *IEEE Trans. Broadcast.*, vol. 54, no. 2, pp. 182–187, June 2008.

[107] H. Venkataraman and G. Muntean, *Cognitive Radio and its Application for Next Generation Cellular and Wireless Networks*. Springer, 2012.

[108] S. Mishra, A. Sahai, and R. Brodersen, "Cooperative sensing among cognitive radios," in *Proc. IEEE ICC*, vol. 4, June 2006, pp. 1658–1663.

[109] C. Jiang, N. Beaulieu, L. Zhang, Y. Ren, M. Peng, and H.-H. Chen, "Cognitive radio networks with asynchronous spectrum sensing and access," *IEEE Network*, vol. 29, no. 3, pp. 88–95, May 2015.

[110] G. Ganesan and Y. Li, "Cooperative spectrum sensing in cognitive radio, part ii: Multiuser networks," *IEEE Trans. Wireless Commun.*, vol. 6, no. 6, pp. 2214–2222, June 2007.

[111] Y. C. Liang, K. C. Chen, G. Y. Li, and P. Mahonen, "Cognitive radio networking and communications: an overview," *IEEE Trans. Veh. Tech.*, vol. 60, no. 7, pp. 3386–3407, Sept 2011.

[112] A. Sakr and E. Hossain, "Cognitive and energy harvesting-based D2D communication in cellular networks: Stochastic geometry modeling and analysis," *IEEE Trans. Commun.*, vol. 63, no. 5, pp. 1867–1880, May 2015.

[113] M. D. Renzo, "Stochastic geometry modeling and analysis of multi-tier millimeter wave cellular networks," *IEEE Trans. Wireless Commun.*, vol. 14, no. 9, pp. 5038–5057, Sept 2015.

[114] Y. Qu, J. Fang, and S. Zhang, "Nearest neighbor nodes and connectivity of three-dimensional wireless sensor networks with poisson point field," in *Proc. IEEE ICCSIT*, vol. 2, July 2010, pp. 269–272.

[115] A. Busson, B. Jabbari, A. Babaei, and V. Veque, "Interference and throughput in spectrum sensing cognitive radio networks using point processes," *Communications and Networks, Journal of*, vol. 16, no. 1, pp. 67–80, Feb 2014.

[116] H. ElSawy and E. Hossain, "Two-tier hetnets with cognitive femtocells: Downlink performance modeling and analysis in a multichannel environment," *IEEE Trans. Mobile. Computing*, vol. 13, no. 3, pp. 649–663, March 2014.

[117] H. ElSawy, E. Hossain, and M. Haenggi, "Stochastic geometry for modeling, analysis, and design of multi-tier and cognitive cellular wireless networks: A survey," *Communications Surveys Tutorials, IEEE*, vol. 15, no. 3, pp. 996–1019, Third 2013.

[118] N. Lee, X. Lin, J. G. Andrews, and R. W. Heath, "Power control for d2d underlaid cellular networks: Modeling, algorithms and analysis," *CoRR*, vol. abs/1305.6161, 2013.

[119] M. J. Rahman and X. Wang, "Probabilistic analysis of mutual interference in cognitive radio communications," in *Proc. IEEE GLOBECOM*, Dec. 2011, pp. 1–5.

[120] C.-H. Lee and C.-Y. Shih, "Coverage analysis of cognitive femtocell networks," *IEEE Wireless Commun. Lett.*, vol. 3, no. 2, pp. 177–180, April 2014.

[121] C.-H. Lee and M. Haenggi, "Interference and outage in poisson cognitive networks," *IEEE Trans. Wireless Commun.*, vol. 11, no. 4, pp. 1392–1401, Apr. 2012.

[122] A. Rabbachin, A. Conti, and M. Win, "Wireless network intrinsic secrecy," *IEEE Trans. Netw.*, vol. 23, no. 1, pp. 56–69, Feb 2015.

[123] X. Zhang and M. Haenggi, "Random power control in Poisson networks," *IEEE Trans. Commun.*, vol. 60, no. 9, pp. 2602–2611, September 2012.

[124] S. Weber, J. Andrews, and N. Jindal, "The effect of fading, channel inversion, and threshold scheduling on ad hoc networks," *IEEE Trans Info. Theory*, vol. 53, no. 11, pp. 4127–4149, Nov 2007.

[125] Y. Dhungana and C. Tellambura, "Uniform approximations for wireless performance in fading channels," *IEEE Trans. Commun.*, vol. 61, no. 11, pp. 4768–4779, November 2013.

[126] D. Moltchanov, "Distance distributions in random networks," *Ad Hoc Networks*, vol. 10, no. 6, pp. 1146–1166, 2012. [Online]. Available: http://www.sciencedirect.com/science/article/pii/S1570870512000224

[127] D. Stoyan, W. S. Stoyan, Kendall, and J. Mecke, *Stochastic Geometry and it's Applications*. John Wiley & Sons Ltd., 1995.

[128] J. Andrews, F. Baccelli, and R. Ganti, "A tractable approach to coverage and rate in cellular networks," *IEEE Trans. Commun.*, vol. 59, no. 11, pp. 3122–3134, 2011.

[129] Q. Cui, Y. Zhang, and X. Tao, "Hybrid-pilot based downlink CSI feedback scheme with zero-overhead," in *Proc. IEEE VTC*, Sept 2009, pp. 1–4.

[130] M. Haenggi, "Mean interference in hard-core wireless networks," *IEEE Commun. Lett.*, vol. 15, no. 8, pp. 792–794, August 2011.

[131] S. Kusaladharma, P. Herath, and C. Tellambura, "Impact of transmit power control and receiver association on interweave network interference," in *Proc. IEEE VTC*, Sept 2014, pp. 1–5.

[132] P. Madhusudhanan, J. Restrepo, Y. Liu, T. Brown, and K. Baker, "Downlink performance analysis for a generalized shotgun cellular system," *IEEE Trans. Wireless Commun.*, vol. 13, no. 12, pp. 6684–6696, Dec 2014.

[133] S. Atapattu, C. Tellambura, and H. Jiang, *Energy Detection for Spectrum Sensing in Cognitive Radio*. Springer, 2014.

[134] A. Ghasemi and E. Sousa, "Interference aggregation in spectrum-sensing cognitive wireless networks," *IEEE J. Sel. Areas Commun.*, vol. 2, no. 1, pp. 41–56, Feb. 2008.

[135] I. F. Akyildiz, B. F. Lo, and R. Balakrishnan, "Cooperative spectrum sensing in cognitive radio networks: A survey," *Phys. Commun.*, vol. 4, no. 1, pp. 40–62, Mar. 2011. [Online]. Available: http://dx.doi.org/10.1016/j.phycom.2010.12.003

[136] A. Ghasemi and E. Sousa, "Collaborative spectrum sensing for opportunistic access in fading environments," in *Proc. IEEE DySPAN*, Nov 2005, pp. 131–136.

[137] P. Madhusudhanan, Y. Liu, and T. Brown, "On primary user coverage probabilities and faulty cognitive radios," *IEEE Trans. Wireless. Commun.*, vol. 13, no. 11, pp. 6207–6218, Nov 2014.

[138] A. Babaei, P. Agrawal, and B. Jabbari, "Statistics of aggregate interference in cognitive wireless ad hoc networks," in *Proc. IEEE ICNC*, Jan 2012, pp. 397–401.

[139] Y. Sun and B. Mark, "Interference model for spectrum sensing with power control," in *Proc. IEEE CISS*, March 2013, pp. 1–6.

[140] M. Di Renzo, F. Graziosi, and F. Santucci, "Cooperative spectrum sensing in cognitive radio networks over correlated log-normal shadowing," in *Proc. IEEE VTC*, April 2009, pp. 1–5.

[141] S.-C. Hung and K.-C. Chen, "Geometric design of cooperative spectrum sensing for cognitive radios," in *Proc. IEEE PIMRC*, Sept 2013, pp. 2496–2501.

[142] A. Rabbachin, T. Q. S. Quek, H. Shin, and M. Z. Win, "Cognitive network interference," *IEEE J. Sel. Areas Commun.*, vol. 29, no. 2, pp. 480–493, Feb. 2011.

[143] A. Busson, B. Jabbari, A. Babaei, and V. Veque, "Interference and throughput in spectrum sensing cognitive radio networks using point processes," *Journal of Communications and Networks*, vol. 16, no. 1, pp. 67–80, Feb 2014.

[144] P. Madhusudhanan, J. G. Restrepo, Y. Liu, T. X. Brown, and K. Baker, "Modeling of interference from cooperative cognitive radios for low power primary users," in *Proc. IEEE GLOBECOM*, Dec 2010, pp. 1–6.

[145] X. Song, C. Yin, D. Liu, and R. Zhang, "Spatial throughput characterization in cognitive radio networks with threshold-based opportunistic spectrum access," *IEEE J. Sel. Areas Commun.*, vol. 32, no. 11, pp. 2190–2204, November 2014.

[146] A. Patel, S. Biswas, and A. K. Jagannatham, "Multiple beacon based robust cooperative spectrum sensing in MIMO cognitive radio networks," in *Proc. IEEE VTC*, Sept 2013, pp. 1–5.

[147] F. Adelantado, A. Juan, H. Skianis, and C. Verikoukis, "Sensing users selection with overhead reduction for cognitive wireless ad-hoc networks," in *Proc. IEEE GLOBECOM*, Dec 2010, pp. 1–5.

[148] E. Krouk and S. Semenov, *Coding Techniques in Wireless Communications*. Wiley, 2010.

[149] P. Herath, W. Krzymien, and C. Tellambura, "Stochastic geometry modeling of cellular uplink power control under composite rayleigh-lognormal fading," in *Proc. IEEE VTC*, Sept 2015, pp. 1–5.

[150] P. Sharma and R. Singh, "Cell coverage and link budget calculations in GSM systems," *International Journal on Modern Engineering Research*, vol. 2, no. 2, pp. 170–176, Mar. 2012.

[151] X. Hong, J. Wang, C.-X. Wang, and J. Shi, "Cognitive radio in 5G: a perspective on energy-spectral efficiency trade-off," *IEEE Commun. Magazine*, vol. 52, no. 7, pp. 46–53, July 2014.

[152] S. Schwarz, M. Wrulich, and M. Rupp, "Mutual information based calculation of the precoding matrix indicator for 3gpp umts/lte," in *Proc. IEEE WSA*, Feb 2010, pp. 52–58.

[153] P. Madhusudhanan, X. Li, Y. Liu, and T. Brown, "Stochastic geometric modeling and interference analysis for massive MIMO systems," in *Proc. IEEE WiOpt*, May 2013, pp. 15–22.

[154] Q. Ye, O. Y. Bursalioglu, H. C. Papadopoulos, C. Caramanis, and J. G. Andrews, "User association and interference management in massive MIMO hetnets," *IEEE Trans. Commun.*, vol. 64, no. 5, pp. 2049–2065, May 2016.

[155] C. Feng, Y. Jing, and S. Jin, "Interference and outage probability analysis for massive MIMO downlink with MF precoding," *IEEE Signal Process. Lett.*, vol. 23, no. 3, pp. 366–370, March 2016.

[156] A. Adhikary, H. S. Dhillon, and G. Caire, "Massive-MIMO meets hetnet: Interference coordination through spatial blanking," *IEEE J. Sel. Areas Commun.*, vol. 33, no. 6, pp. 1171–1186, June 2015.

[157] S. Kusaladharma, P. Herath, and C. Tellambura, "Underlay interference analysis of power control and receiver association schemes," *IEEE Trans. Veh. Technol.*, vol. PP, no. 99, pp. 1–1, 2016.

[158] M. Peng, Y. Li, T. Quek, and C. Wang, "Device-to-device underlaid cellular networks under rician fading channels," *IEEE Trans. Wireless Commun.*, vol. 13, no. 8, pp. 4247–4259, Aug 2014.

[159] S. Zaidi, D. McLernon, and M. Ghogho, "Breaking the area spectral efficiency wall in cognitive underlay networks," *IEEE J. Sel. Areas Commun.*, vol. PP, no. 99, pp. 1–17, 2014.

[160] Z. Wang and W. Zhang, "Spectrum sharing with limited feedback in poisson cognitive network," in *Proc. IEEE ICC*, June 2014, pp. 1441–1446.

[161] S. Govindasamy, "Uplink performance of large optimum-combining antenna arrays in poisson-cell networks," in *Proc. IEEE ICC*, June 2014, pp. 2158–2164.

[162] M. Kountouris and N. Pappas, "Hetnets and massive mimo: Modeling, potential gains, and performance analysis," in *Proc. IEEE APWC*, Sept 2013, pp. 1319–1322.

[163] X. Zou, G. Cui, M. Tang, and W. Wang, "Base station density bounded by maximum outage probability in massive mimo system," in *Proc. IEEE VTC*, May 2015, pp. 1–5.

[164] X. Lin, R. W. Heath, and J. G. Andrews, "The interplay between massive MIMO and underlaid D2D networking," *IEEE Trans. Wireless Commun.*, vol. 14, no. 6, pp. 3337–3351, June 2015.

[165] S. Shalmashi, E. Bjornson, M. Kountouris, K. W. Sung, and M. Debbah, "Energy efficiency and sum rate when massive MIMO meets device-to-device communication," in *Proc. IEEE ICCW*, June 2015, pp. 627–632.

[166] Q. Zhang, S. Jin, K. K. Wong, H. Zhu, and M. Matthaiou, "Power scaling of uplink massive MIMO systems with arbitrary-rank channel means," *IEEE J. Sel. Topics Signal Process.*, vol. 8, no. 5, pp. 966–981, Oct 2014.

[167] B. Yu, L. Yang, H. Ishii, and S. Mukherjee, "Dynamic TDD support in macrocell-assisted small cell architecture," *IEEE J. Sel. Areas Commun.*, vol. 33, no. 6, pp. 1201–1213, June 2015.

[168] Z. Yazdanshenasan, H. S. Dhillon, M. Afshang, and P. H. J. Chong, "Poisson hole process: Theory and applications to wireless networks," *IEEE Trans. Wireless Commun.*, vol. 15, no. 11, pp. 7531–7546, Nov 2016.

[169] J. Ferenc and Z. Neda, "On the size distribution of poisson voronoi cells," *Phisica A: Statistical Mechanics and its Applications*, vol. 385, no. 2, pp. 518–526, Nov 2007.

[170] T. Novlan, H. Dhillon, and J. Andrews, "Analytical modeling of uplink cellular networks," *IEEE Trans. Wireless Commun.*, vol. 12, no. 6, pp. 2669–2679, June 2013.

[171] Z. Chen, L. Qiu, and X. Liang, "Area spectral efficiency analysis and energy consumption minimization in multiantenna poisson distributed networks," *IEEE Trans. Wireless Commun.*, vol. 15, no. 7, pp. 4862–4874, July 2016.

[172] M. Xie, X. Jia, M. Zhou, and L. Yang, "Study on energy efficiency of D2D underlay massive MIMO networks with power beacons," in *Proc. IEEE WCSP*, Oct 2016, pp. 1–5.

[173] Y. Liu, L. Wang, S. A. R. Zaidi, M. Elkashlan, and T. Q. Duong, "Secure D2D communication in large-scale cognitive cellular networks: A wireless power transfer model," *IEEE Trans. Commun.*, vol. 64, no. 1, pp. 329–342, Jan 2016.

[174] S. Kusaladharma and C. Tellambura, "Secondary user interference characterization for spatially random underlay networks with massive mimo and power control," *IEEE Trans. Veh. Technol.*, vol. PP, no. 99, 2017.

[175] S. Kitazawa, H. Ban, and K. Kobayashi, "Energy harvesting from ambient RF sources," in *Proc. IEEE MTT-S*, May 2012, pp. 39–42.

[176] S. Atapattu and J. Evans, "Optimal energy harvesting protocols for wireless relay networks," *IEEE Trans. Wireless Commun.*, vol. 15, no. 8, pp. 5789–5803, Aug 2016.

[177] L. Jiang, H. Tian, Z. Xing, K. Wang, K. Zhang, S. Maharjan, S. Gjessing, and Y. Zhang, "Social-aware energy harvesting device-to-device communications in 5G networks," *IEEE Wireless Commun.*, vol. 23, no. 4, pp. 20–27, August 2016.

[178] G. P. Wijesiri, S. S. Chowdhury, and F. Y. Li, "Energy harvesting-aware backoff algorithms for distributed device-to-device communication," in *Proc. IEEE VTC*, May 2016, pp. 1–5.

[179] Z. Zhou, G. Ma, C. Xu, and Z. Chang, "A game-theoretical approach for green power allocation in energy-harvesting device-to-device communications," in *Proc. IEEE VTC*, May 2016, pp. 1–5.

[180] S. J. Darak, H. Zhang, J. Palicot, and C. Moy, "An efficient policy for D2D communications and energy harvesting in cognitive radios: Go bayesian!" in *Proc. EUSIPCO*, Aug 2015, pp. 1231–1235.

[181] U. Saleem, H. K. Qureshi, S. Jangsher, and M. Saleem, "Transmission power management for throughput maximization in harvesting enabled D2D network," in *Proc. IEEE ISCC*, June 2016, pp. 1078–1083.

[182] T. C. Hsu, Y. W. P. Hong, and T. Y. Wang, "Optimized random deployment of energy harvesting sensors for field reconstruction in analog and digital forwarding systems," *IEEE Trans. Signal Process.*, vol. 63, no. 19, pp. 5194–5209, Oct 2015.

[183] S. Jangsher, H. Zhou, V. O. K. Li, and K. C. Leung, "Joint allocation of resource blocks, power, and energy-harvesting relays in cellular networks," *IEEE J. Sel. Areas Commun.*, vol. 33, no. 3, pp. 482–495, March 2015.

[184] R. Atat, L. Liu, N. Mastronarde, and Y. Yi, "Energy harvesting-based D2D-assisted machine-type communications," *IEEE Trans. Commun.*, vol. PP, no. 99, pp. 1–1, 2016.

[185] J. Ding, L. Jiang, and C. He, "Dynamic spectrum allocation for energy harvesting-based underlaying D2D communication," in *Proc. IEEE VTC*, May 2016, pp. 1–5.

[186] H. H. Yang, J. Lee, and T. Q. S. Quek, "Heterogeneous cellular network with energy harvesting-based D2D communication," *IEEE Trans. Wireless Commun.*, vol. 15, no. 2, pp. 1406–1419, Feb 2016.

[187] P. Lakhlan and A. Trivedi, "Energy harvesting-based two-hop D2D communication in cellular networks," in *Proc. IEEE ICACCI*, Sept 2016, pp. 328–332.

[188] K. Huang, M. Kountouris, and V. O. K. Li, "Renewable powered cellular networks: Energy field modeling and network coverage," *IEEE Transactions on Wireless Communications*, vol. 14, no. 8, pp. 4234–4247, Aug 2015.

[189] H. S. Dhillon, Y. Li, P. Nuggehalli, Z. Pi, and J. G. Andrews, "Fundamentals of heterogeneous cellular networks with energy harvesting," *IEEE Trans. Wireless Commun.*, vol. 13, no. 5, pp. 2782–2797, May 2014.

[190] S. Gupta, R. Zhang, and L. Hanzo, "Energy harvesting aided device-to-device communication underlaying the cellular downlink," *IEEE Access*, vol. PP, no. 99, pp. 1–1, 2016.

[191] M. Xie, X. Jia, M. Zhou, and L. Yang, "Study on energy efficiency of D2D underlay massive MIMO networks with power beacons," in *Proc. IEEE WCSP*, Oct 2016, pp. 1–5.

[192] M. D. Renzo and W. Lu, "System-level analysis and optimization of cellular networks with simultaneous wireless information and power transfer: Stochastic geometry modeling," *IEEE Trans. Veh. Technol.*, vol. 66, no. 3, pp. 2251–2275, March 2017.

[193] P. Guan and M. D. Renzo, "Stochastic geometry analysis and optimization of uplink cellular networks with fractional power control and optimum combining," in *Proc. IEEE ICC*, May 2016, pp. 1–6.

[194] H. ElSawy and E. Hossain, "Two-tier hetnets with cognitive femtocells: Downlink performance modeling and analysis in a multichannel environment," *IEEE Trans. Mobile Comput.*, vol. 13, no. 3, pp. 649–663, March 2014.

[195] T. Bhandari, H. S. Dhillon, and R. M. Buehrer, "The impact of proximate base station measurements on localizability in cellular systems," in *Proc. IEEE SPAWC*, July 2016, pp. 1–5.

[196] S. Kusaladharma and C. Tellambura, "Energy harvesting random underlay cognitive networks with power control," in *Proc. IEEE ICC*, May 2017, pp. 1–6.

[197] D. Liu, L. Wang, Y. Chen, M. Elkashlan, K. K. Wong, R. Schober, and L. Hanzo, "User association in 5g networks: A survey and an outlook," *IEEE Commun. Surveys and Tut.*, vol. 18, no. 2, pp. 1018–1044, Secondquarter 2016.

[198] T. S. Rappaport, S. Sun, R. Mayzus, H. Zhao, Y. Azar, K. Wang, G. N. Wong, J. K. Schulz, M. Samimi, and F. Gutierrez, "Millimeter wave mobile communications for 5G cellular: It will work!" *IEEE Access*, vol. 1, pp. 335–349, 2013.

[199] J. Qiao, X. S. Shen, J. W. Mark, Q. Shen, Y. He, and L. Lei, "Enabling device-to-device communications in millimeter-wave 5G cellular networks," *IEEE Commun. Mag.*, vol. 53, no. 1, pp. 209–215, January 2015.

[200] A. Gupta and R. K. Jha, "A survey of 5G network: Architecture and emerging technologies," *IEEE Access*, vol. 3, pp. 1206–1232, 2015.

[201] D. Maamari, N. Devroye, and D. Tuninetti, "Coverage in mmwave cellular networks with base station cooperation," *IEEE Trans. Wireless Commun.*, vol. 15, no. 4, pp. 2981–2994, April 2016.

[202] W. Lu and M. D. Renzo, "Accurate stochastic geometry modeling and analysis of mmwave cellular networks," in *Proc. IEEE ICUWB*, Oct 2015, pp. 1–5.

[203] K. Venugopal, M. C. Valenti, and R. W. Heath, "Device-to-device millimeter wave communications: Interference, coverage, rate, and finite topologies," *IEEE Trans. on Wireless Commun.*, vol. 15, no. 9, pp. 6175–6188, Sept 2016.

[204] Y. Niu, L. Su, C. Gao, Y. Li, D. Jin, and Z. Han, "Exploiting device-to-device communications to enhance spatial reuse for popular content downloading in directional mmwave small cells," *IEEE Trans. Veh. Technol.*, vol. 65, no. 7, pp. 5538–5550, July 2016.

[205] M. Mirahsan, R. Schoenen, S. S. Szyszkowicz, and H. Yanikomeroglu, "Measuring the spatial heterogeneity of outdoor users in wireless cellular networks based on open urban maps," in *Proc. IEEE ICC*, June 2015, pp. 2834–2838.

[206] Z. Guizani and N. Hamdi, "mmwave E-band D2D communications for 5G-underlay networks: Effect of power allocation on d2d and cellular users throughputs," in *Proc. IEEE ISCC*, June 2016, pp. 114–118.

[207] T. Bai, R. Vaze, and R. W. Heath, "Analysis of blockage effects on urban cellular networks," *IEEE Trans. Wireless Commun.*, vol. 13, no. 9, pp. 5070–5083, Sept 2014.

[208] G. R. MacCartney, J. Zhang, S. Nie, and T. S. Rappaport, "Path loss models for 5G millimeter wave propagation channels in urban microcells," in *Proc. IEEE GLOBECOM*, Dec 2013, pp. 3948–3953.